State University of Gent
Faculty of Applied Sciences
Laboratory of Electromagnetism and Acoustics
Director: Prof. Dr. Ir. P. Lagasse

ANALYSIS OF NOISE AND SPECTRAL BEHAVIOUR OF DFB LASER DIODES

GEERT MORTHIER
electrotechnical engineer

Promotor: Prof. Dr. R. Baets

Academic Year 1990-1991

PREFACE

This work was done in the frame of the optical modelling activities of the Laboratory of Electromagnetism and Acoustics. I therefore wish to express my gratitude to the director, Prof. dr. ir. P. Lagasse for giving me the opportunity to work at his well-organized laboratory. The promotor, Prof. dr. ir. R. Baets is acknowledged for his help in outlining the content of this work and for all the usefull hints and directives which he gave me.

I am also indebted to the partners of the European RACE-projects R1010 (CMC) and R1069 (EPLOT) and of the analog laser project (i.e. Alcatel Alshtom Recherche and Alcatel-SEL). The collaboration with each of the partners has certainly influenced the final contents of this Ph. D. thesis. It would take too far to mention all persons, but I feel obliged to make an exception for Dr. C. Park and Dr. J. Buus of Plessey Research (Caswell, Engeland), who gave me the opportunity to do experimental work for one month. Not only did they help me with this work, but together with other collegues they also turned it in a time which I have enjoyed.

I also like to thank the supervisors of my M.Sc. thesis dr. J.-P. Van De Capelle and dr. P. Vankwikelberge, my collegues K. David and J. Willems and my thesisstudents P. Devos and G. Depestel. The many discussions with each of them undoubtedly have contributed to the level of this work.

The IWONL (Institute for Scientific Research in Industry and Agriculture) is acknowledged for its financial support during three years.

I finally want to express my gratitude to my parents and relatives, and to the many friends (among which many collegues) for the support, the attention and the joy they gave me.

Gent, June 1991
G. Morthier

Chapter I

INTRODUCTION

The subject of this Ph. D. dissertation is the analysis of the spectral and modulation properties of DFB laser diodes and the latters optimalisation for use in optical communication systems. In this theoretical study, we have tried to establish a compromise between a rigourous mathematical treatment and a more simple, physical description, while at the same time we tried to include all of the features which are characteristic for DFB lasers.

In this introductory chapter, the general frame in which this study has to be situated is described and an overview of the goals and the content of the dissertation is given.

I.1 Laser diodes and optical communication systems

A substantial fraction of the present-day research in semiconductor lasers is directed towards their application in optical communication systems [1.1]. In such systems, the original electrical information is converted into an optical signal, which is transmitted along an optical fibre and reconverted in an electrical signal at the receiver end. Interest in such optical communication systems is largely stimulated by the low loss and the large bandwidth of optical fibres. The reader is referred to ref. [1.2] for a brief overview on optical fibres.

The expansion of the optical communication field is clearly illustrated by fig.1.1, where the annual growth rate of U.S. manufacturer's shipments of selected telecommunication equipment is depicted. While the present laser diode production mainly supplies the needs of existing markets such as optical data recording, laser printing, audio and video discs or bar code readers, future production may show an increasing portion of lasers required by optical communication needs.

Laser diodes are the ideal light sources for optical communication, not in the least as a result of their high external efficiency and easy electronic modulation in comparison with other laser types. Furthermore, integration of laser diodes with other electronic components on a single chip seems to be a future potential. However, a full exploitation of laser diodes in optical communication requires a carefull design in function of the applied communication scheme.

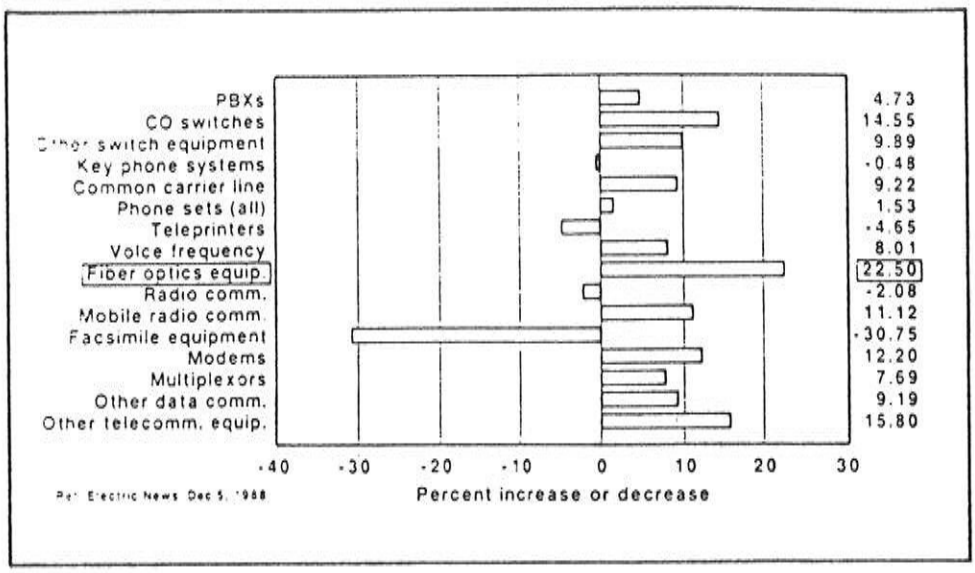

Fig.1.1: Annual growth rate of U.S. manufacturer's shipments of selected telecommunication equipment from 1984-1988 (from [1.1])

Optimum performance is achieved by the application of coherent communication. Both digital and analog systems are considered at present and the attention focusses on FM- as well as AM-modulation schemes ([1.3] - [1.6]). In this case, stable, dynamic single mode lasers are required to make heterodyne detection possible and to restrict the chromatic and modal dispersion during propagation in the fibre. In addition, depending on the coding, a low FM- or AM-noise, a uniform FM- or AM-response and a high linearity may be required.

Applications of coherent communication can be found in the areas of long-haul communication, data networking and subscriber broadband networks (e.g. cable distribution of high definition television).

I.2 Laser diodes and their characteristics

Each laser diode is basically nothing more than an oscillator, conceived as an electromagnetic resonator in a cavity filled with semiconductor material. In its most simple form, as a Fabry-Perot laser (fig.1.2), it consists of a waveguide, which is limited in the longitudinal direction by the partly-reflecting semiconductor facets. The waveguide consists of a thin active layer, sandwiched between cladding layers with a lower refractive index. A population inversion in the active layer is achieved by current injection, usually through a stripe.

This population inversion results in spontaneous and stimulated emission, which compensates for the optical power loss, through the facets and by absorption in the semiconductor material. However, stimulated and spontaneous emission only occur for wavelengths in the neighbourhood of the bandgap-wavelength. Therefore and since optical fibres exhibit a minimal attenuation for wavelengths around 1.55 μm and a minimal dispersion for wavelengths around 1.3 μm, lasers for optical communication purposes usually have an InGaAsP active layer ($In_{.61}Ga_{.39}As_{.84}P_{.16}$ for λ= 1.55 μm and $In_{.72}Ga_{.28}As_{.6}P_{.4}$ for λ=1.3 μm) and InP cladding layers [1.7], [1.8].

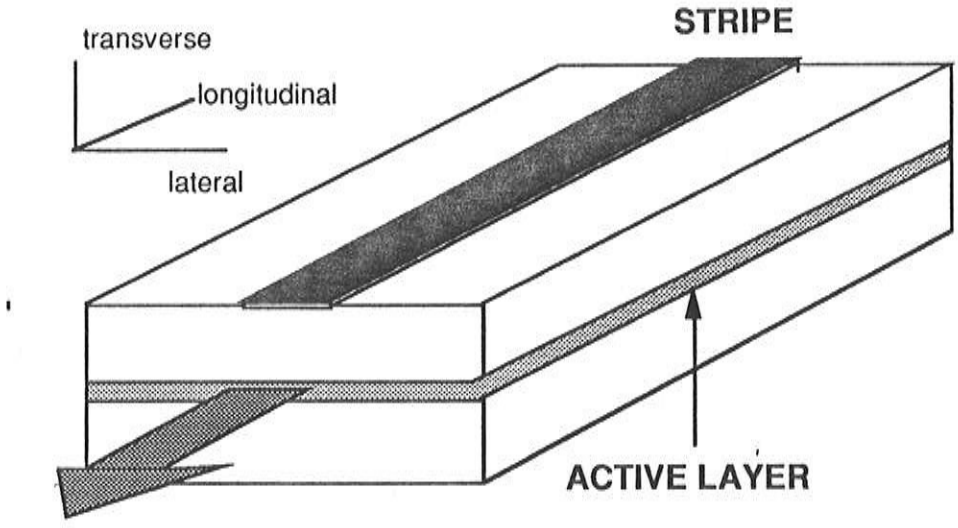

fig.1.2: schematic view of a laser diode

Real laser structures usually are far more complex than the structure of fig.1.2 [1.9]. In the lateral/transverse direction, more than 3 layers are often grown in order to achieve improved electrical, optical and crystallic properties. E.g., current blocking layers and buffer layers can be introduced to this end. In the longitudinal direction, the structure can consist of multiple, separately controlled sections with different waveguide structures and some sections can be provided with a grating in the active or passive layers. Lasers having a grating are called DFB lasers ('Distributed Feedback Lasers') or DBR lasers ('Distributed Reflector Lasers'), if the grating is only present in a passive section (i.e. with a stimulated emission-free active layer). Moreover, the active layer may be composed of ultra thin layers (or even wires), the so-called quantum wells (or quantum wires and boxes). Such layers, which are thinner than the carrier scattering length, exhibit specific properties due to the additional quantisation (quantum size effect) in this case [1.10].

The details about the internal structure of a laser diode should, for use in communication or other systems, be completed by the lasers external characteristics. It is, in fact, the knowledge of these characteristics which often allows to select the most appropriate laser for each specific application. Both the static and dynamic characteristics are usually relevant in this.

Static characteristics of primary importance are the optical power-current (P/I) relation and the far-field pattern. The far-field pattern defines the coupling of the laser light into the transmission system and it is determined by the waveguiding mechanism (e.g. the number of excited waveguide modes) and by the reflection at the facets [1.11], [1.12]. The P/I relation on the other hand defines the efficiency and depends on the temperature and on the different losses. The requirements of optical communication systems are not very stringent for what concerns the static P/I-relation and the far-field pattern. A certain minimum power level (e.g. 5 mW) should be attainable with a reasonable efficiency, while the influence of the temperature and the beam width should not be too high.

A static characteristic of great importance in optical communication applications is the optical spectrum, i.e. the spectral

distribution of the optical power. Fig.1.3 shows a typical spectrum, where, in general, several longitudinal and lateral modes can be present [1.13]. As has been mentioned earlier, optical communication requires that only one mode is present, even under modulation, and that no mode hops occur if a variation in temperature or current takes place. Only some lasers in which a grating is incorporated (DFB or DBR lasers) can fulfill this requirement. In practice, such a laser is called single mode if the side modes are suppressed by 30 dB or more.

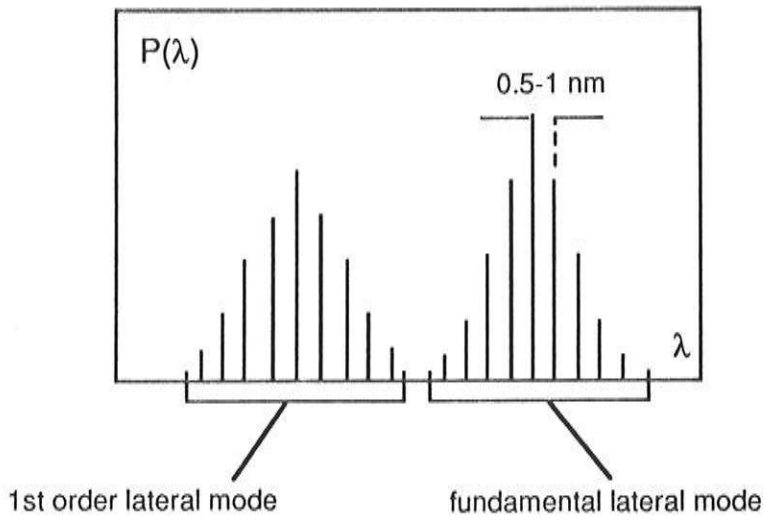

fig.1.3: typical spectrum of a laser diode

In lasers serving as local oscillator in a heterodyne detection system, the main mode must further have a tunable wavelength, since the emission wavelength must be tuned on the wavelength of the received light signal. Special multi-section DFB lasers or DBR lasers need to be considered for this application.

Even the spectrum of single mode lasers still has a certain width, called the linewidth, of 1-100 MHz. This linewidth is determined by the FM-noise, which has its origin in spontaneous emission fluctuations and carrier shot noise. It normally decreases proportional with the inverse power level at low to moderate power levels, whereas at high power levels, it saturates or rebroadens. This is illustrated by the experimental results in fig.1.4 [1.14].

A low linewidth results in a considerably better sensitivity of the receiver in coherent communication schemes and hence noticeable effort has been spent on the reduction of the linewidth. The use of AM-coding also requires a low intensity noise (expressed by the RIN or 'Relative Intensity Noise'). This RIN is caused by identical sources as the FM-noise and can often be minimised simultaneously with the linewidth.

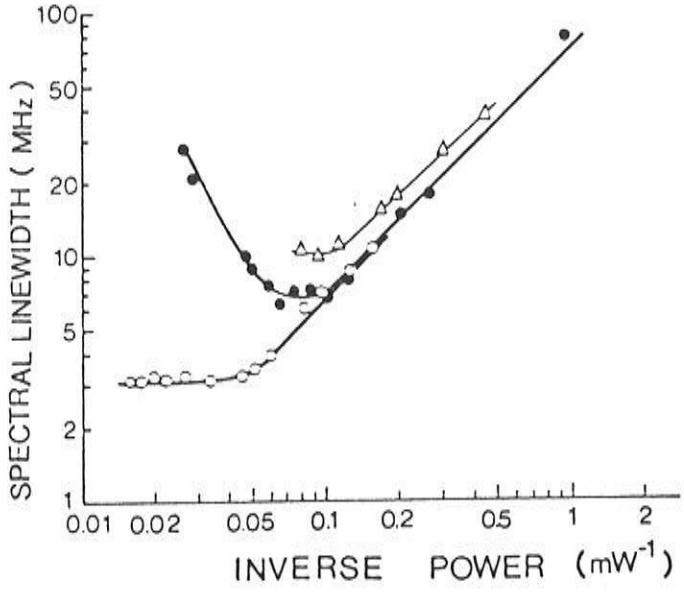

Fig.1.4: Typical evolution of the linewidth in DFB lasers [1.14]

o: 1.3 μm DFB laser
o: 1.55 μm DFB laser
Δ: 1.55 μm 'λ/4-shifted' DFB laser

The static operation of laser diodes results in a monochromatic light signal without information content. Modulation of the light signal and thus of the laser diode is necessary for the transmission of information. The dynamic properties of the laser can not be ignored in this case. One can distinct between large signal and small signal characteristics, although the former are relevant only for analog systems, where the (harmonic and non-linear) disortion must be restricted. The dynamics are largely determined by the detailed interaction between the carriers and the wave propagation in the cavity. In addition, thermal effects seem to play an impor-

tant role at low modulation frequencies (e.g. below 1 MHz), while the influence of parasitics (resulting from the different junctions and contacts) or the mounting (e.g. bonding wires) may not be underestimated at high frequencies (above 1 GHz) [1.15].

The small signal characteristics refer to the FM- and AM-response of the laser when a small sinusoidal current is super-posed on the static bias current. An example of an experimental AM-response is shown in fig. 1.5. The peak in the GHz-region is caused by a resonance in the carrier-photon interaction and limits the maximum modulation frequency. The bandwidth of coherent systems, which demand a uniform FM- or AM-response, is restricted by this resonance frequency on one side and by the linewidth on the low frequency side.

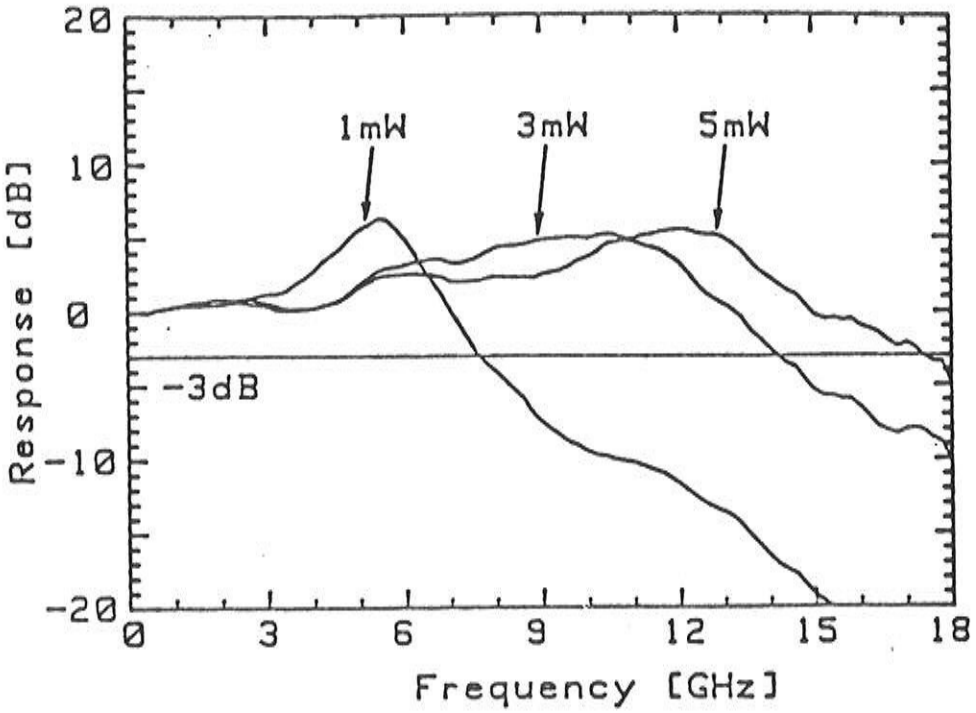

Fig.1.5: Experimental AM-response of a laser diode [1.16]

It must finally be remarked that the static and dynamic properties can be heavily deteriotated in the presence of external reflections (e.g. originating from the fiber in communication systems). The feedback sensitivity of a laser diode quantifies the dependence of its characteristics on external reflections and can therefore be called a characteristic itself. At the present time, ex-

ternal reflections need to be eliminated by the use of one or more (expensive) optical isolators.

I.3 Goals and approach of this work

This work reports on the theoretical investigation of the spectral and (to some extend) the dynamic properties of semiconductor lasers, and of DFB lasers in particular. It explores the mechanisms that determine the side mode suppression at low and high bias level, the noise and the modulation characteristics. Special attention is paid to finding possible explanations for the linewidth rebroadening, a phenomenon which was not at all understood at the time this work started. The tunability and the whole field of tunable DBR lasers on the other hand are not considered in this work. We refer to the work of K. David [1.17] for this.

The backbone of our research is formed by the computer model CLADISS ('Compound Laser Diode Simulation Software'). The basic version of this model, which provided a tool for the single mode analysis of the static and the small signal AC-behaviour, has been developped by Dr. P. Vankwikelberge [1.18]. In the framework of this Ph. D. thesis, it has been extended to a multi mode model which also allows an analysis of the noise behaviour and of the harmonic distortion during modulation. Especially those porperties by which DFB and DBR lasers distinct themselves from other lasers have been emphasised in the model. Some phenomena, which have a similar effect on Fabry-Perot, DFB and DBR lasers and hence cannot offer an explanation for the specific properties of DFB and DBR lasers have thus been ignored. Variations in the lateral/transverse direction e.g. have been averaged, while the current injection and spreading have been approximated in a very simple way. Longitudinal variations in the fields and the carrier density on the other hand are included in an accurate way, for this effect causes a power dependence of the mirror loss in lasers with a grating. It was also found useful, regarding the importance of the spectral laser characteristics, to implement a detailed wavelength dependence of the distributed reflections, the gain and the refractive index.

In addition, effort has been spent on giving physically intuitive explanations for some of the observed phenomena. An adaption

of the standard rate equation description of laser diodes was found to be a useful help in this. To some extend, we also tried to assess the influence of some effects, not included in the modelling.

I.4 Brief overview of the contents

This thesis is divided into 5 general parts. The second chapter treats the mathematical description of laser diodes and as such it forms the basis of the consecutive chapters. It shows how the complexity of an actual laser diode can be reduced to a level suitable for easy mathematical description. First, a z-dependent description (with z being the longitudinal coordinate), consisting of a set of coupled wave equations and a carrier rate equation, is derived from Maxwell's equations and the principle of conservation of charge. This also includes a detailed account of the applied numerical approximations and iterations. The chapter concludes with a derivation of a z-independent description, which results in an extension of the standard rate equation description. This mathematical model, which has not been implemented numerically, is used throughout the remaining chapter as a help in the qualitative understanding.

The numerical implementation of the longitudinal mathematical model, resulting in the computer model CLADISS, is given subsequently in chapter 3. This also includes a detailed account of the applied numerical approximations and iterations.

The analysis of the DC-behaviour of DFB lasers is then treated in detail in chapter 4. The discussion is thereby focussed on the side mode rejection and the design of lasers with a stable, high side mode suppression. The deterioration of the side mode rejection due to spatial hole burning at high power levels and the influence of some parameters in this are investigated, but is also shown how this spatial hole burning can be reduced by the introduction of a gain grating or by specially designed index-coupled lasers.

The fifth chapter considers the noise characteristics of laser diodes. Both the linewidth (or the FM-noise) and the intensity noise are discussed, although the emphasis is on the discussion of possible causes for the linewidth rebroadening. Possible causes, such as

the influence of side modes, the bias dependence of the linewidth enhancement factor and the bias dependence of the dispersion are demonstrated. Attention is furthermore also paid to the effect of external reflections on the linewidth and the RIN.

Finally, the behaviour of laser diodes under modulation is investigated in the last chapter. Only a brief overview of the small signal characteristics, the AM- and FM-responses, is given since this subject has been covered already in the work of Dr. Vankwikelberge (see e.g. [1.18] or [1.19]). The harmonic distortion in the AM- and FM-responses is the main subject in this chapter. It is shown how the distortion is determined strongly by the spatial and spectral hole burning and how it can be minimised.

References

[1.1] A. DeMaria, 'Photonics vs. electronics technologies', Optics News, pp.22-37, April, 1989.

[1.2] S. Nagel, 'Optical Fiber - The Expanding Medium', IEEE circuits and devices magazine, pp. 36-45, March, 1989.

[1.3] T. Okoshi, K. Kikuchi, Coherent Optical Fiber Communications, KTK Publishers, Tokyo, 1988.

[1.4] R. Gross, R. Olshansky, 'Multichannel Coherent FSK Experiments Using Subcarrier Multiplexing Techniques', IEEE Journ. Lightw. Techn., Vol. 8, pp. 406-415, March, 1990.

[1.5] F. Dawson, 'AM systems bring fiber to cable television', Laser Focus World, pp.129-137, February, 1990.

[1.6] L. Kazovski, 'Phase- and Polarization-Diversity Coherent Optical Techniques', IEEE Journ. Lightw. Techn., Vol. 7, pp. 279-292, February, 1990.

[1.7] M. Toda, 'Material selection for double heterojunction lasers - A higher bandgap does noet necessarily mean lower refractive index', IEEE Journ. Quant. El., Vol. 23, pp. 483-486, May 1987.

[1.8] D. Botteldooren, 'Theoretische studie van de optische eigenschappen van III-V bulkhalfgeleiders, quantum wells en superroosters', Ph. D. thesis, University of Gent, 1989.

[1.9] G. Agrawal, N. Dutta, Long-wavelength semiconductor lasers, Van Nostrand Reinhold Company, New York, 1986.

[1.10] L.C. Liu, A. Yariv, 'Quantum well lasers', Journ. of Luminiscence, 30, pp. 551-561, 1985.

[1.11] R.Baets, 'Theoretische en technologische aspekten bij het ontwerp en de vervaardiging van GaAs-AlGaAs halfgeleiderlasers', Ph. D. Thesis, University of Gent, 1984.

[1.12] J. Van de Capelle, 'Modellering en fabricage van dubbelheterojunctie GaAs laserdiodes', Ph. D. thesis, University of Gent, 1987.

[1.13] H. Casey, M. Panish, 'Heterostructure Lasers: Part A, Fundamental Principles', Academic Press, 1978 .

[1.14] K. Kobayashi, I. Mito, 'Single Frequency and Tunable Laser Diodes', Journ. Lightw. Techn., Vol. 6, pp. 1623-1633, November, 1988.

[1.15] R. S. Tucker, 'High-Speed Modulation of Semiconductor Lasers', IEEE Journ. Lightw. Techn., Vol. 3, pp. 1180-1192, December, 1985.

[1.16] N. Chinone, K. Uomi, 'Advances in high speed semiconductor lasers', pp.137-143,.

[1.17] K. David, Ph. D. thesis, university of Gent, to be published.

[1.18] P. Vankwikelberge, 'Theoretische studie van statische en dynamische longitudinale effecten in Fabry-Perot en DFB-diodelasers', Ph. D. thesis (in Dutch), university of Gent.

[1.19] P. Vankwikelberge, F. Buytaert, A. Franchois, R. Baets, P. Kuindersma, C. Fredriksz, 'Analysis of the carrier-induced FM-response of DFB lasers: theoretical and experimental case studies', IEEE Journ. Quant. El., Vol. 25, pp.2239-2254, November, 1989.

Chapter II

MATHEMATICAL MODELS FOR LONG WAVELENGTH LASER DIODES

This chapter describes how a practical laser diode, with its complex structure and its complex physical interactions can be simulated mathematically and numerically. Two mathematical models are presented, with the common feature of both models being that variations in the lateral and transverse direction, as well as the electronic transport problem are treated in a most simplified way. A justification for this simplification, as well as a few limitations of the approach will be given in section II.1.

The two mathematical models are presented in the following sections. The first model takes into account longitudinal and spectral variations and has been implemented numerically on a VAX computer. This computer model, which is described in chapter 3, has been used intensely in obtaining the results of chapter 4, 5 and 6 and it is more or less the backbone of this Ph. D. dissertation. The second model is obtained from the first by further averaging in the longitudinal direction. This then results in a generalisation of the standard rate equation description [2.1], which were and still are often used in deriving simple analytical formulas. In this dissertation, we will generalise some formerly derived formulas and use the formulas rather for the sake of easy understanding.

II.1 From practical device to model

II.1.1 Geometry of a laser diode

Fig.2.1.1 shows the schematic cross section of an etched-mesa buried heterostructure laser, with its typical dimensions. Many other geometrical configurations can be found in literature (see e.g. [2.2], [2.3] and [2.4]), but the lateral/transverse geometry always seems to have a similar degree of complexity. The active la-

yer typically has a width w of 2μm, a thickness d of 0.1-0.2μm and a length L of 300-1000μm.

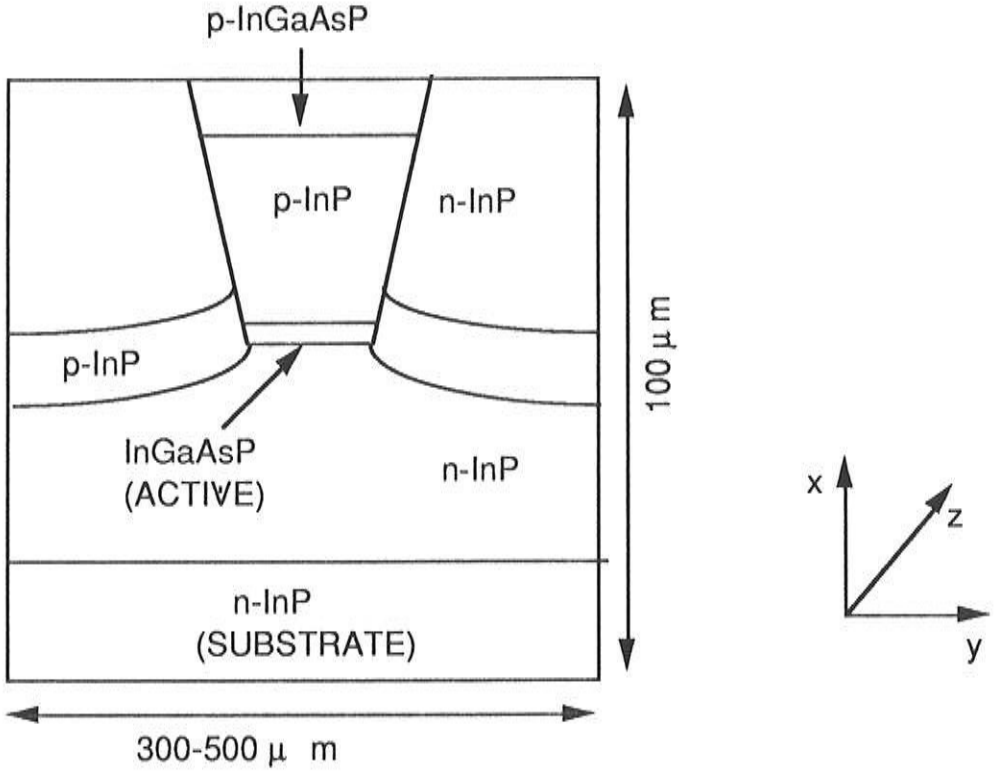

Fig. 2.1.1: schematic cross-section of an etched-mesa buried heterostructure laser.

The double heterojunction formed by the p-InP layer, by the InGaAsP layer and by the n-InP layer helps to confine the carriers in the active InGaAsP layer, where they can recombine (spontaneous and stimulated emission) to produce light. The banddiagram of this heterojunction under zero (a) and forward (b and c) bias is depicted in fig.2.1.2. Obviously, an efficient carrier confinement can only be obtained when the bandgap of the active layer is sufficiently small with respect to the bandgap of the cladding layers.

In practice there will always be some current leakage: over the heterojunction, but in part also over the p-n-p-n InP layers. These p-n-p-n layers act as a thyristor [2.2]. At low current levels (when the thyristor is switched off), the leakage through this path is negligible. At higher current levels, when the thyristor is turned on, this leakage may become significant however.

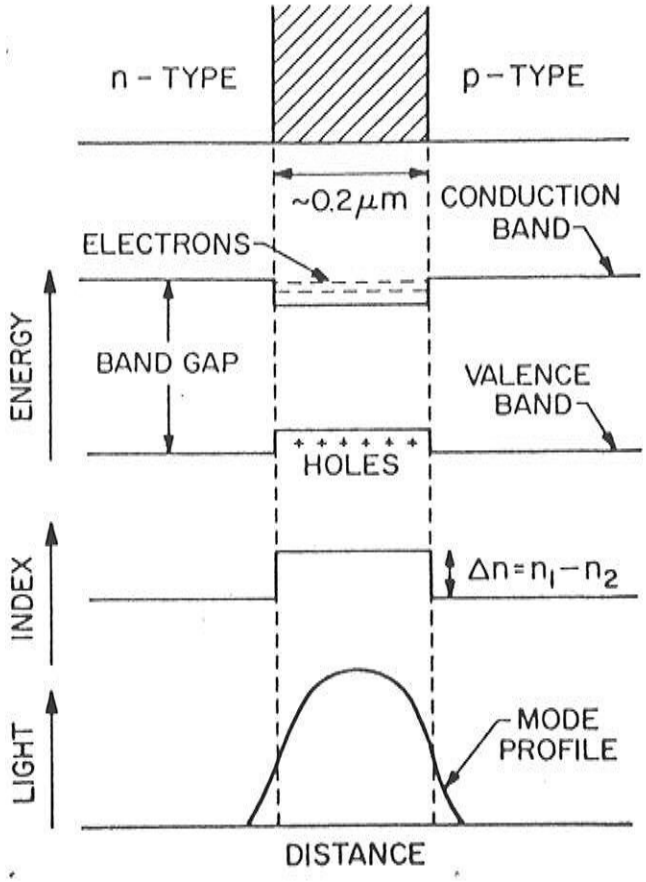

Fig.2.1.2: Energy-band diagram of the double heterojunction at (a) zero bias, (b) and (c) forward bias.

The double heterojunction also assures the optical confinement, i.e. it provides the waveguiding mechanism. The confinement in the transverse direction x is generally of the index-guiding type; the refractive index of the active layer is larger than the index of both cladding layers. The guiding in the lateral direction y on the other hand can be either index- or gain-guiding. Gain guiding occurs in lasers, such as the ridge waveguide laser (fig.2.1.3), where the active layer is not restricted in the lateral direction and where only part of the active layer is pumped. This results in gain (stimulated emission) in the central part of the active layer and loss in the surrounding parts, which causes the guiding. Lasers for optical communication purposes are usually strongly index-guided and we

will therefore restrict ourselves to such lasers in the following. For more information on gain-guiding we refer to the existing literature ([2.2], [2.5]).

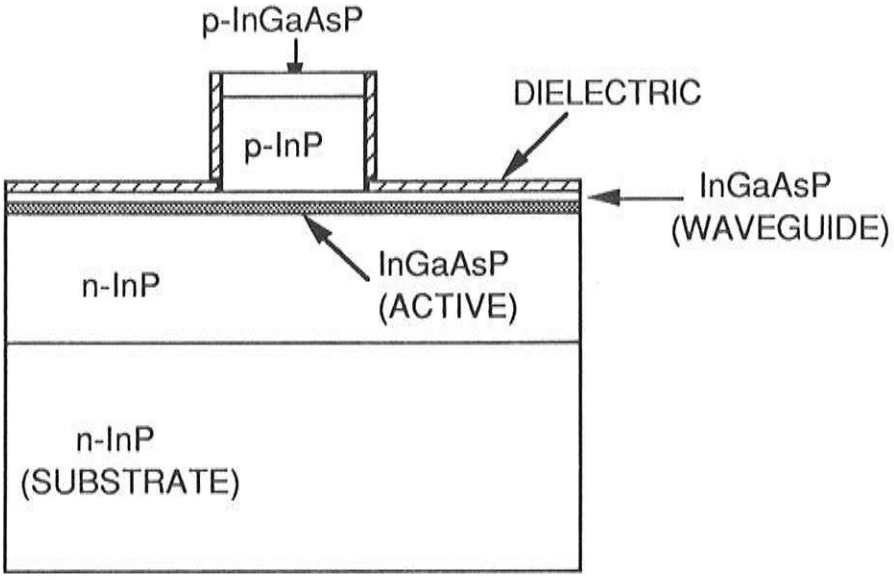

Fig. 2.1.3: Schematic cross-section of a ridge waveguide laser.

Fig.2.1.4 shows a typical longitudinal view of a laser diode. The most general case is considered here. The laser can consist of several sections in the longitudinal direction, whereby each section can be pumped independently and can have a different lateral/ transverse geometry. A grating, causing distributed reflections in the longitudinal direction, can be present in the cladding layers or in the active layer. Furthermore, discrete reflections can occur at the interfaces between two sections or at the front and rear facet. The reflectivity at the interfaces depends on the discontinuities in the waveguide geometry between the sections, whereas the reflectivity at the facets is determined by the cleaving and/or the coating of the facets. It must also be noticed that, in the most general case, the active layers in different sections may be composed of different alloys. In the extreme case, one of the sections may even represent external reflections, originating from e.g. mirrors, lenses etc., and be filled with air.

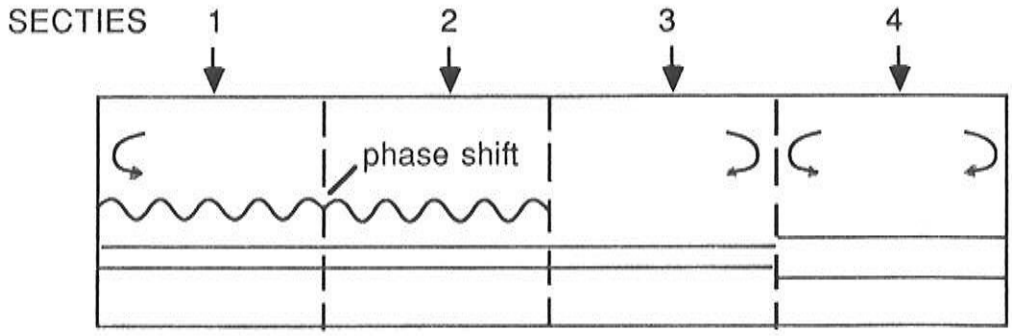

Fig. 2.1.4: Longitudinal structure of a general laser diode

II.1.2 The physical processes and their approximation

A detailed description of a laser diode would require the determination of the carrier density N, the electrical potential V and the optical field E in each point (x,y,z) of the laser. In addition, one must bear in mind that the carrier density in one point determines the stimulated and spontaneous emission, the absorption and the refractive index in that point and therefore the optical field in all points of the laser cavity. On the other hand, the carrier density and the potential in each point are determined by carrier diffusion and drift in all three dimensions, by stimulated emission and absorption (which depend on the optical field intensity) and by the Fermi-level in each layer.

The detailed solution of this complex problem seems a far too ambitious, if not an unattainable goal. Furthermore, the physical insight and hence the derivation of easy design rules would not really benefit from such a complicated model. In the next sections, we will show how a simplification can be brought about and we'll introduce approximations for the carrier density dynamics, for the field propagation and for the interaction between field and carriers.

II.1.2.1 The rate equation for the carrier density

We assume that all sections are current controlled and that, due to the leakage, only a fraction η of the injected carriers reach the active layer, where they distribute uniformly in the lateral and

transverse direction. No doping is assumed and hence it follows from the neutrality condition that the hole density equals the electron density. We can then write down the following rate equation for the carrier density N(z,t) in the active layer at the longitudinal position z and at a time t:

$$\frac{\partial N(z,t)}{\partial t} = \frac{\eta J}{qd} - \frac{N}{\tau} - B_0 N^2 - C_0 N^3 - R_{st} \qquad (2.1.1)$$

The first term on the right hand side of (2.1.1) represents the current injection, with J being the current density, q the electron charge and d the active layer thickness. N/τ represents spontaneous carrier recombination via traps and at surfaces. This recombination rate is proportional with the carrier density since only one carrier (besides one trap) is involved in the process. B_0N^2 represents the bimolecular recombination (or spontaneous emission) rate and this rate is proportional with N^2 since two carriers (an electron and a hole) are now involved. The C_0N^3-term stands for the Auger recombination rate. In this process, the energy released during an electron-hole recombination is transferred to another electron (or hole), which is excited to a high energy state and relaxes back by losing energy to lattice vibrations. This Auger recombination, which is proportional with N^3 as a result of the three carriers involved, is generally the dominant non-radiative process in long wavelength lasers (as used in optical communication). The last term in (2.1.1) expresses the stimulated emission, which will be treated in more detail in section II.1.2.3.

It must be noticed that carrier diffusion, in the lateral/transverse direction as well as in the longitudinal direction is neglected here. Ignorance of the longitudinal diffusion is justified by the fact that the corresponding diffusion length is generally small with respect to the typical distance on which the carrier density varies due to the other terms in (2.1.1). It must finally be noticed that the rate equation (2.1.1) also implies that current leakage from one section to another is neglected which, principally, is correct only if all sections are isolated electrically.

II.1.2.2 Description of the optical field

The lateral/transverse cross section forms an optical waveguide, of which we assume that it only sustains the lowest order TE-mode. The small dimensions of the active layer justify this assumption. The forward (+) and backward (-) propagating parts of the lateral electrical laser field can therefore in each waveguide section be expanded as:

$$E_y^+(x,y,z,t) = \mathrm{Re}\left\{ \phi(x,y) \sum_m R_m^+(z,t)\, e^{j(\omega_m t - \beta_g z)} \right\}$$

$$E_y^-(x,y,z,t) = \mathrm{Re}\left\{ \phi(x,y) \sum_m R_m^-(z,t)\, e^{j(\omega_m t + \beta_g z)} \right\} \qquad (2.1.2)$$

This field expansion relies also on the assumption that the waveguiding properties and the eigenmode ϕ of the cross-section are independent of time t and axial position z.

The waveguiding actually depends on the refractive index in each layer and hence an axial variation in the refractive index of any layer can cause a z-dependence of the eigenmode ϕ. Such an axial variation exists in the passive layers if a grating is present. Since most practical lasers only make use of shallow gratings (gratings at relatively large distance from the active layer and with small amplitudes), we can neglect the effect on the eigenmode. A second axial variation in the refractive index may exist in the active layer. In this case, the refractive index depends on the carrier density, which is generally not uniform in the axial direction due to the non-uniform optical power density. At practical power levels however, the variations in the active layers refractive index are of the order of 0.1 % of the average index and they have no significant influence.

The expansion (1.2.2) finally assumes that the eigenmode is identical for all longitudinal modes m. On one hand, it is known that the eigenmode depends on the optical frequency and that the longitudinal modes m have different optical frequencies ω_m. On the other hand, it will become clear in the following that these optical

frequencies are located very closely one to another and as such they correspond with almost identical eigenmodes.

The complex amplitudes $R_m^{\pm}$ in (1.2.2) represent the slowly varying (with time and axial position) parts of the fields. All rapid variations are included in the exponentials, although the choice of ω_m and β_g is not uniquely defined. ω_m and β_g can be considered as a reference frequency and a reference propagation constant, the choice of which only must lead to slowly varying amplitudes $R_m^{\pm}$. In what follows, we will always choose ω_m so that it coincides with the optical frequency of the m-th longitudinal mode when only static current is injected. For β_g, we choose the Bragg-number $\beta_g = n\pi/\Lambda$ if the section contains a grating of order n. Λ denotes the period of the grating in this case and is, in practical devices, usually chosen so that β_g nearly equals the propagation constant of the waveguide. When a section is not provided by a grating, β_g is set equal to the propagation constant β_m of the lowest order TE-mode of the unperturbed waveguide (i.e. the waveguide without absorption or stimulated emission) at the frequency ω_m.

II.1.2.3 The electron-field interaction

A part of the optical field intensity, propagating inside the laser cavity, is lost through absorption or through the front and rear facets. In lasers, this loss is compensated by the stimulated emission in the active region, which amplifies the intensity during propagation. The amplification is expressed mathematically by the gain g, which, in semiconductors, depends on the carrier density and on the wavelength λ (or the frequency $\omega = 2\pi c/\lambda$) of the light:

$$\frac{\partial(|E(\lambda)|^2)}{\partial s} = g(N,\lambda)\,|E(\lambda)|^2 \qquad (2.1.3)$$

$E(\lambda)$ represents the field component with wavelength λ and propagating in the s direction. From equation (2.1.3), it can be readily seen how g corresponds with an imaginary refractive index, given by:

$$n = \frac{j\,g}{2\,(\omega/c)} \qquad (2.1.4)$$

g can be calculated quantummechanically from the Fermi-functions of electrons and holes, from the densities of states and from the transition probability for a transition from conduction to valence band [2.6]. The same calculation also results in a theoretical estimation for the bimolecular recombination coefficient B_o. From such a calculation, one readily finds that the gain is approximately linear in the carrier density N and that the gain can be positive only for wavelengths in the neighbourhood of the bandgap wavelength λ_g ($=1.24\mu m/E_g$, E_g in eV).

The expression (2.1.3) however, is, strictly speaking, no longer valid when large optical intensities exist in the active layer. The stimulated emission becomes non-linear in this case and the gain becomes intensity dependent. The reason is that a strong field, e.g. at wavelength λ_q, causes a strong stimulated emission and a large electron-hole recombination rate. Since the moment must be conserved in this recombination, only electrons with a certain energy level in the conduction band and only holes with a certain energy level in the valence band will recombine. The large stimulated recombination at these particular energy levels then deforms the energy distribution of the carriers, as if a hole is burned in the spectral distribution of the carriers. (The effect is referred to as 'spectral hole burning', after this visual representation.) After a small, but finite time, the hole is refilled by intraband relaxation, while the energy of the carriers is redistributed through scattering, e.g. electron-phonon scattering.

The non-linearity can be taken into account in gain calculations based on the density matrix formalism, as was first proposed by Asada and Suematsu [2.7]. From curve-fitting, applied on the numerical results obtained with such a gain model, it follows that the gain can be approximated analytically as:

$$g(\lambda) = [a(\lambda)\, N - b(\lambda)] \left\{ 1 - \sum_m \varepsilon(\lambda,\lambda_m)\, P_m \right\} \qquad (2.1.5)$$

in which P_m denotes the power density of the mode m at wavelength λ_m. Expressions for the functions a, b and ε and a list of the used material constants are given in appendix II.A.

The carriers not only cause gain, but also absorption. One can distinct between intervalence band absorption, which has its origin in transitions inside the valence band and is dominant in 1.55μm semiconductors, and free carrier absorption, which is a consequence of the plasma behaviour of the electron-hole gas. Additional absorption also occurs in the passive layer, where the photons can be scattered by e.g. impurities or phonons. We will not take into account a detailed wavelength and carrier density dependence of the absorption and just include all absorption in one constant absorption coefficient α_{int}.

So far, we have described only the stimulated emission and the absorption (which both correspond with an imaginary part of the refractive index). The real part of the refractive index, to which the carrier density also contributes, is of equal importance for the wave propagation. The carrier-induced refractive index contributions are connected with the gain and absorption through the well-known Kramers-Kronig relations [2.8]. From these relations, it can be concluded that the refractive index Δn_r corresponding with the gain and the absorption is again a linear function of the carrier density. However, we don't include an optical power dependence of the refractive index (as was done for the gain). This approximation is most valid for single mode lasers. Indeed, since $\varepsilon(\lambda,\lambda_m)$ is symmetric around λ_m, it follows from the Kramers-Kronig relations that the influence of an optical field at λ_m on the refractive index is asymmetric around λ_m. Hence, the refractive index at λ_m is independent of the intensity of the mode at λ_m. The field at λ_m might nevertheless have some influence on the refractive index at the wavelength λ_q of another mode in the case of multimode lasers. However, such lasers are not studied in detail in this Ph. D. study; after all, they are of little interest for optical communication systems.
An analytical expression for the refractive index of 1.55 μm InGaAsP material is given again in appendix II.A.

II.1.2.4 The influence of the temperature

The majority of the optical properties of semiconductors show a non-ignorable temperature dependence. This is not surpri-

sing if one recalls that most of these properties depend on the temperature dependent statistics of the carriers (Fermi-Dirac statistics) and the photons (Bose-Einstein statistics). The temperature dependence is, more in particular, found (experimentally and theoretically) for the gain, the refractive index, the carrier lifetime τ and the bimolecular and Auger recombination coefficients B_o, resp. C_o [2.9].

On the other hand, it must be recognised that a laser diode is a rather inefficient device, in which any production of optical power is accompanied by heat production. The temperature in the active layer can therefore easily vary with bias current level.

Nevertheless, in our calculations, we will always (unless if it is stated otherwise) use a constant active layer temperature, defined as the room temperature T=300K. Implications of this approach are e.g. that the calculated variation of the optical power and of the wavelength with the bias currents will not fit to experimental results. An alternative formulation of this is that our static results actually correspond with slowly modulated (e.g. at 1 MHz) currents, for which temperature effects have no longer an impact [2.10]. Finally, it must also be stressed that temperature variations hardly have an influence on the static side mode suppression, on the power spectrum and the intensity noise spectrum and (as already mentioned) on the modulation performance.

II.2 The longitudinal field equations

II.2.1 The coupled wave equations

A rigourous derivation of the coupled wave equations, which describe the longitudinal wave propagation in a section with a uniform waveguide structure, can be found in many textbooks on optics. Contributions from spontaneous emission however are usually omitted in these derivations and therefore we present an extension of the theory here. Some steps in the derivation may seem rather intuitive, in which case we refer to the literature (e.g. [2.11] and [2.12]) for more details.

II.2.1.1 The three dimensional wave equation

Maxwell's equations provide the basic relations, which the optical field must satisfy. For semiconductors, they can be expressed as:

$$\nabla \times \mathbf{E} = -\mu \frac{\partial \mathbf{H}}{\partial t} \qquad (2.2.1.a)$$

$$\nabla \times \mathbf{H} = \frac{\partial \mathbf{D}}{\partial t} \qquad (2.2.1.b)$$

$$\nabla \cdot \mathbf{D} = 0. \qquad (2.2.1.c)$$

with **E** being the electric field, **H** the magnetic field and **D** the electric induction corresponding with the optical field. μ is the magnetic permeability of the semiconductor ($\mu = \mu_0 = 4\pi.10^{-7}$H/m). The last equation of (2.2.1) can, for semiconductors such as AlGaAs and InGaAsP which are isotropic for optical phenomena, be replaced by:

$$\nabla \cdot \mathbf{E} = 0. \qquad (2.2.2)$$

Taking the curl of the first equation of (2.2.1) and substituting **D** by:

$$\mathbf{D} = \varepsilon_0 \mathbf{E} + \mathbf{P} \qquad (2.2.3)$$

,with **P** being the polarisation of the medium, results in the wave equation:

$$\nabla^2 \mathbf{E} = \mu \varepsilon_0 \frac{\partial^2 \mathbf{E}}{\partial t^2} + \mu \frac{\partial^2 \mathbf{P}}{\partial t^2} \qquad (2.2.4)$$

The polarisation **P** in this equation consists of three distinctive parts: the polarisation $\mathbf{P}_0$ of the structure without its grating, the polarisation $\mathbf{P}_{pert}$ induced by a possible grating and the polarisation $\mathbf{P}_{spont}$ corresponding with the fluctuating spontaneous emission. The polarisations $\mathbf{P}_0$ and $\mathbf{P}_{pert}$ can be expressed with the help of the refractive index for numerical calculations:

$$\mathbf{P}_0 = \varepsilon_0 n^2(x,y,z)\,\mathbf{E} = \varepsilon_0 (n_0(x,y) + \Delta n(x,y,z))^2 \mathbf{E} \qquad (2.2.5a)$$

$$\mathbf{P}_{pert} = \varepsilon_0 n_p^2(x,y,z)\,\mathbf{E} \qquad (2.2.5b)$$

The perturbation in the refractive index Δn, represents the influence of the carrier density on the complex refractive index and includes contributions such as gain, absorption and carrier induced refractive index. Δn is assumed to be small.

In theory, the refractive index n can also vary with time, especially under dynamic circumstances (e.g. current modulation). This time variation is determined by the time variation of the carrier density. The frequency to which the carrier density can respond is limited to about 10 GHz, which implies that the time variation of the refractive index can be neglected when compared with the time variation of the optical field (with an optical frequency of the order of 10^5 GHz.

The wave equation (2.2.4) can now be written as:

$$\nabla^2\mathbf{E} - \mu\varepsilon_0\{n_0^2(x,y)+2n_0(x,y).\Delta n(x,y,z)\}\frac{\partial^2\mathbf{E}}{\partial t^2} = \mu\frac{\partial^2(\mathbf{P}_{pert}+\mathbf{P}_{spont})}{\partial t^2} \qquad (2.2.6)$$

This equation can be solved theoretically by expanding **E** in the modes of the waveguide formed by the lateral/transverse cross-section. Since only the lowest order TE-mode, corresponding with a lateral electrical field, can reach the threshold in most laser diodes (see e.g. [2.13]), we only need to consider the lateral component ($\mathbf{E} = E\mathbf{1}_y$) of the fields and the wave equation becomes scalar:

$$\nabla^2 E - \mu\varepsilon_0\{n_0^2+2n_0.\Delta n\}\frac{\partial^2 E}{\partial t^2} = F(x,y,z,t)+\mu\varepsilon_0 n_p^2\frac{\partial^2 E}{\partial t^2} \qquad (2.2.7)$$

The spontaneous emission term is now, for the sake of a simple notation, denoted by F. The stochastic nature of spontaneous emission implies that F represents a stochastic driving force or a so-called Langevin function ([2.14], [2.15]) for the wave equation.

II.2.1.2 The Langevin force

It can be assumed that the Langevin force has a negligible spatial and temporal correlation, at least if we denote by F the spontaneous emission, averaged over a small volume ΔV and during a short time Δt. Indeed, spontaneous emissions can only be correlated if they originate from the same carrier and if that carrier has not been scattered (and lost its phase information) in the time between the successive emissions. ΔV and Δt are thus determined by the typical scattering time ($\sim 10^{-13}$s) and the scattering distance ($\sim 10^{-2}$ μm).

The averaging over ΔV and Δt further implies that F can be approximated as a gaussian process since it is the result of many processes. F is therefore completely characterised by the first and second order moments, which can be calculated quantummechanically or semiclassical. A simple, semiclassical calculation has been reported by Henry [2.16], who derived the moments of F by requiring the spontaneously emitted light to be in equilibrium with the semiconductor. The moments are then found to be:

$$\langle F(x,y,z,t) \rangle = 0$$

$$\langle F(x,y,z,t)\, F(x',y',z',t') \rangle = 2\, D_{FF}\, \delta(t-t')\, \delta(x-x')\, \delta(y-y')\, \delta(z-z')$$

$$2\, D_{FF} = \frac{4\omega^3 \hbar}{\varepsilon_0 c^3}\, g\, n\, n_{sp} \qquad (2.2.8)$$

with g being the gain, n the refractive index, ω the optical frequency and

$$n_{sp} = \frac{1}{1 - \exp\left(\frac{\hbar\omega - eV}{kT}\right)} \qquad (2.2.9)$$

the so-called inversion factor. eV is the difference between the Fermi-levels of conduction and valence band. We will further consider n_{sp} as a constant (with a numerical value of 2). D_{FF} is called the diffusion constant of the stochastic process .

II.2.1.3 Reduction in the lateral/transverse direction

The (x,y)-dependence in (2.2.7) can be eliminated by substitution of the field expansions (2.1.2). The eigenmode $\phi(x,y)$ of the lowest order TE-mode of the waveguide obeys, for the longitudinal mode m at the frequency ω_m, the 2-dimensional Helmholtz equation:

$$\nabla_{xy}^2\phi + \omega_m^2\mu_0\varepsilon_0\, n^2(x,y,z)\,\phi = \beta_{c,m}^2\,\phi \qquad (2.2.10)$$

where, as already mentioned, ϕ is assumed to be identical for all longitudinal modes m and independent of the longitudinal coordinate z. The complex eigenvalue $\beta_{c,m}$ on the other hand is treated as a m- and z-dependent quantity.

ϕ and $\beta_{c,m}$ can, for a given waveguide cross-section, be determined by various methods such as the finite elements method [2.17] or the staircase method [2.18]. However, in our case, we prefer to avoid these time-consuming calculations. ϕ is therefore approximated by ϕ_0, the (real) eigenmode of the unperturbed waveguide, while $\beta_{c,m}$ is expressed as a function of β_m, the propagation constant of the unperturbed waveguide, and Δn. ϕ_0 and β_m obey the equation:

$$\nabla_{xy}^2\phi_0 + \omega_m^2\mu_0\varepsilon_0\, n_0^2(x,y)\,\phi_0 = \beta_m^2\,\phi_0 = \left(\frac{2\pi}{\lambda_m} n_{eff}\right)^2 \phi_0 \qquad (2.2.11)$$

n_{eff} is called the effective refractive index and it is considered as constant in our approximation.

An expression for $\beta_{c,m}$ can be derived from the equations (2.2.10) and (2.2.11) and one finds (see appendix II.B):

$$\beta_{c,m} = \frac{2\pi}{\lambda_m}\{n_{eff} + \Gamma\,\Delta n_a + (1-\Gamma)\,\Delta n_{cl}\} \qquad (2.2.12)$$

with Γ being the confinement or power filling factor,

$$\Gamma = \frac{\iint_{act.\ layer} \phi_0^2(x,y)\,dxdy}{\iint_{(x,y)-plane} \phi_0^2(x,y)\,dxdy} \qquad (2.2.13)$$

and Δn_a, resp. Δn_{cl} the perturbations in the complex refractive index of the active layer, resp. the cladding layers:

$$\Delta n_a = \frac{j(g(\lambda) - \alpha_{ac})}{2\,(\omega/c)} + \Delta n_r \qquad (2.2.14a)$$

$$\Delta n_{cl} = \frac{-j\alpha_{cl}}{2\,(\omega/c)} \qquad (2.2.14b)$$

α_{ac}, resp. α_{cl} represents the absorption in the active layer, resp. the cladding layers.

The complex propagation number $\beta_{c,m}$ finally becomes:

$$\beta_{c,m} = \frac{2\pi}{\lambda_m}(n_{eff} + \Delta n_r \Gamma) + j0.5\ \Gamma g(\lambda_m) - j0.5\ \alpha_{int} \qquad (2.2.15)$$

with:

$$\alpha_{int} = \Gamma\alpha_{ac} + (1-\Gamma)\,\alpha_{cl} \qquad (2.2.16)$$

Substitution of the expansions (2.1.2), which we rewrite as:

$$E(x,y,z,t) = Re\left\{ \phi_0(x,y) \sum_m g_m(z,t) e^{j\omega_m t} \right\} \qquad (2.2.17)$$

and taking into account that g_m is a slowly varying function of the time, gives:

$$\phi_0 \sum_m \left\{ \frac{d^2 g_m}{dz^2} + \beta_{c,m}^2\, g_m - j\omega_m \frac{2n^2}{c^2} \frac{dg_m}{dt} \right\} e^{j\omega_m t} =$$

$$F' - \phi_0 \frac{n_p^2}{c^2} \sum_m \omega_m^2\, g_m\, e^{j\omega_m t} \qquad (2.2.18)$$

It must be noticed here that F' in (2.2.18) is slightly different from F in (2.2.7). Indeed, F' is the analytical signal derived from F, i.e.

$$F' = F + jG \qquad (2.2.19)$$

with G being the Hilbert transform of F. From the properties of the Hilbert transform, it follows for the second order moments:

$$\langle F'(x,y,z,t)\, F'^{*}(x',y',z',t')\rangle = 2\,\langle F(x,y,z,t)\, F(x',y',z',t')\rangle \qquad (2.2.20a)$$

$$\langle F'(x,y,z,t)\, F'(x',y',z',t')\rangle = 0. \qquad (2.2.20b)$$

Multiplication of the equation (2.2.18) with ϕ_0 and integration over the x,y-plane eliminates the x,y-dependence:

$$\sum_m \left\{ \frac{d^2 g_m}{dz^2} + \beta_{c,m}^2\, g_m - 2j \frac{\beta_m}{v_g} \frac{dg_m}{dt} \right\} e^{j\omega_m t} =$$

$$f(z,t) - \frac{n_{p,eff}^2}{c^2} \sum_m \omega_m^2\, g_m\, e^{j\omega_m t} \qquad (2.2.21)$$

v_g represents the group velocity and is assumed to be a constant:

$$\frac{\omega_m}{c^2} \frac{\iint_{(x,y)-plane} n^2\, \phi_0^2\, dxdy}{\iint_{(x,y)-plane} \phi_0^2\, dxdy} = \frac{\beta_m}{v_g} \qquad (2.2.22)$$

f and $n_{p,eff}$ are given by:

$$n_{p,eff}^2 = \frac{\iint_{(x,y)-plane} n_p^2\, \phi_0^2\, dxdy}{\iint_{(x,y)-plane} \phi_0^2\, dxdy} \qquad (2.2.23a)$$

$$f(z,t) = \frac{\iint_{(x,y)-plane} F'(x,y,z,t)\, \phi_0\, dxdy}{\iint_{(x,y)-plane} \phi_0^2\, dxdy} \qquad (2.2.23b)$$

Equation (2.2.20) can be decomposed into equations for each longitudinal mode separately by integrating over a few periods T, with T being defined by the mode spacing $\Delta\omega_m$: $T = 2\pi/\Delta\omega_m$. $\Delta\omega_m$ is typically of the order of 100 GHz, and hence the resulting equations are only valid for modulation frequencies up to a few times 10 GHz. The field quantities then denote the average values over a few ti-

mes 10 psec. The longitudinal equation for each mode m can be written as:

$$\frac{d^2 g_m}{dz^2} + \beta_{c,m}^2 g_m - 2j\frac{\beta_m}{v_g}\frac{dg_m}{dt} = \frac{1}{nT}\int_{nT} f\, e^{-j\omega_m t} dt - \frac{n_{p,eff}^2}{c^2}\omega_m^2 g_m \qquad (2.2.24)$$

The correlation function of the resulting Langevin forces can easily be derived from the correlation function of F'. The Langevin forces are mutually uncorrelated. This issue is treated furtheron however.

II.2.1.4 Derivation of the coupled wave equations

The second term on the r.h.s. of (2.2.24) can be transformed by remarking that, for a grating of period Λ, $n^2_{p,eff}$ is a periodic function of z and can be expanded in a Fourier series:

$$n_{p,eff}^2 = \sum_{q=-\infty}^{+\infty} a_q\, e^{j\frac{2q\pi}{\Lambda}z} \qquad (2.2.25)$$

Such a series also exists for a quasi-periodic grating, i.e. a grating of which the period or the amplitude vary slowly in the longitudinal direction. The corresponding coefficients a_q are no longer constant in this case and their phase, resp. amplitude is z-dependent.

Substitution of (2.2.25) in (2.2.24), together with

$$g_m(z,t) = R_m^+(z,t)\, e^{-j\beta_g z} + R_m^-(z,t)\, e^{j\beta_g z} \qquad (2.2.26)$$

results in the equation:

$$\left\{-2j\beta_g\frac{\partial R_m^+}{\partial z} - 2j\frac{\beta_m}{v_g}\frac{\partial R_m^+}{\partial t} + (\beta_{c,m}^2 - \beta_g^2)\, R_m^+\right\} e^{-j\beta_g z} +$$

$$\left\{2j\beta_g\frac{\partial R_m^-}{\partial z} - 2j\frac{\beta_m}{v_g}\frac{\partial R_m^-}{\partial t} + (\beta_{c,m}^2 - \beta_g^2)\, R_m^-\right\} e^{j\beta_g z} =$$

$$f_m - \frac{\omega_m^2}{c^2}(R_m^+ e^{-j\beta_g z} + R_m^- e^{j\beta_g z}) \sum_{q=-\infty}^{+\infty} a_q\, e^{j\frac{2q\pi}{\Lambda}z} \qquad (2.2.27)$$

In the derivation of (2.2.27), it has been taken into account that $R_m^{\pm}$ is a slowly varying function of z. f_m is the time-averaged Langevin force, given by the integral in (2.2.24). Averaging (2.2.27) over a few grating periods and noticing that $\beta_g = n\pi/\Lambda$ results in the coupled wave equations:

$$\frac{\partial R_m^+}{\partial z} + \frac{1}{v_g}\frac{\partial R_m^+}{\partial t} + j(\beta_{c,m}-\beta_g)\,R_m^+ = \frac{j}{n\Lambda 2\beta_g}\int_{n\Lambda} f_m e^{j\beta_g z}dz - \frac{j\omega_m^2 a_{-n}}{2\beta_g c^2}\,R_m^-$$

$$-\frac{\partial R_m^-}{\partial z} + \frac{1}{v_g}\frac{\partial R_m^-}{\partial t} + j(\beta_{c,m}-\beta_g)\,R_m^- = \frac{j}{n\Lambda 2\beta_g}\int_{n\Lambda} f_m e^{-j\beta_g z}dz - \frac{j\omega_m^2 a_n}{2\beta_g c^2}\,R_m^+ \qquad (2.2.28)$$

In the derivation of (2.2.28), it has been taken into account that $\beta_{c,m} \approx \beta_g$. In the absence of a grating, the averaging can occur over a few wavelengths. The a-coefficients vanish in this case. The coupled wave equations are usually written in the form:

$$\frac{\partial R_m^+}{\partial z} + \frac{1}{v_g}\frac{\partial R_m^+}{\partial t} + j\Delta\beta_m\,R_m^+ = F_m^+ + \kappa_{FB}\,R_m^-$$

$$-\frac{\partial R_m^-}{\partial z} + \frac{1}{v_g}\frac{\partial R_m^-}{\partial t} + j\Delta\beta_m\,R_m^- = F_m^- + \kappa_{BF}\,R_m^+ \qquad (2.2.29)$$

in which the coupling coefficients κ_{FB} and κ_{BF}, the complex Bragg-deviation $\Delta\beta_m$ and F_m^+ and F_m^- are defined by:

$$\kappa_{FB} = -\frac{j\omega_m^2 a_{-n}}{2\beta_g c^2}\ ,\ \kappa_{BF} = -\frac{j\omega_m^2 a_n}{2\beta_g c^2}\ ,\ \Delta\beta_m = \beta_{c,m}-\beta_g \qquad (2.2.30a)$$

$$F_m^{\pm} = \frac{j}{n\Lambda 2\beta_g}\int_{n\Lambda} f_m e^{\pm j\beta_g z}dz \qquad (2.2.30b)$$

For a pure index grating, i.e. a periodic variation of the real refractive index, the Fourier coefficients of the real function $n^2_{p,eff}$ obey the relation $a_n = a_{-n}^*$ and hence $\kappa_{BF} = -\kappa_{FB}^*$. A gain grating corresponds with an imaginary $n^2_{p,eff}$ and $\kappa_{BF} = \kappa_{FB}^*$. κ_{BF} and κ_{FB} can, in the

most general case, be slowly varying functions of z. We will treat the coupling coefficients in the following as given constants.

The equations (2.2.29) are the standard equations used in the analysis of laser diodes with or without a grating. Only the moments of the Langevin forces still need to be determined. These moments depend on the field normalisation, which will be treated in section 2.2.

II.2.1.5 Moments of the new Langevin forces

The Langevin forces $F_m^{\pm}$ are obtained from the original Langevin function F' by purely linear transformations. Their first order moments are therefore zero and the second order moments can easily be calculated. Starting from the relations (2.2.20) and (2.2.23), it follows:

$$<f(z,t)f^*(z',t')> = \delta(t-t')\,\delta(z-z')\,\frac{8\omega^3\hbar n_{sp}}{\varepsilon_0 c^3}\,\frac{\iint_{(x,y)} dxdy\ \phi_0^2\, g\, n}{\left[\iint_{(x,y)} dxdy\ \phi_0^2\right]^2}$$

$$= \frac{8\omega^3\hbar n_{sp}\, n_{eff}\, \Gamma g}{\varepsilon_0 c^3 \iint_{(x,y)} dxdy\ \phi_0^2(x,y)}\,\delta(t-t')\,\delta(z-z') \qquad (2.2.31)$$

The correlation functions of the Langevin forces f_m are calculated as:

$$<f_l(z,t)f_m^*(z',t')> = \frac{1}{(nT)^2}\int_{nT} d\tau_1 \int_{nT} d\tau_2 <f(z,\tau_1)f^*(z',\tau_2)> e^{j[\omega_m\tau_1-\omega_l\tau_2]}$$

$$= \frac{8\omega_m^3\hbar n_{sp} n_{eff}\Gamma g}{\varepsilon_0 c^3 \iint_{(x,y)} dxdy\ \phi_0^2}\,\delta(z-z')\,\frac{1}{(nT)^2}\int_{nT} d\tau_1 \int_{nT} d\tau_2\,\delta(\tau_1-\tau_2)e^{j(\omega_m-\omega_l)\tau_1}$$

$$= \frac{8\omega_m^3\hbar n_{sp} n_{eff}\Gamma g}{\varepsilon_0 c^3 \iint_{(x,y)} dxdy\ \phi_0^2}\,\delta(z-z')\,\frac{1}{(nT)^2}\,\delta_{lm}\int_{nT} d\tau_1 \int_{nT} d\tau_2\,\delta(\tau_1'-\tau_2) \qquad (2.2.32)$$

with δ_{lm} being the Kronecker delta, which is a result of the averaging of the exponential function. The double integration in the last

expression of (2.2.32) vanishes when τ_1 and τ_2 belong to different time intervals. More exactly, one has:

$$\frac{1}{(nT)^2}\int_t^{t+nT} d\tau_1 \int_{t'}^{t'+nT} d\tau_2\, \delta(\tau_1-\tau_2) = \frac{1}{nT}\left(1-\frac{|t-t'|}{nT}\right), |t-t'|<nT$$
$$= 0 \qquad , |t-t'|>nT \qquad (2.2.33)$$

This function approaches the Dirac δ-function for small nT, which implies that on our timescale (of the order of 0.1 nsec.) the moments of f_m can be expressed as:

$$<f_l(z,t)f_m^*(z',t')> = \frac{8\omega_m^3\hbar n_{sp}n_{eff}\Gamma g}{\varepsilon_0 c^3\iint_{(x,y)} dxdy\ \phi_0^2}\,\delta(z-z')\,\delta_{lm}\,\delta(t-t') \qquad (2.2.34)$$

At first sight, it looks remarkable that all f_l, which are the components of f, have an energy equal to that of f. In reality however, we have, by approximating the function (2.2.33) by a δ-function, reduced the bandwidth of f_l with respect to that of f. The time averaging filters the white spectrum. The moments of $F_m^{\pm}$ can now be derived in a similar way from the moments of f_m. We finally find:

$$<F_l^{\pm}(z,t)F_m^{\pm *}(z',t')> = 2\,\frac{\omega_m^3\hbar n_{sp}n_{eff}\Gamma g\,\delta(z-z')\,\delta(t-t')}{\varepsilon_0 c^3\iint_{(x,y)} dxdy\ \phi_0^2\,|\beta_g|^2}\,\delta_{lm}\,\delta_{+-} \qquad (2.2.35)$$

The presence of δ_{+-} in (2.2.35) indicates that Langevin forces corresponding with forward propagating waves are uncorrelated with the ones corresponding with backward propagating waves. The averaging over a few periods now implies a reduction of the spatial bandwidth (i.e. the bandwidth of the spatial Fourier transform). The spatial Fourier transform of $F_l^{\pm}$ is thereby located in a small band around $\pm\beta_g$. From the relation (2.2.20b), it follows, furthermore that:

$$<F_l^{\pm}(z,t)F_m^{\pm}(z',t')> = 0 \qquad (2.2.36)$$

II.2.2 The coupled wave equations II

This section explores the full physical meaning of the coupled wave equations and discusses alternative forms of the equations. We first describe a proper choice for the field normalisation. This is followed by the transformation of the equations (2.2.29) into longitudinal rate equations. Both steps make the physical interpretation, which is given subsequently, considerably more simple.

II.2.2.1 The field normalisation

The normalisation of ϕ will further be chosen so that the average optical power in the + or - direction can be expressed as:

$$P^+ = \sum_m P_m^+ = \sum_m |R_m^+|^2$$

$$P^- = \sum_m P_m^- = \sum_m |R_m^-|^2 \qquad (2.2.37)$$

This optical power flux can be calculated by integration of the Poynting vector [2.19] over the lateral/transverse cross-section:

$$P_z = P^+ - P^- = \frac{1}{2}\,\mathrm{Re}\iint_{(x,y)-\mathrm{plane}} (\mathbf{E}\times\mathbf{H}^*)_z\,dxdy$$

$$= \frac{1}{2}\,\mathrm{Re}\iint_{(x,y)-\mathrm{plane}} (-E_y H_x^*)\,dxdy \qquad (2.2.38)$$

where E_y is given by (2.1.2) , while H_x can be derived with the help of :

$$E_y = \phi_0(x,y)\sum_m (R_m^+ e^{-j\beta_g z} + R_m^- e^{j\beta_g z})\, e^{j\omega_m t}$$

$$H_x = \frac{-j}{\mu_0\omega}\frac{\partial E_y}{\partial z} = -\frac{\beta_g\phi_0}{\mu_0\omega}\sum_m (R_m^+ e^{-j\beta_g z} - R_m^- e^{j\beta_g z})\, e^{j\omega_m t} \qquad (2.2.39)$$

When calculating the product $E_y H_x^*$, it can be taken into account that cross products of different mode fields will vanish after averaging over a time of e.g. 10 psec. The power P_z then reduces to:

$$P_z = \frac{\beta_g}{2\mu_0\omega} \iint_{(x,y)\text{-plane}} |\phi_0(x,y)|^2 dxdy \sum_m (|R_m^+|^2 - |R_m^-|^2) \qquad (2.2.40)$$

Consistency with (2.2.37) thus requires the normalisation:

$$\iint_{(x,y)\text{-plane}} |\phi_0(x,y)|^2 dxdy = \frac{2\mu_0\omega}{\beta_g} \approx \frac{2\mu_0 c}{n_{eff}} \qquad (2.2.41)$$

The energy density (per unit distance in the longitudinal direction) inside the laser cavity on the other hand can be calculated as [2.19]:

$$u = \frac{1}{4} \iint_{(x,y)} dxdy \; (\varepsilon_0 n^2 |E_y|^2 + \mu_0 |H_x|^2) \qquad (2.2.42)$$

with:

$$|E_y|^2 = \phi_0^2(x,y) \sum_m \{|R_m^+|^2 + |R_m^-|^2 + 2\mathrm{Re}(R_m^+ R_m^{-*} e^{-2j\beta_g z})\}$$

$$|H_x|^2 = \frac{\beta_g^2 \phi_0^2(x,y)}{\mu_0^2\omega^2} \sum_m \{|R_m^+|^2 + |R_m^-|^2 - 2\mathrm{Re}(R_m^+ R_m^{-*} e^{-2j\beta_g z})\} \qquad (2.2.43)$$

where cross products of different mode fields can again been neglected after time-averaging. Substitution of (2.2.43) in (2.2.42) results in the following expression for u:

$$u = \frac{1}{v_g} \sum_m (|R_m^+|^2 + |R_m^-|^2) \qquad (2.2.44)$$

This energy obviously is connected with the photon density inside the cavity. From (2.2.37) and (2.2.44), it can be concluded that the number of photons $i_m^{\pm}$ in mode m per unit length in the

longitudinal direction and propagating in the +, - direction is given by:

$$i_m^{\pm} = \frac{|R_m^{\pm}|^2}{v_g \hbar \omega_m} \qquad (2.2.45)$$

The relation between the field amplitudes and the photon densities makes a transformation of the coupled wave equations (2.2.29) into equations for the field amplitudes and phases attractive for physical interpretation. It will also become clear then how the Langevin forces are related to photon processes. The normalisation discussed here gives rise to new expressions for the second order moments of these Langevin forces:

$$\langle F_l^{\pm}(z,t) F_m^{\pm *}(z',t') \rangle = \hbar \omega_m n_{sp} \Gamma g(\omega_m) \delta(z-z') \delta(t-t') \delta_{lm} \delta_{+-} \qquad (2.2.46)$$

II.2.2.2 Longitudinal rate equations

Complex quantities such as $R_m^{\pm}$, $F_m^{\pm}$ are often characterised by their amplitude and phase for practical interpretations. We therefore write:

$$R_m^{\pm}(z,t) = r_m^{\pm}(z,t)\, e^{j\varphi_m^{\pm}(z,t)} \qquad (2.2.47a)$$

$$F_m^{\pm}(z,t) = |F_m^{\pm}(z,t)|\, e^{j\varphi_{F,m}^{\pm}(z,t)} \qquad (2.2.47b)$$

$$\Delta\beta_m(z,t) = \Delta\beta_{m,r}(z,t) + j\Delta\beta_{m,i}(z,t) \qquad (2.2.47c)$$

$$\kappa_{FB} = |\kappa|\, e^{j\varphi_\kappa} \qquad (2.2.47d)$$

where all quantities on the r.h.s. are now real functions.

Substitution of (2.2.47) in (2.2.29) results in the longitudinal rate equations:

$$\pm\frac{\partial r_m^{\pm}}{\partial z}+\frac{1}{v_g}\frac{\partial r_m^{\pm}}{\partial t}-\Delta\beta_{m,i}r_m^{\pm}=|F_m^{\pm}|\cos(\varphi_{F,m}^{\pm}-\varphi_m^{\pm})\pm|\kappa|\,r_m^{\mp}\cos(\varphi_\kappa+\varphi_m^{-}-\varphi_m^{+})$$

or

$$\frac{1}{v_g}\frac{dr_m^{\pm}}{dt_{f,b}}-\Delta\beta_{m,i}\,r_m^{\pm}=F_{r,m}^{\pm}\pm|\kappa|\,r_m^{\mp}\cos(\varphi_\kappa+\varphi_m^{-}-\varphi_m^{+}) \qquad (2.2.48a)$$

and

$$\pm\frac{\partial\varphi_m^{\pm}}{\partial z}+\frac{1}{v_g}\frac{\partial\varphi_m^{\pm}}{\partial t}+\Delta\beta_{m,r}=\frac{|F_m^{\pm}|}{r_m^{\pm}}\sin(\varphi_{F,m}^{\pm}-\varphi_m^{\pm})+|\kappa|\,\frac{r_m^{\mp}}{r_m^{\pm}}\sin(\varphi_\kappa+\varphi_m^{-}-\varphi_m^{+})$$

or

$$\frac{1}{v_g}\frac{d\varphi_m^{\pm}}{dt_{f,b}}+\Delta\beta_{m,r}=F_{\varphi,m}^{\pm}+|\kappa|\,\frac{r_m^{\mp}}{r_m^{\pm}}\sin(\varphi_\kappa+\varphi_m^{-}-\varphi_m^{+}) \qquad (2.2.48b)$$

where d/dt_f ($=\partial/\partial t+v_g\partial/\partial z$), resp. d/dt_b ($=\partial/\partial t-v_g\partial/\partial z$) designates the time variation as it is experienced by the forward, resp. the backward propagating wave packet itself.

Three processes contribute to the time variation of the field amplitudes and hence to the time variation of the power or of the photon density: the absorption and the stimulated emission (expressed by $\Delta\beta_{m,i}$), the spontaneous emission (expressed by $F^{\pm}_{m,r}$) and the distributed reflections (caused by a grating and expressed by $|\kappa|$)

The effect of stimulated emission and absorption is more or less obvious. The increment of the amplitude (or of the photon density) is proportional with the amplitude (or with the photon density). This can be understood as a logical consequence of the interpretation of stimulated emission, resp. absorption as a "collision" between a photon and a conduction electron, resp. between a photon and a valence electron or an impurity. The proportionallity follows from the fact that only one photon is involved in each "collision".

The Langevin functions on the right hand side of (2.2.48a) represent the spontaneously emitted photons that couple into the mode. The spontaneous emissions add up to the fields $r_m^{\pm}$, but only in an incoherent way. The presence of $F^{\pm}_{r,m}$ causes fluctuations in the modal photon densities, but it also contributes to the average photon densities. The latter effect however is not easily seen from (2.2.48a) and we will therefore treat the spontaneous emission in more detail in section (2.2.3).

The last term on the r.h.s. of (2.2.48a) corresponds with reflected power of the backward (forward) propagating wave that couples into the forward (backward) propagating wave. The mechanism becomes quite clear after discretisation of the grating (fig. 2.2.1). The difference in complex effective index of two neighbouring points can be approximated as:

$$\Delta n_{eff} = \frac{a_{-n}}{2n_{eff}} \{ e^{-2j\beta_g\left(z+\frac{\Delta z}{2}\right)} - e^{-2j\beta_g\left(z-\frac{\Delta z}{2}\right)} \}$$

$$= -\frac{j\beta_g a_{-n}}{n_{eff}} \Delta z\, e^{-2j\beta_g z} \qquad (2.2.49)$$

The reflection and transmission of the fields at the intersection boundary are then obtained as:

$$r = \frac{\Delta n_{eff}}{n_{eff}(z) + n_{eff}(z+\Delta z)} = -\frac{j\beta_g a_{-n}}{2n_{eff}^2} \Delta z\, e^{-2j\beta_g z} \approx \kappa_{FB}\Delta z\, e^{-2j\beta_g z} \qquad (2.2.50a)$$

$$t = \sqrt{1 - |r|^2} = 1 \text{ to first order in } \Delta z \qquad (2.2.50b)$$

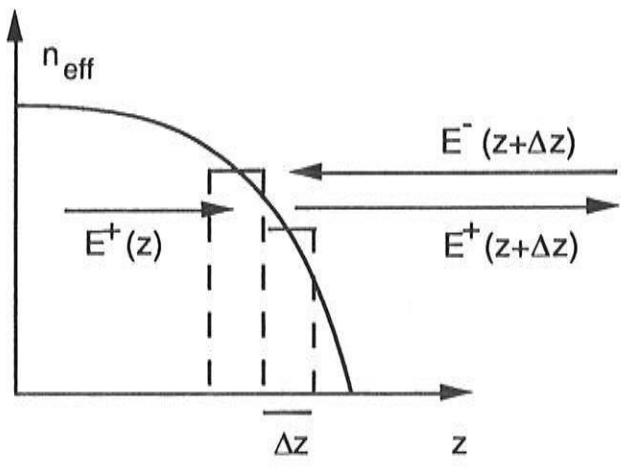

Fig. 2.2.1: Discretisation of the grating

Expression of the field continuity at the intersection boundary now readily leads to:

$$R^+(z+\Delta z)e^{-j\beta_g(z+\Delta z)} = t\ R^+(z)e^{-j\beta_g z} + r\ R^-(z+\Delta z)e^{j\beta_g(z+\Delta z)}$$

or

$$\frac{R^+(z+\Delta z) - R^+(z)}{\Delta z} = \kappa_{FB}\ R^-(z+\Delta z) \qquad (2.2.51)$$

One readily finds the contribution of the distributed reflections as it appears in equations (2.2.29) when Δz is infinitely small.

The reflected backward (forward) propagating fields are not necessarily in phase with the forward (backward) propagating fields. The phase mismatch, expressed by $\varphi_\kappa+\varphi^- - \varphi^+$ in (2.2.48), results in an imperfect energy (photon) transfer from the reflected waves. It is included in the coupling term in (2.2.48a) through the cosine factor.

The interference effect also affects the phases of forward and backward propagating waves, as can be seen from equations (2.2.48b). The influence of the interference obviously depends on the relative strength of reflected and transmitted waves; e.g. a weak reflected wave r^- will only have a small impact (expressed by r^-/r^+) on the phase of the resulting field $r^+ + r^-$.

Other contributions to the phase variation have the origin in spontaneous emission and the Bragg deviation. The first contribution is related to the character of the spontaneously emitted photons, which are not coherent but which interfere with the laser photons. The random phase of the spontaneously emitted photons results in random fluctuations in the phases of the laser fields. The phase variation due to the Bragg deviation accounts for the discrepancy between actual wave vector and the as reference wave vector chosen Bragg vector. It is the result of our choice for the field representation (2.1.2) and has only a physical meaning when a grating is present, i.e. when κ is non-zero. The Bragg deviation determines the phase mismatch in this case and hence the efficiency of the distributed feedback.

II.2.2.3 The spontaneous emission

Before discussing the new Langevin functions, we first remark that equation (2.2.46) can also be written as:

$$< F_l^{\pm}(z,t)\, F_m^{\pm *}(z',t') >= \frac{\hbar\omega_m}{v_g} S_m\, \delta(z-z')\, \delta(t-t')\, \delta_{lm}\, \delta_{+-} \qquad (2.2.52)$$

with $S_m = \Gamma g n_{sp} v_g$ being the rate of spontaneous emission that couples into the mode m, as it can be derived from the famous Einstein relations [2.6]. S_m is a fraction of the total spontaneous emission rate $B_0 N^2 V_a$ (see II.1.2.1), and it can be expressed alternatively as [2.20]:

$$S_m = \beta_{sp} B_0 N^2 V_a \quad ; \quad \beta_{sp} = \frac{\Gamma \lambda_m^4 v_g}{4\pi^2 n_{eff}^2 c V_a \Delta\lambda} \qquad (2.2.53)$$

with $\Delta\lambda$ being the mode spacing, i.e. the wavelength difference between longitudinal modes.

By taking the statistical average of equations (2.2.48a), it can be shown that, if $F^{\pm}_{r,m}$ has zero mean, the spontaneous emission doesn't affect the field amplitudes. On the other hand however, there is a contribution from the spontaneous emission to the average power (or photon number) in the mode. This can be proven by integration of (2.2.29), in which the time dependence can be removed by Fourier transformation. After integration, we find for the fields:

$$R_m^{\pm}(z,t) = \frac{1}{2\pi}\int_{-\infty}^{+\infty} d\Omega\, e^{j\Omega t} \left\{ \frac{1}{a_m} \int^{z} \sin[a_m(z-z')]\, G_m^{\pm}(z',\Omega) dz' \right. \qquad (2.2.54)$$

$$\text{with: } a_m(\Omega) = \left[\left(\frac{\Omega}{v_g} + \Delta\beta_m \right)^2 - |\kappa|^2 \right]^{1/2}$$

$$G_m^{\pm}(z,\Omega) = \int_{-\infty}^{+\infty} dt\, e^{-j\Omega t} \left\{ \frac{\partial F_m^{\pm}}{\partial z} - \kappa_{FB} F_m^{\pm} - j\Delta\beta_m F_m^{\pm} - \frac{1}{v_g} \frac{\partial F_m^{\pm}}{\partial t} \right\}$$

Multiplication of the first equation of (2.2.29) with $R_m{}^{+*}$, adding the complex conjugate of the resulting expression and taking the statistical average of the expression, results in:

$$\frac{\partial<(r_m^+)^2>}{\partial z}+\frac{1}{v_g}\frac{\partial<(r_m^+)^2>}{\partial t}-2\Delta\beta_{m,i}<(r_m^+)^2>=2|\kappa|<r_m^- r_m^+\cos(\varphi_\kappa+\varphi_m^- -\varphi_m^+)>$$

$$+<R_m^{+*}(z,t)\,F_m^+(z,t)>+<R_m^+(z,t)\,F_m^{+*}(z,t)> \qquad (2.2.55)$$

Replacing R_m^+ by the expression (2.2.54) in the last two terms of (2.2.55) and taking into account the $\delta(z-z')$-function in (2.2.46) shows that R_m^+ in (2.2.55) can be replaced by:

$$R_m^+(z,t)=\frac{1}{2\pi}\int dt'\int d\Omega\, e^{j\Omega(t-t')}\left\{\frac{1}{a_m}\int^z \sin[a_m(z-z')]\frac{\partial F_m^+(z',t')}{\partial z'}\right\}dz'$$

$$=\frac{1}{2\pi}\int dt'\int d\Omega\, e^{j\Omega(t-t')}\int^z dz'\, F_m^+(z',t)\cos[a_m(z-z')] \qquad (2.2.56)$$

And hence:

$<R_m^+(z,t)F_m^{+*}(z,t)>=$

$$\frac{1}{2\pi}\int^z dz\left\{\int dt'\int d\Omega\, e^{j\Omega(t-t')}<F_m^+(z',t')F_m^{+*}(z,t)>\cos[a(z-z')]\right\}$$

$$=\frac{1}{2\pi}\int^z dz\left\{\int dt'\int d\Omega\, e^{j\Omega(t-t')}<F_m^+(z',t')F_m^{+*}(z,t)>\right\}$$

$$=\int^z dz'<F_m^+(z,t)F_m^{+*}(z',t)> \qquad (2.2.57)$$

The last term, for which the integrand is only non-zero at the integration boundary, cannot be calculated unambiguously. However, the problem can be overcome by using a more exact function (2.2.33 in the time as well as in the axial variable) for the correlation. This gives:

$$<R_m^{+*}(z,t)\,F_m^+(z,t)>+<R_m^+(z,t)\,F_m^{+*}(z,t)>=$$

$$\frac{2h\omega_m}{v_g T}S_m\int_{z-n\Lambda}^z\frac{1}{n\Lambda}\left(1-\frac{z-z'}{n\Lambda}\right)dz'=\frac{h\omega_m}{v_g T}S_m=\frac{h\omega_m}{2L}S_m \qquad (2.258)$$

The value of T in this formula is defined by the bandwidth of the Langevin function and hence by the modal spacing ($\Delta f = v_g/2L$). We

have chosen the value n=1 in (2.2.32) and (2.2.33) to include the complete spectral content of the mode; a higher value for n would imply a filtering of this spectrum.

Equation (2.2.55) can be transformed into an equation for the average photon density per unit longitudinal distance propagating in the ± direction:

$$\frac{d\langle i_m^+\rangle}{dt_f} - 2\Delta\beta_{m,i} v_g \langle i_m^+\rangle = \frac{S_m}{2L} + \frac{2|\kappa|}{\hbar\omega_m}\langle r_m^- r_m^+ \cos(\varphi_\kappa + \varphi^- - \varphi^+)\rangle \qquad (2.2.59)$$

A similar equation also holds for $\langle i_m^-\rangle$. Equation (2.2.59) indicates that the spontaneous emission rate (S_m/L per unit distance in the longitudinal direction) is divided equally between the forward and backward propagating waves (or more generally that the spontaneously emitted photons have a uniformly in space distributed propagation direction). It also implies that the field amplitudes include contributions from the Langevin forces.

The equation for $i_m^\pm$ can now be written as:

$$\frac{di_m^\pm}{dt_{f,b}} - 2\Delta\beta_{i,m} v_g i_m^\pm = \frac{S_m}{2L} \pm 2|\kappa| v_g \sqrt{i_m^+ i_m^-}\cos(\varphi_\kappa + \varphi_m^- - \varphi_m^+) + F_{i,m}^\pm(z,t)$$

$$\text{with: } F_{i,m}^\pm = \frac{R_m^{\pm *} F_m^\pm + R_m^\pm F_m^{\pm *} - \langle R_m^{\pm *} F_m^\pm + R_m^\pm F_m^{\pm *}\rangle}{\hbar\omega_m} \qquad (2.2.60)$$

The new Langevin functions $F_{i,m}$ now have a zero mean. Their second order moments can easily be calculated from the property that $\langle x^4\rangle = 3\langle x^2\rangle^2$ for a gaussian variable x with zero average. The calculation of the second order moments involves such a fourth order moment due to the stochastic part of $R_m^\pm$ (2.2.56). Nonetheless, under the assumption that the energy of this stochastic part is relatively small when compared with the energy of the coherent part, one can neglect this fourth order moment and one then readily finds:

$$\langle F_{i,m}^\pm(z,t) F_{i,l}^\pm(z',t')\rangle = 2\frac{\langle r_m^\pm\rangle^2}{v_g\hbar\omega_m} S_m \delta(z-z')\,\delta(t-t')\,\delta_{lm}\,\delta_{+-}$$

$$\approx 2\, S_m \langle i_m^\pm\rangle \delta(z-z')\,\delta(t-t')\,\delta_{lm}\,\delta_{+-} \qquad (2.2.61)$$

It must be noticed that the last expression for the autocorrelation holds for all modes (below or above threshold), despite the fact that our assumption in general only holds for the modes above threshold and not for very weak side modes (below threshold). The proof for this follows from a more exact quantummechanical calculation [2.21].

The Langevin functions for the phase equations can be characterized in a similar way. Multiplying e.g. the first equation of (2.2.29) with R_m^{+*} and subtracting the complex conjugate of the resulting equation, gives:

$$\pm \frac{1}{v_g} \frac{d\varphi_m^{\pm}}{dt_{f,b}} + \Delta\beta_{m,r} = |\kappa| \frac{r_m^{\mp}}{r_m^{\pm}} \sin(\varphi_\kappa + \varphi_m^- - \varphi_m^+) - \frac{j}{2} \left\{ \frac{F_m^{\pm}}{R_m^{\pm}} - \frac{F_m^{\pm *}}{R_m^{\pm *}} \right\} \qquad (2.2.62)$$

Again, fourth (and higher) order moments will appear in the correlation of $F_{\varphi,m}$, as can be seen by expanding the stochastic part of R_m in a Taylor series. However, the assumption of a small energy of this stochastic part again allows us to neglect the higher order moments and one finds:

$$\begin{aligned} <F_{\varphi,m}^{\pm}(z,t) F_{\varphi,l}^{\pm}(z',t')> &= \frac{S_m \hbar\omega_m}{2v_g <r_m^{\pm}>^2} \delta(z-z')\,\delta(t-t')\,\delta_{lm}\,\delta_{+-} \\ &\approx \frac{S_m}{2(v_g)^2 <i_m^{\pm}>} \delta(z-z')\,\delta(t-t')\,\delta_{lm}\,\delta_{+-} \end{aligned} \qquad (2.2.63)$$

A more intuitive theory of the spontaneous emission contributions can be established from fig.2.2.2, where it is shown how a spontaneous emission alters the intensity and the phase of the fields in a discontinuous way. Notice also that, since we are dealing with discrete particle processes, i_m^+ must be interpreted as the number of photons in one unit of longitudinal distance (i.e. a number in stead of a density). From this figure, it is easily seen that the change in photon number Δi_m^+ and in phase $\Delta\varphi_m^+$, due to a spontaneous emission in the (+)-direction at (z,t), can be expressed as:

$$\Delta i_m^+ = 1 + 2\sqrt{i_m^+}\cos\theta_i \qquad (2.2.64a)$$

$$\Delta\varphi_m^+ = \frac{\sin\theta_i}{\sqrt{i_m^+}} \qquad (2.2.64b)$$

The first term on the r.h.s. of (2.2.64a) obviously leads to the steady-state contribution $S_m/2L$ in (2.2.60), where as the second terms on the r.h.s. of (2.2.64a) and on the r.h.s. of (2.2.64b) are equivalent with the Langevin functions $F_{i,m}$ and $F_{\varphi,m}$. Since all spontaneous emissions occur at random times t_i and at random places z_j (located in the unity interval under consideration), we can write:

$$F_{i,m}^+(z,t) = 2\sqrt{i_m^+}\sum_{i,j}\cos[\theta(i,j)]\,\delta(t-t_i)\,\delta(z-z_j) \qquad (2.2.65a)$$

$$F_{\varphi,m}^+(z,t) = \frac{1}{v_g\sqrt{i_m^+}}\sum_{i,j}\sin[\theta(i,j)]\,\delta(t-t_i)\,\delta(z-z_j) \qquad (2.2.65b)$$

with the angles $\theta(i,j)$ being randomly distributed.

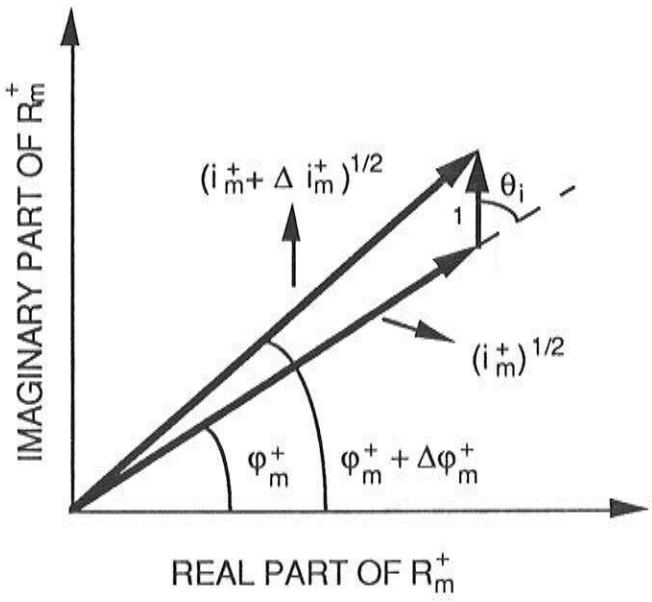

Fig. 2.2.2: Phasor representation of the fields

Therefore, the first order moments are zero, while the second order moments can be written as:

$$F^{+}_{i,m}(z,t)F^{+}_{i,m}(z',t') = 4i^{+}_{m}\sum_{i,j}\cos^2[\theta(i,j)]\delta(t-t_i)\delta(t'-t_i)\delta(z-z_j)\delta(z'-z_j)$$

$$= 4\, i^{+}_{m}\,\delta(t-t')\delta(z-z')\sum_{i,j}\cos^2[\theta(i,j)]\delta(t-t_i)\delta(z-z_j) \qquad (2.2.66a)$$

$$F^{+}_{\varphi,m}F^{+}_{\varphi,m} = \frac{1}{i^{+}_{m}}\delta(t-t')\delta(z-z')\sum_{i,j}\sin^2[\theta(i,j)]\delta(t-t_i)\delta(z-z_j) \qquad (2.2.66b)$$

These equations can be averaged by replacing $\cos^2$ and $\sin^2$ by their average value (1/2). Furthermore, it must be recalled that all quantities already have been averaged over a time T (= $1/\Delta f$, with Δf the mode spacing). The unity interval under consideration has propagated over a distance $v_gT=2L$ in that time and it has been the location of S_mT spontaneous emissions. We can therefore write, with $dt_i=O(T)$:

$$\sum_{i,j}\delta(t-t_i)\,\delta(z-z_j) = S_m\int dt_{i,f}\,\delta(t_f - t_{i,f});\ t_f = t - v_gz$$

$$= S_m \qquad (2.2.67)$$

which, when substituted in (2.2.66), immediately leads to the results given in (2.2.61) and (2.2.63).

We conclude this section by presenting an alternative form for the amplitude rate equations. To this end, we define new amplitudes by the relation:

$$v_g\hbar\omega_m i^{\pm}_m = \langle r^{\pm}_m\rangle^2 + 2\langle r^{\pm}_m\rangle(r^{\pm}_m - \langle r^{\pm}_m\rangle) = \langle r^{\pm}_m\rangle^2 + 2\langle r^{\pm}_m\rangle\Delta r^{\pm}_m \qquad (2.2.68)$$

in which Δr is now due to the noise and is assumed to be small. Substitution of this definition into the equation (2.2.60) and linearisation in Δr then results in 2 equations, one for the average amplitude and one for the fluctuation. It turns out that the resulting equations are identical to those obtained from averaging (for $\langle r\rangle$) or linearisation (for Δr) of:

$$\frac{1}{v_g}\frac{dr^{\pm}_m}{dt_{f,b}} - \Delta\beta_{m,i}r^{\pm}_m = \frac{\hbar\omega_m S_m}{4\,L\,r^{\pm}_m} \pm |\kappa| r^{\mp}_m\cos(\varphi_\kappa + \varphi^{-}_m - \varphi^{+}_m) + \frac{F^{\pm}_{i,m}\hbar\omega_m}{2\langle r^{\pm}_m\rangle} \qquad (2.2.69)$$

II.2.3 The rate equation for the carrier density

A simplified rate equation for the carrier density in the active layer has already been given in section II1.2.1. We are now in a position to express the stimulated emission term in equation (2.1.1) as a function of the field amplitudes and the carrier density. Indeed, from (2.2.13), (2.2.42) and (2.2.44), it follows that the average photon density of mode m in the active layer is given by $\Gamma u_m/\hbar\omega_m wd$. The stimulated emission rate is then easily found by multiplying this average photon density with the gain g_m (assumed to be uniform in the active layer). The total stimulated emission rate is obtained by summing over the longitudinal modes and one finds the carrier rate equation:

$$\frac{\partial N}{\partial t} = \frac{\eta J}{qd} - \frac{N}{\tau} - B_0N^2 - C_0N^3 - \frac{\Gamma}{wd}\sum_m \frac{g(\omega_m)}{\hbar\omega_m}\left[(r_m^+)^2 + (r_m^+)^2\right] \qquad (2.2.70)$$

with the gain g being given by (with $\lambda_m = 2\pi c/\omega_m$):

$$g(\lambda_m) = \left[a(\lambda_m)\,N - b(\lambda_m)\right]\left\{1 - \sum_l \varepsilon(\lambda_m,\lambda_l)\left[(r_l^+)^2 + (r_l^+)^2\right]\right\} \qquad (2.2.71)$$

In the carrier rate equation, we have treated the carrier density as a continuous quantity, while the recombination and creation (e.g. interband absorption) rates have been approximated as continuous processes. However, in reality, the carrier density is quantised with a unit equal to the inverse active layer volume and the recombination and creation processes occur in a discrete way. This discrete character can be accounted for by adding a Langevin force to (2.2.70).

$$\frac{\partial N}{\partial t} = \frac{\eta J}{qd} - \frac{N}{\tau} - B_0N^2 - C_0N^3 - \frac{\Gamma}{wd}\sum_m \frac{g(\omega_m)}{\hbar\omega_m}\left[(r_m^+)^2 + (r_m^+)^2\right] + F_N(z,t) \qquad (2.2.72)$$

For the same reasons as those given in section II.2.1.2, we can assume that $F_N(z,t)$ and $F_N(z',t')$ are gaussian and uncorrelated for $|t-t'| > 10^{-13}$s and $|z-z'| > 10^{-2}\mu$m. Again, F_N has zero average.

A part of F_N has its origin in the spontaneous emission and is thus related to the Langevin functions which we encountered in the previous section. However, spontaneous emissions induce opposite changes in photon number and in carrier number (one spontaneous emission increases the photon number by one, but it decreases the carrier number by one). We can therefore write:

$$\text{wd } F_N(z,t) = \text{wd } F_S(z,t) - \sum_m \{ F^+_{i,m}(z,t) + F^-_{i,m}(z,t) \} \qquad (2.2.73)$$

The multiplication with wd is necessary to obtain the number of carriers per unit length in the longitudinal direction, a quantity similar to i_m. It can also be noticed here that $F_{i,m}$ can as well be interpreted as shot noise associated with the stimulated emission and the interband absorption (see e.g. [2.22] and [2.23]).

wdF_S represents the shot noise related to the spontaneous carrier recombination. This shot noise is not correlated with the shot noise in the stimulated emission and absorption (independent processes) and its second order moment can be derived from the standard formula for shot noise. One finds:

$$< F_S(z,t)\, F_S(z',t') > = \frac{2}{wd}\left(\frac{N}{\tau} + B_0 N^2 + C_0 N^3 \right) \delta(t-t')\, \delta(z-z') \qquad (2.2.74)$$

Obviously, F_S is not correlated with one of the Langevin functions appearing in the field phase equations. F_N consists entirely of shot noise, which never has a direct influence on the field phases.

II.2.4 Boundary conditions

The coupled wave equations and the carrier rate equation are valid only in a section with a uniform waveguide structure. In the case of lasers, consisting of different sections with different waveguiding properties, we can use the coupled wave and the carrier rate equations in each section separately. The fields and the carrier density in two different sections A and B are thereby connected by the boundary conditions at the sections' interface ($z=z_{AB}$). The boundary conditions express the continuity of the tangential

components of the electric and magnetic optical fields and of the carrier density.

The continuity of the carrier density however can not be taken into account unless carrier diffusion is included. The diffusion length in the longitudinal direction on the other hand is so small that it allows large carrier density variations over a small distance. We can therefore, by denoting by N the average carrier density over a certain distance (e.g. a few μm), translate the boundary condition so that discontinuities in the average carrier density are permitted.

The boundary conditions for the electromagnetic fields can be expressed as usual in terms of a reflection (ρ_j) and a transmission (t_j) coefficient. The boundary conditions impose the following relations between the fields in two neighbouring sections A and B:

$$\begin{pmatrix} E_m^+ \\ E_m^- \end{pmatrix}_B = \frac{1}{t_j} \begin{pmatrix} 1 & -\rho_j \\ -\rho_j & 1 \end{pmatrix} \begin{pmatrix} E_m^+ \\ E_m^- \end{pmatrix}_A \qquad (2.2.75)$$

with:

$$(E_m^{\pm})_A = \lim_{z \to z_{AB}^-} R_m^{\pm} e^{\pm j\beta_0 z} \qquad (2.2.76a)$$

$$(E_m^{\pm})_B = \lim_{z \to z_{AB}^+} R_m^{\pm} e^{\pm j\beta_0 z} \qquad (2.2.76b)$$

The reflection and transmission coefficient are determined by the difference in lateral/transverse mode or in effective refractive index between the different sections. The sum of their squared moduli equals one. In the following, we will treat them as given constants.

The relations (2.2.75) also apply at the output facets, i.e. the boundary between the semiconductor and the air. One of the fields ($(E_m^+)_A$ for z=0 and $(E_m^-)_B$ for z=L, L: laser length) vanishes in this case and the boundary conditions reduce to:

$$E_m^+(z=0) = \rho_f E_m^-(z=0) \; ; \; E_m^-(z=L) = \rho_b E_m^+(z=L) \qquad (2.2.77)$$

with $\rho_{f,b}$ being the field reflection coefficient at the left (right) facet.

It is convenient in DFB laser theory to use complex field reflectivities. The phase of the reflectivity can then account for the random variations in the phase of the grating at z=0 and z=L. This phase of the grating, which cannot be controlled with the current technological means and which practically varies from chip to chip (fig.2.2.3), could also be included in the coupling coefficient and by considering small random variations in the laser length. However, one usually assumes a constant phase at z=0 (phase zero in our case) and a constant laser length.

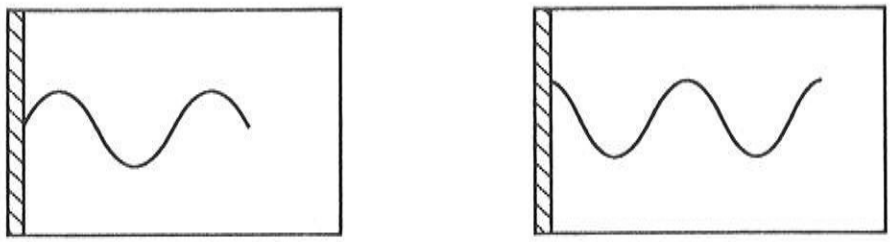

Fig. 2.2.3: Variation in the phase of the grating at the facets for different lasers of the same wafer.

It must also be noticed that, for structures where different sections have different grating periods, the phase of each grating is defined at z=0 even if the grating doesn't start at z=0.

II.3 z-independent rate equations for single section lasers

The rate equations, which describe the time evolution of the total number of carriers in the laser cavity, of the total number of photons in each mode and of the optical frequency of each mode, provide a very simple mathematical model for laser diodes [2.23]. In their usual form, these equations are valid only for single section lasers, although, in recent years, they have also been extended to other lasers such as external cavity lasers [2.24], [2.25]. The usefulness of the rate equations mainly lies in their easy manipulation, by which analytical approximations for the power spectrum and the RIN or the AC-response can be derived.

In the subsequent sections, we will derive the rate equations from the longitudinal field equations, compare these equations with the standard rate equations that can be found in literature and discuss some differences or extensions in more detail. We thereby restrict ourselves to single section lasers. We'll first derive the standard rate equations and discuss some solutions which still are often quoted (even nowadays) when experimental results need to be explained. Next, attention is paid to some modifications due to e.g. longitudinal spatial hole burning or dispersion. This should allow us to evaluate our own specific approach, based on numerical solution of the longitudinal equations, in the next chapters.

II.3.1 Standard rate equations

The standard rate equations can be derived only under the assumption of a longitudinally uniform carrier density, which, practically, only occurs when all longitudinal modes possess either a uniform or a negligible power density. The carrier density can thus be written as:

$$N(z) = N_0 \text{, with } N_0 \text{ being a constant} \qquad (2.3.1)$$

We also introduce the total number of photons I_m carried by the mode m and write:

$$(r_m^+)^2 + (r_m^-)^2 = \frac{\hbar\omega_m v_g}{L} I_m \,(1 + f_m(z))$$

$$\text{with } \int_0^L f_m(z)dz = 0 \text{ for all } m \qquad (2.3.2)$$

The rate equation for the uniform carrier density is now readily obtained by averaging the equation (2.2.72) in the longitudinal direction. The gain appearing in this equation is given in detail in appendix II.A. Since the carrier density dependence of the linear gain and of the gain suppression is almost identical, we will assume the following expression here:

$$g_m = [\, a(\omega_m)\, N_0 - b(\omega_m)\,] \left\{ 1 - \sum_s \varepsilon_{ms} \{ (r_s^+)^2 + (r_s^-)^2 \} \right\} \qquad (2.3.3)$$

We then find:

$$\frac{\partial N_0}{\partial t} = \frac{\eta J}{qd} - \left(\frac{N_0}{\tau} + B_0 N_0^2 + C_0 N_0^3 \right) - \frac{1}{V_a} \sum_m G(N_0,\omega_m)\, I_m + F_{N,0}(t) \qquad (2.3.4)$$

The modal gain G defined therein can be written as:

$$G(N_0,\omega_m) = [\, A(\omega_m)\, N_0 - B(\omega_m)\,] \left\{ 1 - \sum_s \xi_{ms} I_s \right\}$$

with $A(\omega_m) = \Gamma a(\omega_m) v_g$, $B(\omega_m) = \Gamma b(\omega_m) v_g$

and $$\xi_{ms} = \varepsilon_{ms} \frac{\hbar \omega_m v_g}{L} \left(1 + \frac{1}{L} \int_0^L f_m(z) f_s(z) dz \right) \qquad (2.3.5)$$

while $F_{N,0}$ denotes the spatial average of $F_N(z,t)$.

An equation for the photon number I_m can be derived from the equation (2.2.29) and a similar equation for i_m^-. Adding the two equations and integrating the resulting equation over the laser length gives, after substitution of $\Delta\beta_{m,i}$ (from 2.2.15):

$$\frac{dI_m}{dt} = [\, G(N_0,\omega_m) - \alpha_{int} v_g \,]\, I_m + S_m + F_{I,m}(t)$$
$$+ v_g \{ i_m^+(L) - i_m^-(L) \} + v_g \{ i_m^-(0) - i_m^+(0) \} \qquad (2.3.6)$$

The last two terms on the r.h.s. of (2.3.6) are easily interpreted as the photons that leave the cavity through the right, resp. the left facet. This facet loss is proportional with I_m, at least for a uniform carrier density, and it can be expressed symbolically as $\gamma_{fac} I_m$. The photon rate equation then reduces to the standard form:

$$\frac{dI_m}{dt} = [\, G(N_0,\omega_m) - \gamma \,]\, I_m + S_m + F_{I,m}(t)$$

with $\gamma = \gamma_{fac} + \alpha_{int} v_g$ (2.3.7)

It can be remarked that the equations (2.3.4) and (2.3.7) are identical for both Fabry-Perot and DFB lasers. Only the facet loss will be

different for both lasers. Moreover, the loss generally depends on the mode number m in DFB lasers [2.26], i.e. γ must be replaced by γ_m. Due to the dependence of G on the carrier density and on the photon numbers, the system remains highly non-linear.

An equation for the mode frequencies can be derived in a similar way from the equations (2.2.48b). Summation of the equations for φ^+ and φ^- and averaging over the longitudinal direction results in:

$$\frac{d}{dt}\left(\frac{1}{2Lv_g}\int_0^L(\varphi_m^+ + \varphi_m^-)dz\right) + \frac{\omega_m}{c}(n_{eff} + \Gamma\Delta n_r(N_0))$$

$$= \frac{\varphi_m^-(L) - \varphi_m^+(L) + 2\beta_g L}{2L} + \frac{\varphi_m^+(0) - \varphi_m^-(0)}{2L} + \frac{1}{2L}\phi_{fb} + F_{\varphi,m}(t) \qquad (2.3.8)$$

The phase ϕ_{fb} appearing in this equation is due to the distributed reflections (it vanishes for Fabry-Perot lasers) and is given by:

$$\phi_{fb} = |\kappa|L\,\frac{1}{L}\int_0^L\left(\frac{r_m^+}{r_m^-} + \frac{r_m^-}{r_m^+}\right)\sin(\varphi_\kappa + \varphi_m^- - \varphi_m^+)\,dz \qquad (2.3.9)$$

The first two terms on the r.h.s. of (2.3.8) are determined by the phases of the field reflection coefficients ρ_f and ρ_b and they can be considered as constants. By including all reflection phases (i.e. also the phase from the distributed reflections) into one phase ϕ_R, we can again write a common equation for both Fabry-Perot and DFB lasers:

$$\frac{d}{dt}\left(\frac{1}{2Lv_g}\int_0^L(\varphi_m^+ + \varphi_m^-)dz\right) + \frac{\omega_m}{c}(n_{eff} + \Gamma\Delta n_r(N_0))$$

$$= \frac{1}{2L}\phi_R + F_{\varphi,m}(t) \qquad (2.3.10)$$

This last equation can, in general, only be solved in the low-frequency case (i.e. d/dt = 0) and for Fabry-Perot lasers (for which ϕ_R is a constant). Furtheron, we will see that also a few special DFB lasers with a constant (or zero) ϕ_R exist, i.e. lasers for which the sin-function in (2.3.9) vanishes for all longitudinal positions. Equa-

tion (2.3.10) is then usually replaced by its small signal approximation:

$$\frac{\Delta\omega_m}{v_g} = -\frac{\omega_m}{c}\,\Gamma\,\frac{\partial(\Delta n_r)}{\partial N_0}\,\Delta N_0 + F_{\varphi,m} \approx \frac{\alpha}{2v_g}\,\frac{\partial G(N_0,\omega_m)}{\partial N_0}\,\Delta N_0 + F_{\varphi,m}$$

$$\text{with: } \alpha = -2\frac{\omega_m}{c}\,\frac{\dfrac{\partial n_r}{\partial N_0}}{\dfrac{\partial g}{\partial N_0}} \qquad (2.3.11)$$

α is called the linewidth enhancement or antiguiding factor [2.27], [2.28]. Its introduction follows more or less in a natural way from the fact that both the refractive index and the gain depend linearly on the carrier density. α is usually considered as a wavelength dependent constant. It must further be noticed that the use of the group velocity v_g on the l.h.s. of the frequency equation is a consequence of the frequency dependence of the refractive index.

The equation (2.3.11) also is often used for DFB lasers and in non-static cases, although, in principle, one needs to solve the separate phase equations (2.2.48b) in these cases. We'll discuss the validity of this approximation furtheron. Furthermore, it must be remarked that the refractive index doesn't depend on the power levels, as does the gain (gain suppression). For this reason, α should be considered as a bias dependent quantity.

The Langevin functions appearing in the equations (2.3.4), (2.3.7) and (2.3.11) are given by:

$$F_{I,m}(t) = \int_0^L [F^+_{i,m}(z,t) + F^-_{i,m}(z,t)]\,dz$$

$$F_{\varphi,m}(t) = \frac{1}{2L}\int_0^L [F^+_{\varphi,m}(z,t) + F^-_{\varphi,m}(z,t)]\,dz$$

$$F_{N,0}(t) = \frac{1}{L}\int_0^L F_S(z,t)dz - \frac{1}{V_a}\sum_m F_{I,m}(t) = F_{S,0}(t) - \frac{1}{V_a}\sum_m F_{I,m}(t) \qquad (2.3.12)$$

As linear combinations of functions with zero average, they all have a zero average. Since the z-dependent Langevin functions are uncorrelated in space, the second order moments can easily be cal-

culated by integration of the original second order moments. Of course, the uniform carrier density also implies a uniform spontaneous emission rate. One readily finds that all new Langevin functions are mutually uncorrelated and that they have second order moments given by:

$$<F_{I,m}(t)\,F_{I,n}(t')> = 2\,S_m I_m\,\delta_{mn}\,\delta(t-t')$$

$$<F_{\varphi,m}(t)\,F_{\varphi,n}(t')> = \frac{S_m}{8L^2 v_g^2}\int_0^L\left(\frac{1}{i_m^+}+\frac{1}{i_m^-}\right)dz\;\delta_{mn}\,\delta(t-t')$$

$$<F_{S,0}(t)\,F_{S,0}(t')> = \frac{2}{V_a}\left(\frac{N_0}{\tau}+B_0N_0^2+C_0N_0^3\right)\delta(t-t') \qquad (2.3.13)$$

The second order moments of the phase Langevin functions are thereby often calculated under the assumption that the power densities of both the forward and backward propagating waves are uniform and equal to $I_m/2L$ (as is the case in a Fabry-Perot laser with high facet reflectivities). This results in:

$$<F_{\varphi,m}(t)\,F_{\varphi,n}(t')> = \frac{S_m}{2v_g^2\,I_m}\,\delta_{mn}\,\delta(t-t') \qquad (2.3.14)$$

II.3.2 Some basic solutions

Simple, but basic formula for the static side mode suppression, the power spectrum and the linewidth, the RIN and the AC-response can be obtained from analytical solution of the rate equations. Except for the calculation of the side mode suppression, one thereby applies a small signal approximation and considers the loss γ_m as a constant.

Here, we give an overview of these well-known formulas for future reference.

II.3.2.1 The static side mode suppression

The side mode suppression in a laser where only one mode (m) has reached the threshold can be calculated from the equations (2.3.4). Assuming the laser to be driven far above its threshold cur-

rent (where the main mode m starts lasing), one has $G(N_0, \omega_m) = \gamma_m$ (i.e. the gain compensates the loss) and the side mode suppression (for the side mode s) can be expressed as:

$$SMSR = \frac{I_m}{I_s} = \frac{\gamma_s - G(N_0,\omega_s)}{S_s} I_m \approx \Delta g_{th} L \frac{\bar{P}}{\gamma_m n_{sp} \hbar \omega_m} \qquad (2.3.15)$$

$\bar{P}$: average power density in the cavity

Δg_{th}: difference in threshold gain between main and side mode

We also assumed that the gain (and hence the spontaneous emission) depends only weakly on the mode frequency ω_m.

By using typical values in (2.3.15), e.g. $n_{sp} = 2$, $\gamma_m = 100\ cm^{-1}$ and an average intracavity power of 2 mW (which, for cleaved facets, corresponds with 1 mW output power), we find that a static side mode suppression of 30 dB requires a normalized threshold gain difference $\Delta g_{th}L$ of $\pm$ 0.1. The threshold gain difference in DFB lasers depends in general on the specific longitudinal structure and even on the bias level. Its value, calculated at threshold, then can only give an indication of the single mode behaviour.

The side mode suppression as a function of the threshold gain difference $\Delta g_{th}L$ depends for DFB lasers again strongly on the specific structure. The influence of the normalized coupling coefficient κL e.g. can be illustrated by noticing that higher coupling coefficients result in a smaller loss as well as in a higher value of the average intracavity power for a given output power. A given value of the threshold gain difference at a given output power will therefore lead to a higher suppression ratio for high κL-values than it does for low κL-values.

II.3.2.2 The IM- and FM-response

The IM- and FM-response can be obtained after linearisation of (2.3.4) and (2.3.7). We restrict ourselves here to truly single mode lasers with a side mode suppression of 30 dB or more. Side modes have no impact on the AC-response of the main mode in this case [2.29]. By introducing the expansions:

$$J = J_0 + \mathrm{Re}\{\Delta J e^{j\Omega t}\}$$

$$I_m = I_{m,0} + \mathrm{Re}\{\Delta I_m e^{j\Omega t}\}$$

$$N_0 = N_{00} + \mathrm{Re}\{\Delta N_0 e^{j\Omega t}\} \qquad (2.3.16)$$

we find the small signal equations:

$$\left(j\Omega + \frac{S_m}{I_{m,0}} + \xi_{mm}(AN_0-B)I_{m,0}\right)\Delta I_m = A\,\Delta N_0\,(1-\xi_{mm}I_{m,0})\,I_{m,0}$$

$$\left(j\Omega + \frac{1}{\tau_{rd}} + A\,\frac{I_{m,0}}{V_a}\,(1-\xi_{mm}I_{m,0})\right)\Delta N_0 = \frac{\eta\Delta J}{qd} -$$

$$(AN_0-B)\,(1-2\xi_{mm}I_{m,0})\,\frac{\Delta I_m}{V_a}$$

$$\text{with}\quad \frac{1}{\tau_{rd}} = \frac{1}{\tau} + 2\,B_0N_0 + 3\,C_0N_0^2 \qquad (2.3.17)$$

These equations can easily be solved for ΔI_m (which gives the IM-response) and ΔN_0 (which through (2.3.11) gives the FM-response). They can easily be extended for the multi mode case. From (2.3.17), it follows that the spontaneous emission will only be important at low bias levels. One finds the formulas (in which we have left the mode indices behind and neglected $\xi I_{m,0}$ with respect to 1):

$$\Delta I = \frac{A I_0\,\dfrac{\eta\Delta J}{qd}}{\left\{j\Omega + \dfrac{S}{I_0} + \xi I_0(AN_0-B)\right\}\left\{j\Omega + \dfrac{1}{\tau_{rd}} + A\dfrac{I_0}{V_a}\right\} + A\dfrac{I_0}{V_a}(AN_0-B)} \qquad (2.3.18a)$$

$$\Delta\omega = \frac{\dfrac{\alpha}{2}A\left(j\Omega + \dfrac{S}{I_0} + \xi I_0(AN_0-B)\right)\dfrac{\eta\Delta J}{qd}}{\left\{j\Omega + \dfrac{S}{I_0} + \xi I_0(AN_0-B)\right\}\left\{j\Omega + \dfrac{1}{\tau_{rd}} + A\dfrac{I_0}{V_a}\right\} + A\dfrac{I_0}{V_a}(AN_0-B)} \qquad (2.3.18b)$$

It must be noticed that the actual IM-response further depends on the relation between output power and photon number I. Equation (2.3.18a) however gives the exact modulation frequency dependence of the IM-response.

The modulation frequency dependence in the denominator of (2.3.18) gives rise to a resonance phenomenon, better known as the relaxation oscillation. This resonance is also subject to a damping, mainly caused by spontaneous emission and gain suppression. The resonance frequency f_r and the damping ϑ of the relaxation oscillation are given by [2.30]:

$$(2\pi f_r)^2 \approx A \frac{I_0}{V_a}(AN_0 - B) = \frac{A I_0 \gamma}{V_a}$$

$$\vartheta = \frac{1}{\tau_{rd}} + \frac{S}{I_0} + \frac{A I_0}{V_a} + \xi \gamma I_0 \qquad (2.3.19)$$

The resonance frequency and the damping are seen to increase with increasing bias level I_0 and with increasing differential gain A. A considerable contribution to the damping is given by the gain suppression ξ and (at very low power levels) by the spontaneous emission. Typical values for the resonance frequency are of the order of magnitude of a few GHz.

The relaxation oscillations describe the resonant exchange of energy between photons and carriers (electrons) via the processes of stimulated emission and absorption. The oscillation can be described by assuming that a surplus of electrons with respect to the equilibrium exists. The gain exceeds the loss in this case and the stimulated emission creates more and more photons, resulting in an increasing stimulated emission rate. This in turn depletes the carriers inside the cavity, so that eventually the gain can no longer overcome the loss. At this point, the number of photons decreases again, the stimulated emission rate decreases and the carrier density increases again above its equilibrium value, where a new cycle starts. This picture also shows why spontaneous emission and carrier recombination (which make that not all carriers and photons participate to the stimulated recombination) or gain suppression (which restricts the increase of stimulated recombination for increasing photon numbers) cause a damping of the 'oscillation.

From (2.3.18), it also follows that the static (i.e. at modulation frequencies of 1 MHz) IM-response, which is an indication for the internal efficiency, is proportional with the inverse threshold gain. The static FM-response on the other hand, is, at practical po-

wer levels, mainly proportional with the linewidth enhancement factor and the gain suppression coefficient ξ.

II.3.2.3. The power spectrum, the linewidth and the intensity noise

The spectra of the FM-noise and of the intensity noise are derived in a similar way as the AC-response. The Langevin functions (or better their Fourier components at frequency Ω) now act as driving source in stead of a sinusoidal current. It turns out that, at practical bias levels, the 3 dB width of the power spectrum (the linewidth) only depends on the low frequency value of the FM-noise and therefore one can neglect the dynamics in solving the rate equations. We'll also ignore the steady-state spontaneous emission here (we assume a relatively high bias level) and we consider a single mode laser. The static fluctuations in frequency and in intensity are then given by:

$$\Delta N_0 = \frac{\xi V_a F_S - \dfrac{F_{I,m}}{I_{m,0}}}{\xi \dfrac{V_a}{\tau_{rd}} + A} \Rightarrow \Delta\omega_m = \frac{\alpha}{2} A \frac{\xi V_a F_S - \dfrac{F_{I,m}}{I_{m,0}}}{\xi \dfrac{V_a}{\tau_{rd}} + A} + v_g F_{\varphi,m}$$

$$\Delta I_m = \frac{A\, I_{m,0} F_S + \dfrac{F_{I,m}}{\tau_{rd}}}{I_{m,0}(AN_0 - B)\left(\dfrac{A}{V_a} + \dfrac{\xi}{\tau_{rd}}\right)} \qquad (2.3.20)$$

Substitution of typical values for A ($10^4 \mu m^3/s$), V_a ($100 \mu m^3$), ξ (10^{-7}) and τ_{rd} (10^{-9}s) in (2.3.20) shows that F_S can be neglected for not too high a power level and that $\xi V_a/\tau_{rd}$ can be neglected with respect to A. The expressions (2.3.20) are valid for frequencies up to ± 1GHz and on a time scale of a few nanoseconds, one then finds (when leaving the mode index m behind):

$$\langle \Delta\omega(t)\, \Delta\omega(t') \rangle = \frac{S}{2I_0} (1 + \alpha^2)\, \delta(t - t')$$

$$\langle \Delta I(t)\, \Delta I(t') \rangle = 2 \frac{S V_a^2}{A^2 (AN_0 - B)^2 \tau_{rd}^2 I_0} \delta(t - t') \qquad (2.3.21)$$

The spectral density of the FM-noise and of the RIN can now be calculated straightforward [2.31] :

$$S_{\Delta\omega}(f) = \int_{-\infty}^{+\infty} dt \; <\Delta\omega(t)\,\Delta\omega(0)> e^{j2\pi ft} = \frac{S}{2I_0}(1+\alpha^2)$$

$$RIN = \frac{S_{\Delta I}(f)}{I_0^2} = 2\,\frac{S\,V_a^2}{A^2(AN_0-B)^2\tau_{rd}^2 I_0^3} \qquad (2.3.22)$$

The values predicted by (2.3.22) will, in reality, only be found at frequencies which are sufficiently below 1 GHz. In some cases, one is also interested in the spectra at higher frequencies and a more detailed calculation, taking into account the dynamics, is then required.

The power spectrum however can often be calculated in an accurate way by assuming a white spectrum for the FM-noise, with a spectral density given by (2.3.22). The RIN is also neglected thereby and one expresses the single mode field, emitted through one of the facets [2.22], as:

$$E(t) = Re\{E_c(t)\} = Re\left\{E_0\, e^{-j\left(\omega_0 t + \int^t \Delta\omega(t')dt'\right)}\right\} \qquad (2.3.23)$$

with E_0 and ω_0 being constants. The power spectrum, defined as the spectral density of the field is given by:

$$S_E(f) = \int_{-\infty}^{+\infty} dt \; <E_c^*(t)E_c(0)> e^{j2\pi ft}$$

$$= |E_0|^2 \int_{-\infty}^{+\infty} dt \; <e^{j\int_0^t \Delta\omega(t')dt'}> e^{j2\pi(f-f_0)t} \qquad (2.3.24)$$

At this point, it must be noticed that, due to the gaussian character of the Langevin forces, $\Delta\omega$ and its integral can also be treated as gaussian variables (for which $< e^{jx} > = \exp(-0.5<x^2>)$). In addition, it follows that:

$$<\left(\int_0^t \Delta\omega(t')dt'\right)^2> = \int_0^t dt_1 \int_0^t dt_2 <\Delta\omega(t_1)\,\Delta\omega(t_2)> = \frac{S}{2I_0}(1+\alpha^2)\,|t| \qquad (2.3.25)$$

(2.3.24) then reduces to:

$$S_E(f) = \frac{|E_0|^2}{2\pi} \frac{\Delta\nu}{(f-f_0)^2 + \left(\frac{\Delta\nu}{2}\right)^2} \text{ with } \Delta\nu = \frac{S}{4\pi I_0}(1+\alpha^2) \qquad (2.3.26)$$

The power spectrum has a Lorentzian lineform with a 3 dB width of $\Delta\nu$. The expression for $\Delta\nu$ given in (2.3.26) is better known as Henry's formula. It predicts that the linewidth $\Delta\nu$ decreases proportionally with the inverse power level.

II.3.3 Extensions of the rate equations

No matter how useful they may be, the standard rate equations stand for a very simplified description of laser diodes and, in recent years, various modifications have been proposed. Such work has been stimulated a lot by the, at the time, unexplainable behaviour of the linewidth at high power levels, where rebroadening or saturation occurs.

Here, we'll mainly discuss the effect of longitudinal spatial hole burning (i.e. the non-uniform carrier density) and of dispersion (i.e. the wavelength dependence of gain and loss) on the rate equations. Both effects will only be described for a few well-chosen lasers, since giving a general description of these effects seems to be too ambitious. We nevertheless believe that these examples provide sufficient evidence for further discussion in the chapters 5 and 6, which deal with the detailed noise and AC-behaviour of laser diodes.

II.3.3.1 Longitudinal spatial hole burning.

We show how spatial hole burning results in a power dependence of the gain, of the mirror loss and of the feedback phase. We now assume that only one mode is present and leave the mode index

m behind. For the sake of simplicity, we also neglect the gain suppression and the Langevin functions. Again, we use the expansion (2.3.2) for the optical power density and write:

$$(r^+)^2+(r^-)^2=\frac{\hbar\omega v_g}{L}\,I\,(1+f)\ \text{with}\ \int_0^L f\,dz=0 \qquad (2.3.27)$$

Substitution of this expansion in the carrier rate equation (2.2.72) immediately shows that the carrier density will be non-uniform as well and we can approximate it to the first order as:

$$N(z,t)=N_0(t)+N_1(t)\,f(z) \qquad (2.3.28)$$

Since N_1 has its origin in the non-uniformity of the optical power, it can be assumed to be much smaller than N_0 (at least at low or moderate power levels).

The carrier rate equation

Substitution of (2.3.27) and (2.3.28) in the carrier rate equation now allows to determine both N_0 and N_1. One finds the equations:

$$\frac{\partial N_0}{\partial t}=\frac{\eta J}{qd}-\left(\frac{N_0}{\tau}+B_0N_0^2+C_0N_0^3\right)-\frac{(AN_0-B)}{V_a}\,I-\frac{AN_1}{V_a}\,I\,\frac{1}{L}\int_0^L f^2\,dz \qquad (2.3.29a)$$

$$\frac{\partial N_1}{\partial t}=-\frac{N_1}{\tau_{rd}}-\frac{AN_1}{V_a}\,I-\frac{(AN_0-B)}{V_a}\,I \qquad (2.3.29b)$$

From (2.3.29b), it can be seen that the dynamics of N_1 are governed by a time constant T_1, given by:

$$T_1=\left(\frac{1}{\tau_{rd}}+\frac{A\,I}{V_a}\right)^{-1} \qquad (2.3.30)$$

This implies that the amplitude of N_1 decreases rapidly for frequencies higher than $1/T_1$. By inserting typical values in (2.3.30), it follows that the spatial hole burning has a cut-off frequency in

the neighbourhood of 1 GHz. This cut-off frequency also increases with increasing bias level.

Furtheron, we'll only consider frequencies below this cut-off frequency. Solution of (2.3.29b) and substitution of N_1 in (2.3.29a) then gives:

$$\frac{\partial N_0}{\partial t} = \frac{\eta J}{qd} - \left(\frac{N_0}{\tau} + B_0 N_0^2 + C_0 N_0^3 \right) - \frac{(AN_0 - B)}{V_a} (1 - \xi_{spat} I) I$$

$$\text{with: } \xi_{spat} = \frac{A}{V_a \tau_{rd}^{-1} + A I} \frac{1}{L} \int_0^L f^2 dz \qquad (2.3.31)$$

Spatial hole burning thus results in a gain suppression just as spectral hole burning does. However, the suppression coefficient now decreases with increasing bias level as can be seen from (2.3.31). The gain suppression obviously depends on the non-uniformity of the power, but also on the carrier lifetime and on the differential gain. Again, we emphasize here that the obtained results are valid only at low to moderate power levels.

The photon rate equation

It is easily verified that the existence of N_1 results in an identical suppression of the gain in the photon rate equation. Below, we will show that, in addition, a suppression of the mirror loss exists. Only a few representative examples and the static case (i.e. frequencies relatively far below the resonance frequency of the relaxation oscillation) will be discussed.

- a F-P laser with facet reflectivities R_1 (z=0) and R_2 (z=L)

Integration of the coupled wave equations, taking into account the non-uniform carrier density and neglecting the spontaneous emission, now gives for the forward and backward propagating power:

$$P^+(z) = (r^+)^2 = P^+(0)\exp\left[\int_0^z (\Gamma g - \alpha_{int})dz'\right]$$

$$P^-(z) = (r^-)^2 = P^-(0)\exp\left[-\int_0^z (\Gamma g - \alpha_{int})dz'\right] \qquad (2.3.32)$$

Combination of these formulas with the boundary conditions at z=0 and z=L gives the threshold condition for a Fabry-Perot laser:

$$A\,N_0 - B - \alpha_{int}v_g = \frac{v_g}{2L}\ln\left(\frac{1}{R_1R_2}\right) \qquad (2.3.33)$$

It follows that, in spite of the gain suppression, there is still a clamping of the carrier density to the threshold value (determined by (2.3.33)). This can only be explained by assuming a similar power dependence of the total loss. This power dependence is entirely due to a power dependence of the mirror loss. The power dependence of the mirror loss actually implies a non-linear relation between output power and photon number, which is to be considered whenever the IM-response or the RIN is studied. It must be noticed though that, due to its cut-off frequency of about 1 GHz, spatial hole burning has no influence on the damping of the relaxation oscillation.

The relation between output power and photon number can be calculated approximately by using (2.3.32) [2.32]. One finds:

$$v_g[i^-(0) - i^+(0)] = \frac{(1-R_1)\,I\,\{(AN_0-B)\,(1-\xi_{spat}I) - \alpha_{int}v_g\}}{\left(1-\sqrt{R_1R_2}\right)\left(1+\sqrt{\frac{R_1}{R_2}}\right)}$$

$$v_g[i^+(L) - i^-(L)] = \frac{(1-R_2)\,I\,\{(AN_0-B)\,(1-\xi_{spat}I) - \alpha_{int}v_g\}}{\left(1-\sqrt{R_1R_2}\right)\left(1+\sqrt{\frac{R_2}{R_1}}\right)} \qquad (2.3.34)$$

Fig. 2.3.1 gives the numerical values of ξ_{spat} for symmetric, 300 μm long Fabry Perot lasers as a function of the facet reflectivity $R=R_1=R_2$. The photon number has been replaced by the average intracavity power and hence ξ_{spat} is expressed in W^{-1}. Furthermore, an inter-

nal loss of 50 cm^{-1} has been assumed. Comparison of the gain suppression coefficients with the gain suppression resulting from spectral hole burning allows to conclude that spatial hole burning has only a minor influence in ordinary F-P lasers (e.g. with cleaved facets $R_1=R_2=0.32$).

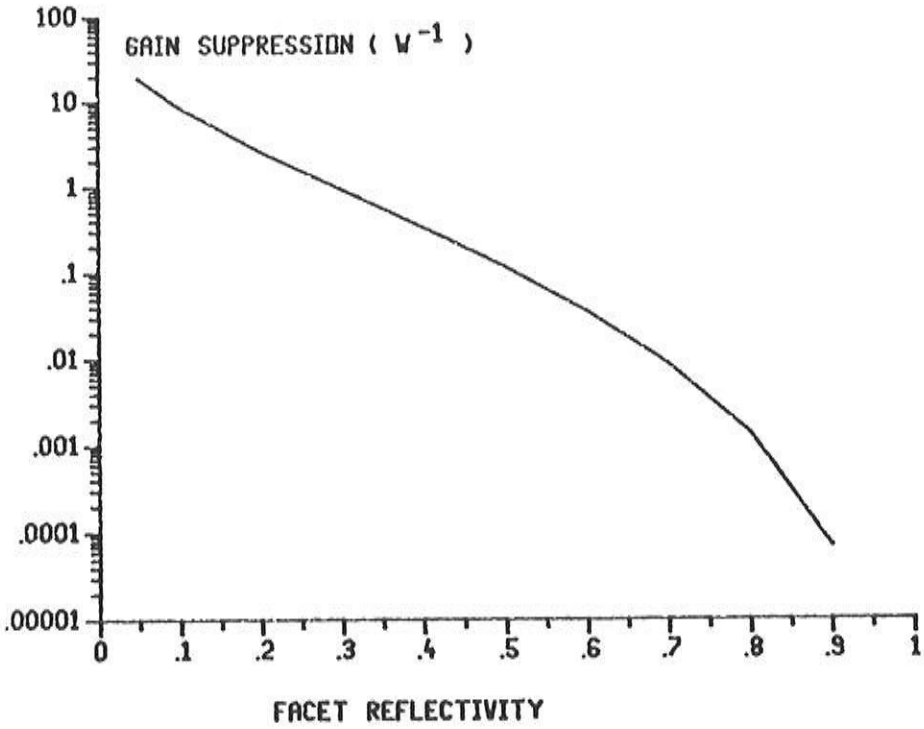

Fig.2.3.1: gain suppression (ξ_{spat}) in 300 μm long, symmetric F-P lasers vs. facet reflectivity.

- AR-coated λ/4-shifted DFB lasers

λ/4-shifted DFB lasers are lasers where the grating has a phase discontinuity of π in the centre (z=L/2). Such lasers emit at the Bragg-wavelength, i.e. $\Delta\beta_r=0$ and possess an optical power density that is symmetric with respect to z=L/2 (see [2.32]).

By introducing the expansion:

$$\Delta\beta_i = \Delta\beta_{io} + \Delta\beta_{i1} f \quad , \text{ with } \Delta\beta_{i1} = \frac{AN_1}{2v_g} \qquad (2.3.35)$$

,one can derive the following wave equation for r^+ and r^- from the amplitude equations:

$$\frac{\partial^2 r^{\pm}}{\partial z^2} = \left(\Delta\beta_{io}^2 + \kappa^2 \cos^2(\varphi_\kappa + \varphi^- - \varphi^+) + 2\Delta\beta_{io}\Delta\beta_{i1} f \pm \Delta\beta_{i1}\frac{\partial f}{\partial z} \right) r^{\pm} \qquad (2.3.36)$$

For most lasers emitting at the Bragg-wavelength, the sum of phases in (2.3.36) is either 0 or π. Hence the derivative of the cosine function vanishes and, to first order, variations in the phase caused by spatial hole burning must not be included.

The equation (2.3.36) can be solved by decomposing the fields r^+ and r^-, corresponding with the non-uniform carrier density, as:

$$r^{\pm} = r_0^{\pm} (1 + F^{\pm}) \qquad (2.3.37)$$

with $r_0^{\pm}$ being the fields corresponding with $\Delta\beta_{io}$. Solution of (2.3.36) again shows how a power dependence of the mirror loss arises. More details about this solution are given in appendix II.C. One now has:

$$v_g i^-(0) = v_g i^+(L) = \frac{v_g I}{\int_0^L dz\, g_+(z)} \{ 1 - \xi_{spat,2} I \}$$

$$\text{with: } \{r_0^+(z)\}^2 + \{r_0^-(z)\}^2 = g_+(z) \{r_0^-(0)\}^2 \qquad (2.3.38)$$

$\xi_{spat,2}$ is different from ξ_{spat} and is given by:

$$\xi_{spat,2} = \frac{(AN_0 - B)\, A \int_0^L dz\, f(z) \int_0^z dz'\, g_-(z')}{v_g (V_a \tau_{rd}^{-1} + AI) \int_0^L dz\, g_+(z)}$$

$$\text{with: } \{r_0^+(z)\}^2 - \{r_0^-(z)\}^2 = g_-(z) \{r_0^-(0)\}^2 \qquad (2.3.39)$$

Fig. 2.3.2 gives numerical values of the gain and loss suppression for 300 μm long $\lambda/4$-shifted lasers as a function of the normalized coupling coefficient. An internal loss of 50 cm^{-1} has again been assumed. It can be seen that the values generally are much larger

than they are for Fabry Perot lasers. It should also be noticed that the loss suppression can now be either positive or negative. In general, the loss increases, resp. decreases with increasing power level for low, resp. high κL-values.

- other DFB lasers

A similar power dependence of the loss can be expected for other DFB lasers. In the most general case however, one must also consider a bias dependence of the phases when calculating the loss. This bias dependence then also influences the feedback phase ϕ_{fb}. The value of $\xi_{spat,2}$ can then no longer be expressed in a simple way, nor is it guarantied that $\xi_{spat,2}$ decreases with bias level.

It must further be emphasized that the previous treatment of spatial hole burning is restricted to relatively small power levels and that no side modes have been included. Nevertheless, it must be obvious that, in general, one must consider both the gain, the loss and the feedback phase as quantities which depend on the power in the different modes.

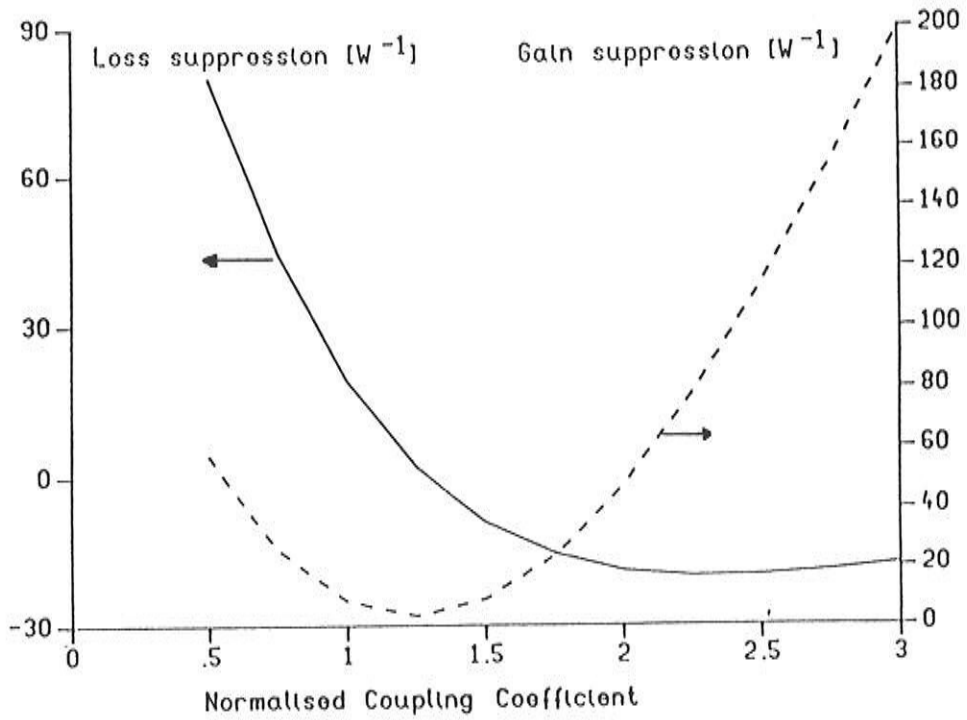

Fig.2.3.2: gain and loss suppression in 300 μm long, λ/4-shifted lasers vs. normalized coupling constant.

II.3.3.2 Dispersion in gain and loss.

The linearisation of the photon rate equation, as given in (2.3.17), is based on the assumption of a constant mode loss γ_m. This is indeed the case for a Fabry-Perot laser, where:

$$\gamma_m = \frac{v_g}{2L} \ln\left(\frac{1}{R_1 R_2}\right) \qquad (2.3.40)$$

However, the loss in lasers with a grating (such as DFB and DBR lasers) strongly depends on the wavelength or the optical frequency. As a consequence, this dispersion should be accounted for when linearising the rate equations, i.e. the loss ought to be linearised in the small signal frequency deviation $\Delta\omega_m$. The wavelength dependence of the gain function g implies that a similar linearisation of $G(N_0, \omega_m)$ in $\Delta\omega_m$ and (because of the spectral hole burning) in $\Delta\omega_s$ ($s \neq m$) must be considered.

The dispersion in the gain can easily be calculated from the functions given in appendix II.A. The dispersion in the loss on the other hand can be derived from solution of the coupled wave equations and determination of the gain required to obtain amplitude resonance. The amplitude resonance can be determined by dividing the laser in 2 equal parts at z=L/2, calculating the reflectivities from both the left and right sides and requiring their product to have an amplitude of one.

Fig. 2.3.3. shows the calculated facet loss $\gamma_{fac}.L/v_g$ as a function of the normalized real Bragg deviation $\Delta\beta_r L$ for a perfectly AR-coated DFB laser with $\kappa L=1.5$ and at very low power levels (i.e. for a uniform carrier density). The dispersion is seen from the sharp minimum in the loss. For a typical 1.55 μm laser (where the Bragg wavelength is located near 1.5 μm, with a length of 300μm and a refractive index of approximately 3), this minimum has a width of the order of magnitude of a few nanometers. The width of the gain curve on the other hand is typically a few tens of nanometers and hence the dispersion in the gain can often by neglected with respect to the dispersion in the loss.

It must be remarked that in DFB lasers, one also has a dispersion in the feedback phase ϕ_{fb}. This dispersion is not easily calcu-

lated however. Furthermore due to the spatial hole burning (and the associated non-uniform refractive index or the non-uniform Bragg deviation), the dispersion in DFB lasers more generally also depends on the bias level (as does the loss itself). More attention to the bias dependence of the dispersion will be given in chapter 5.

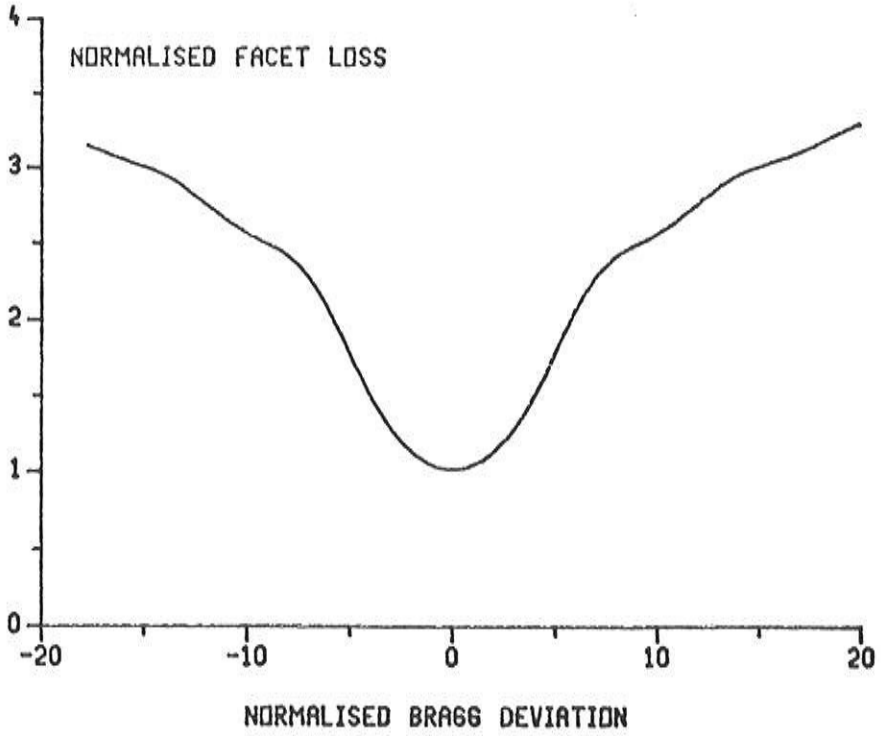

Fig.2.3.3: facet loss vs. Bragg deviation for an AR-coated DFB laser with κL=1.5.

II.3.3.3 Other important factors

The previous effects were treated in more detail because of their special importance in DFB lasers. There are however still other effects, which are not included in our theory , but that also result in an extra non-linearity. Among these effects are the lateral carrier diffusion and spatial hole burning (see e.g. [2.33]) and the formation of a grating as a result of the cavity standing waves (see e.g. [2.34]) by far the most important.

Appendix II.A: Analytical functions for gain and refractive index

We have implemented the density matrix based model for gain, absorption and refractive index [2.7], [2.35] on the computer, which allowed us to calculate the linear gain, the gain suppression, the intervalence band absorption and the associated real refractive index as a function of carrier density, photon energy and temperature. Analytical functions were then easily extracted from the data by the application of the ACM program for curve-fitting: 'NL2SOL'. (for more information on this, we refer to [2.37]).

Below, we will only give the gain and the real refractive index at room temperature (T=300K) and for 1.55 μm InGaAsP. For other materials, for the influence of the temperature and for a description of the intervalence band absorption, we refer to [2.36].

As was already mentioned in II.1.2.3, it follows that the gain can be approximated by:

$$g(\lambda) = g^{(1)}(N,\lambda) - \sum_m g^{(3)}(N,\lambda,\lambda_m) \frac{\Gamma}{w d n_{eff}} \{(r_m^+)^2 + (r_m^-)^2\} \qquad (2.A.1)$$

With the definition E = hω = 1.24 eV/λ (in μm),one finds for $g^{(1)}$ an expression of the form:

$$g^{(1)} = a(\lambda)\, N - b(\lambda) = C_1(E-C_2)^{C_3} N - C_4(E-C_5)^{C_6} \qquad (2.A.2)$$

where for 1.55μm InGaAsP, the constants C_i have the value:

C_1 = .4684235 10^{-6} μm^2	C_4 = 102.8845 μm^{-1}
C_2 = .7477408	C_5 = .6236856
C_3 = .774253	C_6 = 4.172654

The gain suppression can be fitted to a function of the form:

$$g^{(3)} = \frac{D_1 N + D_2}{(E-E_m)^2 + D_3^2} \{ D_4(E_m-D_5)^2 + D_6(E_m-D_5) + 1 \} \qquad (2.A.3)$$

The constants D_i have, for 1.55μm InGaAsP, the value:

$D_1 = 1.30418\ 10^{-11}\ \mu m^4/W$ $D_2 = -1.56402\ 10^{-7}\ \mu m/W$

$D_3 = .60106\ 10^{-2}$ $D_4 = -1550.$

$D_5 = 0.8$ $D_6 = -18.6$

The carrier induced refractive index (associated with the gain and the absorption) is linear in the carrier density as well and can be approximated as:

$$\Delta n_r(E) = F_1 N + F_2 + F_3 u^2 \{1 + F_5 u (1 + F_6 u)\} ; u = E - F_4 \qquad (2.A.4)$$

with the constants having, for 1.55μm InGaAsP, the value:

$F_1 = -0.169\ 10^{-7}\ \mu m^3$ $F_2 = -0.2076\ 10^{-2}$

$F_3 = 14.203$ $F_4 = .8013$

$F_5 = 8.6$ $F_6 = -49.33$

Appendix II.B: Proof of (2.2.12) and (2.2.22)

Formula (2.2.22) can be derived straightforward from equation (2.2.10), in which ϕ can be approximated by ϕ_0, and where the frequency dependence of both ϕ_0 and n^2 is neglected. Multiplication of equation (2.2.10) with ϕ_0 (which is a real function) and integration over the lateral/transverse cross-section gives:

$$\beta_{c,m}^2 = \frac{\iint_{(x,y)-\text{plane}} dxdy\ [\,\phi_0 \nabla_{xy}^2 \phi_0 + \omega_m^2 \mu_0 \varepsilon_0 n^2 \phi_0^2]}{\iint_{(x,y)-\text{plane}} dxdy\ \phi_0^2} \qquad (2.B.1)$$

Application of the definition of the group velocity and taking into account that ϕ_0 and n^2 are regarded as frequency-independent then readily leads to:

$$\frac{1}{v_g} = \frac{d\beta_{c,m}}{d\omega_m} = \frac{\omega_m}{c^2 \beta_{c,m}} \frac{\iint_{(x,y)-\text{plane}} dxdy\ n^2 \phi_0^2}{\iint_{(x,y)-\text{plane}} dxdy\ \phi_0^2} \qquad (2.B.2)$$

Formula (2.2.12) can be proven by multiplying equation (2.2.10) with ϕ_0, multiplying equation (2.2.11) with ϕ, subtracting the resulting equations and integrating over the lateral/transverse cross-section. One then finds:

$$\beta_{c,m}^2 - \beta_m^2 = \frac{\iint_{(x,y)} dxdy[\phi_0 \nabla_{xy}^2 \phi - \phi \nabla_{xy}^2 \phi_0]}{\iint_{(x,y)} dxdy\ \phi_0 \phi} + \frac{\omega_m^2 \mu_0 \varepsilon_0 \iint_{(x,y)} dxdy\ (n^2 - n_0^2)\, \phi_0 \phi}{\iint_{(x,y)} dxdy\ \phi_0 \phi} \qquad (2.B.3)$$

The first term on the r.h.s. of (2.B.3) can be shown to vanish by applying one of Green's theorems on it. A further simplification is also obtained by approximating ϕ by ϕ_0 in the integration and by assu-

ming that n and n_0, and $\beta_{c,m}$ and β_m are only different by a small amount. (2.B.3) then becomes:

$$\beta_{c,m} - \beta_m = \frac{\omega_m^2}{c^2 \beta_m} \frac{\iint_{(x,y)} dxdy\ n_0 (n - n_0) \phi_0^2}{\iint_{(x,y)} dxdy\ \phi_0^2} \qquad (2.B.4)$$

in which β_m can be replaced by its definition (2.2.11). Approximation of n and n_0 as constants in each layer i (e.g. i = active or cladding layers) results in:

$$\beta_{c,m} = \frac{2\pi}{\lambda_m} \left\{ n_{eff} + \sum_i (n_i - n_{0i}) \left(\frac{n_{0i}}{n_{eff}} \right) \Gamma_i \right\}$$

$$\text{with: } \Gamma_i = \frac{\iint_{\text{layer i}} dxdy\ \phi_0^2}{\iint_{(x,y)\text{-plane}} dxdy\ \phi_0^2} \qquad (2.B.5)$$

Equation (2.B.5) reduces to (2.2.12) when we consider only small variations in the unperturbed refractive index n_{0i}, so that (n_{0i}/n_{eff}) can be approximated by one, and when only two layers (active and cladding) are included.

Appendix II.C Solution of equation (2.3.36)

Substitution of:

$$r^{\pm}(z) = r_0^{\pm}(z)\,(1 + F^{\pm}(z)) \tag{2.C.1}$$

into the equation:

$$\frac{\partial^2 r^{\pm}}{\partial z^2} = \left\{ \Delta\beta_{i0}^2 + \kappa^2\cos^2(\varphi_\kappa+\varphi^- -\varphi^+) + 2\,\Delta\beta_{i0}\,\Delta\beta_{i1} f \pm \Delta\beta_{i1}\frac{\partial f}{\partial z} \right\} r^{\pm} \tag{2.C.2}$$

gives the following equation for $F^{\pm}$:

$$\frac{\partial F^{\pm}}{\partial z} = \pm\,\Delta\beta_{i1}\left[f - \frac{2\kappa}{(r_0^{\pm})^2}\int_0^z dz' f\; r_0^- r_0^+ \cos(\varphi_\kappa+\varphi^- -\varphi^+) \right]$$

$$= \pm\,\Delta\beta_{i1}\left[f - \frac{2\kappa}{(r_0^{\pm})^2}\chi(z) \right] \tag{2.C.3}$$

It can be noticed that for λ/4-shifted (or similar) lasers, the integrand appearing in χ is asymmetric around z=L/2 (due to the asymmetric cosine function) and hence that χ is symmetric. For the integration of this equation, one can choose the boundary conditions such that $r^-(0) = r_0^-(0)$ and $r^+(L) = r_0^+(L)$. This results in the solution:

$$F^+ = \Delta\beta_{i1}\left[\int_0^z f(z')\,dz' - \int_L^z dz' \frac{2\kappa}{\{r_0^+(z')\}^2}\chi(z') \right]$$

$$F^- = -\,\Delta\beta_{i1}\left[\int_0^z f(z')\,dz - \int_0^z dz' \frac{2\kappa}{\{r_0^-(z')\}^2}\chi(z') \right] \tag{2.C.4}$$

The symmetric nature of λ/4-shifted-like lasers implies that $r^+(z) = r^-(L-z)$ and hence $F^+(z) = F^-(L-z)$. Calculation of the intracavity power then gives:

$$(r^+)^2 + (r^-)^2 = (r_0^+)^2 + (r_0^-)^2 + 2\Delta\beta_{i1}\{(r_0^+)^2 - (r_0^-)^2\}\int_0^z f\,dz'$$

$$+ 4\,\Delta\beta_{i1}\kappa\left\{(r_0^+)^2\int_z^L dz'\frac{\chi}{(r_0^+)^2} + (r_0^-)^2\int_0^z dz'\frac{\chi}{(r_0^-)^2}\right\} \qquad (2.C.5)$$

The photon number I is obtained by integration of (2.C.5) and is given by:

$$h\omega v_g I = \int_0^L dz\,\{(r_0^+)^2 + (r_0^-)^2\} - 2\Delta\beta_{i1}\int_0^L dz\, f\int_0^z dz'\,\{(r_0^+)^2 - (r_0^-)^2\}$$

$$+ 4\,\Delta\beta_{i1}\kappa\int_0^L dz\,\chi(z)\left[\frac{1}{(r_0^+)^2}\int_0^z dz'(r_0^+)^2 - \frac{1}{(r_0^-)^2}\int_L^z dz'(r_0^-)^2\right] \qquad (2.C.6)$$

The 2nd and 3rd term on the r.h.s. of (2.C.6) are the result of a partial integration. For $\lambda/4$-shifted (or similar) lasers, it follows from numerical calculations that the 3rd term (of which the integrand is symmetric around z=L/2) can be neglected. It can also be remarked that, as a result of the assumed boundary conditions, the output power (proportional with $(r^+(L))^2$ or $(r^-(L))^2$) is determined by the unperturbed fields only, and one can write

$$(r_0^+)^2 \pm (r_0^-)^2 = (r_0^-(0))^2\, g_\pm(z) = v_g h\omega\, i^-(0)\, g_\pm(z) \qquad (2.C.7)$$

with g_+ and g_- being independent of the power level. g_+ and g_- can be calculated from the longitudinal power variation in the absence of spatial hole burning (e.g. calculated at threshold). Substitution of (2.C.7) into (2.C.6) and replacing N_1 by its value as given in (2.3.29b) then readily yields an expression for the reflection loss:

$$v_g i^-(0) = v_g i^+(L) = \frac{v_g I}{\int_0^L dz\, g_+}\left\{1 - \frac{(AN_0 - B)AI}{v_g(\tau_{rd}^{-1}V_a + AI)}\,\frac{\int_0^L dz\, f\int_0^z dz' g_-}{\int_0^L dz\, g_+}\right\} \qquad (2.C.8)$$

The functions f, g_+ and g_- can, for a given laser, be calculated analytically or numerically. They are depicted in figs. 2.C.1, 2.C.2 and

2.C.3 for 300 μm long λ/4-shifted lasers with κL=1 and κL=2. Fig. 2.C.1 shows the functions f, g₋ and the integral of g₋ for the case κL=1 and fig. 2.C.2 for the case κL=2. Fig. 2.C.3 shows the product of f and the integral of g₋ for both cases.

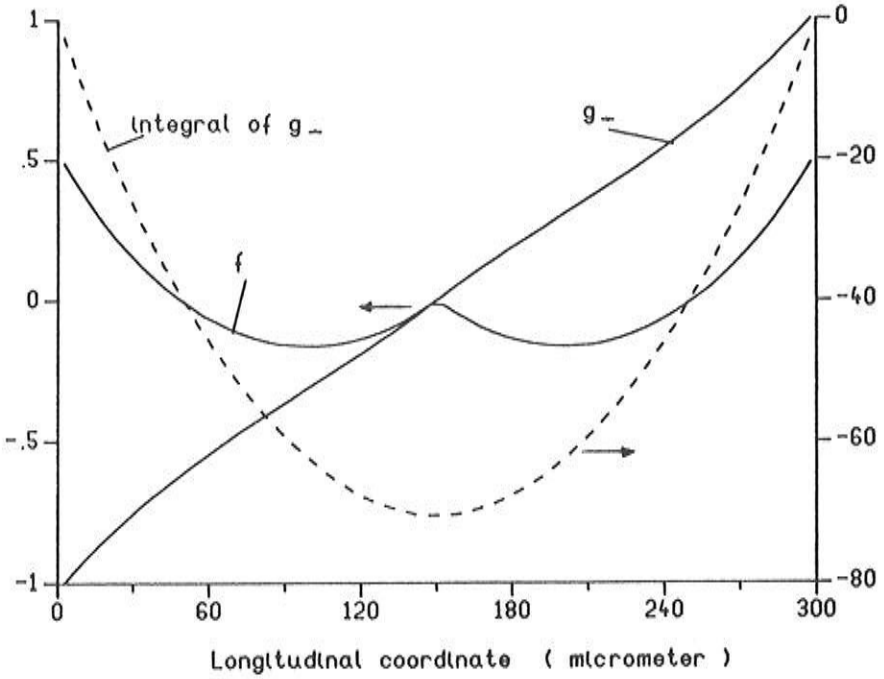

Fig.2.C.1: f, g₋ and the integral of g₋ for a λ/4-shifted laser with κL=1.

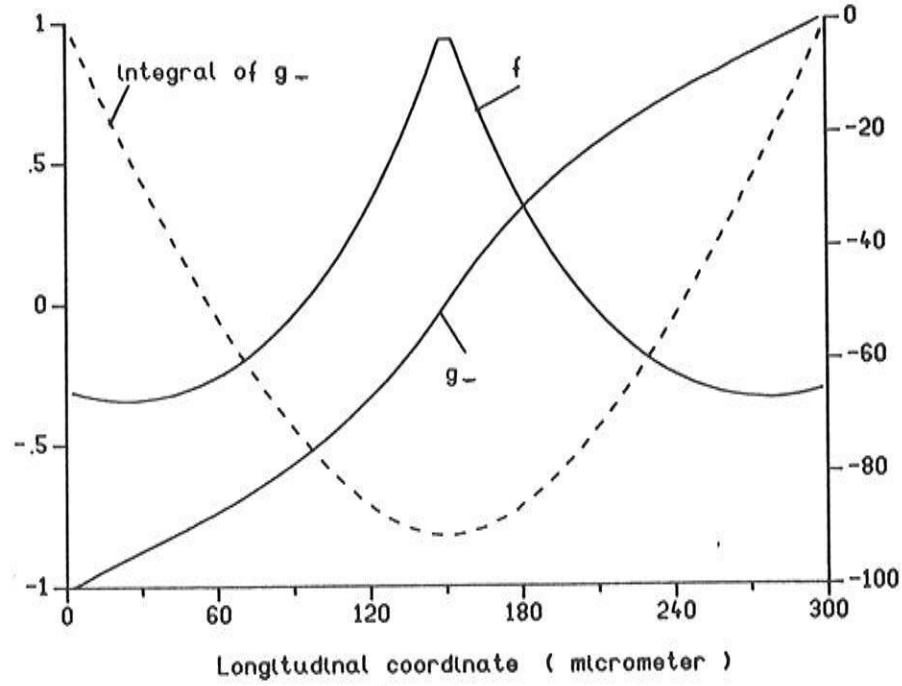

Fig.2.C.2: f, g₋ and the integral of g₋ for a λ/4-shifted laser with κL=2.

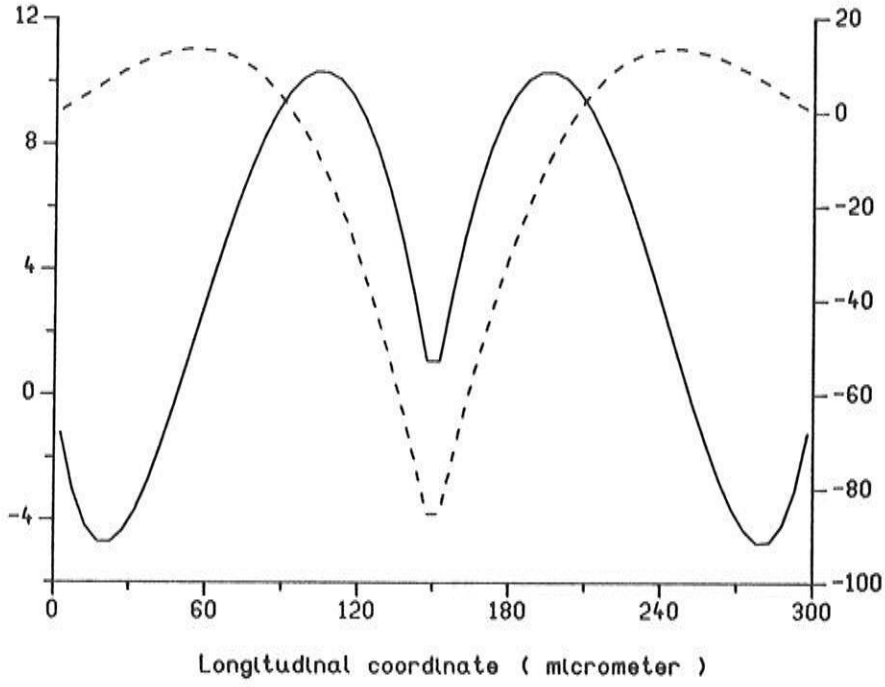

Fig.2.C.3: product of f and the integral of g. for λ/4-shifted laser with κL=1 (—) and κL=2 (---).

References

[2.1] K Petermann, 'Laser Diode Modulation and Noise', KTK Publishers, Tokyo, 1988.

[2.2] G. Agrawal, N. Dutta, 'Long-wavelength semiconductor lasers', Van Nostrand Reinhold, New York, 1986.

[2.3] M. Amann, 'New stripe-geometry laser with simplified fabrication process', El. Lett., Vol. 15, pp.441-442, July, 1979.

[2.4] K. Saito, R. Ito, 'Buried-heterostructure AlGaAs lasers', IEEE Journ. Quant. El., Vol. 16, pp. 205-215, February, 1980.

[2.5] D. Cook, F. Nash, 'Gain-induced guiding and astigmatic output beam of GaAs lasers', Journ. Appl. Phys., Vol. 46, p. 1660, 1975.

[2.6] H. Casey, M. Panish, 'Heterostructure Lasers, part A: Fundamental Principles', Academic Press, New York, 1978.

[2.7] M. Asada, Y. Suematsu, 'Density-matrix theory of semiconductor lasers with relaxation broadening model: gain and gain-suppression in semiconductor lasers', IEEE Journ. Quant. El., Vol. 21, pp. 434-442, May, 1985.

[2.8] A. Yariv, 'Quantum Electronics', 2nd Ed., Wiley , New York, 1980.

[2.9] R. Olshansky, C. B. Su, J. Manning, W. Powazinik, 'Measurement of Radiative and Nonradiative Recombination Rates in InGaAsP and AlGaAs Light Sources', IEEE Journ. Quant. El., Vol. 20, pp. 838-855, August 1984.

[2.10] H. Ghafoori-Shiraz, 'Temperature, Bandgap-Wavelength, and Doping Dependence of Peak-Gain Coefficient Parabolic Model Parameters for InGaAsP/InP Semiconductor Laser Diodes', Journ. Lightw. Techn., Vol. 6, pp. 500-506, April, 1988.

[2.11] D. Marcuse, 'Principles of Quantum Electronics', Academic Press, New York, 1980.

[2.12] P. Vankwikelberge, 'Theoretische studie van statische en dynamische longitudinale effecten in Fabry-Perot en DFB-diodelasers', Ph. D. thesis (in Dutch), university of Gent, 1990.

[2.13] G. Thompson, 'Physics of semiconductor laser devices', Wiley, New York, 1980.

[2.14] M. Lax, 'Fluctuations from the Nonequilibrium Steady State', Rev. Mod. Phys., Vol. 32, pp. 25-64, January, 1960.

[2.15] M Lax, 'Classical Noise IV: Langevin Methods', Rev. Mod. Phys., Vol. 38, pp. 541-566, July, 1966.

[2.16] C. Henry, 'Theory of Spontaneous Emission Noise in Open Resonators and its Application to Lasers and Optical Amplifiers', Journ. Lightw. Techn., Vol. 4, pp. 288-297, March, 1986.

[2.17] B. Rahman, J. Davies,' Finite element solution of integrated optical waveguides', Journ. Lightw. Techn., Vol. 2, pp. 682-688, 1984.

[2.18] M. Adams, 'An Introduction to Optical Waveguides', Wiley, Chichester, 1981.

[2.19] J. D. Jackson, 'Classical Electrodynamics', Wiley, New York, 1962.

[2.20] K. Petermann, 'Calculated spontaneous emission factor for double-heterostructure injection lasers with gain-induced waveguiding', IEEE Journ. Quant. El., Vol. 15, pp. 566-570, July, 1979.

[2.21] M. Lax,'Quantum Noise X: Density matrix treatment of field and population difference fluctuations', Phys. Rev., Vol. 157, pp. 213-231, 1967.

[2.22] C. Henry, 'Phase Noise in Semiconductor Lasers', Journ. Lightw. Techn., Vol. 4, pp. 298-311, March, 1986.

[2.23] K. Lau, A. Yariv, 'High-Frequency Current Modulation of Semiconductor Injection Lasers', Semiconductors and Semimetals, Vol. 22, Pt. B, Ch. 2, 1985.

[2.24] R. Lang, K. Kobayashi, 'External Optical Feedback Effects on Semiconductor Injection Laser Properties', IEEE Journ. Quant. El., Vol. 16, pp. 347-355, 1980.

[2.25] G. Agrawal, 'Line Narrowing in a Single-Mode Injection Laser Due to External Optical Feedback', IEEE Journ. Quant. El., Vol.20, pp. 468-471, 1984.

[2.26] Y. Suematsu, S. Arai, 'Integrated Optics Approach for Advanced Semiconductor Lasers', Proceedings of the IEEE, Vol. 75, pp. 1472-1487, Nov. 1987.

[2.27] M. Osinski, J. Buus, 'Linewidth broadening factor in semiconductor lasers - An overview', IEEE Journ. Quant. El., vol. 23, pp. 9-29, 1987.

[2.28] K. Vahala, L. Chiu, S. Margalit, A. Yariv, 'On the linewidth enhancement factor in semiconductor injection lasers', Appl. Phys. Lett., Vol. 42, pp. 631-633, Apr. 1983.

[2.29] C. Harder, J. Katz, S. Margalit, J. Shacham, A. Yariv, 'Noise equivalent circuit of a laser diode', IEEE Journ. Quant. El., Vol. 17, pp. 333-337, March, 1982.

[2.30] R. Olshansky, P. Hill, V. Lanzisera, W. Powazinik, 'Frequency Response of 1.3 μm InGaAsP High Speed Semiconductor Lasers', IEEE Journ. Quant. El., Vol. 23, pp.1410-1418, Sept. 1987.

[2.31] C. H. Henry, 'Theory of phase noise and power spectrum of a single mode injection laser', IEEE Journ. Quant. El., Vol. 19, pp. 1391-1397, 1983.

[2.32] G. Morthier, F. Libbrecht, K. David, P. Vankwikelberge, R. Baets, 'Theoretical investigation of the 2nd order harmonic distortion in the AM-response of 1.55 μm F-P and DFB-lasers', to be published in IEEE Journ. Quant. El.

[2.33] R. Tucker, D. Pope, 'Circuit modeling of the effect of diffusion damping in a narrow-stripe semiconductor laser', IEEE Journ. Quant. El., vol. 19, pp.1179-1183, July 1983.

[2.34] C. Su, 'Nonlinear gain caused by cavity standing wave dielectric grating as an explanation of the relationship between resonance frequency and damping rate of semiconductor diode lasers', Appl. Phys. Lett., Vol. 53, pp. 950-952, 1988.

[2.35] G. Morthier, 'Quantumfysische aspecten bij de modellering van halfgeleiders', M. Sc. thesis (in Dutch), University of Gent, 1987.

[2.36] D. Botteldooren, 'Theoretische studie van de optische eigenschappen van III-V halfgeleiders, quantumwells en superroosters', Ph. D. thesis (in Dutch), University of Gent, 1990.

[2.37] J. Dennis, D. Gay, R. Welsh, 'NL2SOL', ACM Transactions on Mathematical Software 7, pp. 369-383, 1981.

Chapter III

A NUMERICAL, LONGITUDINAL MODEL: 'CLADISS'

Translation of the longitudinal equations (2.2.48) and (2.2.70) and the boundary conditions ((2.2.75) and (2.2.77)) into an algorithm for numerical solution would result in a very powerful laser diode simulator. Such a laser simulator has been developped at the Laboratory for Electromagnetism and Acoustics in Gent and it is called CLADISS ('Compound Laser Diode Simulation Software'). As was already mentioned, a first basic version of CLADISS, capable of a single mode static and small-signal AC-analysis, has been developped by Dr. P. Vankwikelberge [3.1]. In the framework of this Ph. D. work, it has been cleared of bugs and extended to a multi mode model, which now also allows an analysis of the noise behaviour and of the harmonic distortion during modulation.

CLADISS can handle the analysis of Fabry-Perot lasers, C^3-lasers (Cleaved Coupled Cavity lasers), DFB lasers (including some more exotic types with a longitudinally varying grating amplitude or phase), DBR lasers and external cavity lasers. It consists of three separate modules: for the analysis of the static, the dynamic and the stochastic behaviour. Especially the fact that longitudinal spatial hole burning is included in a detailed way and the multi mode analysis in each module have made CLADISS to one of the most powerful and unique laser models that have been developed in the past years.

In this chapter, we review the implementation of each separate module in some detail. However, we must warn the reader that the review is rather of a descriptive nature and that some numerical algorithms are not fully worked out. Most algorithms are worked out theoretically in ref. [3.1] (even for the multi mode analysis). The extensions such as the analysis of the noise behaviour and the calculation of the distortion during modulation on the other hand have been given considerably more attention.

At the same time, illustrutative numerical examples are given for each module. We conclude this chapter by comparing CLADISS to other existing laser models.

III.1 The analysis of the static behaviour

This analysis aims at calculating quantities such as the total output power and the central wavelength of each line in the optical spectrum, and this for a given static current injection. The laser is assumed to have reached a static (time-independent) regime in this case and all derivatives with respect to the time are thus neglected. Langevin forces, which determine the fluctuations in the output power or the lineform of each line, are not included either. However, when equations (2.2.29) are used, as will be the case for the analysis of the static behaviour, care must be taken to include the average spontaneous emission, coupling into the modes.

It is convenient to distinguish between two parts in the analysis: a threshold analysis and an above-threshold DC analysis. The threshold analysis serves to investigate at which current levels (the threshold currents) a transition from amplifier operation to oscillator operation of the laser occurs. At the same time, the wavelength of the main longitudinal modes and an estimate of the side mode suppression follow from the analysis.

Different approximations and numerical techniques are introduced in both analysises and a separate description of each analysis will be given.

III.1.1 The threshold analysis

The transition from amplifier to oscillator operation takes place when the population inversion in the active layer provides an amount of stimulated emission, sufficient to compensate for the absorption and mirror loss. However, in this situation, the presence of even the slightest photon density will deplete the carrier density and decrease the stimulated emission again below the loss. Oscillator operation then only is possible if no light propagates inside the cavity. In practice, there is no real laser operation in this case and the output power merely consists of amplified spon-

taneous emission. Laser operation begins for current levels immediately above the threshold currents however.

In the theoretical threshold analysis, one must neglect the stimulated emission rate in the carrier rate equation, the power dependence of the gain and the spontaneous emission in the coupled wave equations. The carrier rate equation in a section v with a uniform waveguide geometry and a uniform injection then reduces to:

$$\frac{\eta_v J_v}{q d_v} = \frac{N}{\tau_v} + B_{0v} N^2 + C_{0v} N^3 \qquad (3.1.1)$$

and the (uniform) carrier density is easily found for a given uniform current density J_v (e.g. from Cardano's formula). Equations (2.2.29), in which the Langevin forces and the time dependences are ignored, can be solved for this uniform carrier density and for a uniform grating (i.e. with a constant phase and amplitude):

$$\begin{pmatrix} R_m^+(z) \\ R_m^-(z) \end{pmatrix} = \begin{pmatrix} a_{11}^m(z-z_0) & a_{12}^m(z-z_0) \\ a_{21}^m(z-z_0) & a_{22}^m(z-z_0) \end{pmatrix} \begin{pmatrix} R_m^+(z_0) \\ R_m^-(z_0) \end{pmatrix}$$

with: $a_{11}^m(z) = \cosh(\Delta_m z) - j \frac{\Delta\beta_m}{\Delta_m} \sinh(\Delta_m z)$

$$a_{22}^m(z) = \cosh(\Delta_m z) + j \frac{\Delta\beta_m}{\Delta_m} \sinh(\Delta_m z)$$

$$a_{12}^m(z) = \frac{\kappa_{FB}}{\Delta_m} \sinh(\Delta_m z) \; ; \; a_{21}^m(z) = -\frac{\kappa_{BF}}{\Delta_m} \sinh(\Delta_m z)$$

and: $(\Delta_m)^2 = -[\,(\Delta\beta_m)^2 + \kappa_{FB}\kappa_{BF}\,]$ (3.1.2)

$\Delta\beta_m$, as given in (2.2.15) and (2.2.30a) is now a function of the carrier density and of the wavelength.

Equations (3.1.1) and (3.1.2), together with the boundary conditions (2.2.75)-(2.2.77) can be used to develop a numerical threshold algorithm. To this end, we consider a general multi-section laser as shown in fig. 3.1. For a multi-section laser, it is assumed that the currents injected into the different sections depend linearly on an independent current I_v, injected into the section v. For a given current I_v and a given wavelength, it is then possible to

calculate the Bragg deviation $\Delta\beta$ and the a_{ij}-coefficients in each section.

In practice, a point z_v in the middle of the section v is chosen and the field reflections ρ_L and ρ_R of the left and the right part of the laser cavity are calculated at z_v for a given injection and a given wavelength λ. An oscillation can now be defined as the state where the product $\rho_L\rho_R$ (which is called the roundtrip gain as it denotes the field gain after one roundtrip in the cavity) equals one. The field reflectivities ρ_L and ρ_R can be derived from the propagator matrices (3.1.2),which must be transformed into relations between the fields $E^{\pm}$, and the matrices (2.2.75), expressing the boundary conditions. One can write:

$$\rho_L = \frac{\rho_f (F_L)_{11} + (F_L)_{12}}{\rho_f (F_L)_{21} + (F_L)_{22}} \quad , \quad \rho_R = \frac{(F_R)_{21} + \rho_b (F_R)_{22}}{(F_R)_{11} + \rho_b (F_R)_{12}} \tag{3.1.3}$$

where the propagator matrices F_L and F_R are defined by:

$$\begin{pmatrix} E^+(z_v) \\ E^-(z_v) \end{pmatrix} = F_R \begin{pmatrix} E^+(L) \\ E^-(L) \end{pmatrix}, \quad \begin{pmatrix} E^+(z_v) \\ E^-(z_v) \end{pmatrix} = F_L \begin{pmatrix} E^+(0) \\ E^-(0) \end{pmatrix} \tag{3.1.4}$$

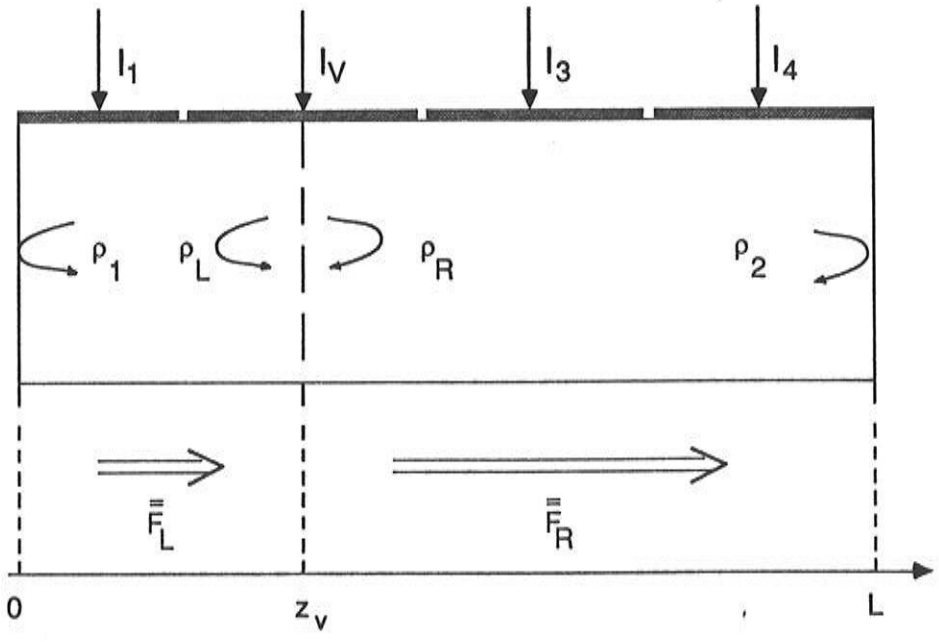

Fig. 3.1: Division of a laser in 2 parts for the calculation of the roundtrip gain.

The determination of the threshold current and of the wavelength of the main modes proceeds as follows. Initially, an estimate of the threshold current I_v and of the wavelength λ_0 of the main mode must be chosen. For this value of I_v, the roundtrip gain is calculated for a wide range of wavelengths around λ_0. The values of the roundtrip gain are subsequently scanned to check whether a resonance occurs. If this is not the case, the current is gradually increased (if all points with zero phase, i.e. if all longitudinal modes, have an amplitude below one) or decreased (if a point with zero phase and an amplitude above one exists) until at least one wavelength gives a zero phase and an amplitude of one. This defines the threshold current, as well as the wavelength λ_m of the most important longitudinal modes.

As an illustration, the complex roundtrip gain at threshold is shown in fig. 3.2 for a 300 μm long DFB laser (laser A) with $\kappa L=1.5$ and with facet reflectivities $\rho_f = 0.566\ e^{j\pi}$ and $\rho_b = 0.224\ e^{j3\pi/2}$. Other parameters are listed in table III.1. The threshold current has the value 21.5 mA in this case. Both the main (lasing) mode and the most important side mode are indicated by an arrow in fig. 3.2.

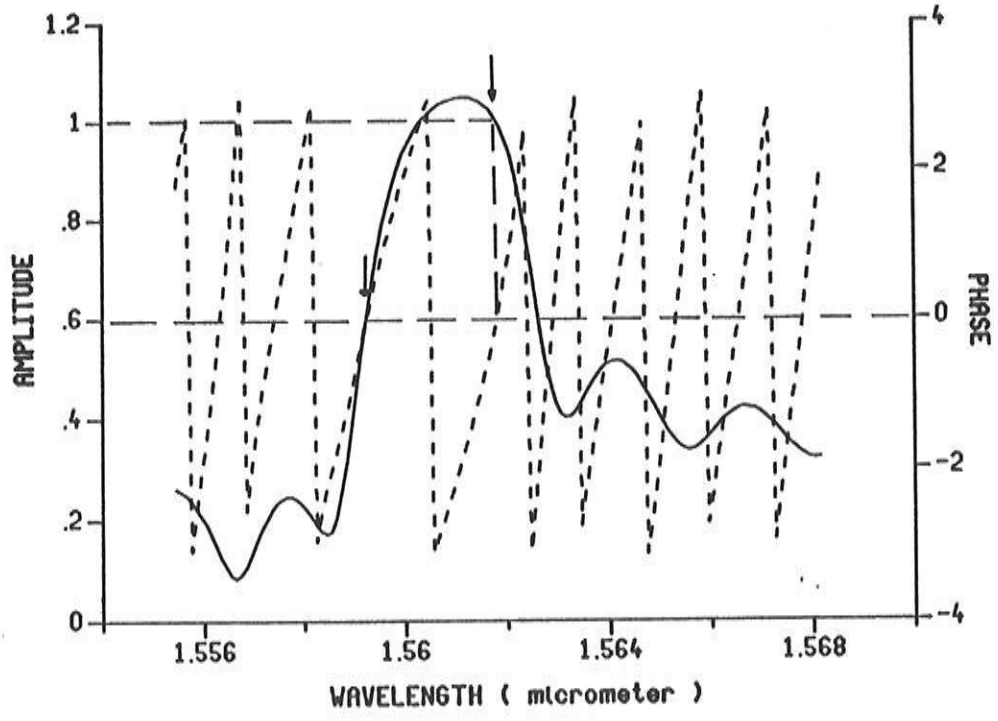

Fig. 3.2: roundtrip gain at threshold for laser A.

The roundtrip gain of the side mode could be considered as a measure for the side mode suppression. A more conventional quantity however is given by the difference in threshold gain ΔgL between main and side mode. This is the difference between the normalized gain g_1L at the threshold current and the gain g_2L for which the side mode starts lasing. For the laser A, this quantity ΔgL has the value 0.25, a value which is generally regarded as guaranteeing a large side mode suppression [3.4], [3.5].

Parameter		Typical value	
w	[μm]	1.5	Stripe width
d	[μm]	0.12	Thickness active layer
Γ		0.5	Confinement factor
L	[μm]	300	Laser length
L	[μm]	0.2413	Grating period
n_e		3.25	Effective refractive index of the unperturbed waveguide
η		0.8	Injection efficiency
τ	[s]	$5.\ 10^{-9}$	Carrier lifetime
B_0	[$\mu m^3/s$]	100	Bimoleculaire recombination
C_0	[$\mu m^6/s$]	$20\ 10^{-5}$	Auger recombination
β_{sp}		10^{-4}	Spontaneous emission factor
n_{sp}		2.	Inversion factor
α_{int}	[μm^{-1}]	$50.\ 10^{-4}$	Internal absorption loss

TABLE III.1

III.1.2 The DC analysis

Above threshold, one can no longer neglect the stimulated emission rate in the carrier rate equation or the power dependence of the gain. Since the optical power is generally not uniform in the longitudinal direction, it follows that a non-uniform carrier densi-

ty (and hence a non-uniform Bragg deviation) might exist in the cavity. Furthermore, one must also include the static contribution from the spontaneous emission. The equations (2.2.29) should therefore be changed into:

$$\frac{\partial R_m^+}{\partial z} + \left\{ j\Delta\beta_m - \frac{S_m}{4L\,|R_m^+|^2} \right\} R_m^+ = \kappa_{FB}\, R_m^-$$

$$-\frac{\partial R_m^-}{\partial z} + \left\{ j\Delta\beta_m - \frac{S_m}{4L\,|R_m^-|^2} \right\} R_m^- = \kappa_{BF}\, R_m^+ \qquad (3.1.5)$$

It can be seen that the spontaneous emission manifests itself as a non-linearity and an exact solution of the coupled wave equations is now no longer possible.

The z-dependence of the Bragg deviation and the spontaneous emission can be taken into account by dividing the cavity in a large number of small segments (with length l_v in a section v), as is illustrated in fig. 3.3. The carrier rate equation and the coupled wave equations can be solved approximately in such small segments (which typically must be a few μm long). We further assume the expression (2.2.53), with β_{sp} being an input parameter, for the spontaneous emission rate S_m, although it must be noted that the expression (2.2.52) is just as valid.

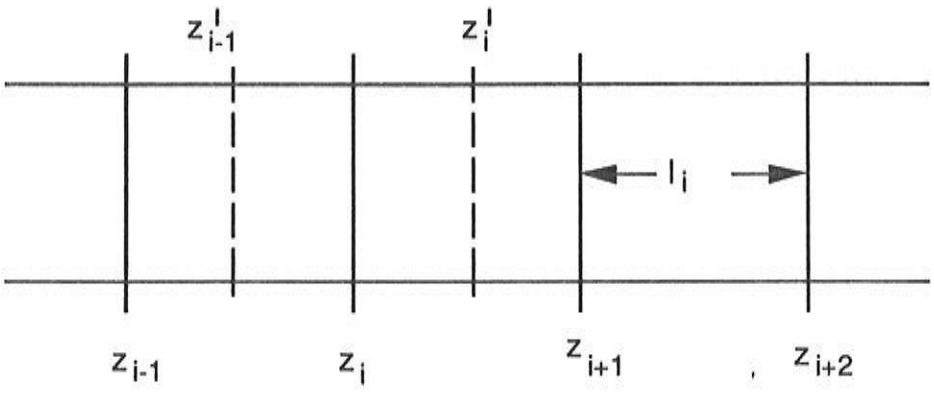

Fig. 3.3: Division of a laser into small sections
z_i : discretisation points for the fields
z'_i : discretisation points for the carrier density

III.1.2.1 Solution in a small section

For small segments, we can approximate both the carrier density N and the optical powers by constants with a value equal to their value in the middle of the segment (at z'_i). The optical powers can thereby be obtained as the average of the power levels at z_i and z_{i+1}, e.g.

$$P_m^{\pm}(z_i') = \frac{1}{2}\{ |R_m^{\pm}(z_i)|^2 + |R_m^{\pm}(z_{i+1})|^2 \} \qquad (3.1.6)$$

For a uniform carrier density and uniform powers, the approximate solution of (3.1.5) reduces to:

$$\begin{pmatrix} R_m^+(z_{i+1}) \\ R_m^-(z_{i+1}) \end{pmatrix} = s_c(l_i) \begin{pmatrix} a_{11}'(l_i) & a_{12}'(l_i) \\ a_{21}'(l_i) & a_{22}'(l_i) \end{pmatrix} \begin{pmatrix} R_m^+(z_i) \\ R_m^-(z_i) \end{pmatrix}$$

with: $s_c(l_i) = \exp\left\{ \frac{S_m l_i}{8L} \left(\frac{1}{P_m^+(z_i')} - \frac{1}{P_m^-(z_i')} \right) \right\}$

and: $a_{ij}' = a_{ij}$ in which $j\Delta\beta_m$ is replaced by :

$$j\Delta\beta_m - \frac{S_m}{8L} \left(\frac{1}{P_m^+(z_i')} + \frac{1}{P_m^-(z_i')} \right) \qquad (3.1.7)$$

The propagator matrix now obviously depends on the resulting fields through $P^{\pm}_m(z'_i)$ and an accurate solution can be achieved only after iteration. E.g. as a first approximation, one can replace the carrier density and the optical powers at z'_i by their value at z_i. Substitution of these values in (3.1.7) yields better estimates for the fields at z_i. This then allows the determination of more accurate values for the carrier density and the optical powers at z_i, which in turn lead to more accurate values for the fields at z_i. This iteration can be repeated until further iterations no longer result in significant changes (typically, only about 5 iterations are needed).

However, care must be taken in a segment, next to a front facet with zero (or small) reflectivity. The first approximation for the optical powers (as defined above) would result in singularities

in this case. The laser model CLADISS automatically introduces a better approximation for $P^{+}_{m}(z'_i)$:

$$P^{+}_{m}(z_i') = \frac{S_m h\omega_m I_i}{2L} \qquad (3.1.8)$$

III1.2.2 Self-consistent determination of the laser state

The field quantities and the carrier density in each point along the longitudinal axis can be determined completely if proper values for the fields at the front facet and for the wavelengths are chosen. More specificly, a value for λ_m and $R^{-}_{m}(z=0)$ (or $R^{+}_{m}(z=0)$, both quantities are related by the boundary condition (2.2.77)) must be chosen for each longitudinal mode m under consideration. We notice that all quantities $R^{-}_{m}(z=0)$ can be considered as real numbers. This is justified by the absence of any phase relation between the different modes (as a result of the time averaging (2.2.24)) and by the fact that, at least for the static regime, the time origin can be chosen arbitrarely.

Assume that q longitudinal modes are included in the calculations. The 2q values for λ_m and $R^{-}_{m}(z=0)$ then allow to determine the fields at the right facet z=L, where the boundary condition must be fulfilled. This boundary condition actually constitutes a complex equation which, for the case of q modes, gives 2q real equations, which the 2q choices of λ_m and $R^{-}_{m}(z=0)$ (m=1,q) must obey. These non-linear equations can be solved by the Newton-Raphson method [3.6].

The complete algorithm can be explained as follows. One chooses initial estimates for λ_m and $R^{-}_{m}(z=0)$. With these values, the fields are propagated subsequently along the small segments (as explained in 1.2.1), until to the right laser facet is reached. At the same time, the derivatives of the fields with respect to λ_m and $R^{-}_{m}(z=0)$ are propagated as well. The resulting system of equations at the right facet and its jacobian can thus be calculated numerically and, if necessary, better approximations for λ_m and $R^{-}_{m}(z=0)$ can be derived by means of the Newton-Raphson algorithm. The iteration can continue until sufficient accuracy has been reached. It must be noticed here that the propagation of the field deriva-

tives can proceed in a very similar way as the field propagation; mainly as a result of the analytical expression for the field propagation over a small segment. (For more details, we refer to [3.1]).

Output facilities of the DC-model include the variation of the output power or the wavelength of several longitudinal modes as a function of the injected currents, as well as the longitudinal variation of the optical power, of the carrier density, the refractive index or the Bragg deviation at a certain bias level. As an illustration, we have shown the longitudinal variation of the power in the main mode (fig. 3.4) and of the carrier density (fig. 3.5) for the laser A. The injected current is chosen so as to obtain an output power of 1 mW.

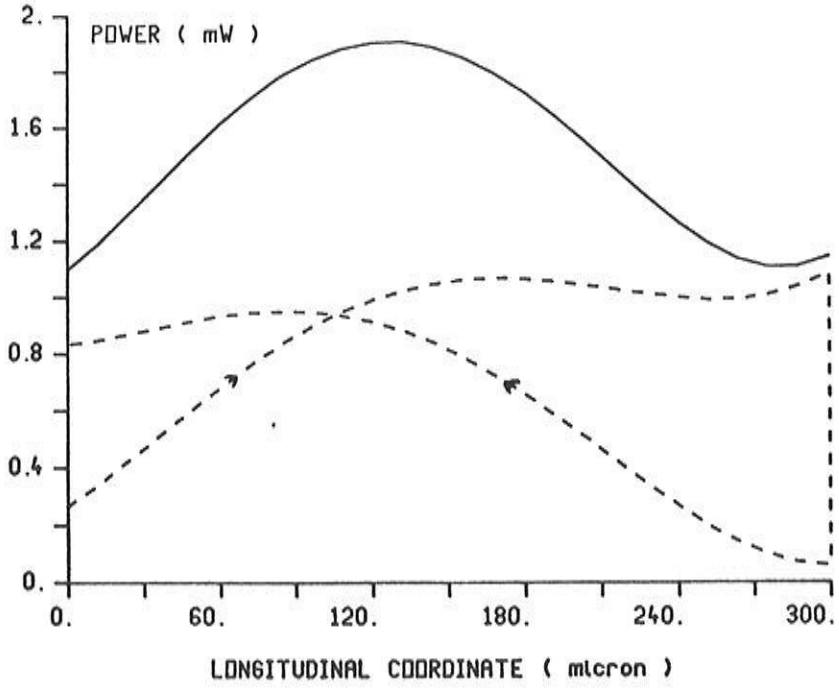

Fig.3.4: Longitudinal variation of the optical power in the main mode for laser A at 1 mW output power.

The DC-analysis furthermore allows to control whether the side modes start lasing at a certain power levels. Two methods can be followed. A first method is to include several modes in the analysis and to calculate the power in each mode for increasing injec-

tion. The lasing of a side mode can be observed as a kink in the power-current relation in this case. The rise of a side mode can even be seen if only the main mode is included in the calculations. In this case, one can calculate the roundtrip gain vs. the wavelength at different bias levels and check whether the roundtrip gain of the side mode reaches one. The roundtrip gain above threshold is calculated in an identical way as the roundtrip gain at threshold, although the gain suppression and the non-uniform carrier density must be taken into account. This implies that many small sections ought to be used now.

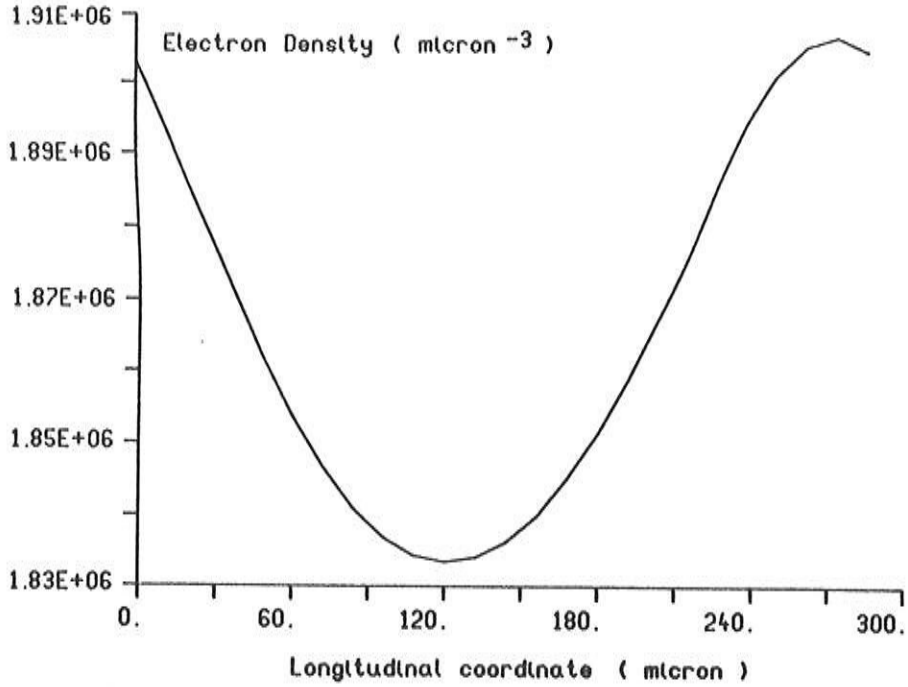

Fig.3.5: Longitudinal variation of the carrier density for laser A at 1 mW output power.

III.2 Analysis of the dynamic behaviour

The noise sources are still ignored in the analysis of the dynamic behaviour. However, the analysis now is based on solution of the equations (2.2.48b), (2.2.69) and (2.2.70), in which the derivatives with respect to time are taken into account as well. We thereby recall that equation (2.2.69), without the Langevin forces, describes the evolution of the statistically averaged field amplitudes.

III.2.1 Assumptions

The analysis is restricted to sinusoidal regimes, i.e. the injected current densities are expressed as:

$$J_v(t) = J_{v0} + \mathrm{Re}\{ J_{v1} e^{j\Omega t} \} \qquad (3.2.1)$$

with J_{v0} being the static current density and J_{v1} the sinusoidal current density, injected into the section v. The periodic excitation makes the assumption of a periodic response plausible and we express the field quantities and the carrier densities as:

$$r_m^{\pm}(z,t) = r_{m0}^{\pm}(z) + \mathrm{Re}\left\{ \sum_{k=1}^{\infty} r_{mk}^{\pm}(z,k\Omega)\, e^{jk\Omega t} \right\}$$

$$\varphi_m^{\pm}(z,t) = \varphi_{m0}^{\pm}(z) + \mathrm{Re}\left\{ \sum_{k=1}^{\infty} \varphi_{mk}^{\pm}(z,k\Omega)\, e^{jk\Omega t} \right\}$$

$$N(z,t) = N_0(z) + \mathrm{Re}\left\{ \sum_{k=1}^{\infty} N_k(z,k\Omega)\, e^{jk\Omega t} \right\}$$

$$\Delta\omega_m(t) = \mathrm{Re}\left\{ \sum_{k=1}^{\infty} \Delta\omega_{mk}(k\Omega)\, e^{jk\Omega t} \right\} \qquad (3.2.2)$$

The terms with subscript 0 obviously represent the static solution, whereas the other terms denote deviations from the static solution, caused by the sinusoidal currents.

It can be remarked that (3.2.2) does not include alll possible solutions of the dynamic laser equations. Indeed, due to the nonlinearity of these equations, a periodic excitation does not necessarily imply a periodic respons with the same period. In fact, responses with different period (e.g. period doubling) and non-periodic responses (e.g. patterning effects) have already been observed experimentally [3.7]. Such effects nevertheless tehd to appear for large modulation currents and at high modulation frequencies. We therefore restrict ourselves to relatively small modulation depths, for which the expansion (3.2.2) can be used. The terms with subscript 1 then represent the linear or small-signal modulation re-

sponses, while the terms with higher subscript are an indication for the harmonic distortion.

It must finally be noted that the time dependent parts of the field phases and of the optical frequencies are not uniquely defined. As a matter of fact, it is actually possible to assign a z-dependent frequency to both the forward and backward propagating waves, according to:

$$\omega_m^{\pm}(z,t) = \omega_{m0} + \mathrm{Re}\left\{ \sum_{k=1}^{\infty} (\Delta\omega_{mk}(k\Omega) + jk\Omega\varphi_{mk}^{\pm}(z,k\Omega))\, e^{jk\Omega t} \right\} \qquad (3.2.3)$$

This ambiguity is removed in CLADISS by requiring $\varphi^{-}_{mk}(z=0,k\Omega)$ to be zero for all m and k. The frequency then denotes the frequency of the light that leaves the laser at the front facet. Up to frequencies of several tens of GHz, this frequency is nearly identical to that defined in (2.3.3) (i.e. the phase has a negligible influence), so that our definition can safely be regarded as 'the' optical frequency.

III.2.2 Approximations and algorithm

We restrict the sums in (3.2.2) to the first three terms, which is acceptable for sufficiently small modulation depths. As a matter of fact, it follows both from experiments [3.8] and theory [3.9] that the terms with index k are proportional with the k-th power of the modulation depth.

The laser equations are solved by substitution of the expansions (3.2.2), whereby the exp(jkΩt)-time variation removes the derivatives with respect to the time. Multiplication of the resulting equations with exp(-jkΩt) and integration over the period corresponding with Ω leads to separate equations for the terms with index k. The separate equations for the terms with index 1 can be written under the form of a matrix equation (i.e. X_k, B_k and A are matrices) as:

$$\frac{dX_1(z,\Omega)}{dz} = A(z,\Omega)\, X_1(z,\Omega) + B_1(J_{v1},z,\Omega)$$

$$\text{with } X_k^T(z,\Omega) = [(\Delta\omega_{mk}, r_{mk}^{+}, r_{mk}^{-}, \varphi_{mk}^{+}, \varphi_{mk}^{-}),\ m=1,q] \qquad (3.2.4)$$

with q being the total number of modes taken into account. For the terms with index 2 or 3, the equations have a similar form:

$$\frac{dX_2(z,2\Omega)}{dz} = A(z,2\Omega)\, X_2(z,2\Omega) + B_2(z,2\Omega,X_1) \qquad (3.2.5a)$$

$$\frac{dX_3(z,3\Omega)}{dz} = A(z,3\Omega)\, X_3(z,3\Omega) + B_3(z,3\Omega,X_1,X_2) \qquad (3.2.5b)$$

As can be seen, the homogeneous parts of the equations (3.2.4) and (3.2.5) are identical, except for the frequency to be used. The equations for $d\Delta\omega_{mk}/dz$, included in (3.2.4) and (3.2.5) are the trivial identities $d\Delta\omega_{mk}/dz=0$.

We will not give the equations (3.2.4) and (3.2.5) in any further detail because they are too extended. Their derivation is nonetheless straightforward. By applying finite differences with the same longitudinal discretisation scheme as in the DC analysis, the equations (3.2.4) and (3.2.5) can be transformed into a set of linear algebraic equations:

$$2\,\frac{X_k(z_{i+1},k\Omega) - X_k(z_i,k\Omega)}{z_{i+1} - z_i} = \text{right memb. at } z_i + \text{right memb. at } z_{i+1} \qquad (3.2.6)$$

The discretised equations, together with the boundary equations can now be solved by standard techniques. The simulator CLADISS uses the ACM software package COLROW, which decomposes the system matrix into triangular matrices [3.10]

The dependence of X_2 on X_1 and of X_3 on X_1 and X_2 defines the order in which the equations must be solved. First, the equations for the first order quantities, which can be obtained also by linearisation of the laser equations and of the boundary equations, and consecutively the equations for the second and third order quantities must be solved.

The AC analysis allows to calculate the small signal FM- (Frequency Modulation) and IM- (Intensity Modulation) response as a function of the modulation frequency $\Omega/2\pi$, as well as the 2nd and 3rd order harmonic distortion in the FM- and IM-response. The exact definitions of these characteristics are given below in table

III.2. An example of the AC-analysis is given in fig.3.6, which depicts the amplitude and the phase of the FM-response vs. the modulation frequency for laser A at different bias points and for a modulation current of 1mA.

$\frac{\Delta\omega_{m1}(\Omega)}{2\pi}$	: FM–response for mode m
$\frac{\Delta\omega_{mk}(k\Omega)}{\Delta\omega_{m1}(\Omega)}$	: k–th order harmonic distortion in the FM–response of mode m
$(1-\lvert\rho_f\rvert^2)\, 2r^-_{m0}(0)r^-_{m1}(0,\Omega)$	: IM–response for mode m at left facet
$\frac{2r^-_{m0}(0)r^-_{m2}(0,2\Omega)+(r^-_{m1}(0,\Omega))^2}{4\, r^-_{m0}(0)r^-_{m1}(0,\Omega)}$	: 2nd order harmonic distortion in the IM–response at the left facet
$\frac{1}{4}\left(\frac{r^-_{m3}(0,3\Omega)}{r^-_{m1}(0,\Omega)}+\frac{r^-_{m2}(0,2\Omega)}{r^-_{m0}(0)}\right)$	: 3rd order harmonic distortion in the IM–response at the left facet
$(1-\lvert\rho_b\rvert^2)\, 2r^+_{m0}(L)r^+_{m1}(L,\Omega)$	: IM–response for mode m at right facet
$\frac{2r^+_{m0}(L)r^+_{m2}(L,2\Omega)+(r^+_{m1}(L,\Omega))^2}{4\, r^+_{m0}(L)r^+_{m1}(L,\Omega)}$	: 2nd order harmonic distortion in the IM–response at the right facet
$\frac{1}{4}\left(\frac{r^+_{m3}(L,3\Omega)}{r^+_{m1}(L,\Omega)}+\frac{r^+_{m2}(L,2\Omega)}{r^+_{m0}(L)}\right)$	: 3rd order harmonic distortion in the IM–response at the right facet

Table III.2

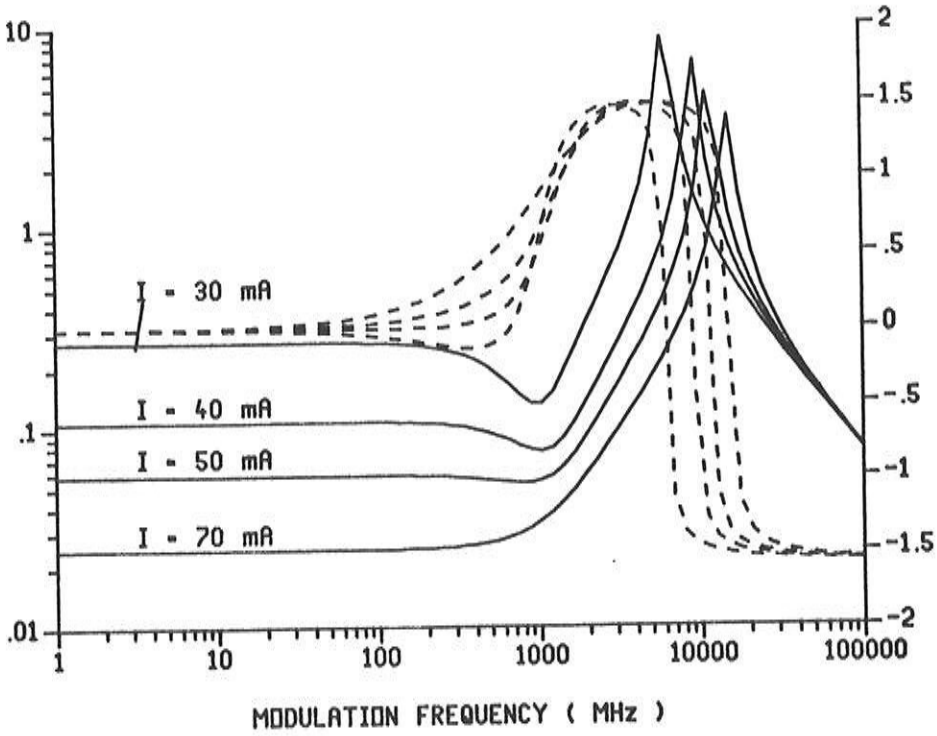

Fig. 3.6: Amplitude (——) and phase (--) of the FM-response of laser A.

III.3 Analysis of the noise behaviour

We restrict the analysis here to situations with static injection only. The fluctuations, mainly caused by spontaneous emission, are nevertheless time dependent and we must use the time-dependent equations (2.2.48b), (2.2.69) and (2.2.72). The Langevin forces, which represent the noise sources, can thereby be regarded as time dependent excitations with a small amplitude.

The small amplitude of these Langevin forces will in general result in small fluctuations of the field amplitudes and phases and of the carrier density. Hence, a linearisation of the laser equations into these small fluctuations is justified. By defining the intensity fluctuations according to (2.2.68), the linearisation of the amplitude equations may even be considered as an exact procedure, as has been mentioned in chapter 2 (section 2.2.3). Anyway, the linearisation can be more generally justified (also for the phase

equations) by the small distortion in the FM- and IM-responses, which is usually found. In order to eliminate the derivatives with respect to the time, we now use the Fourier transform of the fluctuations, i.e. we use the expansions:

$$r_m^{\pm}(z,t) = r_{m0}^{\pm}(z) + \frac{1}{2\pi}\int_{-\infty}^{+\infty} d\Omega\, \Delta r_m^{\pm}(z,\Omega)\, e^{j\Omega t}$$

$$\varphi_m^{\pm}(z,t) = \varphi_{m0}^{\pm}(z) + \frac{1}{2\pi}\int_{-\infty}^{+\infty} d\Omega\, \Delta \varphi_m^{\pm}(z,\Omega)\, e^{j\Omega t}$$

$$N(z,t) = N_0(z) + \frac{1}{2\pi}\int_{-\infty}^{+\infty} d\Omega\, \Delta N(z,\Omega)\, e^{j\Omega t}$$

$$\Delta\omega_m(t) = \frac{1}{2\pi}\int_{-\infty}^{+\infty} d\Omega\, \Delta\omega_m(\Omega)\, e^{j\Omega t} \qquad (3.3.1)$$

The Langevin functions can be Fourier transformed in a similar way. Since they can be considered as stationary (i.e. for time differences of the order of 0.01 nsec. or more), it follows that their Fourier transforms at different Fourier frequencies are also uncorrelated. It can easily be shown that the correlation of the Fourier transforms of two Langevin functions $f_1(t)$ and $f_2(t)$, with the property (as in our case) that:

$$\langle f_1(t)\, f_2(t')\rangle = 2D_{12}\frac{1}{T}\left(1 - \frac{|t-t'|}{T}\right), \; |t-t'| < T$$

$$= 0 \qquad\qquad , \; |t-t'| > T \qquad (3.3.2)$$

,is given by:

$$\langle F_1(\Omega)\, F_2^{*}(\Omega')\rangle = 2D_{12}\, 2\pi\, \delta(\Omega-\Omega')\, \frac{4\sin^2\left(\frac{\Omega T}{2}\right)}{\Omega^2 T^2} \qquad (3.3.3)$$

As long as only the spectral components in a bandwidth of the order of a few tens of GHz are considered (for which ΩT is very small), the transformed second order moments are related to the original moments by a very simple relation. We will further restrict ourselves to this situation and ignore the sinc^2 -function.

III.3.1 Application of the small signal model

Substitution of the Fourier integrals in the small signal (linearised) laser equations, multiplication of the resulting equations with exp(-jΩt) and averaging over a long (theoretically an infinite) time results again in separate equations for the different spectral components of the fluctuations. The obtained system of equations is identical to that obtained in the small signal AC analysis, except that other non-homogeneous terms (i.e. the Fourier transforms of the Langevin functions in stead of the modulation currents) are now present. The system of small signal equations can, symbollically, be written as:

$$\mathcal{A}(\Omega)\,\mathcal{X}(\Omega) = \sum_i \mathcal{C}_i(\Omega)\,F_i(\Omega) \qquad (3.3.4)$$

The F_i represent the different, uncorrelated Langevin functions after Fourier transform and longitudinal discretisation. It can be remarked that the F_i can be obtained by integrating the original Langevin functions over the length of the small segments. It can then easily be proven that the Langevin functions referring to different segments are uncorrelated (the δ(z-z')-function is transformed into a discrete Kronecker delta). $\mathcal{X}(\Omega)$ is a column matrix, containing the fluctuations of the different variables in all discretisation points z_i. $\mathcal{A}(\Omega)$ represents the system matrix (which also appears in the small signal AC analysis) and the $\mathcal{C}_i(\Omega)$ are column matrices with which the Langevin functions have to be multiplied.

The linear character of (3.3.4) and the gaussian character of the Langevin forces allow to calculate the 2nd order moment of $\mathcal{X}(\Omega)$ readily as:

$$<\mathcal{X}(\Omega)\,\mathcal{X}^{\dagger}(\Omega')> = 2\mathcal{A}(\Omega)\left\{\sum_i \mathcal{C}_i(\Omega)\,\mathcal{C}_i^{\dagger}(\Omega)\,D_{ii}\right\}(\mathcal{A}^{\dagger}(\Omega))^{-1}\,\delta(\Omega-\Omega')$$

with D_{ii} being defined by:

$$<F_i(\Omega)\,F_i^{*}(\Omega')> = 2D_{ii}\,\delta(\Omega-\Omega') \qquad (3.3.5)$$

The spectrum of the FM-noise or the relative intensity noise (RIN) can be extracted from $<\mathcal{X}(\Omega)\,\mathcal{X}^{\dagger}(\Omega')>$. The spectrum of the FM-noise and the RIN are defined below in table III.3. The spectrum of

the FM-noise and of the RIN can be defined for each mode separately. In coherent communication systems, the presence of only one lasing mode is required and one then often considers the FM-noise and the RIN for this mode. Sometimes one also considers the relative noise in the overall intensity (sum of the intensities of all modes).

With the definitions: $\langle \Delta\omega_m(\Omega)\, \Delta\omega_m^*(\Omega') \rangle = 2D_{\Delta\omega,m}(\Omega)\, \delta(\Omega-\Omega')$

$\langle \Delta r_m^-(0,\Omega)\, \Delta r_m^{-*}(0,\Omega') \rangle = 2D_{r,m}^-(\Omega)\, \delta(\Omega-\Omega')$

$\langle \Delta r_m^+(L,\Omega)\, \Delta r_m^{+*}(L,\Omega') \rangle = 2D_{r,m}^+(\Omega)\, \delta(\Omega-\Omega')$

the FM–noise and the RIN can be defined as:

$$S_{\Delta\omega,m}(\Omega) = \frac{2D_{\Delta\omega,m}}{2\pi}$$: spectral density of the fluctuations in the pulsation ω_m of mode m.

$$S_{\Delta f,m}(\Omega) = \frac{S_{\Delta\omega,m}(\Omega)}{(2\pi)^2}$$: spectral density of the FM–noise for mode m.

$$S_{\Delta i,m}(\Omega) = \frac{2\, 2D_{r,m}^-}{\pi\, (r_{m0}^-(0))^2} = \frac{2\, 2D_{r,m}^+}{\pi\, (r_{m0}^+(L))^2}$$: spectral density of the relative intensity noise for mode m

$$S_{\Delta i}(\Omega) = \frac{2 \sum_{m=1}^{q} \{(r_{m0}^-(0))^2\, 2D_{r,m}^-\}}{\pi \left\{ \sum_{m=1}^{q} (r_{m0}^-(0))^2 \right\}^2}$$: overall relative intensity noise

TABLE III.3

III.3.2 Power spectrum and linewidth

It has been shown before that the power spectrum and its width (the linewidth) are mainly due to the fluctuations in the optical frequency of each mode [3.11]. We can therefore assume the fields, emitted at each laser facet, to be of the form:

$$E_m(t) = E_{0m} \exp\left\{ j\omega_{m0}t + j\int^t \Delta\omega_m(t')dt' \right. \qquad (3.3.6)$$

As in section II.3 , $\Delta\omega_m$ has a gaussian distribution and the relative power spectrum is thereby given as:

$$S_{\Delta P,m}(\omega) = \mathcal{F}\left\{ e^{j\omega_{m0}t}\, e^{-0.5 < \left(\int_0^\tau \Delta\omega_m(t')dt'\right)^2 >} \right\} \qquad (3.3.7)$$

in which $\mathcal{F}$ denotes the Fourier transform. The exponent can easily be calculated by inverse Fourier transform of the spectral density of the FM-noise:

$$< \left(\int_0^\tau \Delta\omega_m(t')dt'\right)^2 > = \frac{1}{2\pi}\int_0^\tau dt_1 \int_0^\tau dt_2 \int_{-\infty}^{+\infty} d\Omega\, S_{\Delta\omega,m}(\Omega)\, e^{j\Omega(t_1-t_2)} \qquad (3.3.8)$$

In CLADISS, the integration is performed numerically and the Fourier transforms are calculated with the help of FFT-routines [3.12]. In this way, one readily finds the detailed power spectrum, including possible relaxation oscillation peaks (see e.g. chapter 4). However, another option, based on a more simple approximation for the linewidth is also offered by CLADISS. The simple approximation assumes a white FM-noise, which, at not too low a power level, is justified. The spectrum of the FM-noise is usually constant up to ±1 GHz, while the linewidth is usually far below 1 GHz. The linewidth in this approximation is given by:

$$\Delta\nu_m = \frac{S_{\Delta\omega,m}(\Omega=0)}{2\pi} \qquad (3.3.9)$$

and one only needs to calculate the low frequency value of the FM-noise in this case.

As an example, we have shown the power spectrum of the main mode of laser A at 1 mW output power in fig. 3.7. The linewidth is 43.5 MHz.

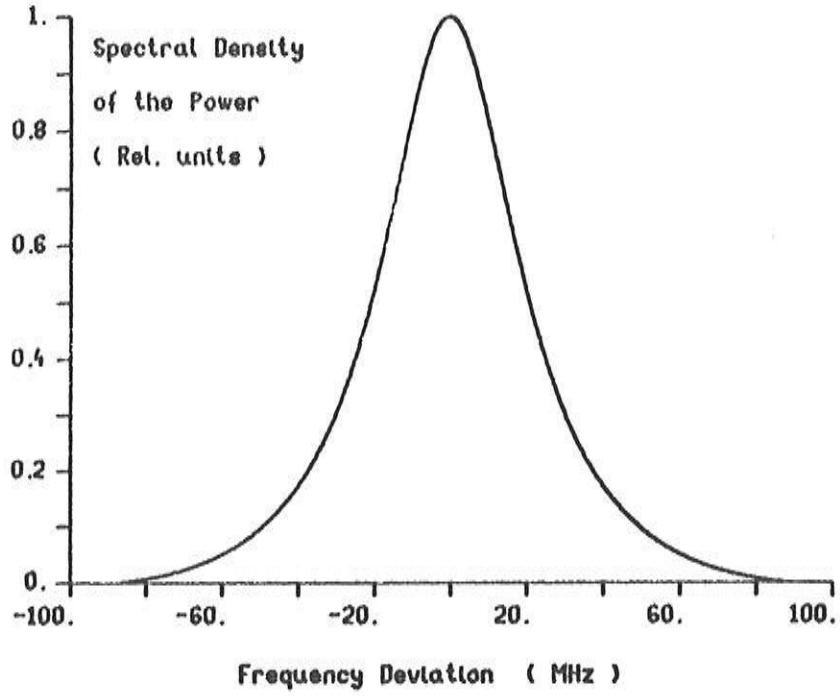

Fig. 3.7: Spectrum for the main mode of laser A at 1 mW.

III.4 Comparison of CLADISS with other existing models

The first longitudinal model for multi-section laser diodes, with or without distributed feedback, has been developped by Whiteaway et all. [3.13]. However, this model was (and still is) restricted to a static analysis, extended in some way for the calculation of the linewidth. Furthermore, this model can not really handle multi mode situations, neither does it include the gain suppression.

A model which takes into account dynamic aspects has been proposed by Tromborg et all. [3.14]. Their model however doesn't include spatial hole burning effects and as such one cannot really call it a longitudinal model. A similar model, which neither inclu-

des spatial hole burning, has been developped by Lowery [3.15]. Both models are often referred to as transmission line models.

All previous models neither allow to calculate the distortion.

CLADISS was the 'first ever' multi-mode model to take into account both longitudinal variations and dynamic effects, as well as noise sources. Particularly the inclusion of longitudinal spatial hole burning in the AC and noise analysis is unique. CLADISS should be considered as the ideal complement of a more theoretical approach based on analytical solution of the rate equations or the coupled wave equations. CLADISS doesn't make the analytical treatment worthless. In fact, the majority of the original results, presented here, were more or less initiated by analytical work.

One drawback of CLADISS is that explicit time-dependent phenomena such as the transient response can not be analyzed. This would require a model which solves the laser equations in the time domain. In contrast with CLADISS, this type of model on the other hand is hardly suited for the investigation of low-frequency phenomena, such as thermal effects or 1/f-noise.

References

[3.1] P. Vankwikelberge, 'Theoretische studie van statische en dynamische longitudinale effecten in Fabry-Perot en DFB-diodelasers', Ph. D. thesis (in Dutch), University of Gent.

[3.2] P. Vankwikelberge, G. Morthier, R. Baets, 'CLADISS, a longitudinal, multi mode model for the analysis of the static, dynamic and stochastic behaviour of diode lasers with distributed feedback', IEEE Journ. Quant. El., October 1990.

[3.3] P. Vankwikelberge, G. Morthier, K. David, R. Baets, 'CLADISS, a new diode laser simulator', Technical Digest Topical Meeting on Integrated Photonics Research, Hilton Head, March, 1990.

[3.4] J. Buus, 'Mode selectivity in DFB lasers with cleaved facets', Electron. Lett., Vol. 21, pp. 179-180, 1985.

[3.5] P. Mols, P. Kuindersma, W. Van Es, I. Baele, 'Yield and device characteristics of DFB lasers: statistics and novel coating design in theory and experiment', IEEE Journ. Quant. El., Vol.25, June, 1989.

[3.6] K. Rektorys, 'Survey of Applicable Mathematics', M.I.T. press, 1969.

[3.7] Y. Chen, H. Winful, J. Liu, 'Subharmonic bifurcations and irregular pulsing behavior of modulated semiconductor lasers', Appl. Phys. Lett., Vol. 47, pp. 208-210, August, 1985.

[3.8] A. Takemoto, H. Watanabe, Y. Nakajima, Y. Sakakibara, S. Kakimoto, H. Namizaki, 'Low harmonic distortion distributed feedback laser diode and module for CATV systems', Proc. of the Opt. Fiber Communications Conf. (OFC'90), San Francisco, p. 213.

[3.9] K. Lau, A. Yariv, 'Intermodulation distortion in semiconductor injection lasers', Appl. Phys. Lett., Vol. 45, pp. 1034-1036, 1984.

[3.10] 'Subroutine COLROW, Algorithm 603, ACM-Trans. Math. Software, Vol. 9, pp. 376-380, September, 1983.

[3.11] K. Vahala, A. Yariv, 'Semiclassical Theory of Noise in Semiconductor Lasers - Part I', IEEE Journ. Quant. El., Vol. 19, pp. 1096-1101, June, 1983.

[3.12] J. Nussbaumer, 'Fast Fourier Transform and Convolution Techniques', Springer-Verlag, New York, 1981.

[3.13] J. Whiteaway, G. Thompson, A. Collar, C. Armistead, 'The design and assessment of $\lambda/4$ phase-shifted DFB laser structures', IEEE Journ. Quant. El., Vol. 25, pp. 1261-1279, June, 1989.

[3.14] B. Tromborg, H. Olesen, X. Pan, S. Saito, 'Transmission line description of optical feedback and injection locking for Fabry-Perot and DFB lasers', IEEE Journ. Quant. El., Vol. 23, pp. 1875-1889, November, 1987.

[3.15] A. Lowery, 'A new dynamic semiconductor laser model based on the transmission line modelling method', IEE Proc., pt. J, Vol. 134, pp. 281-289, 1987.

Chapter IV

ASPECTS OF THE STATIC BEHAVIOUR: THE 'DSM' OPERATION OF DFB LASERS

In this chapter, we will concentrate on the mode discrimination in DFB lasers. This is of great interest in coherent optical communcations where the transmitter and local oscillator lasers must have a side mode suppression of at least 30 dB. Such lasers are called 'dynamic single mode' (DSM), as they remain single mode even if they are modulated . Here we discuss how some DFB lasers, which are single mode at low power levels can become multi mode at higher power levels due to longitudinal spatial hole burning. The influence of several laser parameters on this side mode onset is also reported.

The detrimental influence of spatial hole burning has led us to investigate possible new laser structures with a substantially reduced spatial hole burning. A variety of new, special laser structures have been discovered and therefore, a second major part of this chapter consists of descriptions of these special laser structures.

Other aspects of the static behaviour, such as the variation of the wavelength with the injected currents or the linearity of the L-I curve are not considered here. These topics are partly covered in the chapter 6 or, in the case of multi-section tunable devices, are beyond the scope of this work.

IV.1 Introduction: F-P lasers

The mirror losses in F-P lasers are equal for all modes and hence the mode discrimination can have its origin only in the wavelength dependence of the gain and the internal loss. In the following, we 'll always assume a constant internal loss $\alpha_{int}=50cm^{-1}$. The dispersion in the gain then remains as the only mode discriminating factor for F-P lasers.

From (2.3.13), it can be seen that the output power of the side modes is nearly constant above threshold and that the SMSR increases nearly proportional with the output power in the main mode. Although one must bear in mind that, due to the gain suppression, the dispersion in the gain may change with bias level, it can be argued that gain suppression only has a minor effect on the static behaviour. The above statements (with the words 'nearly' accounting for the gain suppression) are therefore still valid.

The difference in gain between the main mode and a side mode is largely determined by their wavelength difference. Indeed, the curvature of the g(λ)-curve is, for a given material, practically independent of the carrier density and thus of the threshold gain. The side mode suppression can thus be improved by an increase in the mode separation ($\Delta\lambda = \lambda^2/2n_eL$), i.e. by decreasing the laser length.

Parameter		Typical value	
w	[μm]	1.5	Stripe width
d	[μm]	0.12	Thickness active layer
Γ		0.5	Confinement factor
L	[μm]	300	Laser length
L	[μm]	0.2413	Grating period
n_e		3.25	Effective refractive index of the unperturbed waveguide
η		0.8	Injection efficiency
τ	[s]	$5.\ 10^{-9}$	Carrier lifetime
B_0	[$\mu m^3/s$]	100	Bimoleculaire recombination
C_0	[$\mu m^6/s$]	$20\ 10^{-5}$	Auger recombination
β_{sp}		10^{-4}	Spontaneous emission factor
n_{sp}		2.	Inversion factor
α_{int}	[μm^{-1}]	$50.\ 10^{-4}$	Internal absorption loss

TABLE IV.1

As an example, we consider a 300 μm long, as-cleaved F-P laser, of which the roundtrip gain at threshold is shown in fig. 4.1.1 and the output power in main and side modes as a function of the injected current in fig. 4.1.2. The laser parameters used in the calculation are given in table IV.1. To illustrate the capabilities of CLADISS, 5 modes have been included in the calculations. It can be remarked that the amplitude of the roundtrip gain is proportional with exp(gL) and thus fig. 4.1.1 gives an idea of the dispersion in the gain. Fig. 4.1.1 confirms that the power in the side modes remains constant above threshold. It also indicates that the SMSR in F-P lasers of reasonable length is usually well below 20 dB.

The SMSR and the output power in the side modes further depend on the spontaneous emission factor β_{sp}. This is illustrated in fig. 4.1.2, where the power in main and side mode for the same laser is also depicted for a different values (10^{-5}) of β_{sp}. The reduction of β_{sp} by a factor of 10 obviously causes an increase of the SMSR by 10 dB. From the same figure, it also follows that the threshold current (defined as the intercept of the steep line in fig. 4.1.2 with the x-axis) is independent of the value of β_{sp} and equals 14.5 mA here.

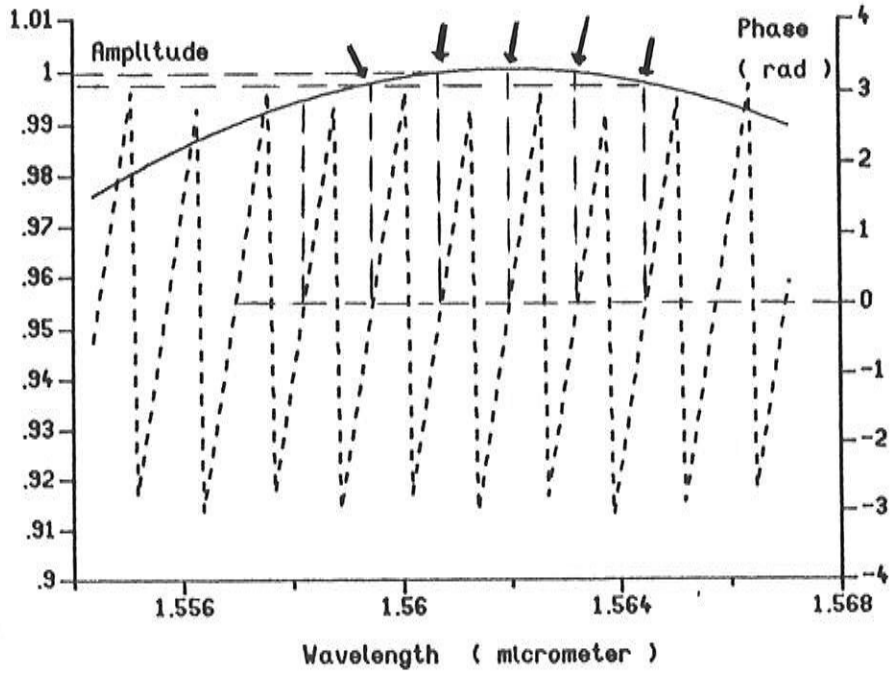

Fig. 4.1.1: Amplitude (—) and phase (--) of the roundtrip gain for a 300 μm long, cleaved F-P laser.

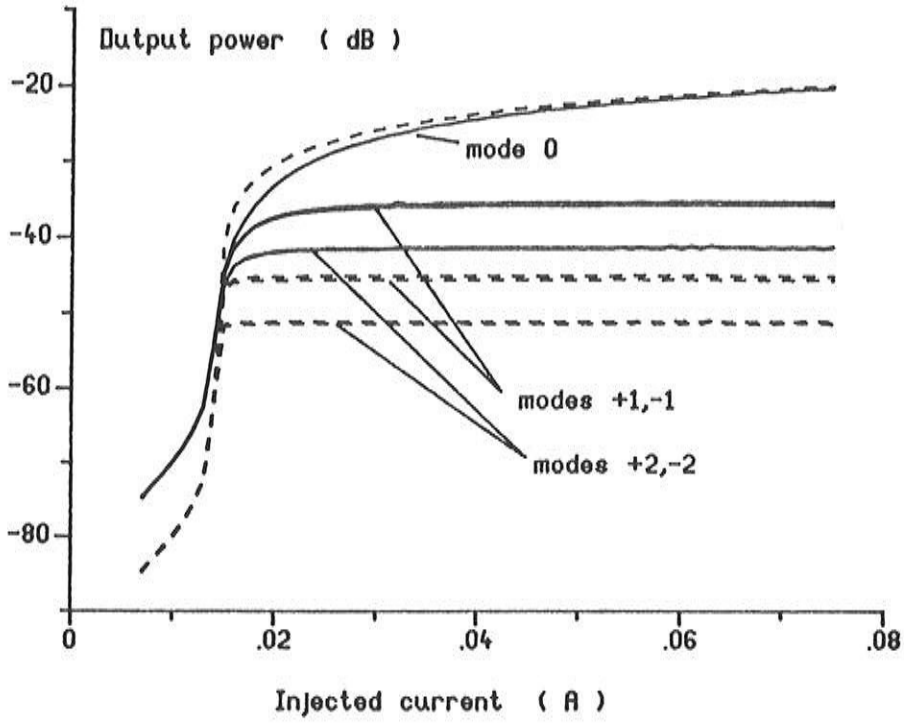

Fig.4.1.2: Output power of main and side mode vs. injected current for a 300 μm long, cleaved F-P laser. (--) : $\beta_{sp} = 10^{-5}$, (—) : $\beta_{sp} = 10^{-4}$

IV.2 Single mode properties of common DFB lasers

IV.2.1 The threshold gain difference ΔgL and associated yield

For DFB lasers, an estimate of the side mode suppression at low power levels can be obtained from the threshold gain difference ΔgL, according to formula (2.3.15). The value of ΔgL strongly depends on the laser structure under consideration and on the normalised coupling constant κL and varies from 0 for AR-coated lasers to more than 1 for some λ/4-shifted or gain coupled lasers. As outlined in chapter 2, a ΔgL value of 0.1 or more would (if spatial hole burning were absent) guarantee a single mode operation (with a SMSR of 30 dB) at ± 1mW output power.

For DFB lasers with partly reflecting facets, ΔgL also depends on the phase of the reflection coefficients. The current technology (i.e. the cleaving or etching processes) does not yet allow to control these phases and one can say that the reflection phases are distributed randomly among the different lasers grown on one wa-

fer. Hence, this random distribution of phases gives rise to a random distribution of ΔgL-values and a yield (the percentage of lasers with a ΔgL-value larger than a certain, predefined value) is therefore defined.

The yield has already been studied in very much detail (see e.g. [4.1], [4.2] and [4.3]). For later reference, we have depicted the yield as a function of ΔgL for 300 μm long, as-cleaved lasers with $\kappa L=2$ in fig.4.2.1. 16 values of the phases, uniformly distributed in the interval $[0,2\pi]$ have been considered for both facets.

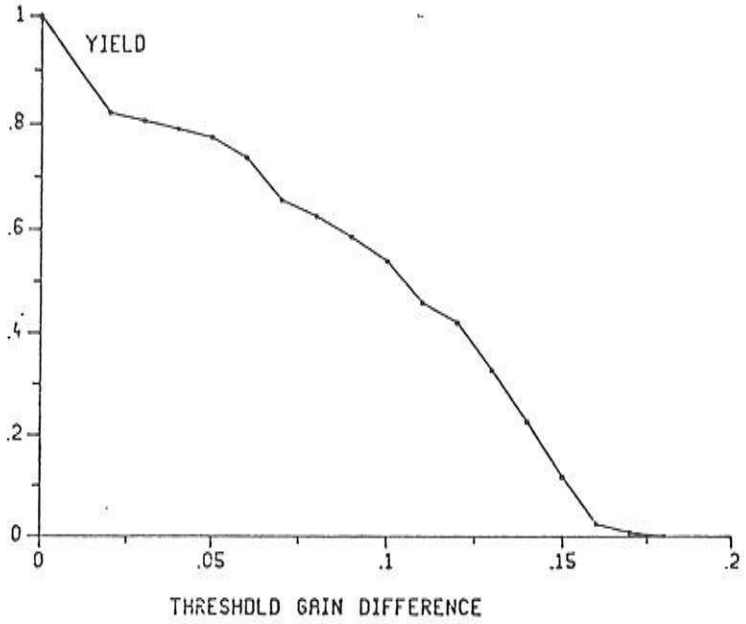

Fig.4.2.1: Yield of as-cleaved DFB lasers with L=300 μm and $\kappa L=2$.

IV.2.2 The onset of side modes at high power levels

IV.2.2.1 Examples and physical explanation

A DFB laser with a relatively high ΔgL-value and being single mode at low power levels can become multi mode at moderate or high power levels due to spatial hole burning [4.4]. We first illustrate this by an example.

To this end, we consider a 600 μm long laser (which for future reference we call laser B) with a κL-value of 3 and with the field reflectivities of the facets being given by $\rho_f = 0.566\, e^{j\pi}$ and

ρ_b = 0.224 $e^{j3\pi/2}$. The parameters are identical to those of table IV.1. Fig. 4.2.2 shows the complex roundtrip gain at threshold of this laser, which has a threshold current of 39.6 mA and a threshold gain difference between main and first side mode of 0.25. In spite of this large ΔgL-value, one finds that the side mode reaches the threshold at 70 mA, corresponding with an ex-facet power of 2 mW (fig. 4.2.3). This side mode onset is also visible on the wavelength dependence of the roundtrip gain calculated at 70 mA, displayed in fig. 4.2.4. From this figure, it should also be clear that all other side modes remain well suppressed. Spectral hole burning has not been taken into account in the previous calculated results.

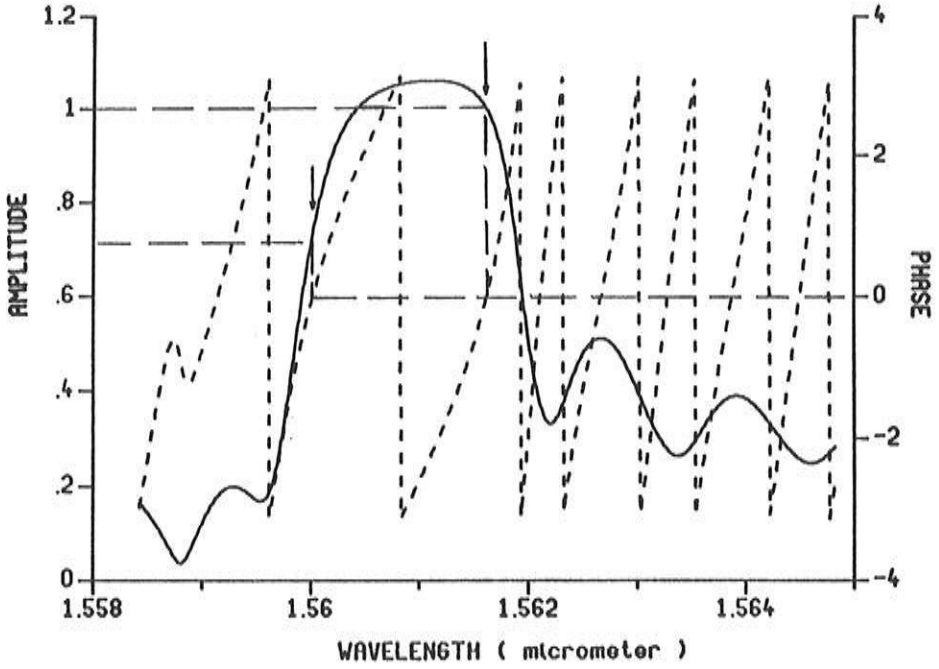

Fig.4.2.2: Amplitude (—) and phase (---) of the roundtrip gain of laser B at threshold.

Evidence for spatial hole burning (i.e. the variation of the carrier density due to the variation of the power) being the cause of the side mode onset can be given as follows. The z-dependence of the carrier density implies that the effective refractive index n_e, the Bragg wavelength ($\lambda_B=2n_e\Lambda$) and the real part of the Bragg deviation $\Delta\beta_r$ also become z-dependent. The reflection losses however depend on $\Delta\beta_r$ and, since the last quantity assumes various values along the z-axis, become less dependent on the wavelength.

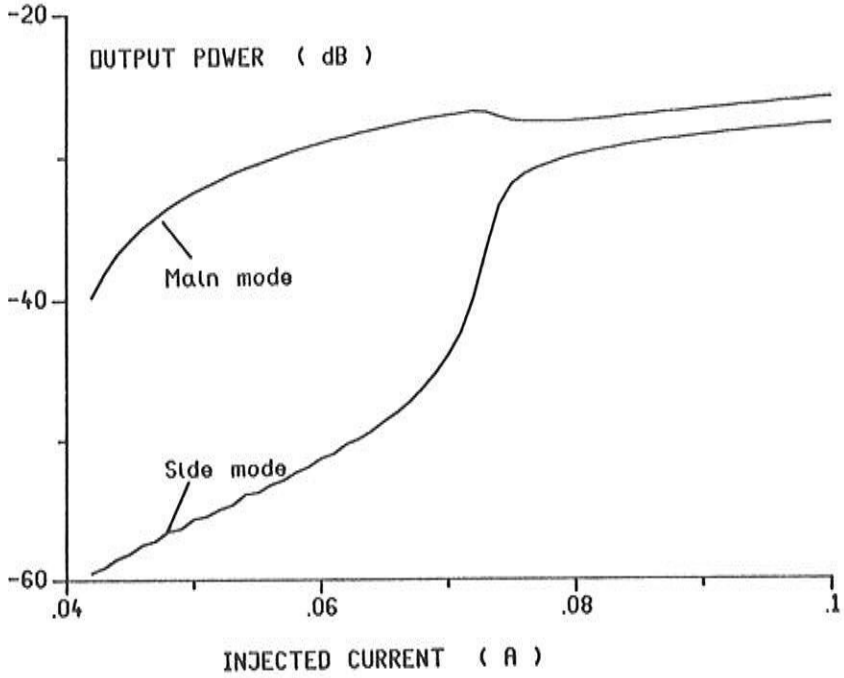

Fig.4.2.3: Output power in main and side mode vs. the injected current for laser B.

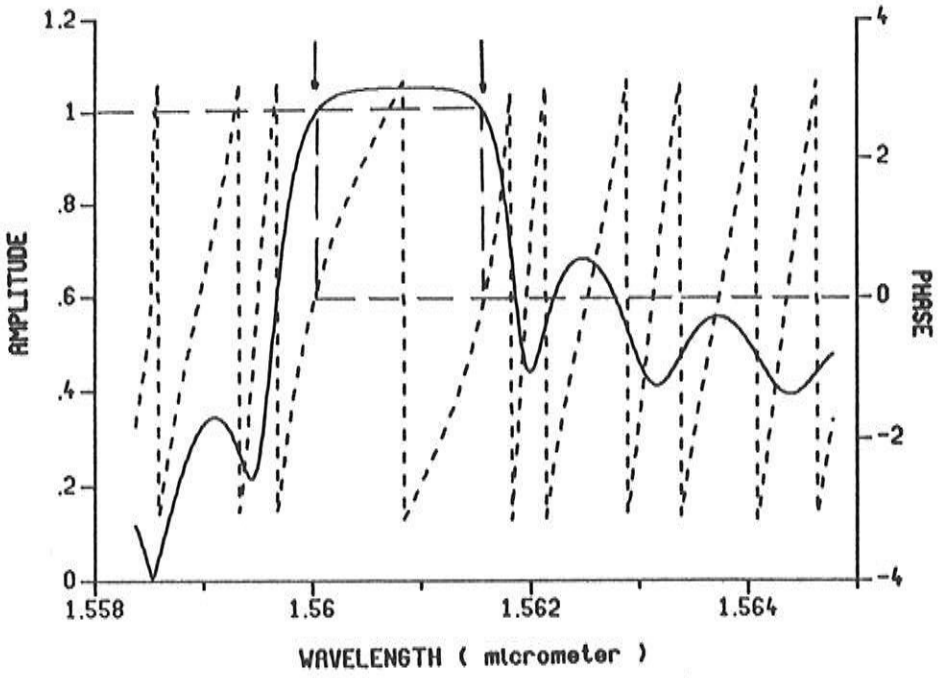

Fig.4.2.4: Amplitude (—) and phase (---) of the roundtrip gain of laser B at 70 mA bias current.

For the specific case of laser B, a large carrier density exists near the facets. This corresponds with a locally smaller Bragg wavelength, which, at sufficiently high excitation, coincides with the wavelength of the side mode. The side mode is then strongly reflected and experiences noticably lower losses.

$\Delta\beta_r$ is depicted in fig. 4.2.5 for both the main and side mode and for different injection levels. One can see how the average Bragg deviation increases for the main mode, while it decreases for the side mode. The first phenomenon is accompanied by an increase in the loss of the main mode and thus, due to gain clamping, an increase in the modal gain for both the main and side mode. The second phenomenon results in a decreased loss of the side mode, which, eventually makes it reach the threshold.

It must be noticed that another non-linearity, associated with the non-uniformity of the gain may have an additional influence. This non-linearity is nevertheless much weaker than the one associated with the non-uniformity of $\Delta\beta_r$ and has a much weaker impact on the side mode onset.

Inclusion of spectral hole burning in this particular case gives an onset of the side mode at an output power of 2.5 mW in stead of 2 mW. A possible explanation for this effect is that spectral hole burning damps the spatial hole burning. In regions with high local optical photon density, it implies a reduced differential gain (dg/dN) and an increased spontaneous carrier recombination (bimolecular and Auger recombination). The latter is due to an increased average carrier density needed to compensate the loss by gain. Both effects result in a smaller influence of the optical power on the carrier density, as can easily be controlled with the help of (2.3.31).

IV.2.2.2 Influence of different laser parameters

The impact of spatial hole burning on the side mode onset depends on the non-uniformity of the carrier density, but equally well on the degree to which this non-uniformity is reflected in a non-uniformity of the refractive index and the Bragg deviation. From the expression (2.3.29) for the non-uniform carrier denstity:

(a)

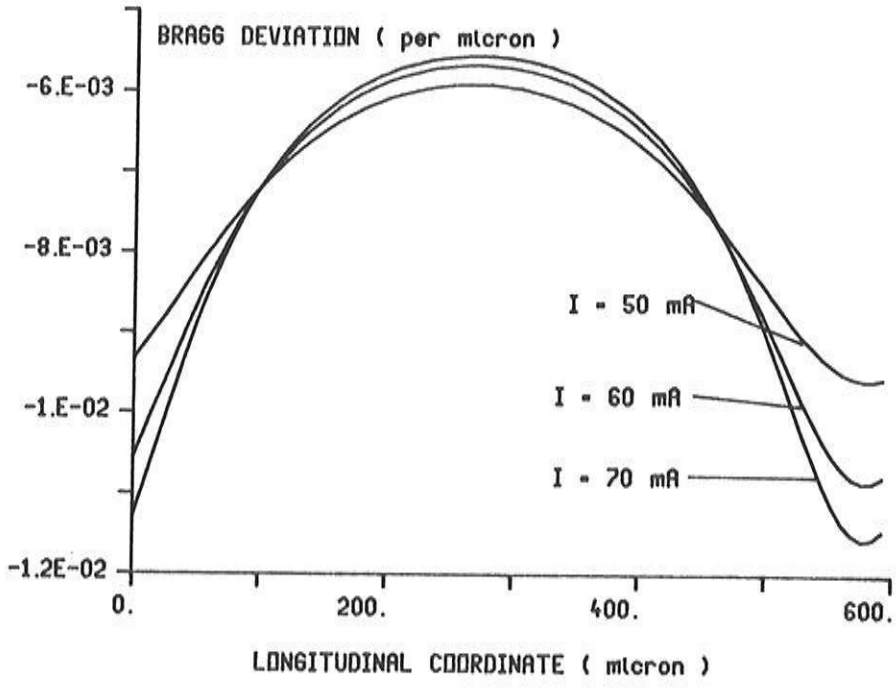

(b)

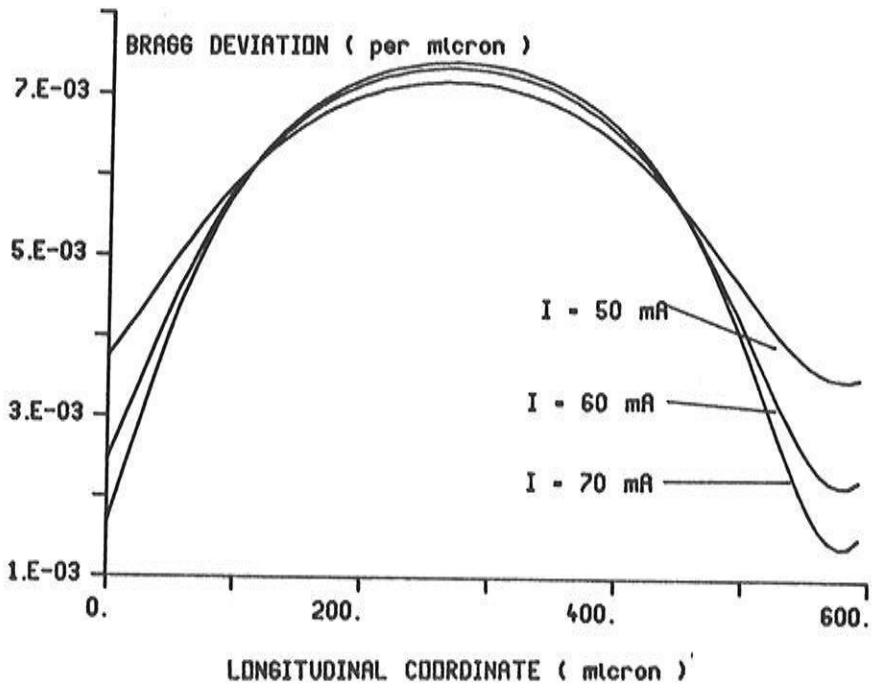

Fig.4.2.5: Longitudinal variation of the Bragg deviation of laser B at different injection levels.
(a) main mode , (b) side mode

$$N_1 f = -\frac{(AN_0 - B)\,I}{(V_a \tau_{rd}^{-1} + AI)}\,f \qquad (4.2.1)$$

, with all symbols being defined as in II.3, it readily becomes clear which parameters are of importance:

- the non-uniformity of the optical power (expressed by f)
- the power level (expressed by I)
- the losses (expressed by the average gain AN_0-B)
- the differential gain A and the carrier lifetime τ_{rd}.
- the 'differential' refractive index dn/dN
- the wavelength separation between main and side mode

The non-uniformity of the power depends on the specific laser structure and on the κL-value. Lasers with high κL-value tend to become rapidly multi mode due the strongly non-uniform power. Indeed, the distributed reflections are stronger for higher κL-values and, in general, the power seems to be concentrated in the central region of the laser. This is illustrated in fig.4.6, which shows the power variation for a 300 μm long λ/4-shifted DFB laser with κL=3 (laser C).

In lasers with high κL-value, it is often the side mode on the short wavelength side of the main mode that can reach the threshold. This mode has a positive Bragg deviation at threshold. However, the concentration of the power in the centre of the laser in this case corresponds with a concentration of the electron density near the facets. Since the refractive index decreases with increasing carrier density, it follows that the Bragg deviation of each mode decreases near the facets and only the Bragg deviation of the side mode on the short wavelength side approaches zero.

It must however be remarked that higher κL-values also imply smaller facet losses and thus a relatively smaller non-uniform carrier density. The loss can further be reduced by decreasing the internal absorption. The non-uniformity of the power is not affected in this case. The absorption depends on the quality of the grown active and passive layers, but also on the carrier density (which itself depends on the loss and gain parameters) and on the wavelength [4.5].

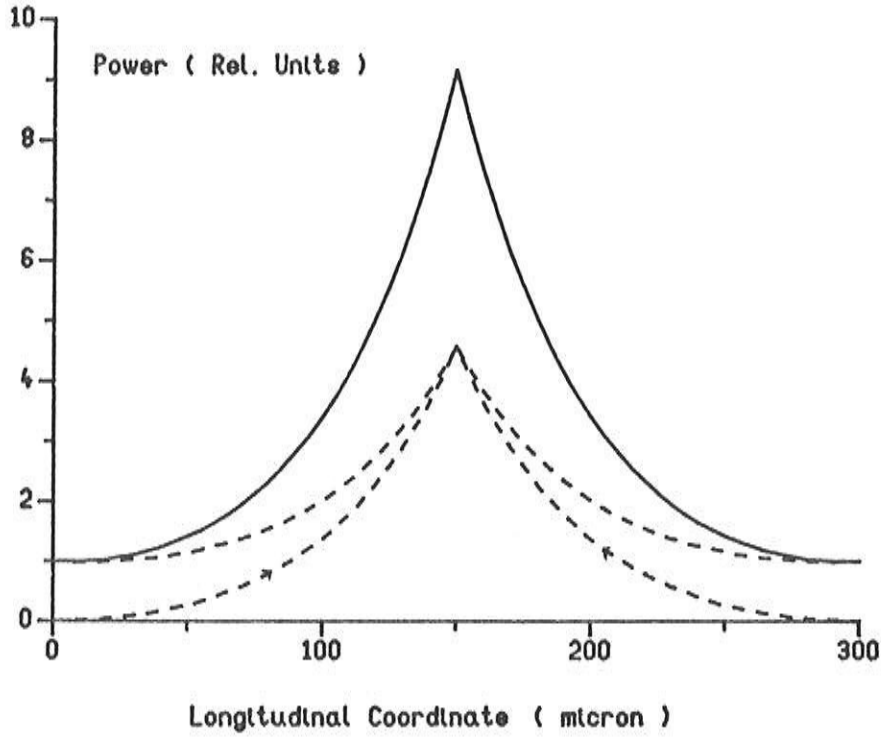

Fig.4.2.6: Longitudinal variation of the power in a λ/4-shifted laser with κL=3.

The non-uniform carrier density can also be reduced by reducing the carrier lifetime or, to a lesser extend, by increasing the differential gain. Both quantities depend on the chosen material (e.g. bulk or quantum well material), on the temperature and on the doping levels in the active layer. The small-signal carrier lifetime furthermore depends on the threshold carrier density (i.e. on the loss) and on the quality of the semiconductor layers.

A change in the carrier dependence of the refractive index on the other hand reduces the non-uniform index or Bragg deviation in stead of the non-uniform carrier density. As shown in IV.2.2.1, it is the non-uniformity in the Bragg deviation which causes the side mode onset. The carrier dependence of the refractive index again depends on the semiconductor material, the temperature and the doping levels.

It must finally be noticed that shorter lasers are more stable with respect to the side mode onset. In many cases, the Bragg deviation of the side mode is inversely proportional with the laser length, and thus larger for shorter lasers. A larger non-uniformity of the refractive index is then required to cause a side mode onset.

All of the dependencies reported here have indeed been confirmed, by experiments as well as by our simulations. As an illustration we show in fig. 4.2.7 the output power in main and side mode for laser A, which is identical to laser B except that it is only half as long. One finds a stable single mode behaviour up to very high power levels and the side mode suppression does not drop below 20 dB, even at an output power of 20 mW.

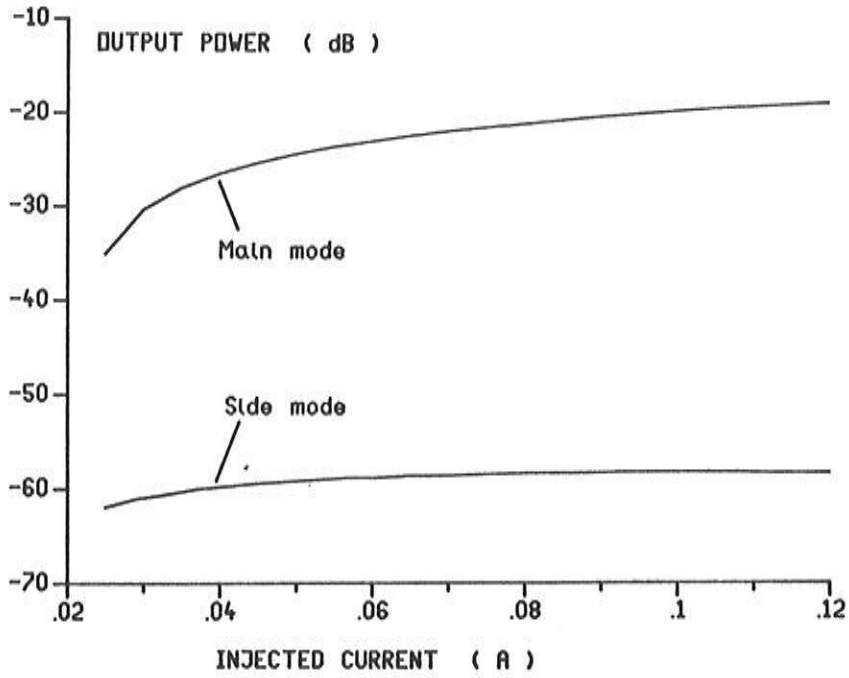

Fig.4.2.7: Output power in main and side mode vs injected current for laser A.

IV.2.2.3 Longitudinal instabilities

According to (4.2.1), the spatial hole burning saturates at high power levels. In the derivation of (4.2.1), it was assumed that the longitudinal variation of the optical power in the main mode remains virtually unchanged above threshold. This is not always the case and the longitudinal mode profile of the main mode may itself be instable. This aspect already has been discussed in detail in ref. [4.6], and therefore we will only briefly review it here.

We consider a 300 μm long DFB laser (laser D) with κL=2 and facet reflectivities ρ_f=-j0.566 and ρ_b=0. Fig. 4.2.8 shows the longitudinal variation of the power in the main mode at threshold and at 5 mW bias output power. One can see that the power in the main mode becomes concentrated more and more near the facet at z=L as the power increases. This is easily understood from the threshold characteristics. At threshold, the Bragg deviation of the laser is positive and the power is concentrated near z=L. Hence, above threshold, the carrier density will be depleted near z=L and an increased Bragg deviation will result. This in turn implies that the Bragg reflections are weakened near z=L and intensified near z=0., so that the power becomes more concentrated near z=L.

This effect occurs mainly in lasers with strongly asymmetric facets or when the main mode emits at the short, resp. long wavelength side of the Bragg wavelength for lasers with high, resp. small κL-value. Obviously, this relatively strong spatial hole burning easily causes the onset of side modes.

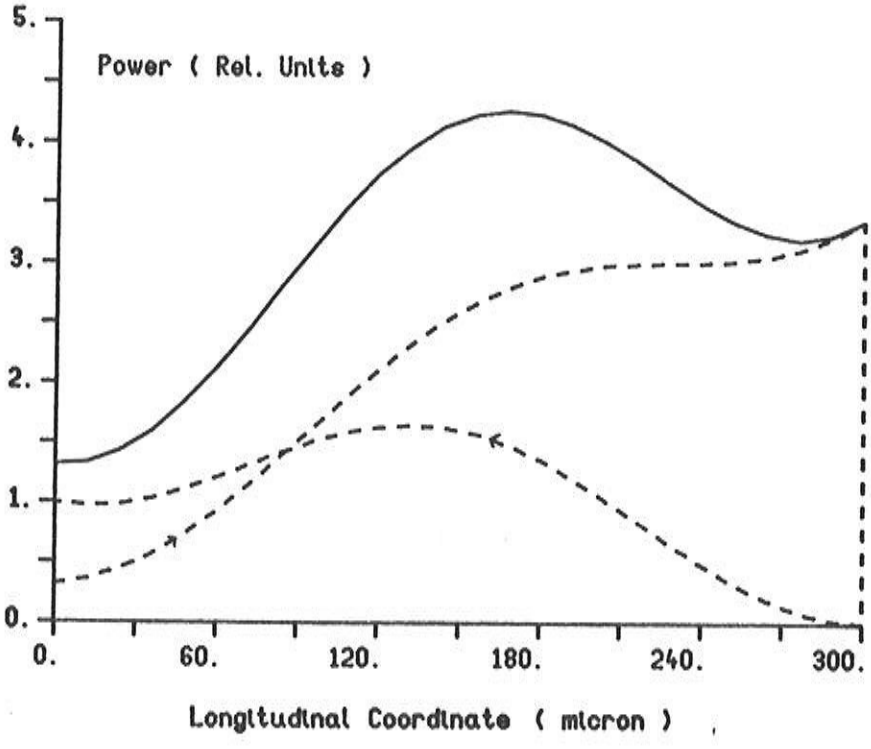

Fig.4.2.8a: Longitudinal variation of the optical power in laser D at threshold.

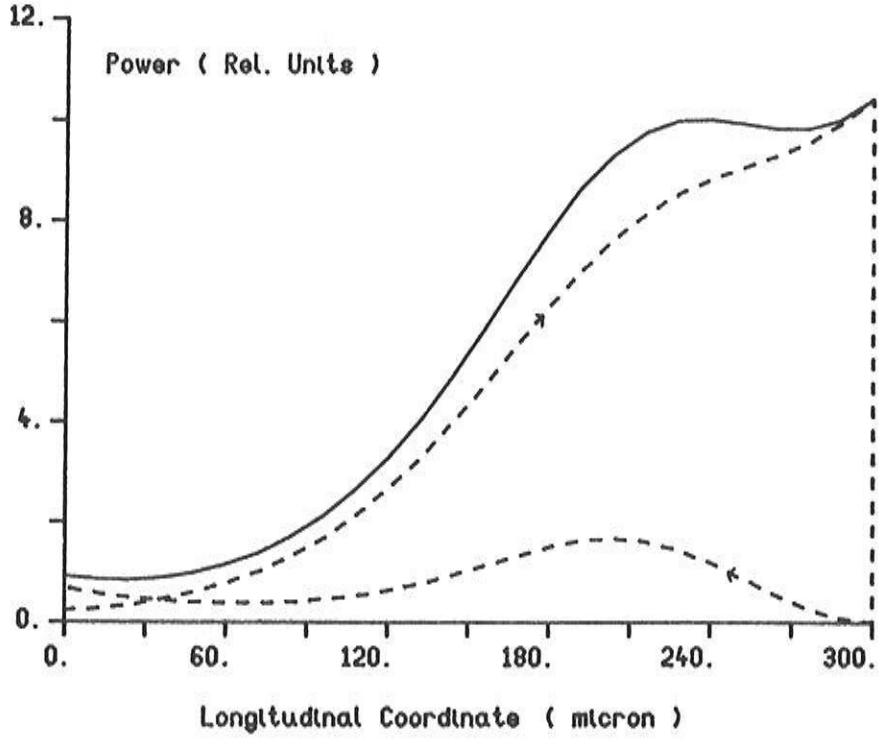

Fig.4.2.8b: Longitudinal variation of the optical power in laser D at a bias level of 5 mW output power.

IV.2.2.4 Impact on the 'yield'

The spatial hole burning and the instabilities indicate that one may not exclusively rely on the value of ΔgL and on the formerly defined yield. In practice as well, the actual yield always appears to be smaller than the theoretical yield.

Nonetheless, CLADISS offers enough possibilities to allow a better predictability of the above threshold yield, e.g. by calculating the SMSR at a certain level above threshold. For cleaved lasers, the yield can then be defined as the percentage of lasers with a certain minimum value of the SMSR. This is illustrated in fig. 4.2.9, which shows the distribution of the SMSR values for the cleaved lasers of IV.2.1 at an injection equal to 3 times the threshold current. The percentage of lasers with an SMSR above 30 dB is a lot smaller than one can expect from the yield of IV.2.1.

Calculation of the above threshold yield as a function of κ and L would principally allow to determine the optimum values of κ and L. Though must also take into account that α_{int} decreases for increasing values of κ and L. Small deviations with respect to the results for a constant α_{int} might then arise.

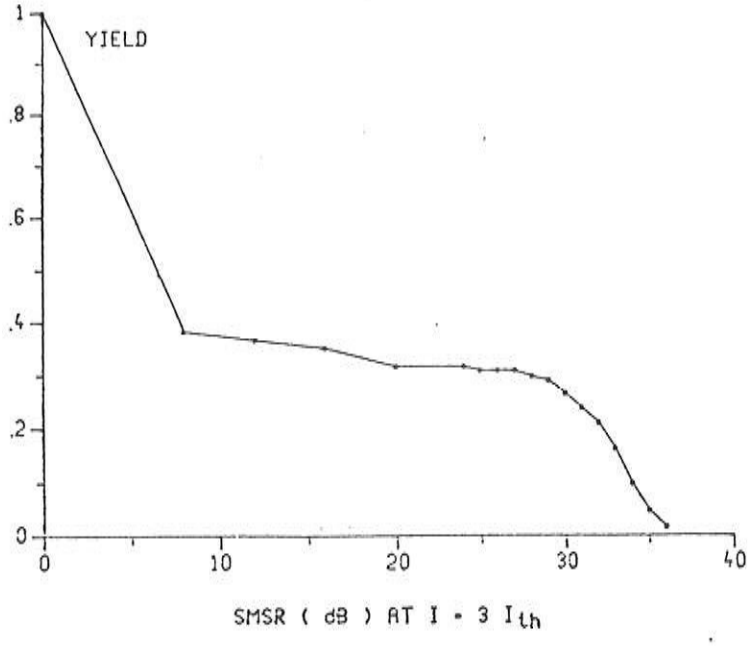

Fig. 4.2.9: Distribution of the SMSR for cleaved lasers with L=300 μm and κL=2.

IV.3 Reduction of spatial hole burning in DFB lasers

An intense search for methods which allow to elevate the detrimental consequences of spatial hole burning has started recently (1989). This search is restricted to perfectly AR-coated lasers, in order to eliminate the uncertainty in the facet reflectivity phases.

IV.3.1 Non-uniform injection

This obviously requires the use of multi-electrode lasers, where the injection into each electrode is adjusted until single mode behaviour is achieved. Numerous examples of this approach have already been given in literature ([4.7], [4.8] and [4.9]). We repeat that such laser types are most suitable for tuning purposes, an aspect which we won't treat however.

As an example, we consider again the λ/4-shifted laser (laser C) with L=300 μm, κL=3 and other parameters as given in table IV.1. The stripe electrode has been divided into three parts, as shown in fig. 4.3.1 , although the first and third part are short-circuited. The laser becomes multi mode at ± 80 mA when uniformly pumped (the

full line in fig.4.3.1). But one easily finds that this can be resolved by pumping the central electrode stronger than the outer electrodes, which is illustrated by the dashed line in fig. 4.3.2 for the case $I_c=1.2I_e$.

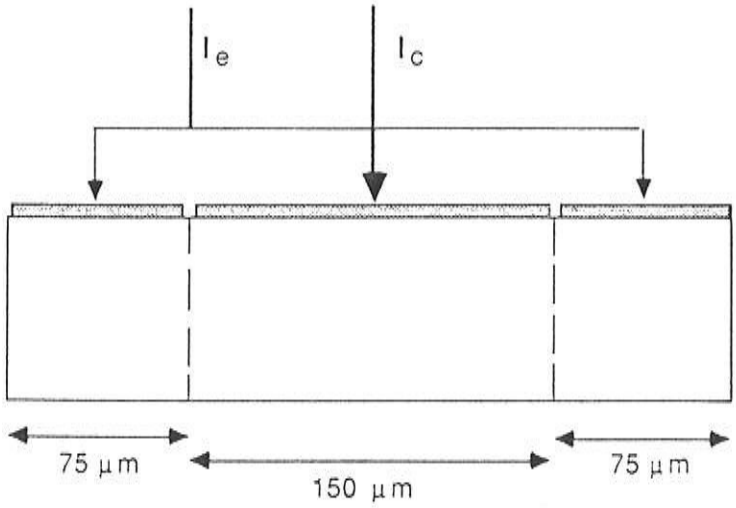

Fig.4.3.1: Schematic view of a multi-electrode laser.

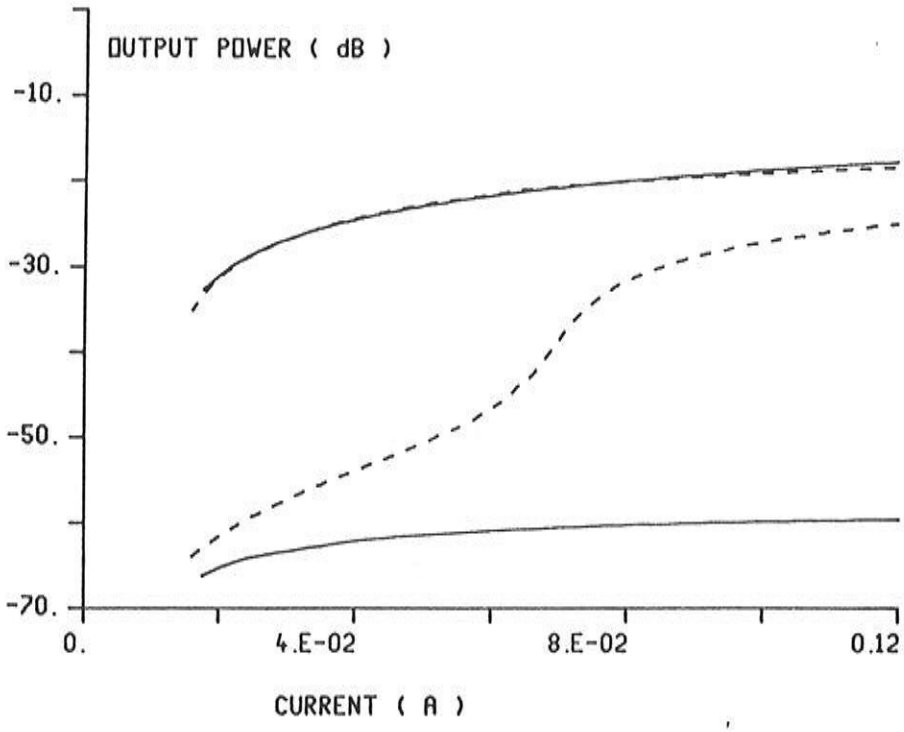

Fig.4.3.2: Power in main and side mode for uniform (—) and non-uniform (- -) injection, for laser C.

IV.3.2 Special index-coupled structures

IV.3.2.1 Introduction

A large part of the recent literature on DFB lasers is formed by discussions of new laser structures, which aim at a more uniform power distribution along the longitudinal axis. Especially multi-phase-shifted lasers (i.e. with several phase shifts in the grating) and chirped grating lasers (gratings with a varying period) were initially considered as 'the solution' to the problem (see e.g. [4.10], [4.11]). Such lasers have also been fabricated ([4.12]).

Some of these laser types have been modelled with the help of CLADISS. As an example, we show the longitudinal variation of the power for a multi-phase-shifted laser (fig. 4.3.3). The laser under consideration has a length of 1200μm and a normalised coupling constant of 2. 3 phase shifts of $4\pi/5$ have been incorporated in the grating every 300 μm. The total optical power density varies only with ± 30 %, which, in comparison with common DFB lasers, is an appreciable reduction. However, our calculations also indicate that this uniformity can't be improved a lot anymore simply by using more phase shifts or chirped gratings.

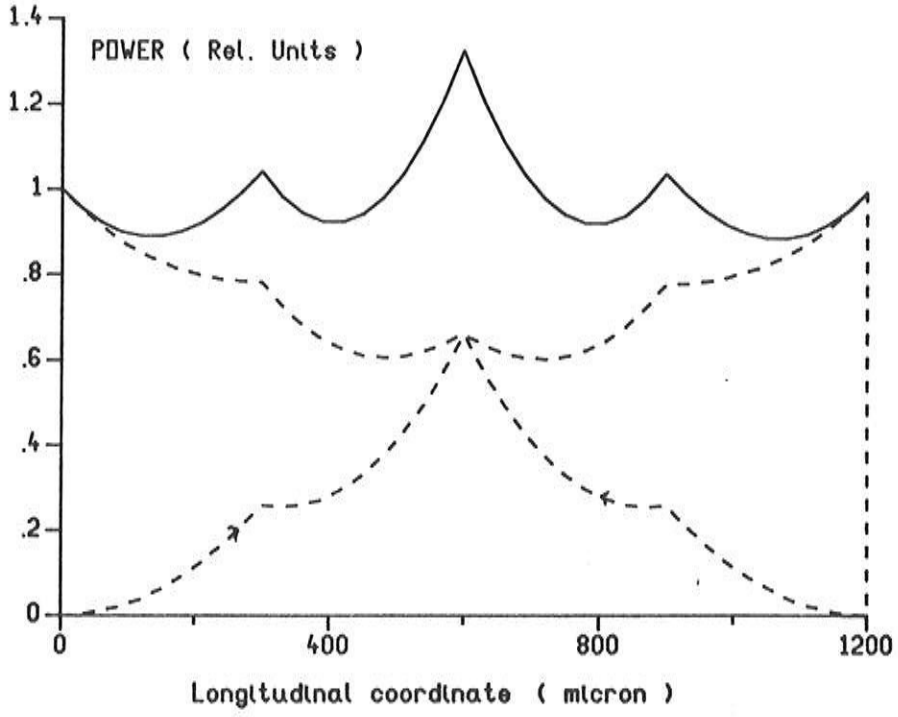

Fig.4.3.3: Longitudinal variation of the power in a multi-phase-shifted laser.

IV.3.2.2 Theory

Complete elimination of spatial hole burning is possible only if a variable coupling constant and/or if a variable gain/loss is allowed. This can easily be shown theoretically with the help of the coupled wave equations (2.2.48), which we rewrite here for the static, single mode regime and with the spontaneous emission being disregarded.

$$\frac{dr^+}{dz} - \Delta\beta_i\, r^+ = |\kappa|\, r^- \cos(\varphi_\kappa + \varphi^- - \varphi^+) \qquad (4.3.1a)$$

$$\frac{dr^-}{dz} + \Delta\beta_i\, r^- = |\kappa|\, r^+ \cos(\varphi_\kappa + \varphi^- - \varphi^+) \qquad (4.3.1b)$$

$$\frac{d\varphi^+}{dz} + \Delta\beta_r = |\kappa|\, \frac{r^-}{r^+} \sin(\varphi_\kappa + \varphi^- - \varphi^+) \qquad (4.3.1c)$$

$$\frac{d\varphi^-}{dz} - \Delta\beta_r = -|\kappa|\, \frac{r^+}{r^-} \sin(\varphi_\kappa + \varphi^- - \varphi^+) \qquad (4.3.1c)$$

Multiplication of equation (4.3.1a) with r^+, of equation (4.3.1b) with r^- and subtration of both resulting equations gives an equation for the z-variation of the optical power $(r^+)^2 + (r^-)^2$, from which it follows that a uniform power requires the following relation:

$$2\,|\kappa| \cos(\varphi_\kappa + \varphi^- - \varphi^+) = \Delta\beta_i\, \frac{(r^-)^2 - (r^+)^2}{r^+ r^-} \qquad (4.3.2)$$

The denominator on the r.h.s. of (4.3.2) approaches infinity if one or both facets are perfectly AR-coated. The requirement can then only be fulfilled if $|\kappa|$ approaches infinity as well or if $\Delta\beta_i$ vanishes at this facet. The case with $\Delta\beta_i$ being identically zero is not really of interest and nor is the case with $|\kappa|$ being identically infinite. Both cases actually correspond with lasers with zero efficiency (i.e. no output power can be extracted).

Structures with uniform optical power can be derived after transformation of the coupled wave equations in the following way. We first remark that the perfect AR-coating of the facets and the

requirement of a uniform power can be expressed by the following relations:

$$r^+(0) = r^-(L) = 0. \qquad (4.3.3a)$$

$$[r^+(z)]^2 + [r^-(z)]^2 = 1 \qquad (4.3.3b)$$

The power is normalized here. A first useful equation can now be derived by multiplication of (4.3.1a) with r^+, multiplication of (4.3.1b) with r^- and subtraction of both equations:

$$\frac{d(r^+)^2}{dz} - 2\Delta\beta_i (r^+)^2 = \frac{d(r^-)^2}{dz} + 2\Delta\beta_i (r^-)^2 \qquad (4.3.4)$$

Taking into account the relation (4.3.3b) readily gives:

$$\frac{d(r^+)^2}{dz} = \Delta\beta_i \qquad (4.3.5)$$

and integration of this last equation gives:

$$\int_0^L \Delta\beta_i(z)dz = 1 \qquad (4.3.6)$$

The power of forward and backward propagating waves is then found to be:

$$(r^+)^2 = \int_0^z \Delta\beta_i(z')dz' \;\; ; \;\; (r^-)^2 = \int_z^L \Delta\beta_i(z')dz' \qquad (4.3.7)$$

Substitution of these functions into (4.3.2) shows that the r.h.s. is completely determined. (4.3.2) allows to determine the required coupling coefficient, provided the phase difference is known. An equation for this phase difference can be derived from (4.3.1c) and (4.3.1d):

$$\frac{d(\varphi^- - \varphi^+)}{dz} - 2\Delta\beta_r = -\Delta\beta_i \frac{[1 - 2(r^+)^2]}{2(r^+)^2 (r^-)^2} \, tg(\varphi_\kappa + \varphi^- - \varphi^+) \qquad (4.3.8)$$

It must be noticed that, due to the AR-coating of the facets, only this phase difference has a physical meaning. The phase φ_κ can be considered as a stepwise constant function. Continuous changes in this phase can be included in $\Delta\beta_r$ since they can also be regarded as changes in the grating period. In fact, phase jumps as in phase shifted lasers could also be included in $\Delta\beta_r$ as Dirac functions.

Several structures with a uniform power density can now be derived from the equations (4.3.6)-(4.3.9), just be choosing appropriate functions for $\Delta\beta_i$, κ and $\Delta\beta_r$. Two of these functions, e.g. $\Delta\beta_i$ and $\Delta\beta_r$, can be chosen freely. It can be remarked however that the equation (4.3.8) is easier to solve if $\Delta\beta_r$ is replaced by another function:

$$\Delta\beta_r(z) = \frac{f(z)}{\cos(\varphi_\kappa + \varphi^- - \varphi^+)} \; ; y = \sin(\varphi_\kappa + \varphi^- - \varphi^+) \qquad (4.3.9a)$$

yielding for (4.3.8):

$$\frac{dy}{dz} + \Delta\beta_i(z)\,\frac{[1 - 2\,(r^+)^2]}{2\,(r^+)^2\,(r^-)^2}\,y = 2\,f(z) \qquad (4.3.9b)$$

The last equation is a first order linear differential equation, which, for a given f, is easily solved. Hence, by choosing functions for f(z) and $\Delta\beta_i$, one can determine the fields and the phases. The required variations of κ and $\Delta\beta_r$ then follow from (4.3.2) and (4.3.9a).

IV.3.2.3 Exact solutions to the problem

- *solutions with uniform $\Delta\beta_i$:*

For this case, one readily finds from (4.3.6) and (4.3.7):

$$\Delta\beta_i = 1/L \quad \text{and} \quad r^+ = \sqrt{z/L}\,; r^- = \sqrt{1 - z/L} \qquad (4.3.10)$$

The power of forward and backward propagating beams varies linearly in the longitudinal direction. A simple solution of (4.3.8) is then:

$tg(\varphi_\kappa + \varphi^- - \varphi^+) = c$, with c an arbitrary real constant

$$\Delta\beta_r = \frac{\left(1 - 2\frac{z}{L}\right)}{4L\frac{z}{L}\left(1 - \frac{z}{L}\right)} c \qquad (4.3.11)$$

The $\kappa(z)$-function can be derived from (4.3.2). It follows that a phase shift of π is needed at z=L/2 in order to keep $|\kappa|$ positive and one finds for κ:

$$\kappa = \frac{1}{2L} \frac{\left(1 - 2\frac{z}{L}\right)}{\sqrt{\frac{z}{L}\left(1 - \frac{z}{L}\right)}} \sqrt{1 + c^2} \qquad (4.3.12)$$

The variation of $\Delta\beta_r$ can practically result from a variation in e.g. the composition of the cladding or active layers (although this usually also implies a small variation of α_{int}) or the grating period. An interesting special case rises when c is chosen zero. Both $\Delta\beta_i$ and $\Delta\beta_r$ are then uniform and the solution corresponds with a uniform waveguide geometry, where the amplitude of the grating varies in the longitudinal direction. Lasing occurs at the Bragg wavelength in this case.

The functions $\Delta\beta_r$, $\Delta\beta_i$ and $|\kappa|$ are depicted in fig. 4.3.4 for a few values of the parameter c. $\Delta\beta_r$ and $|\kappa|$ both increase for increasing values of c. This can be related to the fact that an increase of the Bragg deviation (and thus of c) results in a weakening of the distributed reflections, which must be compensated by an increase of the coupling coefficient (which enhances the distributed reflections). The low value of $|\kappa(z)|$ in the central region of the laser prevents a power concentration in this region. There is little reflection in this region and the longitudinal variation of the power of the forward and backward propagating beams is mainly caused by stimulated emission in this region. This stimulated emission would result in a concentration of power near the facets (as in Fabry-Perot lasers), if it were not for the increase of $|\kappa|$ (or the growth of the reflections) near the facets.

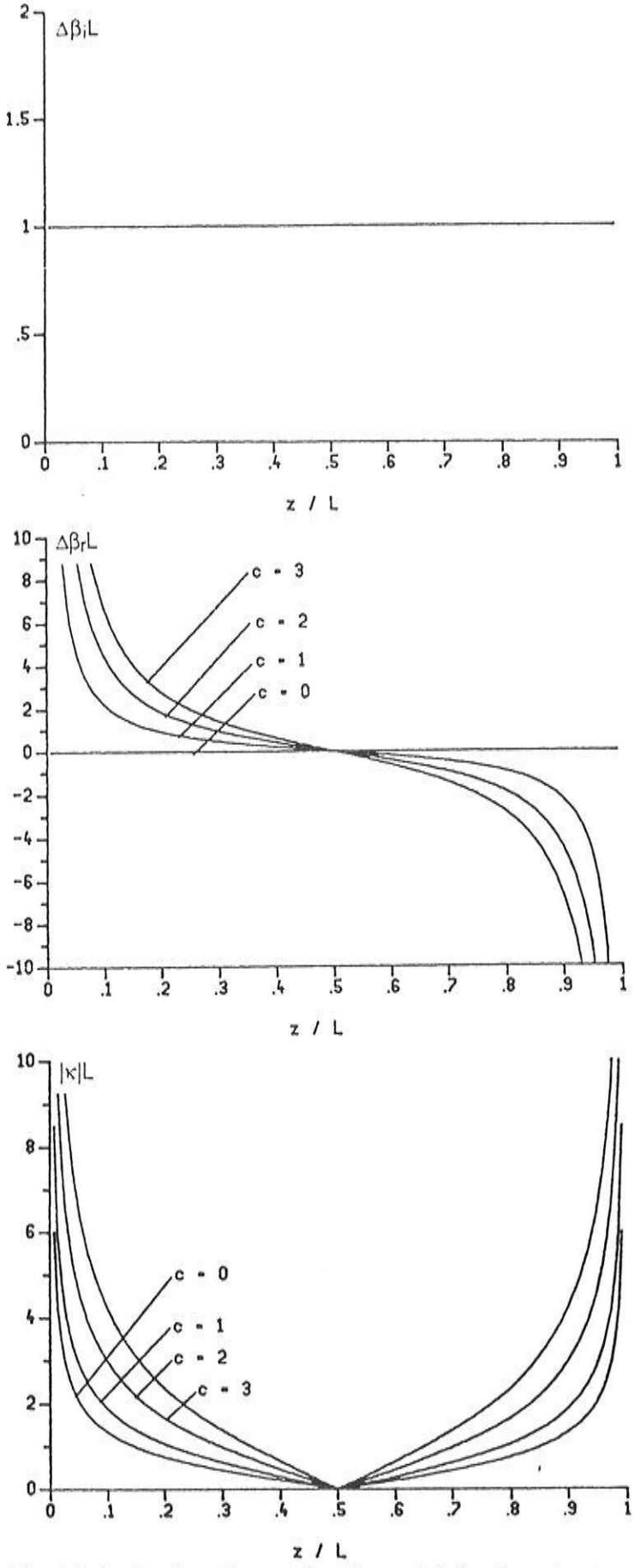

Fig.4.3.4: De functions $\Delta\beta_i$, $\Delta\beta_r$ en $|\kappa|$ for the structure described by (4.3.12) and (4.3.13).

- *solutions with variable* $\Delta\beta_i$:

To remove the singularity in the $\kappa(z)$-function, one can try a solution of the form:

$$\Delta\beta_i \sim r^+ r^- \tag{4.3.13}$$

The solutions are:

$$r^+ = \sin\left(\frac{(2n+1)\pi z}{2L}\right); r^- = \cos\left(\frac{(2n+1)\pi z}{2L}\right) \tag{4.3.14a}$$

$$\Delta\beta_i = \frac{(2n+1)\pi}{2L}\sin\left(\frac{(2n+1)\pi z}{L}\right) \tag{4.3.14b}$$

with n an integer. From the equation (4.3.8), one can see that again a solution with $\Delta\beta_r = 0$ exists. Again, a phase shift of π at z=L/2 is required to keep $|\kappa|$ positive and one finds:

$$\kappa(z) = \frac{(2n+1)\pi}{2L}\cos\left(\frac{(2n+1)\pi z}{L}\right) \tag{4.3.15}$$

A strucure which for n=0 has been reported also in literature [4.13] It must be noticed once more that the variation of $\Delta\beta_i$ (which can be implemented as a variation of the absorption or as a variation of the gain) will often be accompanied by a variation of $\Delta\beta_r$. This is the case when a variable composition of the passive layers (i.e. a variable loss in the passive layers) or a non-uniform injection is applied. The variations of $\Delta\beta_r$ should be restricted or compensated for by a varying grating period.

The functions $\Delta\beta_r$, $\Delta\beta_i$ and $|\kappa|$ are depicted in fig.4.3.5 for n=0 and n=1. For the case n=0, one can again argue that the low $|\kappa|$-value near z=L/2 prevents a concentration of power in the central part of the laser. The concentration of power near the facets however is now anticipated both by an increase of $|\kappa|$ and by a decrease of $\Delta\beta_i$ (i.e. the net stimulated emission is reduced and the reflections have become stronger).

Other solutions can be derived after substitution of f by:

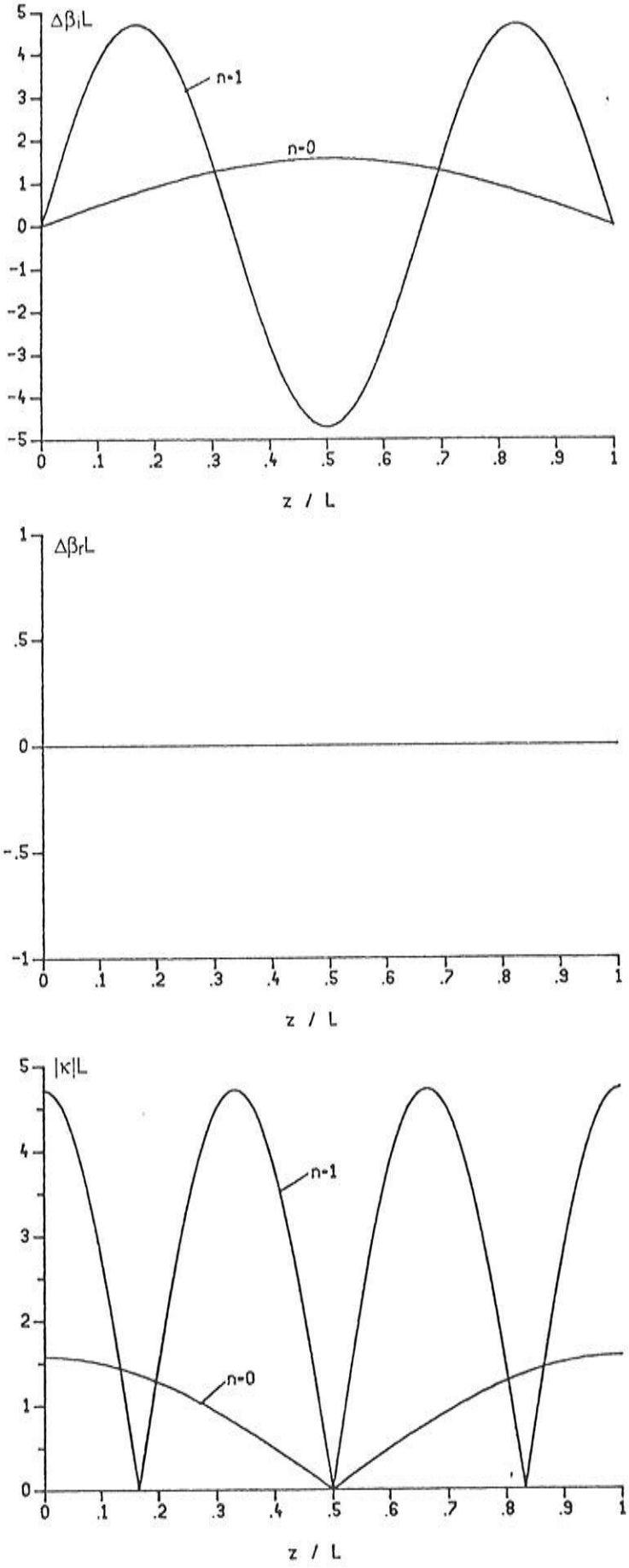

Fig.4.3.5: The functions $\Delta\beta_i$, $\Delta\beta_r$ en $|\kappa|$ for the structure described by (4.3.14) and (4.3.15); n=0 and n=1.

$$f(z) = c\left[\sin\left(\frac{(2n+1)\pi z}{L}\right)\right]^k \cos\left(\frac{(2n+1)\pi z}{L}\right) \qquad (4.3.16)$$

with c being an arbitrary real constant and k an arbitrary integer. The solution of (4.3.9b) for this choice of f becomes:

$$y = \frac{2c\left[\sin\left(\frac{(2n+1)\pi z}{L}\right)\right]^{k+1}}{(2n+1)\,(k+2)\,\pi/L} \text{ with } a = \frac{2cL}{(2n+1)(k+2)\pi} \leq 1 \qquad (4.3.17)$$

The last requirement thereby follows from (4.3.9a). From y and f, the Bragg deviation can be determined via the equation (4.3.9a). The sign of $\cos(\varphi_\kappa+\varphi^- -\varphi^+)$, which also determines $|\kappa|$, can not be determined from (4.3.17). Both + and - sign, as well as changes of the sign along the longitudinal axis are allowed. Though, one must assure that the value of $|\kappa|$ remains positive (e.g. by including phase shifts φ_κ). For the case a=1 and n=0, one finds for κ and $\Delta\beta_r$:

$$\Delta\beta_r = \pm \frac{(k+2)\frac{\pi}{2L}\left[\sin\left(\frac{\pi z}{L}\right)\right]^k}{\sqrt{1+\left[\sin\left(\frac{\pi z}{L}\right)\right]^2+\ldots+\left[\sin\left(\frac{\pi z}{L}\right)\right]^{2k}}} \qquad (4.3.18a)$$

$$|\kappa| = \frac{\pi}{2L}\,\frac{1}{\sqrt{1+\left[\sin\left(\frac{\pi z}{L}\right)\right]^2+\ldots+\left[\sin\left(\frac{\pi z}{L}\right)\right]^{2k}}} \qquad (4.3.18b)$$

The cases with k=0 and k=1 are of most interest. For k=0, one finds a uniform κ ($=\pi/2L$) and lasing at the average Bragg wavelength if $\Delta\beta_r$ is chosen as:

$$\Delta\beta_r = \frac{\pi}{L} \text{ for } 0\leq z\leq L/2 \text{ and } \Delta\beta_r = -\frac{\pi}{L} \text{ for } L/2\leq z\leq L \qquad (4.3.19)$$

For k=1, one finds that $\Delta\beta_r$ and $\Delta\beta_i$ vary in a similar way along the longitudinal axis, while the variation of κ is rather small.

$$\Delta\beta_r = \frac{\pm 3\,\Delta\beta_i}{\sqrt{1+\left[\sin\left(\frac{\pi z}{L}\right)\right]^2}} \qquad (4.3.20a)$$

$$|\kappa| = \frac{\pi}{2L}\,\frac{1}{\sqrt{1+\left[\sin\left(\frac{\pi z}{L}\right)\right]^2}} \qquad (4.3.20b)$$

It must be emphasized that the previous solutions are not necessarily the modes with the lowest threshold gain (current), nor has it been proven that the special structures are single mode. Only when the uniform power solution is the main and single mode will there be an absence of spatial hole burning effects in the laser behaviour. This can be expected for the solutions lasing at the average Bragg wavelength. For the solutions with variable $\Delta\beta_i$, especially the cases where $n\neq 0$ seem to be higher order modes which might not be the main mode.

The variations of $\Delta\beta_r$, $\Delta\beta_i$ and $|\kappa|$ are shown in fig. 4.3.6, resp. 4.3.7 for the solutions (4.3.19), resp. (4.3.20). For these solutions, the value of $|\kappa|$ near $z=L/2$ is not that small anymore, but the distributed reflections are now also suppressed by the larger Bragg deviation $\Delta\beta_r$. This Bragg deviation decreases near the facets for the solution (4.3.20), which, together with the decrease of the net stimulated emission again prevents a power concentration.

We emphasize once more that other interesting structures can be derived from the eqution s (4.3.6)-(4.3.9). Only a few simple solutions have been discussed here and we leave the further exploration of other (and probably also more complex) solutions as future work.

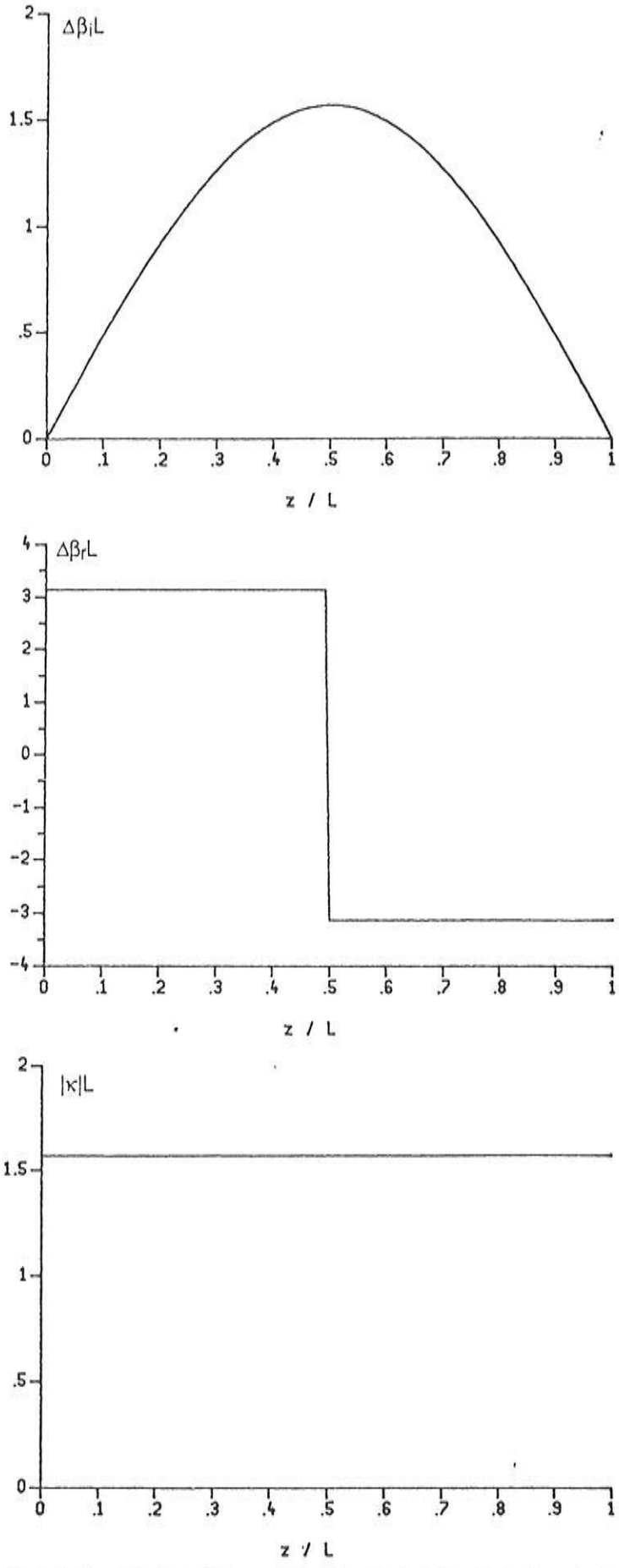

Fig.4.3.6: De functions $\Delta\beta_i$, $\Delta\beta_r$ en $|\kappa|$ for the structure described by (4.3.14) (n=0) and (4.3.19).

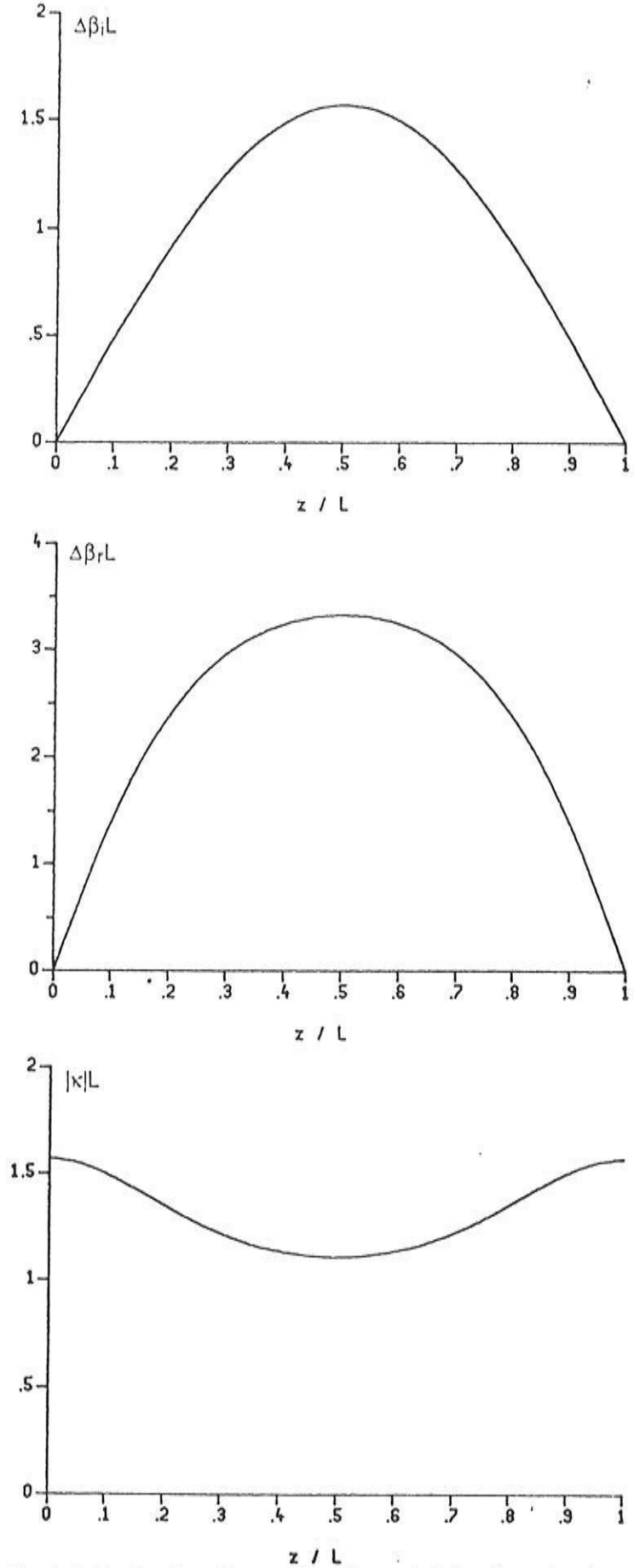

Fig.4.3.7: De functions $\Delta\beta_i$, $\Delta\beta_r$ en $|\kappa|$ for the structure described by (4.3.12) (n=0) and (4.3.20).

IV.3.2.4 Approximations and simulations

- *solutions with uniform* $\Delta\beta_i$:

For c=0, one finds a laser with a grating of which the amplitude varies in the longitudinal direction [4.14]. The $\kappa(z)$-variation can then e.g. be approximated by a linear, a cosine or a stepwise constant function. As a matter of fact, the function can be approximated to any degree if gratings are written by e-beam lithography. One can either vary the actual grating amplitude or the duty cycle of the grating, as shown in fig.4.3.8. A stepwise constant approximation, together with the exact function, is shown in fig. 4.3.9 for a 300 μm long laser. This approximation already results in an extremely uniform optical power (fig. 4.3.10), with variations that are restricted to 5 %. For the threshold gain difference ΔgL, one finds the value 0.17 and therefore, a stable single mode behaviour should be observed for this structure.

A second approximation can be formed by the double exposure of a photoresist to form 2 holographic interference patterns of slightly different periods Λ_1 and Λ_2 ([4.15], [4.16]). This results in a cosine variation of κ. However, the variation of the coupling coefficient will in general be accompanied by a variation of the effective refractive index (and of the Bragg deviation) if the last method is used.[1] The relation between the variation of the coupling coefficient and that of the refractive index depends on the lithography and etching process. One possible structure is shown in fig. 4.3.11, in which case $\Delta\beta_r = 0.5\ |\kappa|$. This is fundamentally different from (4.3.11), which could be approximated somehow as $\Delta\beta_r = c\ \kappa$. The case of a linearly varying coupling coefficient and a linear refractive index variation has been modelled numerically for a 300 μm long laser. Fig. 4.3.12 shows the variation of the optical power, which still is restricted to about 10 %. With Δgl being equal to 0.14, a good mode rejection can still be expected.

[1]Notice that this is also the case for a variable duty cycle.

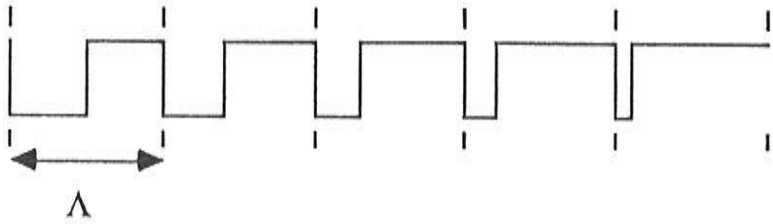

Fig.4.3.8: Grating with variable duty cycle.

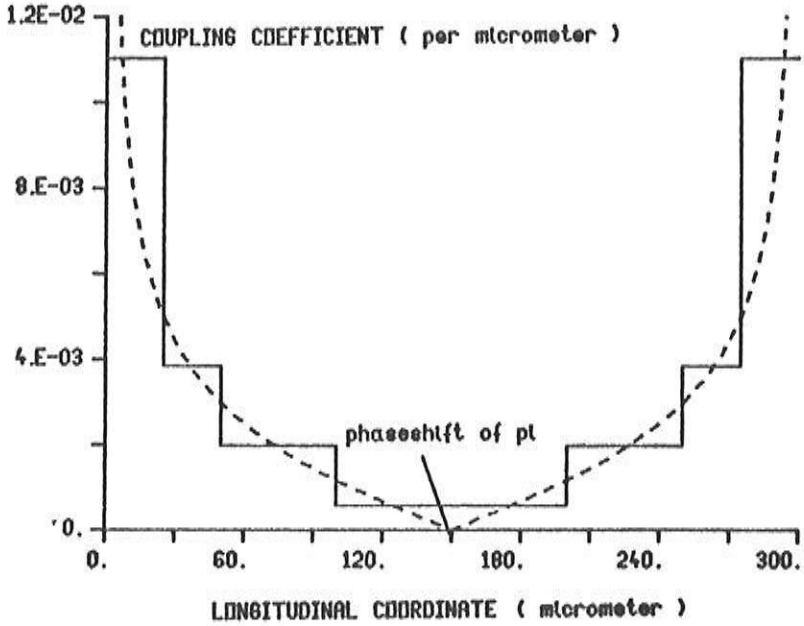

Fig.4.3.9: Longitudinal variation of κ (4.3.12) and stepwise constant approximation for c=1.

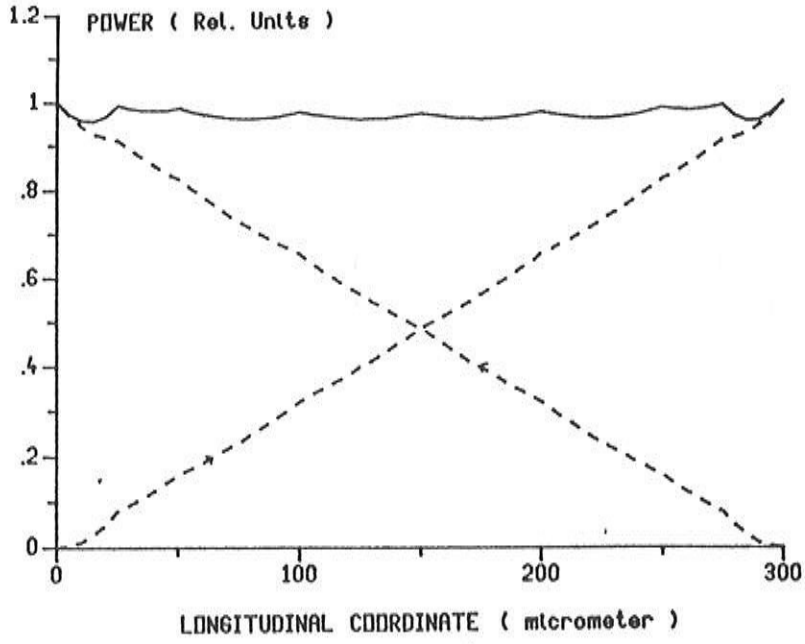

Fig.4.3.10: Longitudinal variation of the power for the stepwise constant approximation of fig. 4.3.5.

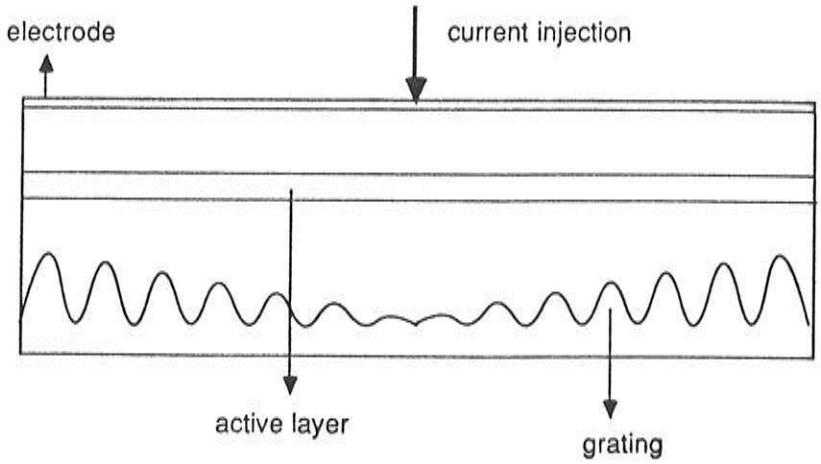

Fig.4.3.11: Grating formed by the double exposure technique.

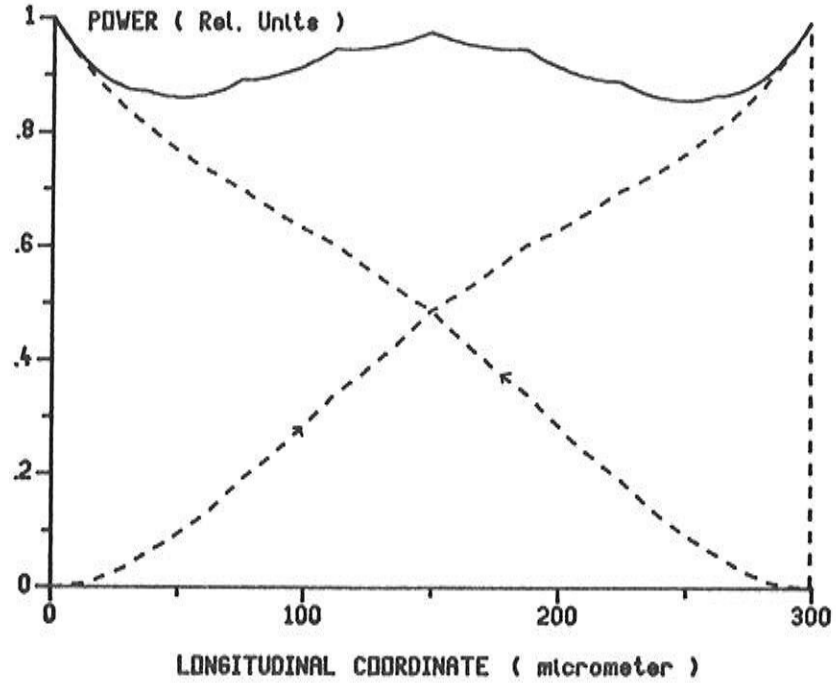

Fig.4.3.12: Longitudinal variation of the power for the laser of fig. 4.3.7.

A last approximation, worthwile mentioning, is a stepwise constant approximation with κ being constant in the outer sections and zero (i.e. no grating) in the central section. One must thereby assure that the π-phaseshift between both gratings near the facets is still present. One possibility is to fabricate a $\lambda/4$-shifted grating of which a central part is removed afterwards.

- *solutions with variable* $\Delta\beta_i$:

The solution given by (4.3.14) and (4.3.15) with n=0 could be fabricated approximately by producing the $\kappa(z)$-function by the double exposure technique. The $\Delta\beta_i$-variation can be approximated by e.g. a stepwise constant variation (with 3 steps) of the cladding layer composition. The additional $\Delta\beta_r$-variation caused by this composition variation will modify the κ-variation, but it also might compensate for the $\Delta\beta_r$-variation caused by the double exposure technique. We further remark that the exact structure (and the stepwise constant approximation) exhibit a high ΔgL-value of ± 0.46.

2 simple structures can further be obtained from approximations of (4.3.19), resp. (4.3.20). For the case (4.3.19) e.g., one can approximate $\Delta\beta_i$ by a constant and divide the laser into 2 halfs with different grating periods, and separated by a $\lambda/4$-shift. We have modelled such a 300 μm long laser with grating periods Λ_1= 241.3 nm and Λ_2=240.9 nm. For the uniform $\Delta\beta_i$, one finds an optimum κL-value of 1.75 (instead of $\pi/2$). fig. 4.3.13 depicts the longitudinal variation of the power. A value of 0.66 was found for ΔgL.

The solution (4.3.20) can be fabricated by introducing a stepwise (or other) variation of $\Delta\beta_i$, which is accompanied by a $\Delta\beta_r \sim \pm 3\Delta\beta_i$. Variations in the absorption (or in the composition of the cladding layers) and in the gain (or in the composition of the active layer) are indeed accompanied by variations of the refractive index of this order of magnitude. If the variation of $\Delta\beta_i$ is implemented as e.g. a non-uniform injection, one has $\Delta\beta_r=-\alpha\Delta\beta_i$, with α being the linewidth enhancement factor and $\alpha \sim 3$. Fig. 4.3.14 shows simulation results for a 300 μm long structure, that is a stepwise constant approximation (with 5 steps) of the required $\Delta\beta_i$-function (implemented as an absorption variation) and for which $\Delta\beta_r=-3\Delta\beta_i$. The power variations are again restricted to 10 % and a ΔgL-value of 0.22 is achieved.

We further mention that also solutions for $\alpha \approx 4,5,..$ can be found, e.g. starting from (4.3.18) with k = 2,3,... The z-dependence of the denominator in (4.3.18) is more important in this case and neglecting it will further reduce the uniform character of the power.

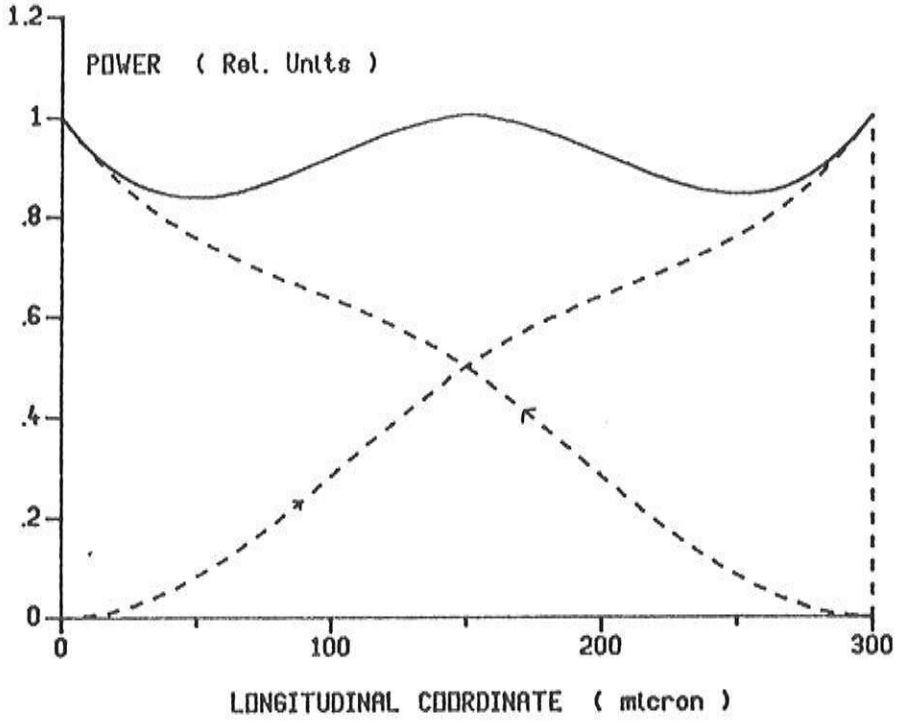

Fig.4.3.13: Longitudinal variation of the power in a laser with 2 different grating periods (see text).

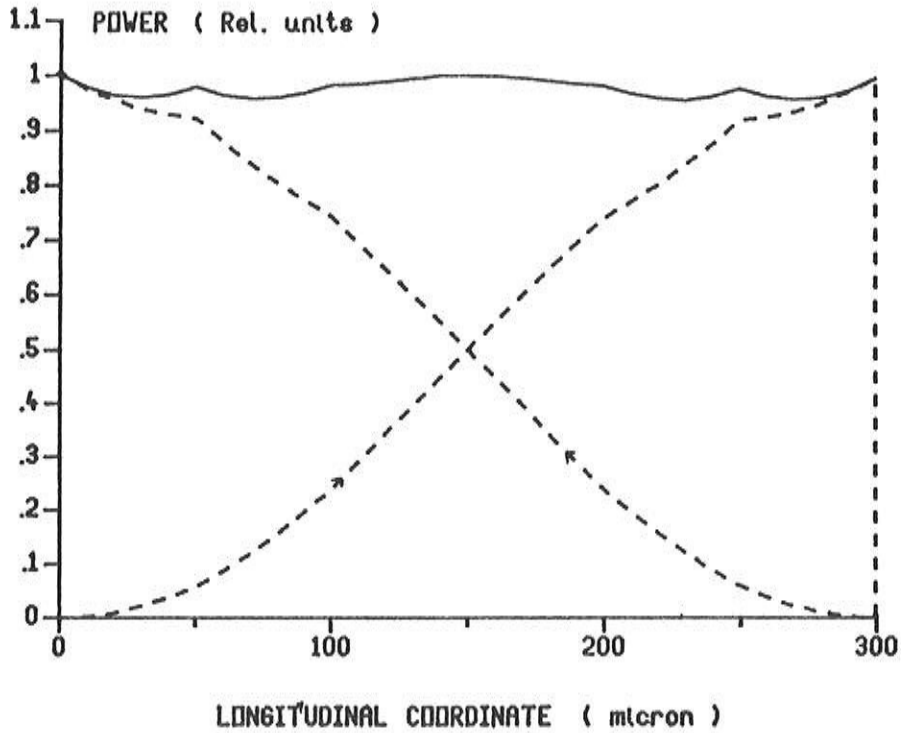

Fig.4.3.14: Longitudinal variation of the power for a 5-step approximation of (4.3.20) (see text).

We finally remark that by neglecting the variation of $\Delta\beta_i$, one retrieves the chirped grating lasers. The variation of the optical power in such lasers is comparable with that in multiple-phase-shifted lasers. Fig. 4.3.15 shows the longitudinal variation of the power for a 300 μm long laser, where $\Delta\beta_r$ is a stepwise constant approximation (with 5 sections) of the function (4.3.20a), and where κ and $\Delta\beta_i$ are constant along the longitudinal axis. For the optimum value of κ, equal to 1.6, one finds power variations that are restricted to 10% and a ΔgL-value of 0.25.

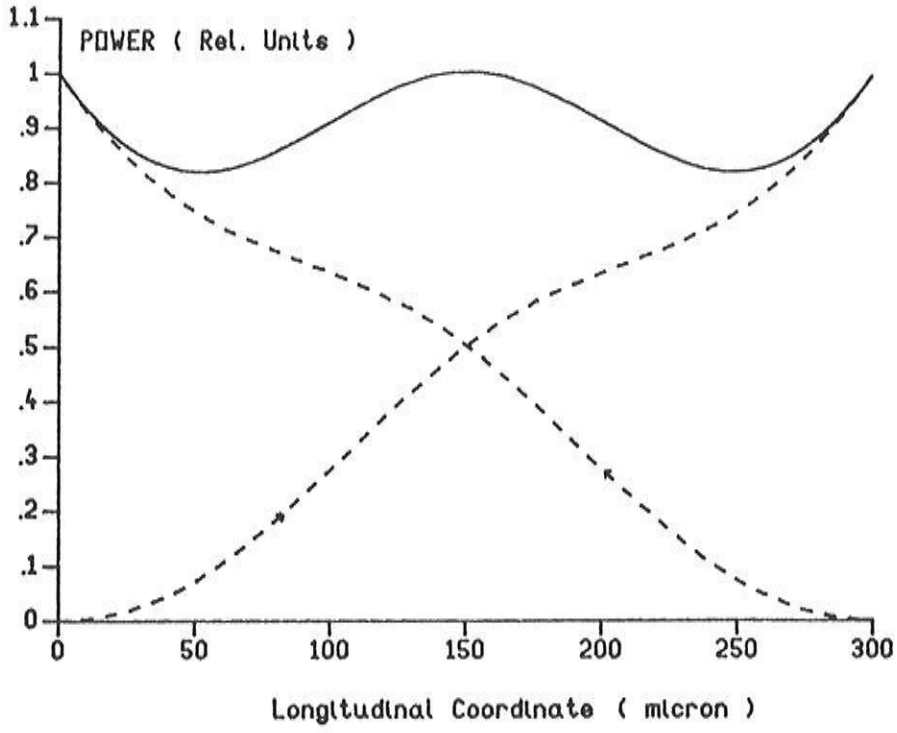

Fig.4.3.15: Longitudinal variation of the power for a 5-section approximation of (4.3.20a) (see text).

IV.3.3 Gain-coupled lasers

The use of gain-coupling (i.e. a periodic variation in gain or loss) provides an alternative for the previous index-coupled structures [4.17]. In the following, it will become clear that by supplying even a small fraction of gain-coupling to the index-coupling one can get very stable single mode lasers with low spatial hole burning. Moreover, gain-coupling also results in both a spectacular decrease of the threshold gain (and current) and a strong increase in threshold gain difference ΔgL. A tremendous performance is already obtained for a gain-coupling equal to a few tenths of the index-coupling. Theoretically, one finds a stable single mode behaviour up to power levels of more than 50 mW in this case.

An analysis of the influence of gain coupling on distributed feedback lasers has already been given by Kapon [4.18], who calculated the threshold behaviour of AR-coated lasers for several values of the normalized coupling coefficient and for various degrees of gain-coupling. We have extended this analysis by considering above-threshold operation and by optimisation of the normalized coupling coefficient in order to obtain minimal spatial hole burning.

Before proceeding with the analysis, we remark that some gain-coupling can also be present in so-called index-coupled lasers. Indeed, the grating in the passive layer modifies the lateral/transverse mode profile and hence also the confinement factor Γ. Furthermore, the standing wave pattern in the power, caused by the interference between the forward and backward propagating beams gives rise to a weak periodic variation of the carrier density, which acts as gain-coupling as well. It is estimated however that the gain-coupling, originating from both effects, only amounts to a few percent of the index-coupling in a typical index-coupled laser. On the other hand, DFB lasers with a considerably higher degree of gain-coupling have been produced [4.19] and they seem to exhibit excellent single mode properties.

The coupled wave equations for DFB lasers with both index- and gain-coupling can be written as:

$$\frac{dR^+}{dz} + j\Delta\beta\ R^+ = (\kappa_g + j\kappa_n)\ R^- \qquad (4.3.21a)$$

$$\frac{dR^-}{dz} - j\Delta\beta\ R^- = -(\kappa_g + j\kappa_n)\ R^+ \qquad (4.3.21b)$$

in which the coupling constants κ_g, resp. κ_n stand for the gain-, resp. the index-coupling. The phases of κ_g and κ_n are assumed to be equal here, which is justified if the gain- and index-coupling are induced by one grating (e.g. a modulation of the active layer thickness). The phase difference between κ_g and κ_n then can only assume the values 0 and π, whereas a phase difference of π would only cause a change in the sign of the Bragg deviation of the lasing mode. In addition, the grating phase at the left facet is chosen such that κ_g and κ_n are both real.

We have calculated the threshold gain $2\Delta\beta_i$, the threshold gain difference ΔgL, the real Bragg deviation $\Delta\beta_r$ and the longitudinal spatial hole burning of AR-coated lasers of length 300 μm as a function of κ_g/κ_n. The value of $|\kappa|$ is optimised so as to achieve minimal spatial hole burning. As a measure for the spatial hole burning, we use the ratio P_{min}/P_{max} with $P_{min(max)}$ denoting the minimum (maximum) value of the power along the longitudinal axis. Above threshold, the power level P_m where the SMSR drops below 20 dB has been calculated.

Fig. 4.3.16 shows the value of $|\kappa|L$ that gives minimal spatial hole burning and the corresponding value of P_{min}/P_{max}. Little spatial hole burning is obtained in all cases and one can see that a uniform power results for pure gain-coupling. $|\kappa|L$ equals the value $\pi/2$ in this case and both $\Delta\beta_i$ and $\Delta\beta_r$ are zero. It can easily be verified that the solution of the coupled wave equations then reduces to:

$$R^+(z) = \sin(\pi z/2L)\ ;\ R^-(z) = \cos(\pi z/2L) \qquad (4.3.22)$$

The longitudinal variation of forward and backward propagating power, as well as the total power is depicted in fig. 4.3.17 for three values of κ_g/κ_n (10^{-2}, 0.5 and 10). A relatively uniform power is also found for the case of weak gain-coupling or almost pure index-coupling. The low threshold gain difference in this case makes

such a laser unattractive however. As $\kappa_g$increases, both R^+ and R^- become more sinusoidal and the power becomes more uniform.

Fig. 4.3.18 shows the variation of $\Delta\beta_i$ and $\Delta\beta_r$ as a function of κ_g/κ_n. The threshold gain and the Bragg deviation, as well as the spatial hole burning are slowly decreasing functions of the gain-coupling for small values of κ_g/κ_n, but they rapidly approach zero if the gain-coupling becomes comparable with or larger than the index-coupling. The threshold gain difference (fig. 4.3.19) on the other hand increases considerably for even a small fraction of gain-coupling. The output power P_m (the dashed curve on fig. 4.3.19) where the SMSR drops below 20 dB also increases rapidly for increasing gain-coupling. E.g. for κ_g/κ_n=0.05 we obtained a genuine single mode behaviour (SMSR > 30 dB) up to an output power level of more than 50 mW.

Due to the gain-coupling, the phase resonances occur no longer at wavelengths that are symmetric with respect to the Bragg wavelength (as in index-coupled AR-coated lasers). This asymmetry in the phase resonance can be seen from the resonance condition, which is easily derived from the coupled wave equations:

$$\exp(2\delta L) = -\frac{\delta + \Delta\beta_i - j\Delta\beta_r}{\delta - \Delta\beta_i + j\Delta\beta_r} \text{ with } \delta^2 = -(\Delta\beta)^2 - (\kappa_g + j\kappa_n)^2 \qquad (4.3.23)$$

In the high gain approximation e.g., $|\Delta\beta| >> |\kappa|$, one finds the phase resonance condition:

$$\left\{\Delta\beta_r + \frac{[2\kappa_g\kappa_n\Delta\beta_i + \Delta\beta_r(\kappa_g^2 - \kappa_n^2)]}{2\,(\Delta\beta_r^2 + \Delta\beta_i^2)}\right\} L = tg^{-1}\left(\frac{\Delta\beta_r}{\Delta\beta_i}\right) + tg^{-1}\left(\frac{\kappa_n}{\kappa_g}\right) + m\pi \qquad (4.3.24)$$

from which it is easily verified that the phase resonances are symmetric with respect to the Bragg wavelength only for κ_g=0 or κ_n=0.

At the same time, a larger effective gain is provided for the cavity mode nearest to the Bragg wavelength. This effect can be understood from the presence of a standing wave pattern, both in the power of the cavity modes (with period $\lambda/2n_e$) and in the gain (period Λ). The overlap of both standing wave patterns, which

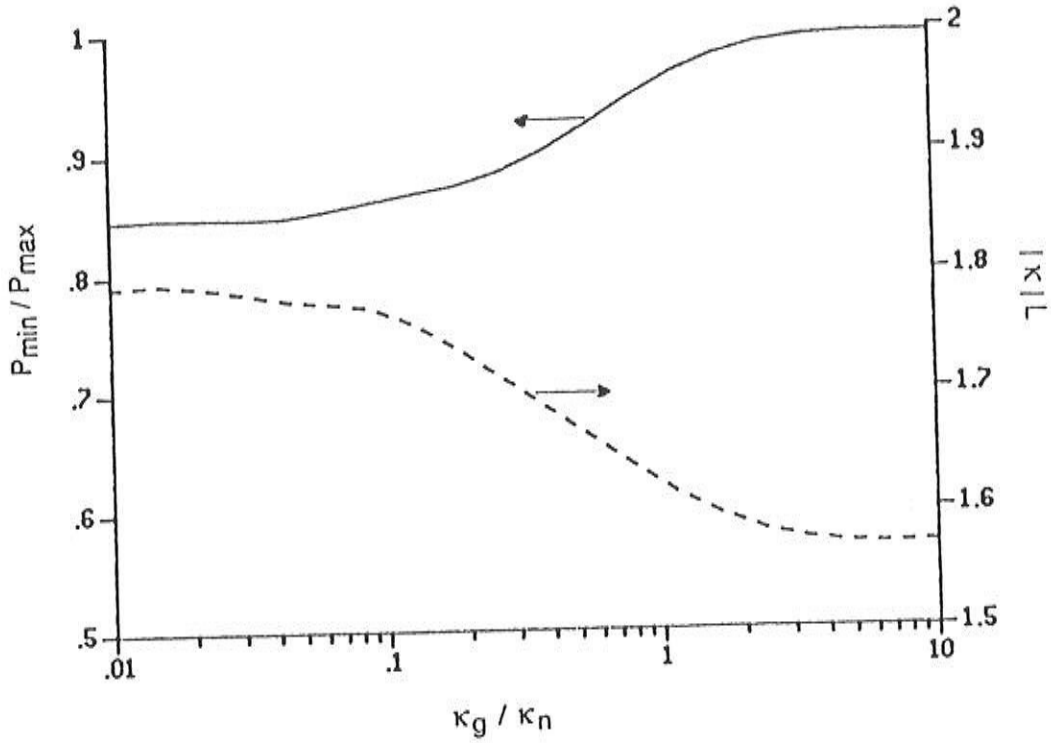

Fig.4.3.16: Optimum value of P_{min}/P_{max} (—) and of κL (--) as a function of κ_g/κ_n.

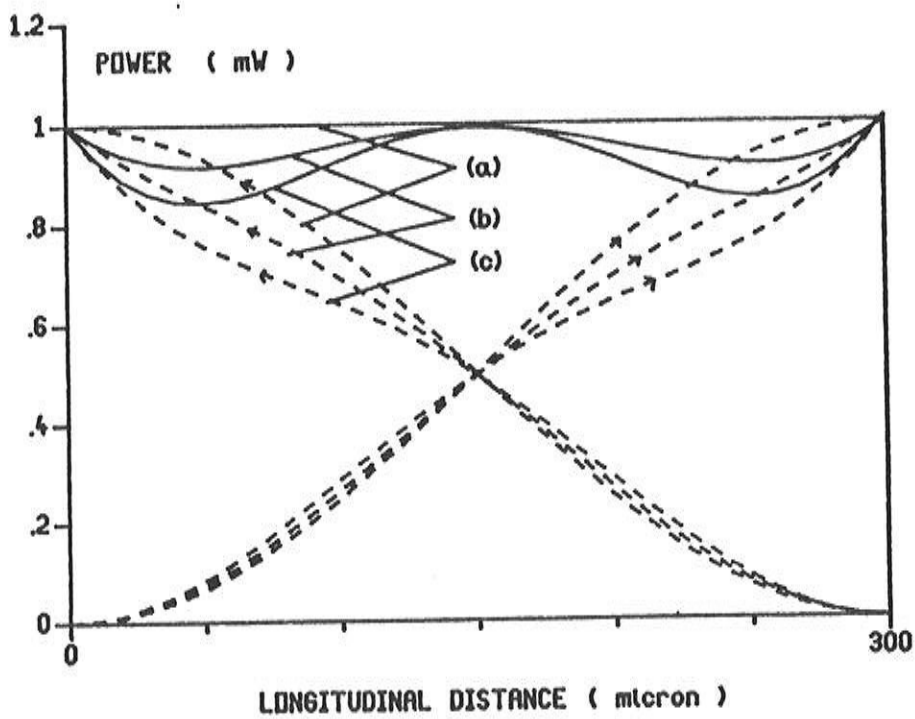

Fig.4.3.17: Longitudinal variation of the power for: κ_g/κ_n=10 (a), κ_g/κ_n=0.5 (b) and κ_g/κ_n=0.01 (c).

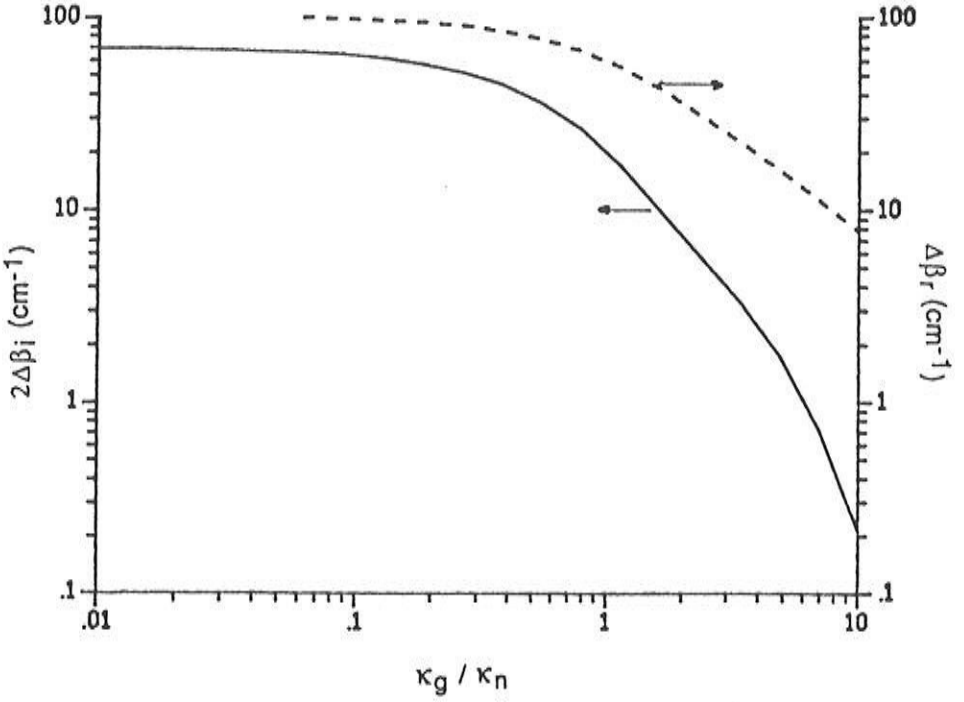

Fig.4.3.18: Variation of $2\Delta\beta_i$ (—) and $\Delta\beta_r$ (---) vs. κ_g/κ_n.

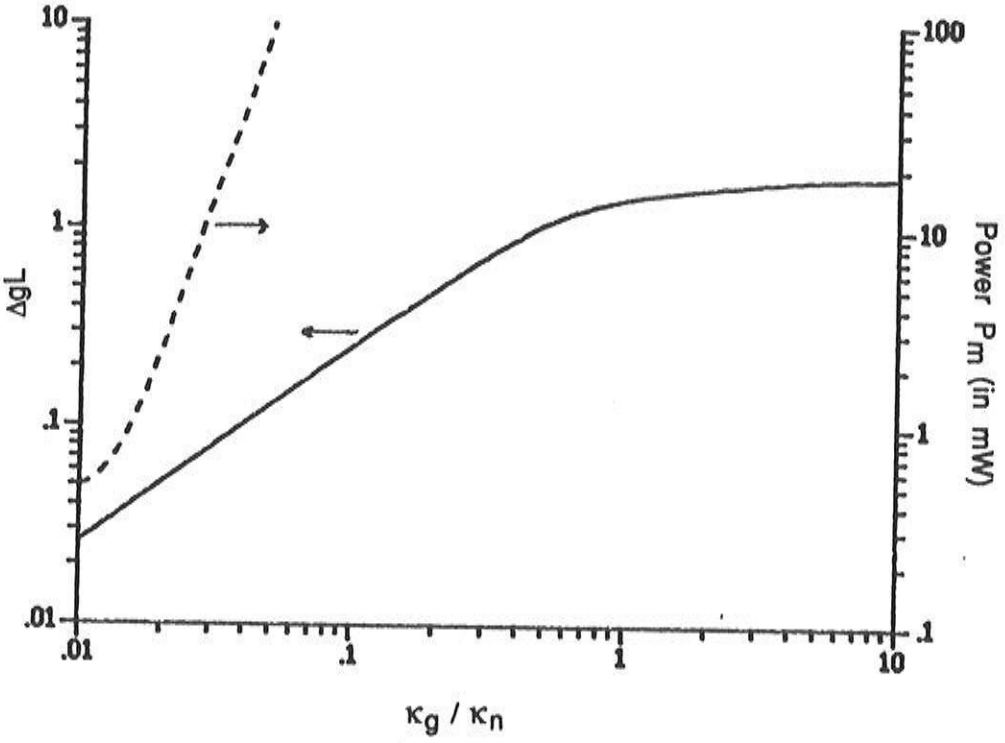

Fig.4.3.19: Variation of ΔgL (—) and P_m (---) vs. κ_g/κ_n.

describes the degree of coincidence of points with high gain and points with large optical power, increases for a decreasing difference between mode wavelength and Bragg wavelength. This results in a larger netto stimulated emission rate.

This standing wave aspect also finds expression in the photon rate equation (2.3.7), which for gain-coupled lasers reads:

$$\frac{dI}{dt} = [G(N_0,\omega) - \gamma]\, I + S + \frac{4\,\kappa_g}{h\omega}\int_0^L r^+ r^- \cos(\varphi^- - \varphi^+)\,dz + F_I \qquad (4.3.25)$$

The 3rd term on the r.h.s. of (4.3.25) is identical to the overlap integral between the standing wave patterns in the power and in the gain. Indeed, the standing wave patterns in the power and in the gain are:

$$|E|^2 = |r^+ e^{j(\varphi^+ - \beta_g z)} + r^- e^{j(\varphi^- + \beta_g z)}|^2$$
$$= (r^+)^2 + (r^-)^2 + 2r^+ r^- \cos(\varphi^- - \varphi^+ + 2\beta_g z)$$
$$\Delta(\Gamma g) = 2\,\kappa_g \cos(2\beta_g z) \qquad (4.3.26)$$

Only the first harmonic of $\Delta(\Gamma g)$ is retained here since the higher harmonics disappear after averaging over the longitudinal coordinate. The overlap integral is given by:

$$\int_0^L dz\; 4\,\kappa_g r^+ r^- \cos(2\beta_g z)\cos(2\beta_g z + \varphi^- - \varphi^+) =$$
$$4\,\kappa_g \int_0^L dz\; r^+ r^- \cos(\varphi^- - \varphi^+) \qquad (4.3.27)$$

It must finally be noticed that the calculations discussed here are valid only for an optimized value of $|\kappa|L$. In practical calculations however, the gain-coupling and thus $|\kappa|L$ generally will depend on the threshold gain (see [4.20]). Such a dependence is not taken into account in our calculations. For values of κ_g not larger than a few tenths of κ_n, there is hardly any influence of κ_g on $|\kappa|L$ and the optimum value solely depends on the choice of κ_n. The threshold gain and Bragg deviation remain almost independent of κ_g

in this case, and practically, κ_g can be calculated from the threshold gain of the corresponding index-coupled laser.

Although we have only considered AR-coated lasers here, it can be mentioned that the introduction of gain-coupling is equally well advantageous for lasers with cleaved facets (or facets with a finite reflection). The phase of the reflection coefficients seems to have less influence in this case and a larger yield of single mode lasers can be expected [4.21].

References

[4.1] P. Mols, P. Kuindersma, M. Van Es-Spiekman, I. Baele, 'Yield and device characteristics of DFB lasers: statistics and novel coating design in theory and experiment', IEEE Journ. Quant. El., Vol. 25, pp. 1303-1319, June 1989.

[4.2] J. Buus, 'Mode selectivity in DFB Lasers with cleaved facets', El. Lett., Vol. 21, pp. 179-180, 1985.

[4.3] J. Kinoshita, K. Matsumoto, 'Yield analysis of SLM DFB Lasers with an Axially-Flattened Internal Field', IEEE Journ. Quant. El., Vol. 25, pp. 1324-1332, June 1989.

[4.4] M. Erman, 'Integrated Guided-Wave Optics on III-V Semiconductors', Proc. of on Gallium Arsenide and Related Compounds, Heraklion, Crete, Greece, Sep. 1987.

[4.5] H. Soda, Y. Kotaki, H. Sudo, H. Ishikawa, S. Yamakoshi, H. Imai, 'Stability in single longitudinal mode operation in GaInAsP/InP phase-adjusted DFB lasers', IEEE Journ. Quant. El., Vol. 23, pp. 804-814, June 1987.

[4.6] P. Vankwikelberge, 'Theoretische studie van statische en dynamische longitudinale effecten in Fabry-Perot en DFB-diodelasers', Ph. D. thesis (in Dutch), University of Gent.

[4.7] Y. Yoshikuni, K. Oe, G. Motosugi, T. Matsuoka, 'Broad wavelength tuning under single-mode oscillation with a multi-electrode distributed feedback laser', El. Lett., Vol. 22, pp. 1153-1154, 1986.

[4.8] M. Usami, S. Akiba, 'Suppression of Longitudinal Spatial Hole-Burning in λ/4-Shifted DFB Lasers by Nonuniform Current Distribution', IEEE Journ. Quant. El., vol. 25, pp. 1245-1253, June 1989.

[4.9] Y. Kotaki, S. Ogita, M. Matsuda, Y. Kuwahara, H. Ishikawa, 'Tunable, Narrow-linewidth and High-power λ/4-shifted DFB Laser', El. Lett., Vol. 25, pp. 990-991, July 1989.

[4.10] T. Kimura, A. Sugimura, 'Coupled Phase-Shift Distributed Feedback Semiconductor Lasers for Narrow Linewidth Operation', IEEE Journ. Quant. El., Vol. 25, pp. 678-683, April 1989.

[4.11] G. Agrawal, J. Geusic P. Anthony, 'Distributed feedback lasers with multiple phase-shift regions', Appl. Phys. Lett., Vol. 53, pp. 178-179, July 1988.

[4.12] S. Ogita, Y. Kotaki, M. Matsuda, Y. Kuwahara, H. Ishikawa, 'Long-cavity, Multi-phase-shift, distribu-ted feedback laser for linewidth narrowing', El. Lett., Vol. 25, pp. 629-630, 1989.

[4.13] T. Schrans, A. Yariv, 'Semiconductor lasers with uniform longitudinal intensity distribution', Appl. Phys. Lett., Vol. 56, pp. 1526-1528, April 1990.

[4.14] G. Morthier, K. David, P. Vankwikelberge, R. Baets, 'A New DFB Laser Diode with Reduced Spatial Hole Burning', IEEE Phot. Techn. Lett., Vol. 2, pp. 170-172, June 1990.

[4.15] G. Heise, R. Max, U. Wolff, 'Phase-shifted holographic gratings for distributed feedback lasers', SPIE, Vol. 651.

[4.16] D. Reid, C. Ragdale, I. Bennion, D. Robbins, J. Buus, W. Steward, 'Moiré Fibre Grating Resonators', MOC/GRIN '89, PD5, pp. 19-22, Tokyo, Japan, 1989.

[4.17] G. Morthier, P. Vankwikelberge, K. David, R. Baets, 'Improved Performance of AR-coated DFB Lasers by the Introduction of Gain Coupling', IEEE Phot. Techn. Lett., Vol. 2, pp. 170-172 , March 1990.

[4.18] E. Kapon, A. Hardy, A. Katzir, 'The effects of complex coupling coefficients on distributed feedback lasers', IEEE Journ. Quant. El., Vol. 18, pp. 66-71, 1982.

[4.19] Y. Luo, Y. Nakano, K. Tada, T. Inoue, H. Hosomatsu, H. Iwaoka, 'Gain-coupled DFB semiconductor laser having corrugated active layer', Proc. 7th Int. Conf. Integrated Opt. and Opt. Fiber Commun., Japan, pp. 40-41, 1989.

[4.20] K. David, J. Buus, G. Morthier, R. Baets, 'Coupling Coefficients in Gain Coupled DFB Lasers: Inherent compromise between coupling strength and loss', IEEE Phot. Techn. Lett., May, 1991.

[4.21] K. David, G. Morthier, P. Vankwikelberge, R. Baets, 'Yield analysis of non-AR-coated DFB lasers with combined index and gain coupling, El. Lett., Vol. 26, pp. 238-239, 1990.

Chapter V

THE NOISE IN DFB LASERS: LINEWIDTH, RIN AND POWER SPECTRUM

This chapter describes the influence of the (spontaneous emission and other) noise on the power spectrum. This influence is twofold: on one hand, it causes phase fluctuations and a broadening of the emission lines (the width of the emission line corresponding with the main mode is then called the linewidth), while on the other hand it also results in fluctuations in the light intensity (expressed by the so-called RIN, Relative Intensity Noise).

Our research in this field principally aimed at understanding the linewidth behaviour, in particular the rebroadening or the saturation of the linewidth at moderate or high power levels. Indeed, according to well-accepted theories (see [5.1], [5.2], [5.3] or chapter 2) the linewidth ought to decrease with increasing power level, whereas experiments show that this is no longer the case at moderate or high power levels. We have found a few original explanations for this phenomenon and a large part of this chapter is dedicated to it.

However, other aspects of the noise are considered here as well. Interesting modelling results, other than those relating to the linewidth rebroadening, have indeed been obtained. In addition, we have tried to touch the most important aspects related to noise. In this respect, we have chosen to introduce a brief overview of the recent literature here. This is then followed by a detailed description of the linewidth and RIN behaviour. The latter also includes topics such as the spectra of the FM-noise, the intensity noise and the power as well and the reduction of linewidth and RIN. A last paragraph describes the influence of external feedback.

We finally remark that this chapter relies heavily on the rate equations and their analytical, small-signal solutions.

V.1 Overview of literature

For a long time, the linewidth and the RIN of DFB lasers have been calculated with the help of the standard rate equation solutions as given in II.3. The mode loss and the relation between photon number and output power are then determined from solution of the coupled wave equations, in which a uniform carrier density is assumed.

Recently, various modifications of these standard formuli for linewidth and RIN have been proposed. First, the longitudinal variation of the optical power was included by the introduction of a structure dependent factor K (the longitudinal Petermann factor) in S [5.4], [5.5]:

$$S_{eff} = S\,K$$

$$\text{with: } K = \frac{\left| \int_0^L [(r^+)^2 + (r^-)^2]\, dz \right|^2}{\left| \int_0^L R^+ R^-\, dz \right|^2} \qquad (5.1.1)$$

The mode index has been left behind here. K can assume values up to 4, but it has only a weak bias dependence, unable to cause a linewidth rebroadening.

The previous approach was given a more theoretical basis by Henry [5.6], who proposed a Green's function approach for the equation (2.2.7). With this theory, the formula (5.1.1) can be retrieved for Fabry-Perot lasers. More accurate formuli are found for DFB-lasers. Henry's paper has given rise to numerous other contributions, e.g. about the application to ordinary DFB lasers [5.7], to multi-phase-shifted lasers [5.8] or to multi-electrode lasers [5.9]. Spatial hole burning, i.e. a non-uniform carrier density is usually not considered when a Green's function is derived. Including it would require extensive numerical treatment anyway.

Some theories further account for the dispersion in gain [5.10] or loss [5.11]. These theories again ignore the spatial hole burning, resulting in a bias dependence of the dispersion. They the-

refore lead to a linewidth that is proportional with the inverse output power.

By solving the rate equations in the multi mode case, it was shown that the presence of relatively strong side modes could cause a substantial enhancement of the linewidth and the RIN [5.12], [5.13], [5.14]. The interaction between main and side mode has thereby been attributed to gain suppression. We will show furtheron how also spatial hole burning can be responsible for the influence of a side mode on the main mode. A linewidth rebroadening due to the presence of side modes can occur when the side mode suppression drops below ±20 dB. However, one finds experimentally that a rebroadening also takes place if the side mode suppression remains well above 30 dB.

A last modification of the standard formuli is based on the introduction of an effective linewidth enhancement factor α_{eff} [5.15]. This effective α-factor can be calculated from a complex, longitudinal confinement factor:

$$\Gamma_z = \Gamma_z' + j\Gamma_z'' = -\frac{R^+ R^-}{\int_0^L R^+ R^- dz} L \qquad (5.1.2)$$

The effective α-factor and the linewidth are given by:

$$\Delta\nu = \frac{S}{4\pi I}(1 + \alpha_{eff}^2)$$

$$\alpha_{eff} = \frac{\int_0^L [\alpha\,\Gamma_z' - \Gamma_z'']\,\Delta N(z)\,dz}{\int_0^L [\Gamma_z' + \alpha\,\Gamma_z'']\,\Delta N(z)\,dz} \qquad (5.1.3)$$

in which $\Delta N(z)$ represents the z-dependent change in carrier density caused by the Langevin forces. This small-signal carrier density can be obtained as a function of the photon density after linearisation of the carrier rate equation. $\Delta N(z)$ can then be expressed in terms of the steady state carrier density and the steady state photon denstiy if one assumes a similar z-dependence for the steady state and the small-signal photon density.

The theory of the effective α-factor can easily be derived from the wave equation and is therefore most justified. It also allows to take into account spatial and spectral hole burning in an easy manner. Its implications are illustrated by fig. 5.1.1, which gives the α_{eff} of AR-coated lasers as a function of κL [5.15]. One can see that the use of α_{eff} could result in a considerable enhancement or reduction of the linewidth. One drawback is that dispersion effects are still not included.

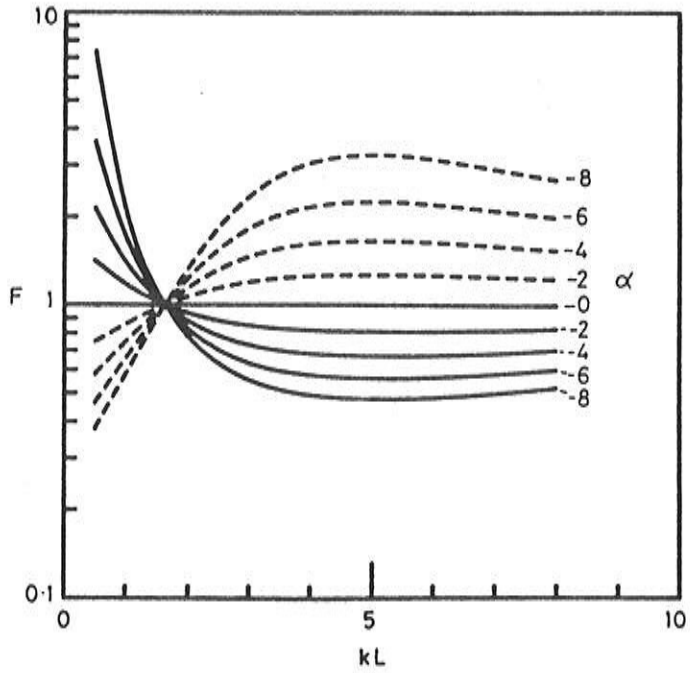

Fig. 5.1.1: correction factor for the linewidth resulting from α_{eff} for AR-coated lasers: (—) $\lambda>\lambda_B$, (--) $\lambda<\lambda_B$.

By solving the coupled wave equations and the carrier rate equation, our model will take all previous effects into account. Moreover, it is more suitable for the analysis of multi-section lasers, such as external cavity lasers. Spatial hole burning, gain suppression and dispersion are all taken into account self consistently and at the same time . The power level and the mode profile of the side modes are calculated self consistently as well, whereas in [5.12] and [5.13] one has to assume a certain power level for the side modes, of which no spatial variation is considered. Finally, our model also offers the possibility to include dynamic effects in a more detailed way.

V.2 The linewidth of DFB lasers

Before discussing possible causes of the linewidth rebroadening, we first illustrate the FM-noise and the adiabatic approximation which is usually applied to it. We then pay attention to the different factors that determine the linewidth, i.e. causes of the rebroadening such as the presence of side modes, gain non-linearities and dispersion and other important factors. We conclude by an overview of methods that allow to reach smaller linewidths.

V.2.1 The adiabatic approximation

For the calculation of the linewidth, the spectrum of the FM-noise is normally approximated as a white noise spectrum. The validity of this approximation is confirmed by fig. 5.2.1, which gives the spectrum of the FM-noise for laser A at 1 mW output power. The spectrum is white (uniform) in a bandwidth of ± 1 GHz. Relaxation oscillations, which are heavily damped by spectral hole burning, occur at a few GHz. The oscillations, which are the expression of a resonant conversion of electrons into photons and vice-versa, due to stimulated emission and absorption, are also damped by spontaneous emission and diffusion. The spectral density of the FM-noise decreases rapidly beyond these oscillations.

The FM-noise has a spectral density of 314 MHz in the flat part of the spectrum. This implies that practically no loss of coherence occurs during the characteristic time of the relaxation oscillations (≤ 1 nsec.) and that these oscillations have no influence on the linewidth. The adiabatic approximation is therefore valid and one finds a linewidth $\Delta\nu$ = 50 MHz, corresponding with a coherence time of 20 nanoseconds.

The presence of relaxation oscillations in the power spectrum is only at low power levels visible in DFB lasers. The relaxation oscillations are not yet heavily damped by spectral hole burning in this case. Fig. 5.1.2 shows the power spectrum of laser A at an output power of 1 mW. The relaxation oscillations occur at frequencies where the spectral density of the power has already decreased to 30 dB below the peak value. The strength of these oscillations decreases strongly with bias power anyway. Fig.5.1.2 clearly illustrates the heavy damping due to spectral hole burning. From

chapter 2 (eq. 2.3.19) we know that the damping is proportional with the gain suppression coefficient ξ.

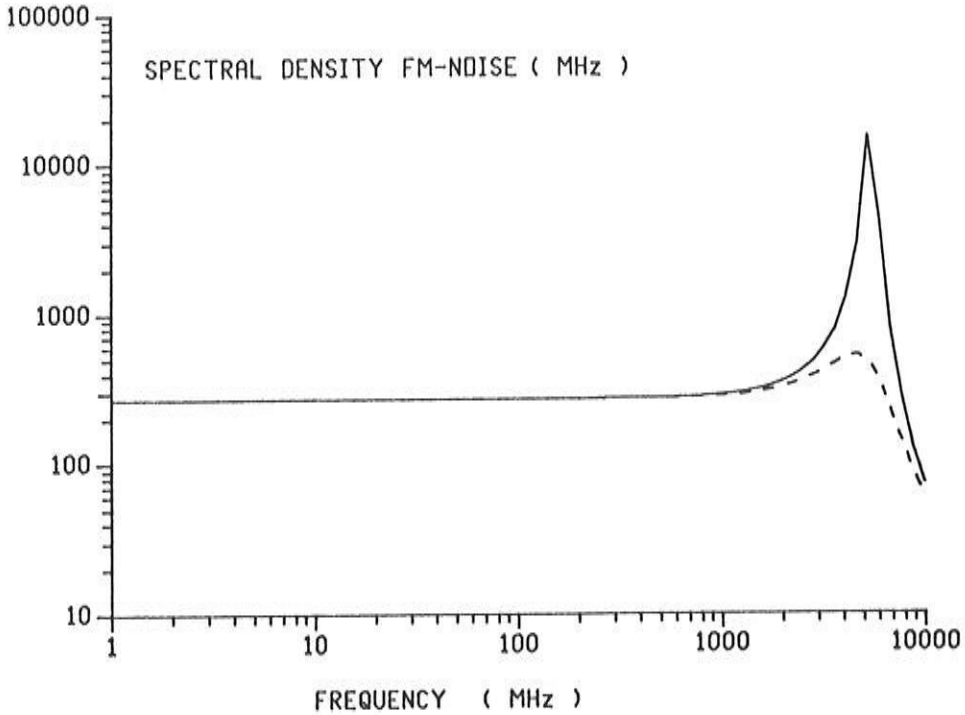

Fig. 5.2.1: FM-noise for laser A at 1 mW bias power with (--) and without (—) gain suppression

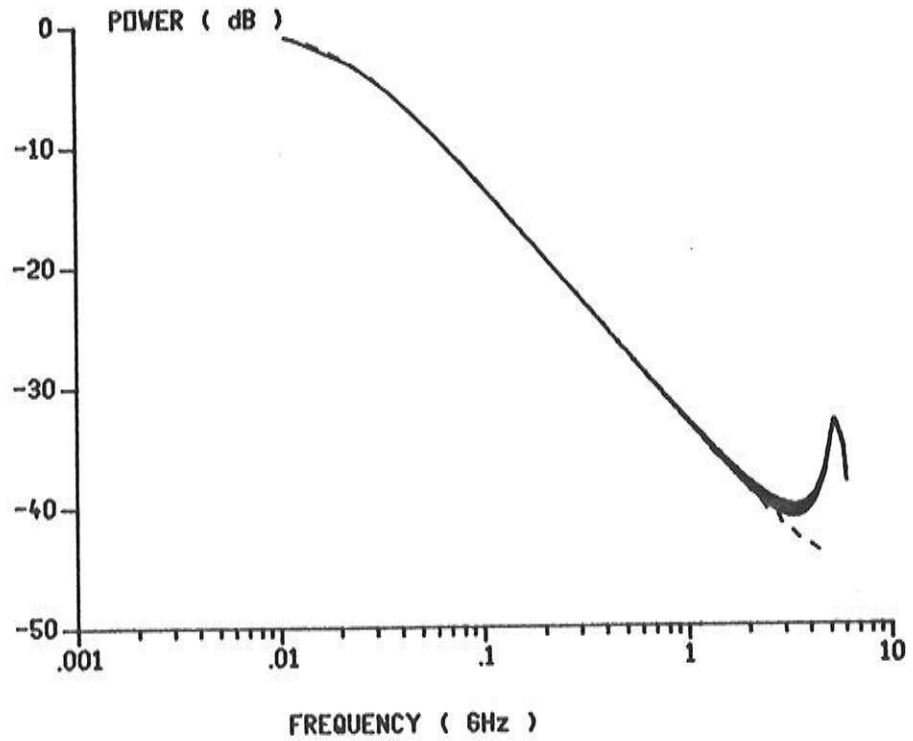

Fig. 5.2.2: Power spectrum of laser A at 1 mW bias power with (--) and without (—) gain suppression

V.2.2 Causes of linewidth rebroadening

V.2.2.1 The presence of side modes

The influence of a side mode (with intensity I_1) on the linewidth of the main mode (with intensity I_0) can, in DFB lasers, have its origin in two non-linearities:

- Spectral hole burning (or more general gain suppression), expressed by the coefficients ξ_{mk} in the rate equations.

- Spatial hole burning, by which, in DFB lasers, mainly the losses γ_0 and γ_1 of main and side mode are affected. These losses depend on the longitudinal variation of the carrier density, which in turn depends on the intensities I_0 and I_1 of both modes.

The interaction via spectral hole burning is easily estimated analytically. In this case, we assume the following:

$$\xi_{00} = \xi_{11}$$
$$\xi_{01} = \xi_{10} < \xi_{00} \qquad (5.2.1)$$

From calculations of the spectral hole burning [5.16] it seems that the coefficients ξ_{mk} (or ε_{mk}) mainly depend on the wavelength difference $|\lambda_m - \lambda_k|$ and that they reach a maximum value for m=k. The maximum value then depends only little on the wavelength λ_m.

From the analytical solution of the rate equations (II.3.1 with 2 modes being taken into account), it follows that one can distinct between 3 regimes.

1/ The side mode is far below threshold (i.e. strongly suppressed) and one has:

$$\frac{\gamma_1}{G_1} - 1 >> \xi_{00} I_1 \text{ or } \frac{S}{G_1} >> \xi_{00} I_1^2 \qquad (5.2.2)$$

The linewidth of the main mode is independent of the side mode intensity in this case. The fluctuations in the intensity of the side

mode are too small to affect the gain via spectral hole burning here. Indeed, the second order moment of the Langevin function $F_{I,1}$ is proportional with the side mode intensity and thus very small. Since the side mode is far below threshold, its gain is far less than its loss. The spontaneous emissions therefore are hardly amplified and only give small fluctuations in the side mode intensity.

2/ The side mode reaches the threshold, but still has a small intensity. One then finds the following approximation for the main mode linewidth:

$$\Delta\nu = \frac{S}{4\pi I_0}\{1+\alpha^2\} + \frac{\alpha^2 G_1^2 I_1^3 (\xi_{00}-\xi_{01})^2}{4\pi S\,(1-\xi_{00} I_0)^2} \qquad (5.2.3)$$

In this regime, an increase of the linewidth occurs when the side mode intensity increases as it reaches the threshold. From (5.2.3), it can be derived that the side mode only has a significant influence when its average intracavity power becomes ± 50 μW or more [5.12], [5.13]. The broadening of the linewidth can be explained by noticing that, since the side mode is just below or at threshold, no clamping of the side mode gain yet exists in this regime. However, the gain of the side mode almost compensates the loss and the enhanced resonance makes that all spontaneous emissions are strongly amplified (they are propagated many times back and forth inside the cavity). Hence, large fluctuations in the side mode intensity and in the gain (due to spectral hole burning) are generated. Since the gain of the main mode must be clamped to a value equal to the main mode loss, the fluctuations in the gain, caused by spectral hole burning, must be compensated by large fluctuations of the carrier density. These large fluctuations in carrier density in turn cause large fluctuations in the refractive index and, as a result of the phase resonance condition, large frequency fluctuations and a large linewidth.

3/ The side mode is far above threshold and its intensity no longer consists of amplified spontaneous emission. In this case, one finds for the linewidth of the main mode (with $2\xi_{av}=\xi_{00}+\xi_{01}$):

$$\Delta\nu = \frac{S}{4\pi I_0} + \frac{\alpha^2 S}{16\pi I_0 I_1} \frac{[I_0(1-2\xi_{av}I_1)^2 + I_1(1-2\xi_{av}I_0)^2]}{[1-\xi_{av}(I_0+I_1)]^2} \qquad (5.2.4)$$

The linewidth decreases again with increasing power in main and side mode in this regime. Both modes are now truly oscillating and the fluctuations of the carrier density are restricted by the fact that the gain of both modes must remain equal to the loss. The fluctuations in the intensity of the side mode are more damped as compared with 2/ and the spectral hole burning effect no longer occurs. The fluctuations of the carrier density are damped by both modes and an increase in the power of one of these modes implies a stronger damping and thus a smaller linewidth.

The influence of the side mode via spatial hole burning can be described in a similar way by expanding the losses γ_0 and γ_1 in the small signal analysis as:

$$\gamma_0 = \Gamma_0 (1 - \sigma_{00}\Delta I_0 - \sigma_{01}\Delta I_1)$$
$$\gamma_1 = \Gamma_1 (1 - \sigma_{10}\Delta I_0 - \sigma_{11}\Delta I_1) \qquad (5.2.5)$$

Numerical values for the coefficients σ_{mk} (which are not necessarily positive numbers) are not easily obtained however. The effect can be investigated numerically in this case, i.e. by setting all spectral hole burning coefficients zero in the model. As an example, we consider again the laser B, of which we know from chapter 4 that it becomes multi mode at an output power of ± 2 mW due to spatial hole burning.

Fig. 5.2.3 shows the linewidth vs. the inverse output power. The linewidth has been calculated both with and without taking into account the presence of the side mode. Fig. 5.2.3 also gives the relative side mode intensity. Again, one can distinguish between 3 regimes. As long as the side mode remains strongly suppressed, the fluctuations in its intensity also remain small and the side mode has no influence on the main mode linewidth.

As soon as the side mode approaches the threshold however, a steep rebroadening of the linewidth occurs. The large fluctuations in the intensity of the side mode now induce large fluctuations in the loss of the main mode via spatial hole burning. Large fluctua-

tions in the carrier density (or the gain), and hence large fluctuations of the refractive index and the frequency, are then needed to compensate the loss at all time. For the numerical example under consideration, the rebroadening starts when the output power of the side mode reaches ± 50 μW, while the output power of the main mode is 2 mW. From other examples, it can be concluded that the rebroadening generally occurs when the side mode suppression decreases below 20 dB.

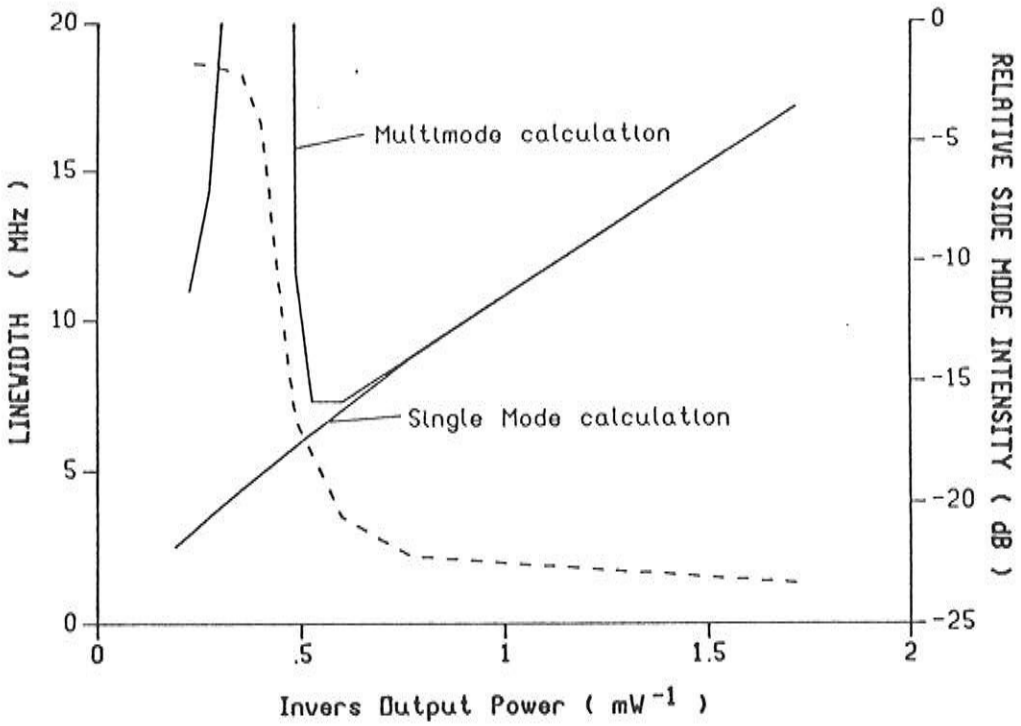

Fig. 5.2.3: Linewidth vs. inverse output power for laser B; Side mode suppression ratio.

As the side mode is far above threshold, one again finds a decreasing linewidth for increasing power level of main and side mode. As for the case of spectral hole burning, the fluctuations of the side mode intensity are no longer determined by the photon rate equation (which now expresses that the gain and the loss of the side mode must be equal), but by the carrier rate equation and they remain limited.

Fig. 5.2.4 show the influence of the side mode on the main mode linewidth when both spectral and spatial hole burning are in-

cluded in the calculations. A similar behaviour as in fig. 5.2.3 can be seen, i.e. the rebroadening occurs when the side mode suppression decreases below 20 dB. It can be noticed however that the side mode now reaches the threshold at an output power of 2.5 mW. Spectral hole burning has a stabilising influence on the side mode onset, as has been explained in chapter 4.

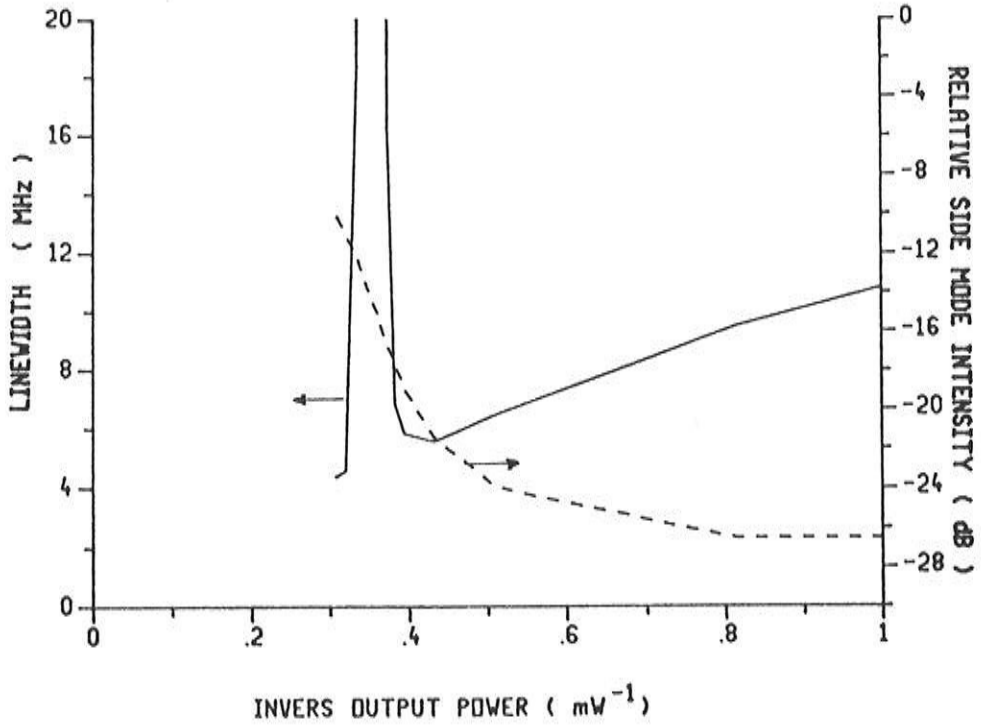

Fig. 5.2.4: Same as fig. 5.2.3, but gain suppression is also included now.

V.2.2.2 Gain suppression

The definition of the linewidth enhancement factor (equation 2.3.11) actually implies that α must be considered as a bias or power dependent quantity and therefore one can write for single mode lasers:

$$\alpha = \frac{\alpha_0}{1 - \xi_{00} I_0} \tag{5.2.6}$$

A gain suppression as in (2.3.3) has been used. Substitution of this expression for α in the linewidth formula (2.3.26) then gives:

$$\Delta\nu = \frac{S}{4\pi I_0} \left\{ 1 + \frac{\alpha_0^2}{(1 - \xi_{00} I_0)^2} \right\} \tag{5.2.7}$$

The bias dependence of α cannot be ignored at high power levels. Important is that it gives rise to a minimum in the linewidth at a bias level corresponding with $I_0 = 1/3\xi_{00}$ [5.17]. The linewidth rebroadening due to the gain suppression, which was proposed simultaneously by the author [5.18] and by Agrawal [5.19], is illustrated in fig. 5.2.5 for a 300 μm long as-cleaved F-P laser (in order to exclude all other effects such as spatial hole burning and dispersion). A value of $4.75\ 10^{-7}$ [5.20], [5.21] has been used for ξ, corresponding with $\varepsilon = 15\ W^{-1}$. Rebroadening of the linewidth occurs at an output power of about 14 mW. This is different from the value 11.5 mW which can be predicted from (5.2.7), but the difference can be attributed to the spontaneous carrier recombination. This recombination causes additional damping of the carrier density fluctuations, as can easily be found by rigourous solution of the static rate equations. One finds:

$$\Delta\nu = \frac{S}{4\pi I_0} \left\{ 1 + \frac{\alpha_0^2 (1 - \xi_{00} I_0)^2}{[(1 - \xi_{00} I_0)^2 + \xi_{00} V_a (A\tau_{rd})^{-1}]^2} \right\}$$

$$+ \frac{\alpha_0^2 \xi^2}{4\pi} \frac{V_a (N_0/\tau + B_0 N_0^2 + C_0 N_0^3)}{[(1 - \xi_{00} I_0)^2 + \xi_{00} V_a (A\tau_{rd})^{-1}]} \tag{5.2.8}$$

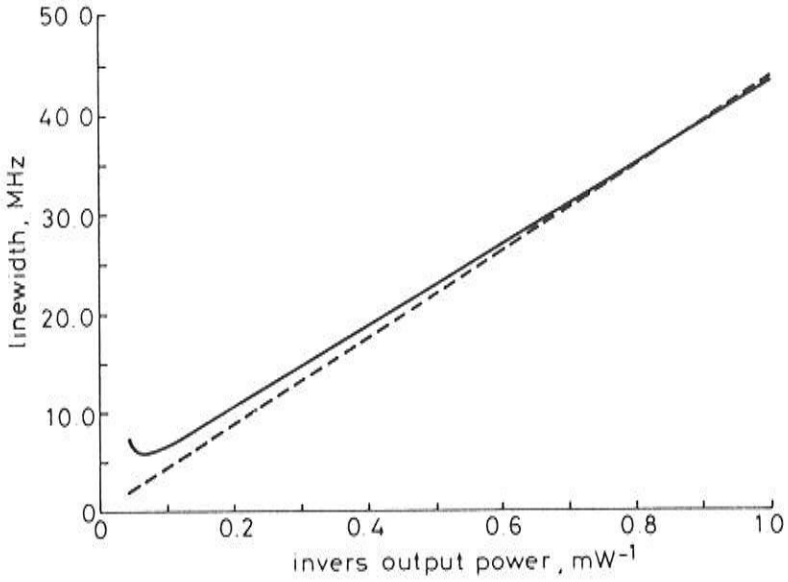

Fig. 5.2.5: Linewidth vs. inverse output power for a 300 μm long, as-cleaved F-P laser, with (—) and without (--) gain suppression taken into account.

The last term in (5.2.8) represents the effect of shot noise, which only has a minor influence in F-P and DFB lasers. It must also be remarked that N_0 (and thus also τ_{rd}) may be slightly bias dependent, due to gain suppression or other non-linearities. This might eventually turn the rebroadening into a saturation, especially if τ_{rd} is rather small.

A similar rebroadening can be found in DFB lasers. This is illustrated in fig. 5.2.6 for laser A. The linewidth has been calculated both with and without taking into account the spontaneous carrier recombination. One can clearly see how the minimum in the linewidth occurs at a higher power level due to the spontaneous carrier recombination.

Experimental evidence for the rebroadening due to spectral hole burning has been given by C. Park and J. Buus [5.22]. They have measured the linewidth at 1 mW output power, the minimum linewidth and the power at which it occurs for two populations of as-cleaved DFB lasers. All lasers were of the buried ridge type and the two populations were detuned from the gain peak by 20 nm and 30

nm respectively. The two populations therefore had different linewidth enhancement factors, being 7.7 and 6.5 respectively.

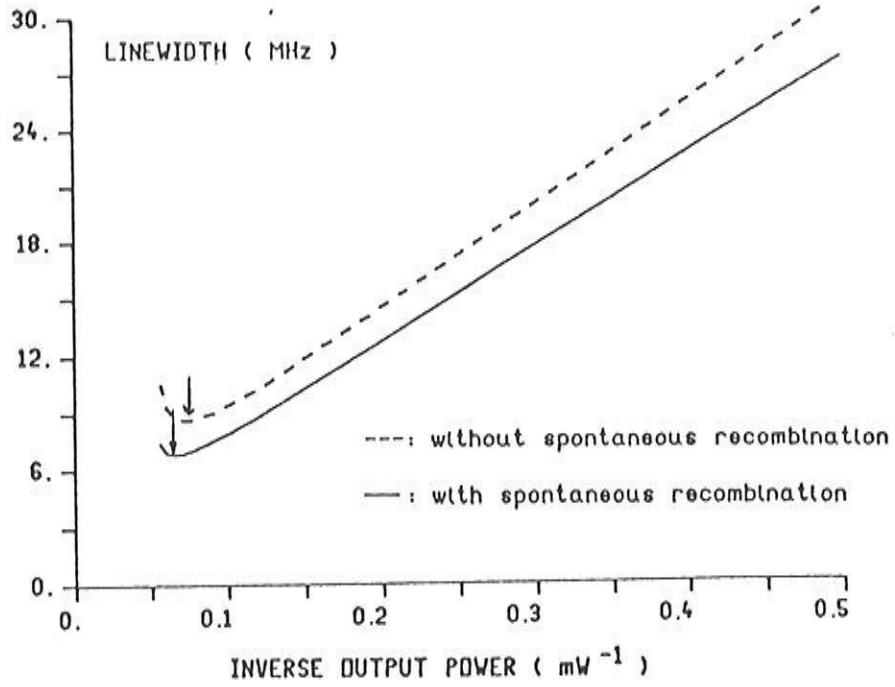

Fig. 5.2.6: Linewidth vs. inverse output power for laser A.

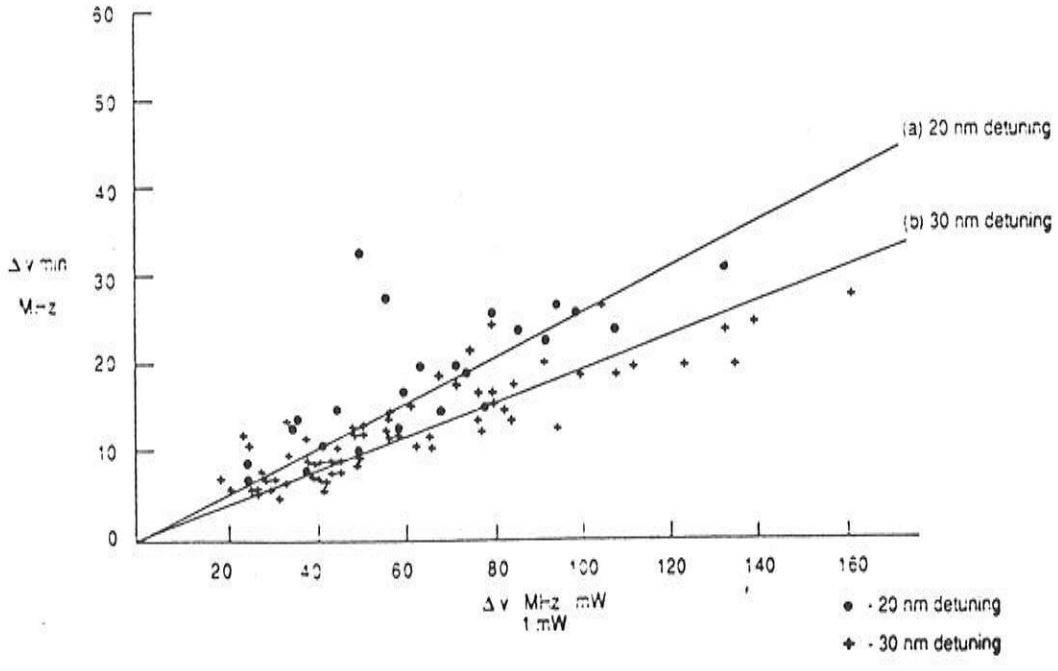

Fig. 5.2.7: Measured minimum linewidths against linewidth at 1 mW power for 2 populations of 1.55 μm DFB lasers [5.22].

Fig.5.2.7 shows the results for the single mode lasers. There seems to be a good correlation between the linewidth at 1 mW and the linewidth floor. The different gradients for different detuning in fig. 5.2.7 are consistent with the weak wavelenght dependence of the gain suppression factor ε.

The average ratio between minimum linewidth and the linewidth at 1 mW is approximately 0.22 mW^{-1} in fig. 5.2.7. This corresponds extremely well with the formula (5.2.7). From this formula, one finds that the ratio between the minimum linewidth and the linewidth at 1 mW (intracavity power) is given approximately by:

$$\Delta\nu_{min}/\Delta\nu_{(1\ mW\ intracavity\ power)} = \frac{27}{4}\varepsilon \qquad (5.2.9)$$

Since, for as-cleaved lasers, an output power of 1 mW corresponds with $\pm$ 2 mW intracavity power, it follows from fig. 5.2.7 that the value of ε is approximately 16 W^{-1} (a value to be compared with the value of 15 W^{-1} which is theoretically found for ε).

We finally remark that other non-linearities, which also have a different impact on gain and refractive index, exist. Standing wave induced gratings, two photon absorption and lateral carrier diffusion can be mentioned here. Moreover, other expressions for the gain suppression (or the power dependence of the gain) are being used, e.g.:

$$G_0 = \frac{AN_0 - B}{1 + I_0/I_s} \quad \text{or} \quad G_0 = \frac{AN_0 - B}{\sqrt{1 + I_0/I_s}} \qquad (5.2.10)$$

A different linewidth behaviour (see appendix V.a) is then found for these expressions.

V.2.2.2 Dispersion in the feedback

The distributed reflections and hence the loss in DFB lasers are strongly wavelength or frequency dependent, as has been outlined in II.3. This frequency dependence of the loss can also be seen from the wavelength dependence of the roundtrip gain. This dispersion may not be neglected in a linearisation of the rate equations.

More generally, the dispersion implies that variations in the frequency (due to modulation or noise) feed back via a variation in the loss. The last variation requires a variation of the carrier density (and thus of the refractive index and the frequency) so that the gain can compensate for the changed loss. Hence, one must, when linearising the rate equations, also include a variation in the loss of the form:

$$\Delta\gamma_0 = \frac{\partial\gamma_0}{\partial\omega_0}\Delta\omega_0 + \frac{\partial\gamma_0}{\partial N}\Delta N_0 \qquad (5.2.11)$$

The variation of the loss with the carrier density is due to e.g. the variation of the average refractive index and of the Bragg wavelength. It accounts for the fact that the loss depends more generally on the Bragg deviation (see e.g. fig. 2.3.3). This variation is also caused by the dispersion (i.e. it is not present if the loss is independent of the Bragg deviation). Notice that the variation with carrier density must be calculated under constant emission frequency and that the variation with frequency must be calculated under constant average carrier density. The equation that expresses the phase resonance must, due to the dispersion also be transformed to:

$$\Delta\omega_0 = \frac{\alpha_0}{2}A\Delta N_0 + \frac{v_g}{2L}\left\{\frac{\partial\phi_R}{\partial\omega_0}\Delta\omega_0 + \frac{\partial\phi_R}{\partial N}\Delta N_0\right\} + F_{\varphi,0} \qquad (5.2.12)$$

Expressions for ϕ_R and γ_0 have been given in chapter 2. It must be noticed that to be exact and due to spatial hole burning, one should also include variations of ϕ_R and γ_0 with varying power. Here we concentrate on the dispersion and neglect these variations. The derivatives of γ_0 and ϕ_R can be included in the α-factor. With these adaptions to the rate equations, the linewidth can be derived to be:

$$\Delta\nu = \frac{S}{4\pi I_0}\frac{(1+\beta^2)}{\left\{1 - \frac{v_g}{2L}\frac{\partial\phi_R}{\partial\omega_0} - \frac{\beta}{2}\frac{\partial\gamma_0}{\partial\omega_0}\right\}^2}\ ;\ \beta = \frac{\alpha A + \frac{v_g}{L}\frac{\partial\phi_R}{\partial N}}{A - \frac{\partial\gamma_0}{\partial N}} \qquad (5.2.13)$$

β can be considered as some kind of effective linewidth enhancement factor.

The term between brackets can cause a considerable linewidth enhancement when γ_0 and/or ϕ_R are strongly increasing functions of the frequency (i.e. in the case of strong dispersion). Moreover, due to spatial hole burning, this term is also power dependent. In some lasers, e.g. where the loss γ_0 increases with bias level and hence its derivative can also be expected to increase, the enhancement increases with bias level. This can give rise to a linewidth floor.

β, $\partial\gamma/\partial\omega$ and $\partial\phi_R/\partial\omega$ are not easily quantified. One possible method to investigate the effect of dispersion numerically is to calculate the linewidth of two DFB-lasers, which are completely identical except for the fact that they have an opposite dispersion. As an example we consider two 300 μm long 1.55 μm DFB-lasers (denoted by E and E') with field reflection coefficients $\rho_f = 0.2324\ e^{j\pi}$ at the left facet and $\rho_b = 0.2324\ e^{j3\pi/2}$ for laser E and $\rho_b = 0.2324\ e^{j\pi/2}$ for laser E' at the right facet.

Both lasers have the same longitudinal distribution of optical power (and hence identical spatial hole burning), but also the same threshold gain and threshold gain difference $\Delta gL = 0.33$. From calculations of the spatial hole burning induced FM-response, it follows that the loss increases with bias level in both lasers. Fig. 5.2.8 shows the complex roundtrip gain (at threshold) as a function of the wavelength for both lasers. The roundtrip gain is defined as the optical field gain after one roundtrip through the cavity. A wavelength independent gain has been assumed and hence this wavelength dependence of the roundtrip gain is completely due to the dispersion in the loss. The amplitudes of the roundtrip gain of both lasers are symmetric with respect to λ_B (λ_B being the Bragg wavelength). The phases however are antisymmetric against λ_B.

Both lasers have an opposite dispersion in γ and an equal dispersion in ϕ_{fb}. E.g. for laser E (E'), it follows from fig. 5.2.8 that a decrease of λ ($\Delta\omega>0$) results in a enhanced (reduced) roundtrip gain and thus an decreased (increased) loss. Thus $\partial\gamma/\partial\omega$ is negative (positive) for laser E (E'). It can also be seen from fig. 5.2.8 that, since λ_B decreases with increasing N, $\partial\gamma/\partial N$ is positive (negative) for laser E (E'). Any difference in linewidth between both lasers can be

attributed to the dispersion in γ and to the different β-values (which also comes down to a power dependent dispersion effect).

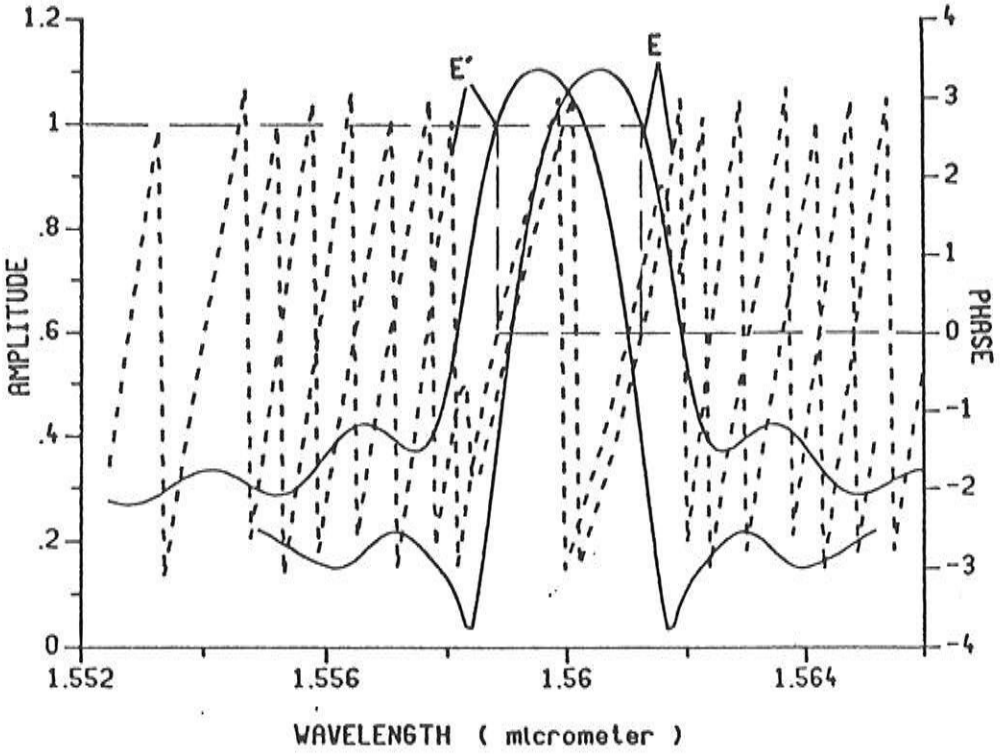

Fig. 5.2.8: Amplitude (—) and phase (--) of the roundtrip gain at threshold for lasers E and E'.

The linewidth as a function of inverse output power is shown in fig. 5.2.9 for both lasers. The α-factor has a value of 3. Spectral hole burning with a saturation power of 67 mW (ε = 15 W^{-1}) has also been taken into account in the calculation. This spectral hole burning leads to an extra term in the denominator of (5.2.13) and weakens the effect of the dispersion. However, the dispersion still causes the linewidth of laser E' to be about 15% larger than that of laser E at low power levels, while the influence of the dispersion still increases with increasing power level. The linewidth of laser E' reaches a minimum of 77 MHz at a power level of about 2 mW and then increases again to a value of 120 MHz at a power level of 3.7 mW. Beyond this power level, the laser becomes multi mode and a steep increase of the linewidth starts.

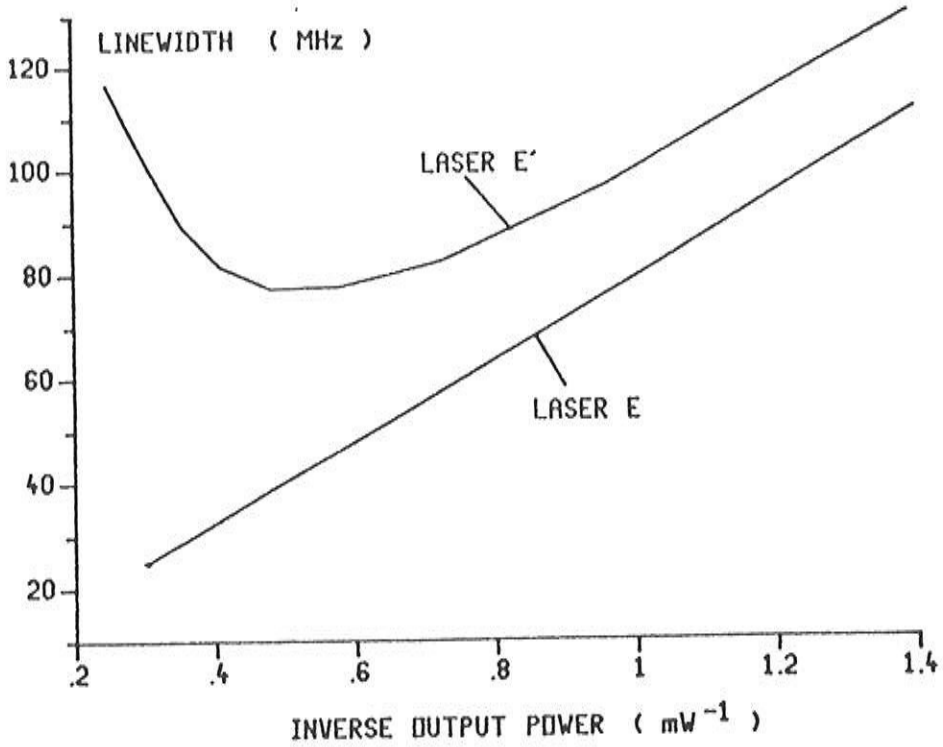

Fig. 5.2.9: Linewidth vs. inverse output power for the lasers E and E'.

Fig. 5.2.10 further shows the roundtrip gain of laser E' at an excitation of 38 mA (where the minimum in the linewidth occurs). It can be concluded that the laser is still single mode at this bias level. Calculation of the slope of the amplitude of this roundtrip gain gives an indication of the increase in dispersion. This slope has increased from 357/μm at threshold to 401/μm for a current of 38 mA and 530/μm at 44 mA (corresponding with 3.7 mW).

This type of rebroadening has theoretically been observed in most lasers where there is a local increase of the loss with the frequency in the neighbourhood of the emission frequency and where the loss increases with bias level. The minimum linewidth and the power at which this minimum occurs depend on the strength of the dispersion and of the spatial hole burning, but also on the value of the linewidth enhancement factor. The dispersion is often much weaker than it is in laser E', but the linewidth enhancement factor is often larger (values of 5 and more are reported).

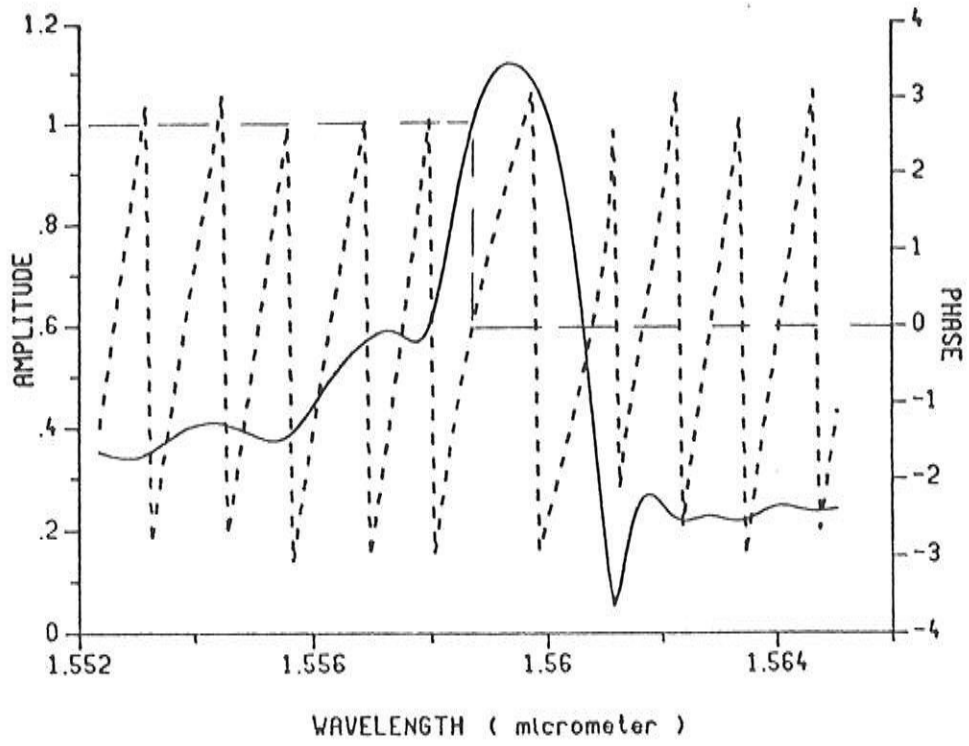

Fig. 5.2.10: Amplitude (—) and phase (--) of the roundtrip gain at 38 mA for laser E'.

As many lasers, emitting on the short wavelength side of the Bragg wavelength, seem to become multi mode at low power levels (they are instable), this rebroadening is only found for a limited number of lasers. When considering again the fig. 5.2.7 with the experimentally measured linewidth floor, one can notice that a few lasers seem to differ quite a lot from the average behaviour. One can wonder if the linewidth floor of these few (pathological) cases is not caused by a dispersion effect.

The implications of dispersion in the gain can be estimated by replacing $\partial\gamma/\partial\omega$ in (5.2.13) by $\partial\gamma/\partial\omega - \partial G/\partial\omega$. From the analytical expressions for the gain, it follows that the dispersion in the gain is equal to 0.0067 for each 10 nm detuning from the gain peak. This would give a slope of the roundtrip gain equal to 17/μm, which is negligible with the slope resulting from the dispersion in the loss. The dispersion in the gain affects the linewidth by less than 1 %.

The previous results also indicate that dispersion of the loss, even if it doesn't result in a linewidth rebroadening, surely can affect the linewidth quite a lot and should not be ignored.

V.2.3 Other important factors

V.2.3.1 Spatial hole burning

Spatial hole burning not only affects the dispersion, but it also influences the linewidth directly. It was already shown in II.3 how spatial hole burning results in a bias dependence of the gain and the loss. In general however, it will also affect the Langevin functions and the feedback phase.

In order to eliminate the dispersion we first consider $\lambda/4$-shifted lasers here. We further neglect the spectral hole burning. Fig. 5.2.11 shows the linewidth vs. the inverse output power for 300 μm long $\lambda/4$-shifted lasers with different κL-values. The linewidth has been divided by the threshold gain and by the facet loss to eliminate the κL-dependence of these quantities. According to Henry's formula, the different curves should then coincide. Any difference can now only be attributed to a difference in spatial hole burning or in mode profile (resulting in a different K-factor or a different α_{eff}). It certainly becomes clear that spatial hole burning results in an offset for the linewidth, an offset which increases with increasing κL [5.23], [5.24]. It is also seen that the offset becomes less at higher power levels and the linewidth eventually approaches zero. This can be related to the expression (2.3.31) for the gain suppression and similar expressions for the power dependence of the loss. At high power levels, the gain and loss suppression saturate and the spatial hole burning only implies a change in the differential gain and in the loss. The linewidth is therefore again proportional with the inverse power level, just other values for the α-factor and for the loss need to be used.

Fig. 5.2.12 and 5.2.13 show the influence of spatial hole burning on the linewidth of lasers A and B. Results obtained with a (non-) uniform carrier density are thereby depicted by a (full) dashed line. When, in addition, spectral hole burning is also taken into account, one finds that spatial hole burning again causes an offset for the linewidth, although it doesn't seem to have much influence on the power level where the minimum in the linewidth occurs.

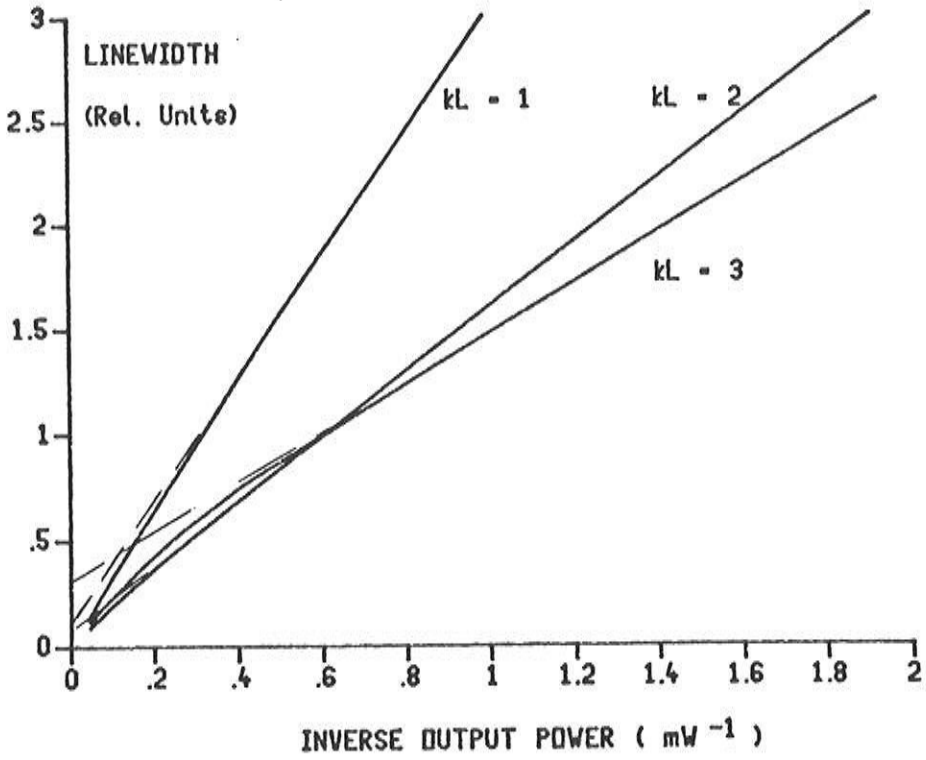

Fig. 5.2.11: Linewidth (divided by the threshold gain and the facet loss) vs. inverse outpower power for 300 μm long λ/4-shifted lasers (in 10^6 MHz/μm^2).

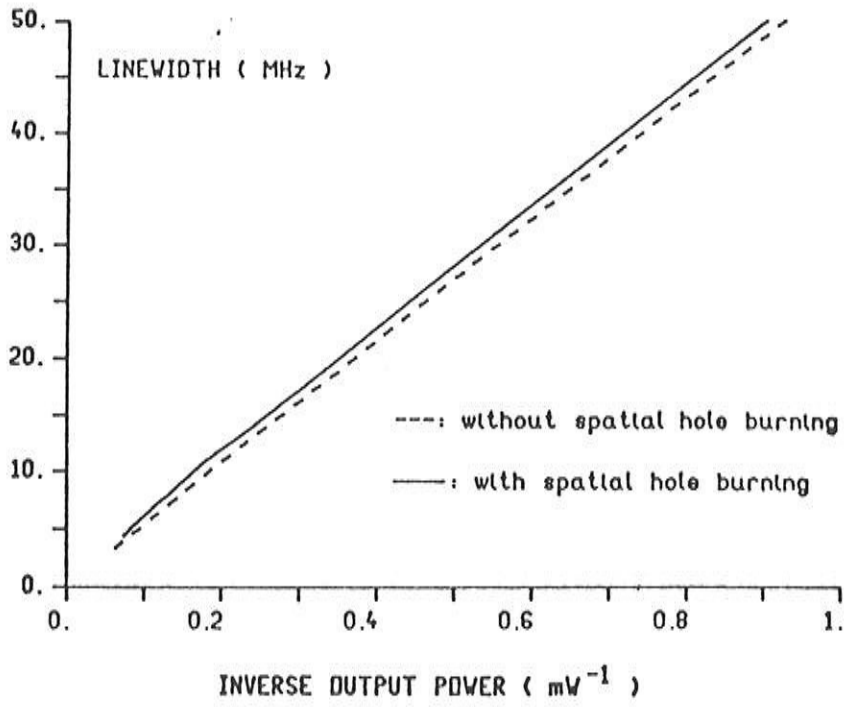

Fig. 5.2.12: Linewidth of laser A vs. inverse output power; calculated with uniform (--) and non-uniform ( ) carrier density

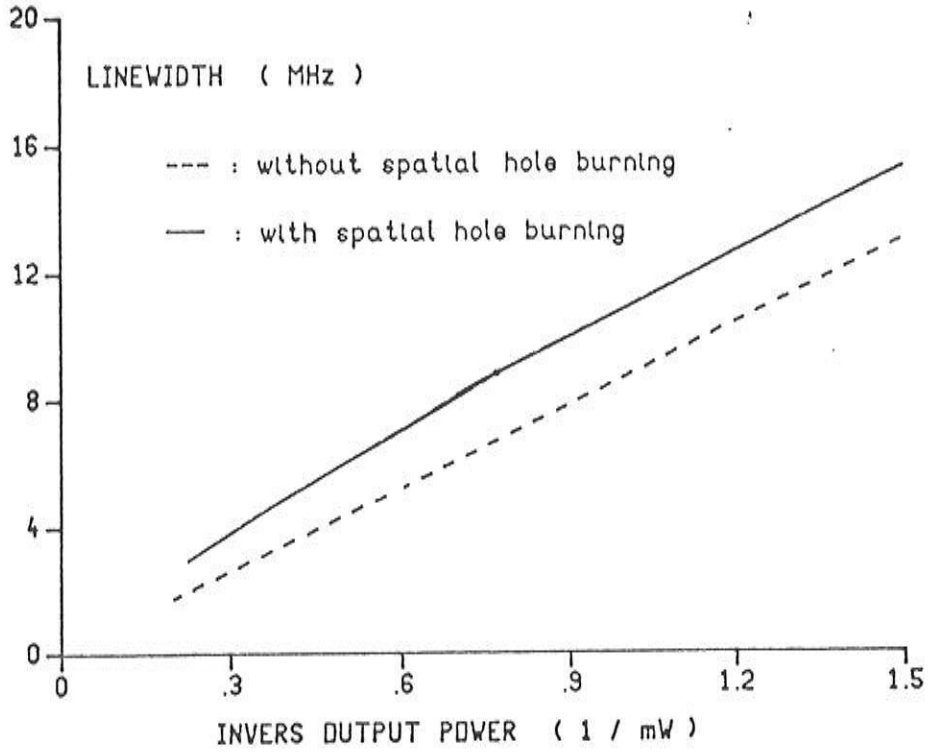

Fig. 5.2.13: Linewidth of laser B vs. inverse output power; calculated with uniform (--) and non-uniform ( ) carrier density

V.2.3.2 1/f-noise and temperature fluctuations

The Langevin function F_S originates from fluctuations in the spontaneous carrier recombinations. A considerable part of the electron energy is converted into heat during these recombinations and this causes a temperature increase ΔT, which depends on the thermal resistance R_T (with typical value 60 K/W). F_S therefore induces temperature fluctuations, which lead to additional noise sources for the rate equations since the gain and the refractive index are temperature dependent. The temperature fluctuations can simply be calculated from F_S, R_T and the bandgap energy E_g:

$$\Delta T = R_T E_g V_a \eta_T F_{S,0} \qquad (5.2.14)$$

with the efficiency η accounting for the fact that F_S is only partly converted into heat.

A detailed description of the numerical implementation of the temperature problem and its incorporation into the small signal models of CLADISS is given elsewhere [5.25]. We only notice that the thermal cut-off frequency is much lower than 1 MHz and

that, as a consequence, the temperature fluctuations can not be treated as white noise.

1/f-noise is another low frequency noise source. It can be taken into account by the introduction of a new Langevin force F_f, uncorrelated with the other Langevin forces, in the equation (2.3.4). The exact origin of F_f is not really known, but its autocorrelation is generally assumed to be [5.26]:

$$< F_f(\Omega)\, F_f^*(\Omega') > = \frac{\alpha_H (2\pi)^2 I_{th}^2}{\Omega\, N_0 V_a}\, \delta(\Omega-\Omega') \qquad (5.2.15)$$

with I_{th} being the threshold current and α_H (Hooge's constant) being an empirical constant equal to $2\ 10^{-3}$. F_f also causes temperature fluctuations and must be included in (5.2.14).

Fig. 5.2.14 shows the spectrum of the FM-noise of laser A at an output power of 10 mW when the additional 1/f-noise and temperature fluctuations are taken into account. Gain suppression was neglected to avoid the rebroadening. One can see that both noise sources only give slowly varying contributions (with a frequency below 1 MHz). The adiabatic approximation can no longer be applied when calculating the linewidth and one must use the Fast Fourier approach.

Fig. 5.2.15 shows the calculated power spectrum. It is clear that, for the laser under consideration and at the power level of 10 mW, both effects result in an increase of the linewidth by about 1 MHz. It must further be noticed that, due to the 1/f-noise, the spectrum is no longer Lorentzian, but Gaussian.

The low frequency contribution to the FM-noise is nearly independent of the power level [5.27]. However, the contribution of the white noise becomes smaller and smaller with increasing power level (at least if gain suppression is neglected). The low frequency FM-noise therefore becomes dominant at high bias levels and it can easily be shown that this results in a saturation of the linewidth. Though, this low frequency noise is little annoying in optical communication systems [5.27] and the phenomenon is rahter of theoretical interest.

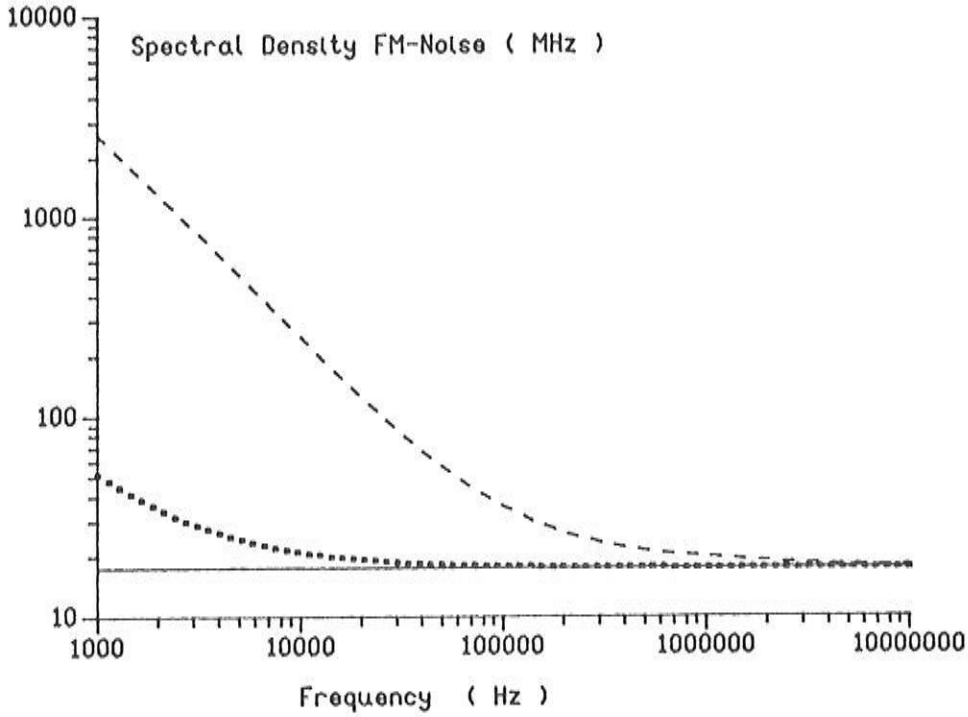

Fig. 5.2.14: FM-noise of laser A at 10 mW output power:
(—) white noise, (···) including 1/f-noise,
(---) 1/f-noise and temperature fluctuations.

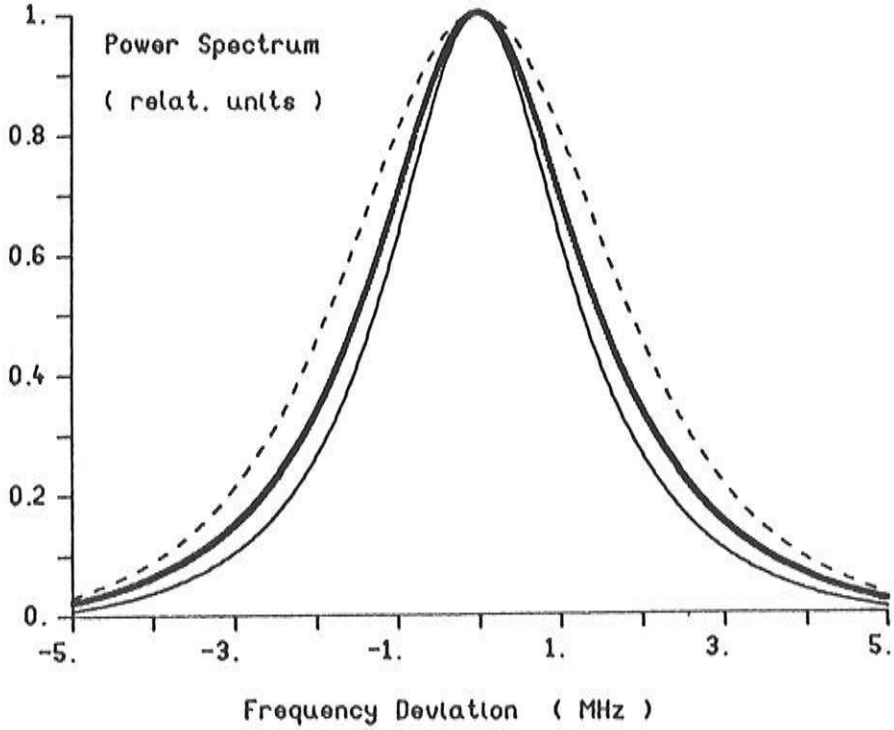

Fig. 5.2.15: Power spectrum of laser A at 10 mW power,
for the same conditions as in fig. 5.2.14.

V.2.4 Reduction of the linewidth

From the previous results, it can be concluded that the attainable minimum linewidth depends on: the stability of the single mode behaviour, the loss and the photon number, the antiguiding factor α, the dispersion and the spatial and spectral hole burning. Minimisation of the linewidth therefore requires the control of these factors. We already noticed that an increase of the photon number and a decrease of the loss can be achieved by an increase of the laser length. The stability of the single mode behaviour can then be guaranteed by using special laser structures (as described in chapter 4). The influence of spatial hole burning on the linewidth is then removed at the same time. We'll briefly discuss the other factors in the following.

V.2.5.1 The loss

From Henry's formula, it follows that the linewidth is proportional with the threshold gain Γg_{th}, which equals the total loss (i.e. the sum of mirror loss and absorption loss). The mirror loss can be reduced by increasing the laser length or the coupling constant. An increased spatial hole burning results in both cases and the method should therefore only be applied if special laser structures are used.

The absorption loss α_{int} has its origin mainly in the free-carrier absorption and can be expressed as:

$$\alpha_{int} = \Gamma\alpha_{ca} + (1-\Gamma)\alpha_{cl} \qquad (5.2.16)$$

with α_{ca} being the absorption in the active layer and α_{cl} the absorption in the cladding layers. Materials research [5.28] indicates that α_{ca} is much larger than α_{cl} for 1.55 μm lasers. α_{int} can therefore be minimised by using a very thin active layer (for which Γ is smaller).

V.2.5.2 The antiguiding factor

The linewidth is nearly proportional with the square of the antiguiding factor α_0. The value of α_0 can, for DFB lasers, be redu-

ced by the choice of a rather short grating period. A shift of the main mode towards shorter wavelengths then occurs and the value of α_0 decreases, as can be seen on fig. 5.2.16 [5.29].

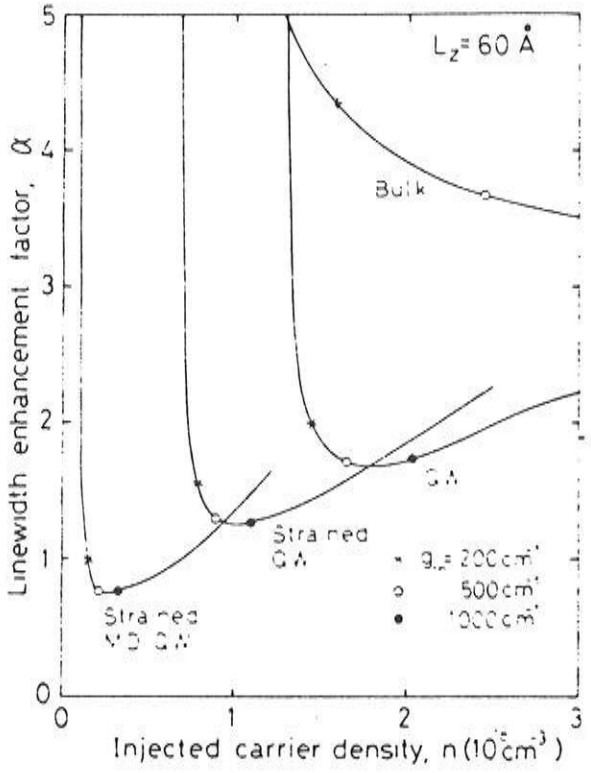

Fig. 5.2.16: α-factor of a F-P laser for bulk and QW material [5.29] (the wavelength decreases with the carrier density).

A larger reduction of α_0 can be obtained by introducing quantum well material. The value of α_0 can even be reduced to below one if 'Strained Modulation Doped Quantum Well' material is used. This means a reduction of α_0 with a factor 3 or 5 and of the linewidth with a factor 10-30, in comparison with bulk material.

V.2.5.3 The spectral hole burning

The spectral hole burning coefficients are little dependent on the wavelength and only a small reduction in minimum linewidth can thus be achieved by detuning. A larger reduction of the spectral hole burning is possibly achieved if other material is used.

V.2.5.4 The dispersion

Losses that decrease with frequency are to be preferred here, although no (first order) dispersion in the loss suffices to avoid the dispersion induced rebroadening. A large dispersion is sometimes introduced via an external cavity to obtain very narrow linewidth, but is must be mentioned that the mode behaviour in such external cavity lasers is not very stable.

V.3 The intensity noise of DFB lasers

The intensity noise, i.e. fluctuations in the emitted optical power, is of special importance under the application of analog or digital AM-communication. Future applications of this can be found in e.g. optical cable television (CATV) systems. [5.30] The carrier to noise ratio (CNR) has a large influence on the system performance in this case and it is determined by the noise of the receiver (e.g. shot noise of the photodetector) as well as by the intensity noise of the laser [5.31].

One must distinct between the noise, which appears in the intensity of a single mode (e.g. the main mode) and the noise which appears in the total intensity (equal to the sum of the intensities of all modes). Mode partition noise [5.32], [5.33] e.g. involves large fluctuations in the intensity of each mode separately, while the fluctuations in the total intensity remain rather small. The fluctuations in the intensities of the different modes are thereby correlated so that their sum remains very small. Mode partition noise should nonetheless be avoided in optical communication systems. Indeed, the correlation between the noise in the modes can be destroyed as a result of the dispersion in the optical fibre (which makes that all modes propagate with different velocity) and it can result in large fluctuations of the total intensity, measured by the photodetector. This noise is easily reduced by working at the wavelength (1.3 μm) where minimum fibre dispersion occurs. Noise in the total intensity of the laser itself is not as easily reduced. Theoretical and experimental investigation of the factors which determine the RIN is therefore required.

V.3.1 Frequency dependence of the RIN in single mode lasers

Fig. 5.3.1. shows a typical spectrum of the RIN of a single mode laser (laser A here). This spectrum is flat for freqencies ranging from 1 MHz up to a few hundred MHz (or more), where it strongly increases as a result of the relaxation oscillation. The spectral density of the RIN again decreases beyond this oscillation.

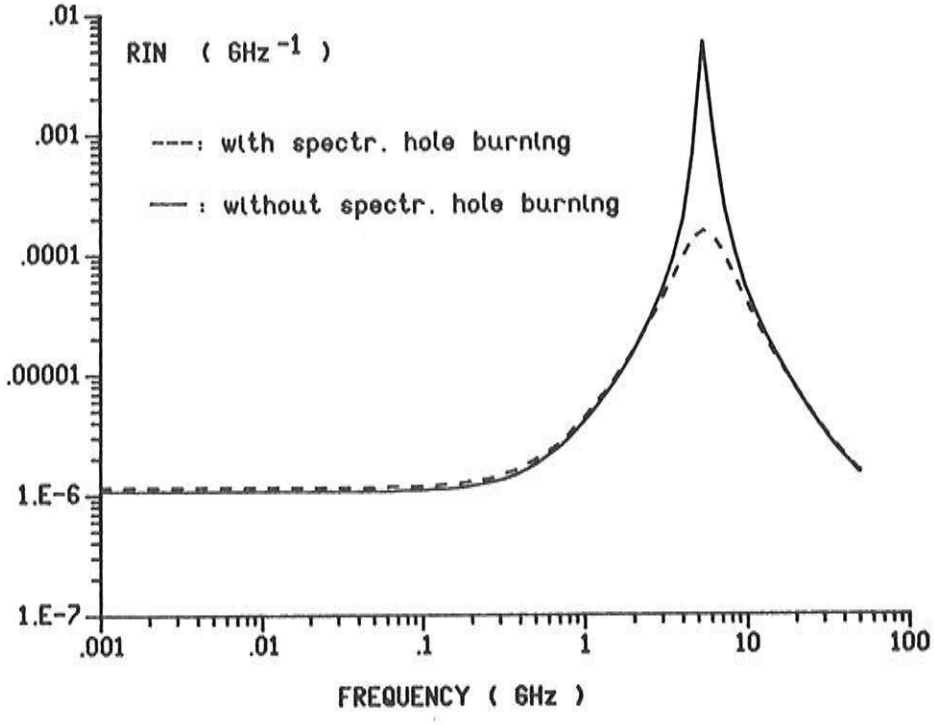

Fig. 5.3.1: Frequency dependence of the RIN for laser A at an output power of 1 mW.

It can no longer be argued, as for the FM-noise, that only the low frequency value of the RIN has implications on the performance of a communication system. The relaxation oscillations in the FM-noise only limit the channel spacing in communication systems. The fibre bandwidth is nevertheless large enough so that a sufficient number of channels are allowed. The relaxation oscillations in the RIN on the other hand limit the maximum modulation frequency. A low value of the RIN at these relaxation oscillations would imply that a larger channel bandwidth can be used.

The frequency dependence of the RIN can be derived from the rate equations. For a Fabry-Perot laser, one finds for the intensity fluctuations at high power levels:

$$\frac{\Delta I}{I_0} = \frac{A\ F_S + (j\Omega + \tau_{rd}^{-1})\ F_I/I_0}{\{j\Omega + \xi I_0(AN_0-B)\}\{j\Omega + \tau_{rd}^{-1} + AI_0V_a^{-1}\} + AI_0V_a^{-1}(AN_0-B)} \qquad (5.3.1)$$

From this expression, it follows that the resonance frequency is approximately proportional with the square root of the photon number (or output power). A high resonance frequency can be obtained by biasing at higher output powers, but also by using shorter lasers or quantum well lasers.

The damping of the relaxation oscillations is mainly caused by the gain suppression. From (5.3.1), it can be derived that the maximum value of the RIN, occuring at the resonance frequency, is proportional with the inverse of the square of ξ and with the inverse of the third power of the photon number. An increase of the output power, will therefore bring about a considerable decrease of the RIN.

1/f-noise and temperature fluctuations only contribute to the intensity noise at low frequencies (below 1 MHz) [5.34]. In practice however, modulation frequencies are always chosen above 1 MHz (also in order to reduce the distortion and to guarantee a uniform FM- or AM-response), and the low frequency noise is of little significance.

V.3.2 Factors determining the low frequency RIN

V.3.2.1 Multi mode lasers

The RIN appears to be very sensitive to the presence of strong side modes. This is first of all the case for the noise in the intensity of the main and side mode separately (partition noise), and is easily explained with the help of the rate equations. The equation (2.3.7) for the side mode intensity (index 1) gives in the low frequency approximation:

$$\Delta I_1 = \frac{F_{I,1} + I_1\ \Delta[G(N_0,\omega_1) - \gamma_1]}{\gamma_1 - G(N_0,\omega_1)} \qquad (5.3.2)$$

Both the side mode intensity I_1 and the fluctuations in gain and loss $\Delta[G(N_0,\omega_1)-\gamma_1]$ are relatively small for a side mode below threshold. The fluctuations in the carrier density are indeed restricted by the oscillation of the main mode and the resulting gain clamping, while non-linearities such as spectral and spatial hole burning can be neglected in first order approximation. The second term in the numerator of (5.3.2) can thus be neglected. The denominator of (5.3.2) however is very small when the side mode reaches the threshold. Its value can be determined from solution of (2.3.7) in the steady state and one then finds for the low frequency intensity noise of the side mode:

$$S_{\Delta I,1}(\Omega=0) = \frac{2\ I_1^3}{S} \qquad (5.3.3)$$

The fluctuations in the side mode intensity are proportional with the 3rd power of the side mode intensity and they can be relatively large if the side mode approaches the threshold.

By neglecting all other Langevin functions and all non-linearities, it follows from the carrier rate equation that the total intensity remains constant. This indicates that the fluctuations in the side mode intensity and in the main mode intensity are cross correlated so that large fluctuations in the main mode intensity will be present. It is as if the photons are just repartitioned over the 2 modes in a stochastic way, a viewpoint giving rise to the name 'partition noise'.

The other Langevin functions and the fluctuations in gain and carrier density are not zero in reality, but their effect is much smaller than the fluctuations in the side mode intensity. The mode partition noise is illustrated in fig. 5.3.2, which gives the fluctuations in the main mode intensity for laser B. This figure also shows that the influence of the partition noise is restricted to low frequencies (up to 100 MHz). The cut-off frequency is given by $[G(N_0,\omega_1)-\gamma_1]/2\pi$, as can be seen after solution of the equation (2.3.7) in the dynamic regime.

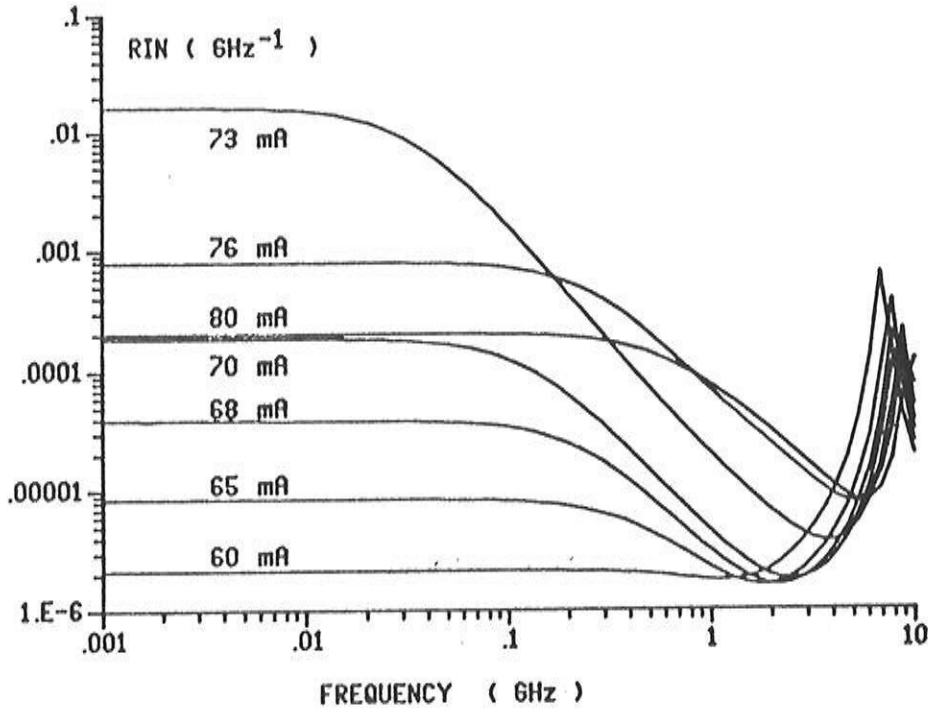

Fig. 5.3.2: RIN of the main mode for laser B and for different bias levels.

The fluctuations in the intensity of main and side mode become again smaller beyond the threshold of the side mode. The side mode then consists no longer of amplified spontaneous emission, but becomes a genuine oscillator mode and the side mode equation now reduces to the condition that the gain must compensate the loss for the side mode. An analytical approximation can be found only if spatial or spectral hole burning are considered.

These non-linearities result furthermore in a strong dependence of the total intensity noise on the side mode strength [5.35], in contrast with what has been believed for a long time. As has already been outlined in V.2, the fluctuations in the side mode intensity induce large fluctuations in the gain or loss of the main mode, which ought to be compensated by large fluctuations in the carrier density to maintain the oscillation condition. The conservation of charge (expressed by the carrier rate equation) makes that the large fluctuations in carrier density now also require large fluctuations in the total intensity. The influence of the side mode inten-

sity on the overall RIN is illustrated in fig. 5.3.3 for laser B. Gain suppression has thereby been neglected. It is clear that the overall RIN strongly increases as soon as the side mode suppression drops below 20 dB and that it decreases again beyond the threshold of the side mode.

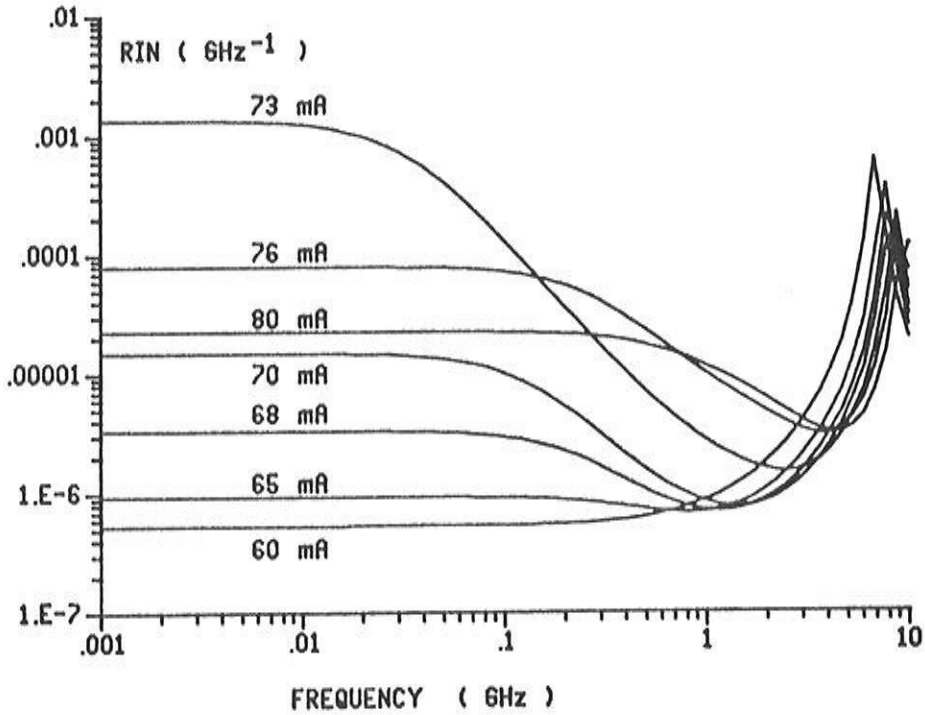

Fig. 5.3.3: Overall RIN for laser B and for different bias levels.

As for the linewidth, the influence of the side modes on the overall RIN can be approximated analytically. Though, the expressions are too long to write down here.

V.3.2 Single mode lasers

As long as a strong side mode suppression (more than 30 dB) exists, the RIN decreases with increasing power, as can be seen from the expression (5.3.1). Gain suppression and spatial hole burning only have a very weak influence in this case. The following expression can be derived if gain suppression is taken into account accurately:

$$\frac{\Delta I}{I_0} = \frac{A F_S (1 - \xi I_0) + \tau_{rd}^{-1} F_I / I_0}{(A N_0 - B) I_0 \{\xi \tau_{rd}^{-1} + A (1 - \xi I_0)^2 V_a\}} \qquad (5.3.4)$$

whereby one can notice that:

$$(A N_0 - B)(1 - \xi I_0) = \gamma = cte \qquad (5.3.5)$$

which implies that the minimum in the RIN would occur for $I_0 = 1/2\xi$. The presence of the term $\xi(\tau_{rd})^{-1}$ will shift this minimum towards even higher power levels, power levels where the first term of the numerator becomes dominant. The minimum then disappears.

The dispersion results in a dependence of the RIN on the linewidth. If gain suppression is neglected, one finds:

$$(AN_0 - B)\frac{\Delta I}{V_a} = F_S + \frac{F_I\left\{\tau_{rd}^{-1} + V_a^{-1}\frac{\partial \gamma}{\partial N}\right\}}{I\left(A - \frac{\partial \gamma}{\partial N}\right)} + \frac{\frac{\partial \gamma}{\partial \omega}\Delta\omega}{\left(A - \frac{\partial \gamma}{\partial N}\right)}\{\tau_{rd}^{-1} + A I_0 V_a^{-1}\} \qquad (5.3.6)$$

Fig. 5.3.4 shows the influence of the dispersion on the RIN of lasers E and E', which, as was shown in V.2.2.2, exhibit an opposite dispersion. The influence of dispersion on the RIN is substantially smaller than its influence on the linewidth; the 2 curves do not deviate by more than 5 dB and no increase of the RIN can be observed.

Fig. 5.3.5 further shows the RIN of laser A as a function of the inverse output power. The RIN decreases as I^{-3} at low power levels, in agreement with (5.3.4). At higher power levels, the shot noise becomes more important; the RIN still decreases, but not as rapidly anymore. It must be noticed however that the observed RIN at these high power levels is usually dominated by the noise of the photodetector, noise which has not been taken into account here.

The previous results indicate that a, for practical purposes, sufficiently low RIN (e.g. -150 dB/Hz) can in general be achieved by biasing at a sufficiently high power level, provided that a sufficient suppression of the external reflections and of the side modes can be guaranteed.

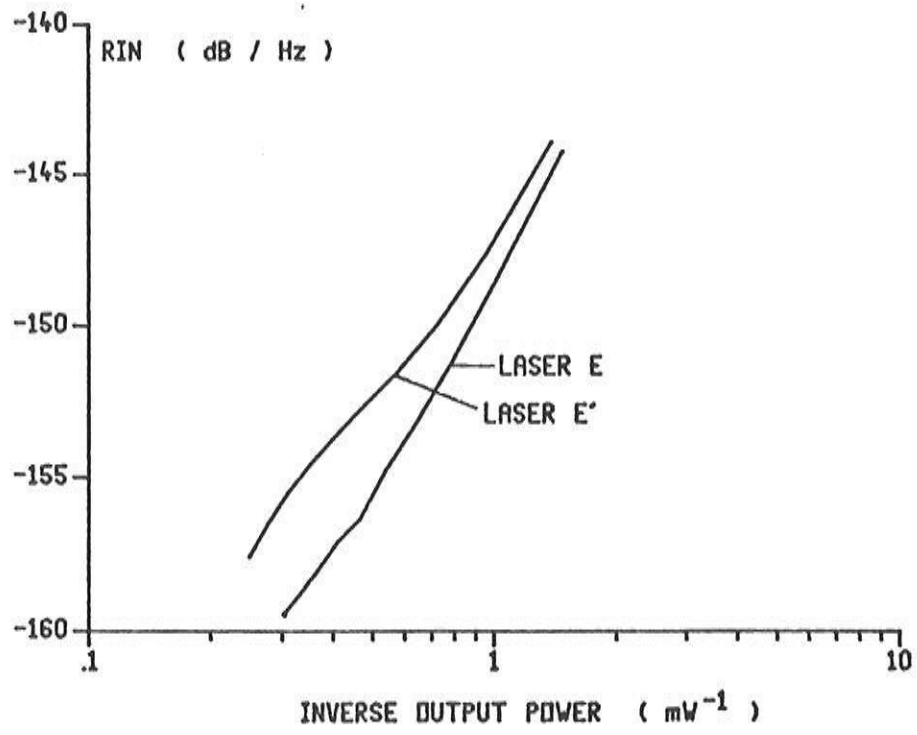

Fig. 5.3.4: Low frequency value of the RIN for the lasers E and E' vs. inverse output power.

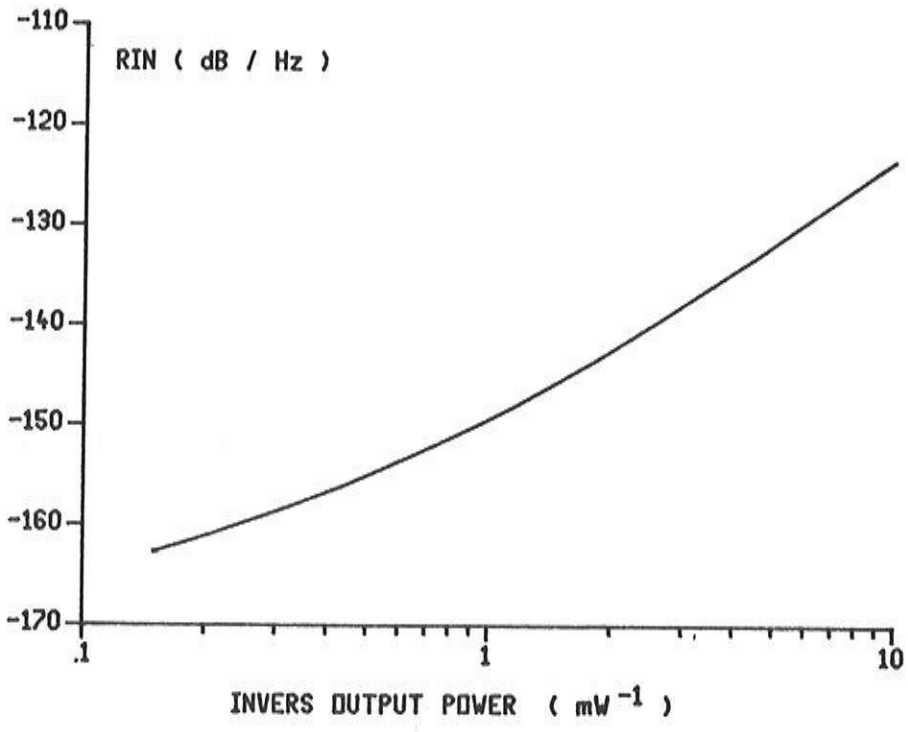

Fig. 5.3.5: Low frequency value of the RIN for laser A vs. inverse output power.

V.4 External feedback

External reflections (e.g. originating from an optical fibre or from lenses) can bring along an enormous increase or decrease of the linewidth and the RIN. The presence of such external reflections can be simulated by attaching an extra, passive section to the actual laser cavity, as is illustrated in fig. 5.4.1. The passive cavity has a length L_e equal to the distance between laser facet and fibre and the material parameters are those of air if the external reflection originates form a fibre or a lens surface. In reality, the reflections can be originating from different surfaces or points in the fibre or real external cavities (with or without grating) can be introduced deliberately. The external field reflection r_3 and L_e are not necessarily independent of the wavelength and the intensity in this case.

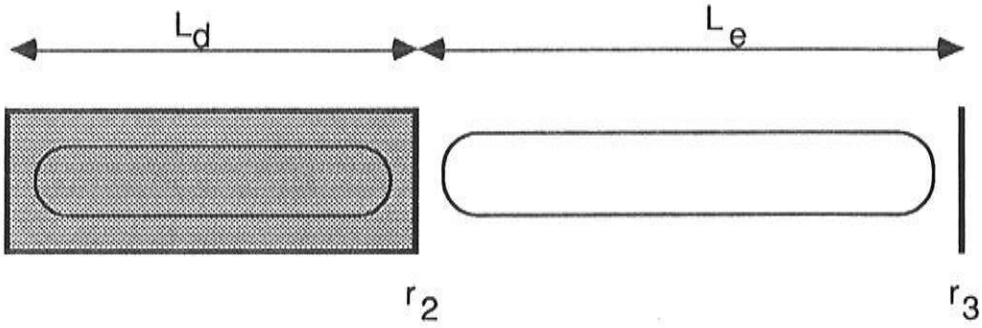

Fig. 5.4.1: Schematic view of an external cavity laser.

For a static or low frequency analysis, the effect of the external cavity can be reduced to a modification of the facet reflectivity r_2. If one assumes that an absorption α_e and a effective refractive index n_e for the external cavity, one finds the following expression for the effective facet reflectivity r_e:

$$r_e = r_2 + \frac{r_3'\,(1-|r_2|^2)}{1-r_2 r_3'} \qquad (5.4.1)$$

with:

$$r_3' = r_3\, e^{-\alpha_e L_e}\, e^{-j4\pi n_e L_e/\lambda} \qquad (5.4.2)$$

The implications of the modification in facet reflectivity can be evaluated with the help of the rate equations. The loss ($\gamma = v_g(\alpha_{int} - L^{-1}\ln|r_1 r_e|)$) becomes frequency dependent, while the phase of r_e, ϕ_e, affects the phase resonance condition:

$$\phi_1 + \phi_e - \frac{4\pi}{\lambda} n_a L_d = 2k\pi \,,\; k \in Z \qquad (5.4.3)$$

with ϕ_1 being the phase of the facet reflectivity r_1, L_d the laser length and n_a the effective refractive index of the active section.

The rate equation for the carrier density (in the active region) remains unchanged, but the other rate equations need to be modified. For the single mode case and leaving the mode index m behind, they can be written as [5.36]:

$$\frac{dI}{dt} = [G(N_0,\omega) - \gamma]\, I + S + 2k_c \sqrt{I(t)I(t-\tau)}$$
$$\cdot \cos(\omega_0\tau + \varphi(t) - \varphi(t-\tau)) + F_I \qquad (5.4.4a)$$

$$\Delta\omega = \frac{d\varphi}{dt} = \frac{\alpha}{2}\frac{\partial G}{\partial N_0}(N_0 - N_{0,th}) + \frac{v_g}{2L}\Delta\phi_R - k_c\sqrt{\frac{I(t-\tau)}{I(t)}}$$
$$\cdot \sin(\omega_0\tau + \varphi(t) - \varphi(t-\tau)) + v_g F_\varphi \qquad (5.4.4b)$$

with τ being the roundtrip delay of the external cavity, γ, ω_0 and $N_{0,th}$ the loss, the emission frequency and the threshold carrier density without external feedback, I the number of photons in the active section and $\Delta\omega$ the frequency deviation caused by the noise and the external feedback. The feedback coefficient k_c is given by:

$$k_c = \frac{1}{\tau_D}\frac{1 - |r_2|^2}{r_2} r_3 \qquad (5.4.5)$$

with τ_D the roundtrip time in the (active) laser cavity. Steady state solution of (5.4.4) gives the change in threshold gain and emission frequency $\Delta\omega$ caused by the external feedback for Fabry-Perot lasers [5.37]:

$$\Delta G_{th} = -2k_c \cos(\omega\tau)$$

$$\Delta\omega\tau = \omega\tau - \omega_0\tau = -C\sin(\omega\tau + tg^{-1}\alpha);\ C = k_c\tau\sqrt{1+\alpha^2} \qquad (5.4.6)$$

while a small signal analysis yields the linewidth narrowing:

$$\Delta\nu = \Delta\nu_0 [1 + C\cos(\omega\tau + tg^{-1}\alpha)]^{-2} \qquad (5.4.7)$$

with $\Delta\nu_0$ denoting the linewidth of the solitary laser diode. k_c (and hence r_2 and r_3) and C are usually assumed to be real, which is justified for Fabry-Perot lasers. Formula (5.4.7) predicts that, depending on the value of $\omega\tau$ and of α, both broadening and narrowing of the linewidth will take place.

Formula (5.4.7) is valid only for C<1. For larger values of C, the feedback induces mode hopping and locking and the feedback can even become incoherent [5.38], [5.39]. A large signal, time domain analysis is required in this case. Five regimes, determined by the value of C and of $|r_3|$, are therefore usually distincted. Fig. 5.4.2 depicts the linewidth in the first four regimes for a 300 μm long, as-cleaved F-P laser at an output power of 5 mW [5.38]. The first regime is defined by the condition C<1 and the linewidth is given by (5.4.7) in this regime. Different values for the linewidth are found for the different values of $\omega\tau$ and of τ. In regime II (C>1), there exist two solutions for the phase condition (5.4.6) and it turns out that the emission frequency will lock to the solution with the lowest phase noise. Mode hopping, yielding a linewidth rebroadening, can therefore occur between modes with a similar amount of phase noise. With increasing feedback, the frequency splitting of the hopping modes approaches the frequency separation between the external cavity modes and the laser will lock more and more to the feedback phase that gives maximum linewidth reduction. The mode hopping disappears and a low linewidth results (regime III). For still higher feedback levels, a dramatic increase of the linewidth appears and this regime (regime IV) is referred to as the coherence-collapse regime. This coherence collapse is not yet completely understood. One explanation for it is that the light has lost its coherence at the time it is fed back into the laser [5.40]. The linewidth can assume values of several GHz. The last regime (regime V,

not shown in fig. 5.4.2) again shows a stable, narrow linewidth. The laser now operates as a long cavity laser.

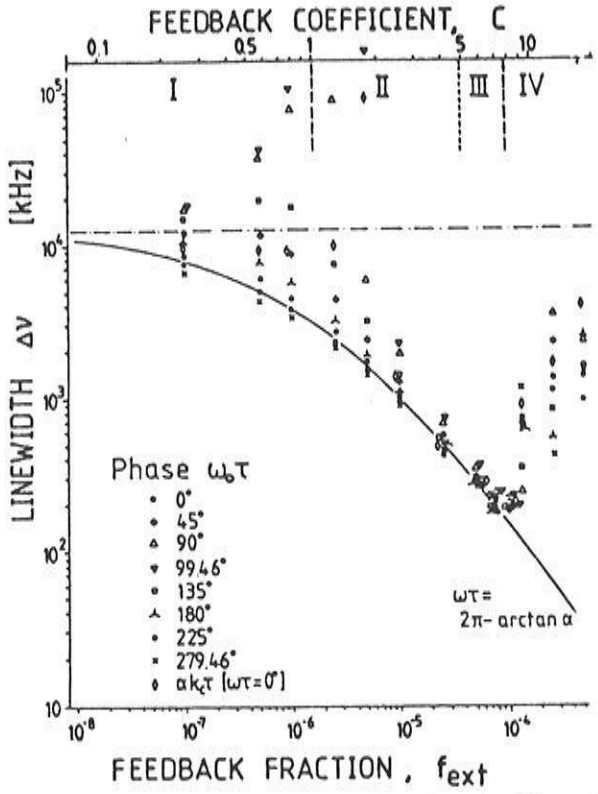

Fig. 5.4.2: Linewidth vs. feedback fraction $|r_3|^2$ and for an external cavity length L_e = 10 cm [5.38].

The relative intensity noise is less sensitive to external reflections. Fig. 5.4.3 shows the caculated RIN, averaged over the frequency range from 5 to 500 MHz, for the same F-P laser. The output power is again 5 mW and different values for the length of the external cavity are considered. It can be seen that the values of the RIN are little scattered and they remain small until the coherence collapse occurs. A strong increase in the RIN is nonetheless found when the coherence collapse starts. The occurence of the coherence collapse depends mainly on the value of α and on the length of the external cavity. The coherence collapse disappears for $\alpha=0$ or for short external cavities (i.e. L_e < a few mm) [5.41].

The previous results have been obtained after solution of the rate equations (5.4.4) and they are not really valid for DFB lasers. No such general calculations for DFB lasers have yet been reported, but the five regimes have been observed experimentally for DFB lasers [5.42]. A large-signal, time-domain model ([5.43]) that solves

the coupled wave equations would be required to analyse the effects of external feedback on DFB lasers in detail. Models such as CLADISS, which rely on solution in the frequency domain, can only handle the first regime.

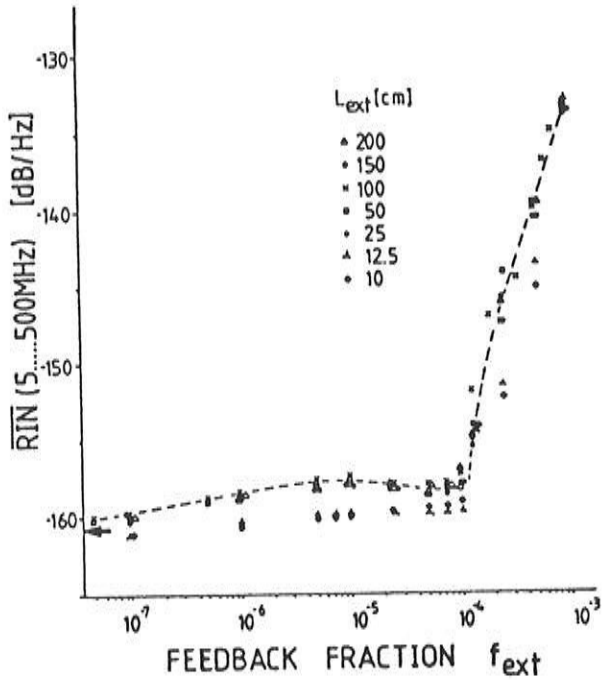

Fig. 5.4.3: RIN vs. feedback fraction $|r_3|^2$ and for several external cavity lengths [5.38].

We illustrate the variation of the linewidth for a 300 μm long DFB laser with $\kappa L=2$ and with facet reflectivities $r_1=0.9e^{j\pi/2}$ and $r_2=0.1e^{j\pi/2}$. We consider the first regime; the external reflection originates from a distance of 3 cm and $r_3=16\ 10^{-3}$. We also assume $\alpha_e=0$ and $n_e=1$. Fig. 5.4.4 shows the variation in the linewidth due to the external reflection for small variations in the distance L_e. One can easily check that the variation of the linewidth corresponds with the formule (5.4.7), at least qualitatively.

The previous results indicate that external reflections must be suppressed to any possible degree, unless a control of the distance L_e and of the feedback fraction can be assured. External cavity lasers, operating in the regime III, are sometimes introduced when narrow linewidth lasers are needed. A carefull design is ob-

viously required to assure operation in the regime III, but even such lasers are little stable. Undesired external reflections on the other hand are usually eliminated by the use of one or more (expensive) optical isolators. In addition, special design of laser diodes might result in a decrease of the feedback sensitivity C. However, it can be shown that this reduced C-value is obtained at the expense of a reduced efficiency [5.44]

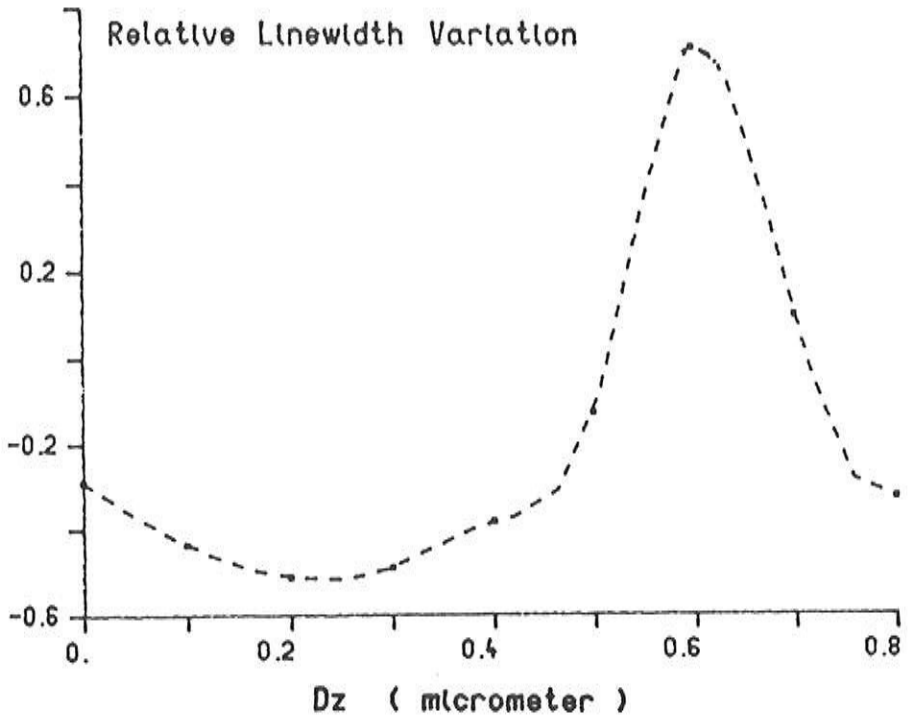

Fig. 5.4.4: Variation in the linewidth of a DFB laser due to external reflections, for small changes in external cavity length.

It is also expected that the feedback sensitivity can be reduced substantially by incorporating the laser diode in a ring configuration. A general structure of such a ring laser is shown in fig. 5.4.5. The laser acts as an amplifier and the ring furthermore consists of an isolator and a directional coupler. The analysis of such a configuration can be based on the introduction of transfer matrices for each element. This matrix can be derived from the coupled wave equations for the laser amplifier. Multiplication of the different transfer matrices then results in some kind of roundtrip matrix. The emission wavelength can be determined as the wavelength

for which the eigenvalue of the roundtrip matrix equals one, while the fields are found from the corresponding eigenvectors.

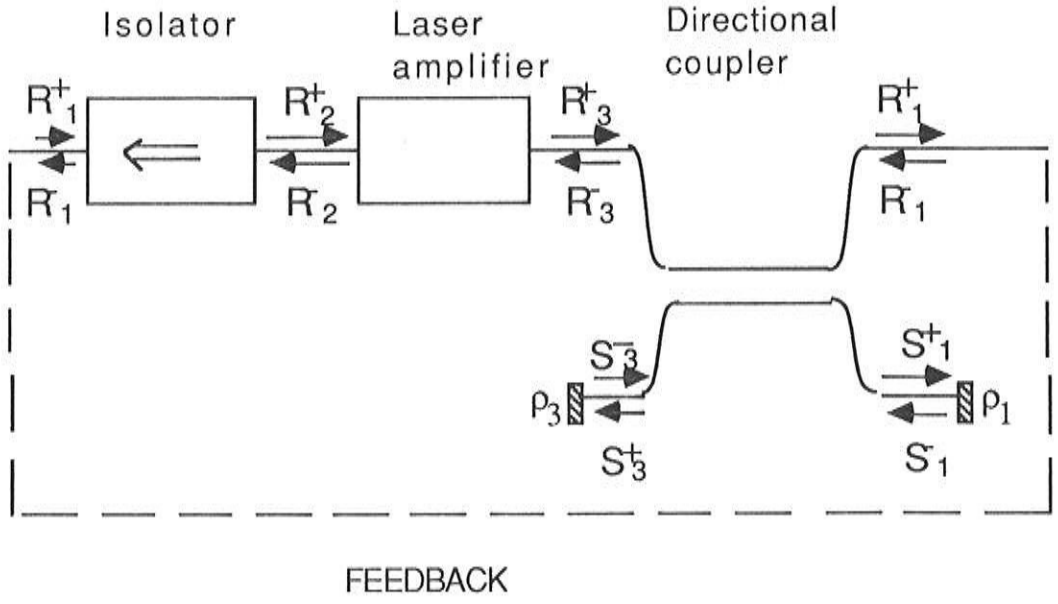

Fig. 5.4.5: Structure of a ring laser.

It has been shown [5.45] that a very low reflection sensitivity can be obtained already for a very weak level of isolation if a travelling wave amplifier is used. The isolator then just serves to assure that only one travelling wave (i.e. in one direction) exists in the ring. The external reflections then give rise to a wave in the direction for which no oscillation occurs and this wave disappears after a few roundtrips. This further requires that all reflections (e.g. on the facets of amplifier, connectors, etc.) be as low as possible since the required level of isolation is determined by these reflections. In that case, a low reflection sensitivity and an acceptable efficiency result at the same time. However, due to the long feedback loop (e.g. a fibre of a few cm), one needs to include a strong wavelength selective filter, such as a Moiré Fibre Grating Resonator [5.46].

Appendix V.A Influence of gain suppression on the linewidth

We derive the linewidth form the single mode static rate equations:

$$[\, G(N_0,\omega) - \gamma \,]\, I + F_I(t) = 0 \qquad (5.A.1a)$$

$$\frac{\eta J}{qd} = \left(\frac{N_0}{\tau} + B_0 N_0^2 + C_0 N_0^3 \right) + \frac{G(N_0,\omega)\, I}{V_a} - F_{S,0}(t) + \frac{F_I}{V_a} \qquad (5.A.1b)$$

$$\Delta\omega = \frac{\alpha}{2} A\, \Delta N_0 + v_g F_\varphi(t) \qquad (5.A.1c)$$

with the different quantities being defined as in II.3.1 and where we have ignored the modeindex. The steady state spontaneous emission has also been neglected.

a) For a gain suppression of the form:

$$G(N_0,\omega) = [A\, N_0 - B]\, \{1 - \xi\, I\} \qquad (5.A.2)$$

we find after linearisation of (5.A.1):

$$A\, \Delta N_0\, (1 - \xi I) - \xi\, (A N_0 - B)\, \Delta I + F_I / I = 0 \qquad (5.A.3a)$$

$$\Delta N_0 \{ V_a \tau_{rd}^{-1} + A I\, (1 - \xi I) \} + (A N_0 - B)(1 - 2\xi I)\, \Delta I = V_a F_{S,0} - F_I \qquad (5.A.3b)$$

Substitution of ΔI, as it can be determined from (5.A.3a), in (5.A.3b) gives an expression for ΔN_0, which, after substitution in (5.A.1c), gives the following expression for the linewidth:

$$\Delta\nu = \frac{S}{4\pi I} \left\{ 1 + \frac{\alpha^2}{\left[(1 - \xi I) + \dfrac{\xi V_a}{\tau_{rd} A\, (1 - \xi I)} \right]^2} \right\} \qquad (5.A.4)$$

b) If the gain suppression is assumed to be of form:

$$G(N_0,\omega) = \frac{A\, N_0 - B}{1 + \xi\, I} \qquad (5.A.5)$$

then the linearisation gives:

$$\frac{A\,\Delta N_0}{1+\xi I} - \frac{\xi\,(AN_0 - B)\,\Delta I}{(1+\xi I)^2} + \frac{F_I}{I} \tag{5.A.6a}$$

$$\frac{\Delta N_0}{\tau_{rd}} V_a + \frac{A\,I\,\Delta N_0}{1+\xi I} + \frac{(AN_0 - B)\,\Delta I}{(1+\xi I)^2} = V_a F_{S,0} - F_I \tag{5.A.6b}$$

and for the linewidth, one finds:

$$\Delta\nu = \frac{S}{4\pi I}\left\{1 + \frac{\alpha^2\,(1+\xi I)^2}{\left(1 + \frac{\xi V_a}{A\,\tau_{rd}}\right)^2}\right\} \tag{5.A.7}$$

A rebroadening will still occur, but the minimum in the linewidth is reached for $\xi I = 1$.

c) For a gain suppression of the form:

$$G(N_0,\omega) = \frac{A\,N_0 - B}{\sqrt{1+\xi I}} \tag{5.A.8}$$

one finds:

$$\frac{A\,\Delta N_0}{\sqrt{1+\xi I}} - \frac{(AN_0 - B)\,\xi\,\Delta I}{2\,(1+\xi I)^{3/2}} + \frac{F_I}{I} = 0 \tag{5.A.9a}$$

$$\frac{\Delta N_0 V_a}{\tau_{rd}} + \frac{A\,\Delta N_0\,I}{\sqrt{1+\xi I}} + \frac{(AN_0 - B)\,\Delta I}{(1+\xi I)^{3/2}}\left(1 + \frac{\xi I}{2}\right) = F_{S,0} V_a - F_I \tag{5.A.9b}$$

and for the linewidth:

$$\Delta\nu = \frac{S}{4\pi I}\left\{1 + \frac{\alpha^2\,(1+\xi I)}{\left(1 + \frac{\xi V_a}{2\tau_{rd} A\sqrt{1+\xi I}}\right)^2}\right\} \tag{5.A.10}$$

The gain suppression now only causes an offset (or a weak rebroadening due to the presence of τ_{rd}).

References

[5.1] C. Henry, 'Theory of the Phase Noise and Power Spectrum of a Single Mode Injection Laser', IEEE Journ. Quant. El., Vol. 19, pp. 1391-1397, Sep. 1983.

[5.2] G. Agrawal, N. Dutta, 'Long-wavelength semiconductor lasers', Van Nostrand Reinhold Company Inc., New York, 1986.

[5.3] K. Vahala, A. Yariv, 'Semiclassical Theory of Noise in Semiconductor Lasers - Part II', IEEE Journ. Quant. El., Vol. 19, pp. 1101-1109, June, 1983.

[5.4] J. Wang, N. Schunk, K. Petermann, 'Linewidth enhancement for DFB lasers due to longitudinal field dependence in the laser cavity', El. Lett., Vol. 23, pp. 715-716, July, 1987.

[5.5] J. Arnaud, 'Natural linewidth of semiconductor lasers', El. Lett., vol. 22, pp. 538-540, May, 1986.

[5.6] C. Henry, 'Theory of Spontaneous Emission Noise in Open Resonators and its Application to Lasers and Optical Amplifiers', IEEE Journ. Lightw. Techn., Vol. 4, pp. 288-297, March. 1986.

[5.7] K. Kojima, K. Kyuma, 'Analysis of the Linewidth of Distributed Feedback Laser Diodes Using the Green's Function Method', Jap. Journ. Appl. Phys., Vol. 27, pp. 1721-1723, Sept. 1988.

[5.8] T. Makino, 'Analysis of the spontaneous emission rate of multiple-phase-shift distributed feedback semiconductor lasers', El. Lett., Vol. 26, pp. 629-630, May, 1990.

[5.9] K. Kikuchi, H. Tomofuji, 'Analysis of linewidht of separated-electrode DFB laser diode', El. Lett., Vol. 25, pp. 916-918, July 1989.

[5.10] K. Vahala, 'Corrections to the rate equation approximation for dynamic considerations in a semiconductor laser', Appl. Phys. Lett., vol. 48, pp.1340-1341, May 1986.

[5.11] B. Tromborg, H. Olesen, X. Pan, S. Saito, 'Transmission line description of optical feedback and injection locking for Fabry-Perot and DFB lasers', IEEE Journ. Quant. El., Vol. 23, pp. 1875-1889, Nov. 1987.

[5.12] U. Krüger, K. Petermann, 'The Semiconductor Laser Linewidth Due to the Presence of Side Modes', IEEE Journ. Quant. El., Vol. 24, pp. 2355-2358, Dec. 1988.

[5.13] S. Miller, 'The effect of Side Modes on Linewidth and Intensity Fluctuations in Semiconductor Lasers', IEEE Journ. Quant. El., Vol. 24, pp. 750-757, May, 1988.

[5.14] M. Adams, 'Linewidth of a single mode in a multimode injection laser', El. Lett., Vol. 19, pp. 652-653, August, 1983.

[5.15] M. Amann, 'Linewidth enhancement in distributed feedback semiconductor lasers', El. Lett., Vol. 26, pp. 569-571, April, 1990.

[5.16] M. Asada, Y. Suematsu, 'Density-Matrix Theory of Semiconductor Lasers with Relaxation Broadening Model - Gain and Gain Suppression in Semiconductor Lasers', IEEE Journ. Quant. El., Vol. 21, pp. 434-442, May 1985.

[5.17] G. Morthier, P. Vankwikelberge, F. Buytaert, R. Baets, 'Influence of gain non-linearities on the linewidth enhancement factor in semiconductor lasers', IEE Proc., Pt. J, Vol. 137, pp. 30-32, Febr., 1990.

[5.18] G. Agrawal, 'Intensity Dependence of the Linewidth Enhancement Factor and Its Implications for Semiconductor Lasers', IEEE Phot. Techn. Lett., Vol. 1, pp. 212-214, August 1989.

[5.19] G. Morthier, P. Vankwikelberge, F. Buytaert, R. Baets, P. Lagasse, 'Linewidth of Single Mode DFB Lasers in the Presence of Spatial and Spectral Hole Burning', Proc. of the European Conf. on Opt. Communications', Sept. 1989, Gothenburg (Sweden).

[5.20] R. Tucker, 'High-Speed Modulation of Semiconductor Lasers', IEEE Journ. Lightw. Techn., Vol. 3, pp. 1180-1192, Dec., 1985.

[5.21] J. Wiesenfeld, R. Tucker, P. Downey, 'Picosecond measurement of chirp in gain-switched single-mode injection lasers', Appl. Phys. Lett., Vol. 51, pp. 1307-1309, 1986.

[5.22] C. Park, J. Buus, 'Prediction of the linewidth floor in DFB lasers', Proc. of the Opt. Fiber Comm. Conf. (OFC'90), San Francisco, p.158.

[5.23] J. Whiteaway, G. Thompson, C. Armistead, A. Collar, S. Clements M. Gibbon, 'The influence of Longitudinal Mode Spatial Hole Burning on the Linewidth and Spectrum of λ/4-Phase Shifted DFB Laser', Proceedings of the 11th International Semiconductor Laser Conference, Boston, USA, Sept. 1988.

[5.24] M. Wu, Y. Lo, S. Wang, 'Linewidth broadening due to longitudinal spatial hole burning in a long distributed feedback laser', Appl. Phys. Lett., Vol. 52, pp. 1119-1121, April 1988.

[5.25] D. Guillemyn, MSc thesis (in Dutch), University of Gent, 1989.

[5.26] D. Wolf (ed.), 'Noise in Physical Systems', Spinger Series in Electrophysics 2, Berlin, 1978.

[5.27] K. Kikuchi, 'Impact of 1/f-type FM-noise on coherent optical communications', El. Lett., Vol. 23, pp. 885-887, Aug., 1987.

[5.28] S. Kakimoto, A. Takemoto, Y. Sakakibara, Y. Nakajima, M. Fujiwara, H. Namizaki, H. Higuchi, Y. Yamamoto, 'Wavelength Dependence of Characteristics of 1.2-1.55 μm InGaAsP/InP P-Substrate Burried Crescent Laser Diodes', IEEE Journ. Quant. El., Vol. 24, pp. 29-35, Jan., 1988.

[5.29] T. Ohtoshi, N. Chinone, 'Linewidth Enhancement Factor in Strained Quantum Well Lasers', IEEE Phot. Techn. Lett., Vol. 1, pp. 117-119, June 1989.

[5.30] K. Sato, 'Intensity noise of semiconductor laser diodes in fiber-optic analog video transmission', IEEE Journ. Quant. El., Vol. 19, pp. 1380-1391, Sept., 1983.

[5.31] W. Way, 'Subcarrier Multiplexed Lightwave System Design Considerations for Subscriber Loop Applications', IEEE Journ. Lightw. Techn., Vol. 7, pp. 1806-1818, Nov., 1989.

[5.32] C. Henry, P. Henry, M. Lax, 'Partition Fluctuations in Nearly Single-Longitudinal-Mode Lasers', IEEE Journ. Lightw. Techn., Vol. 2, pp. 209-216, June, 1984.

[5.33] K. Liou, M. Ohtsu, C. Burrus, U. Koren, T. Koch, 'Power Partition Fluctuations in Two-Mode-Degenerate Distributed-Feedback Lasers', IEEE Journ. Lightw. Techn., Vol. 7, pp. 632-639, April, 1989.

[5.34] R. Lang, K. Vahala, A. Yariv, 'The Effect of Spatially Dependent Temperature and Carrier Fluctuations on Noise in Semiconductor Lasers', IEEE Journ. Quant. El., Vol. 21, pp. 443-451, May, 1985.

[5.35] C. Su, J. Schlafer, R. Lauer, 'Low frequency relative intensity noise in semiconductor lasers', Proc. of the Optical Fiber Communication Conf. (OFC'90), San Francisco, p. 218, 1990.

[5.36] R. Lang, K. Kobayashi, 'External optical feedback effects on semiconductor injection laser properties', IEEE Journ. Quant. El., Vol. 16, pp. 347-355, Mar., 1980.

[5.37] G. Agrawal, 'Generalized Rate Equations and Modulation Characteristics of External-Cavity Semiconductor Lasers', Journ. Appl. Phys., Vol. 56, pp. 3110-3115, Dec., 1984.

[5.38] N. Schunk, K. Petermann, 'Numerical Analysis of the Feedback Regimes for a Single-Mode Semiconductor Laser with External Feedback', IEEE Journ. Quant. El., Vol. 24, pp. 1242-1247, July, 1988 .

[5.39] D. Lenstra, B. Verbeek, A. Den Boef, 'Coherence Collapse in Single-Mode Semiconductor Lasers Due to Optical Feedback', IEEE Journ. Quant. El., Vol. 21, pp. 674-679, June, 1985.

[5.40] J. Cohen, D. Lenstra, 'Spectral properties of the coherence collapsed state of a semiconductor laser with delayed optical feedback', IEEE Journ. Quant. El., Vol. 25, pp. 1143-1151, June, 1989,.

[5.41] N. Schunk, K. Petermann, 'Stability Analysis for Laser Diodes with Short External Cavities', IEEE Phot. Techn. Lett., Vol. 1, pp. 49-51, March, 1989.

[5.42] R. Tkach, A. Chraplyvy, 'Regimes of feedback effects in 1.5 μm distributed feedback lasers', IEEE Journ. Lightw. Techn., Vol. 4, pp. 1655-1661, Nov., 1986.

[5.43] F. Libbrecht, G. Morthier, R. Baets, P. Lagasse, 'Large-signal multimode DFB-laser model as part of an optical communication system simulation tool', Proc. of the Opt. Fiber Comm. Conf. (OFC'91), San Diego, p. 120, Febr., 1991.

[5.44] J. Buus, O. Nilsson, 'A fundamental limit for the feedback sensitivity of semiconductor lasers', Proc. of the 12th International Semiconductor Laser Conference, Davos, Switzerland, Sept. 1990.

[5.45] G. Morthier, K. David, R. Baets, M. Farries, 'Design study on the reflection sensitivity of laser diodes', deliverable RACE 1069 (EPLOT), activity 2.2.5, Febr., 1990 (confidential).

[5.46] D. Reid, C. Ragdale, I. Bennion, D. Robbins, J. Buus, 'Phase-shifted Moiré grating fibre resonator', El. Lett., Vol. 26, pp. 10-12, Jan., 1990.

Chapter VI

THE MODULATION OF DFB LASERS: HARMONIC DISTORTION

In this chapter, we address the behaviour of laser diodes under current modulation. Such a modulation is indispensable for the transmission of information and the performance of a laser diode is therefore judged for a great deal on the basis of its modulation characteristics. In the case of digital coding, only the linear or the small signal characteristics (i.e. under a small modulation current) are of importance. Important is to which degree and over which frequency range these characteristics can be regarded as being independent of the modulation frequency. The small signal charac-teristics have already been the subject of an extensive investiga-tion and a detailed treatment of them has also been given in ref. [6.4]. They therefore do not really belong to the topics of this the-sis, although, for the sake of completeness, we will give a brief review of the recent theories.

In the case of analog modulation, one must also aim at a small (harmonic and intermodulation) distortion. The responses of amplitude and frequency do not longer depend linearly on the current modulation as a result of this distortion and the intensity and the frequency of the light are also modulated with frequencies that differ from the modulation frequency. The total distortion (which must be minimised) in a system actually depends also on the distortion of other components such as the detector.

In this chapter, we will mainly focuss on the second and third order harmonic distortion. The higher order distortions become smaller and less important if the optical modulation depth (OMD) is not too large. Moreover, the causes of all harmonic and intermodulation distortions are practically identical, being spectral and spatial hole burning, spontaneous emission at low power levels and the relaxation oscillations at high modulation frequencies.

We start here, as in the previous chapter, with an overview of the literature, and subsequently give a discussion of the linear mo-

dulation characteristics. We then treat the numerical and analytical results about the harmonic distortion in more detail.

VI.1 Brief overview of the literature on modulation.

Numerous papers on the modulation of laser diodes have already been published. The vast majority of these papers are restricted to the small signal modulation and describe both experimental and theoretical results about the low and high frequency modulation of several types of laser diodes such as F-P, DFB and DBR lasers, multi-electrode lasers and external-cavity lasers.

Temperature effects, which are only important for modulation frequencies below 1 MHz, are described in e.g. [6.1] and [6.2]. In both cases, the analysis is restricted to Fabry-Perot lasers and a good correspondence between experimental and theoretical results is reported. In [6.2], lateral diffusion of carriers and spontaneous emission are also taken into account. Both effects mainly cause a damping of the relaxation oscillations.

The consequences of lateral diffusion were also investigated in [6.3] for narrow-stripe lasers, for which the diffusion is taken into account as an effective gain suppression. In this way, one also finds a contribution to the low frequency FM response, which is not consistent with experimental or other theoretical results [6.4].

An in-depth analysis of the relaxation oscillationss, i.e. of the resonance frequency f_r and of the damping ϑ, is given in [6.5]. The existence of a universal relation between f_r and ϑ was first shown there starting from the rate equations, as in II.3. For not too low a power level, one can show that:

$$\vartheta = K (f_r)^2 \text{ met } K = (2\pi)^2 \xi \frac{V_a}{A} \qquad (6.1.1)$$

[6.5] in addition also treats the influence of parasitic electrical elements.

An excellent review of the AC-response of Fabry-Perot lasers, of the influence of parasitic elements and of the different non-linearities and of circuit models for the modelling is given in [6.6].

DFB lasers must be distincted from Fabry-Perot lasers due to the extra influence of longitudinal spatial hole burning. Mainly the low frequency FM-response is affected by this phenomenon. The contribution of spatial hole burning to the FM is little predictable and can give rise to the presence of a dip in the power or frequency dependence of the FM. Therefore, a lot of attention has been given to this phenomenon [6.7], [6.8]. The dip in the frequency dependence of the FM response can be removed by the use of multi-electrode lasers, as has been demonstrated in [6.9].

Since analog optical communication systems have attracted attention only very recently, only a limited number of studies of the distortion exist. Most of these papers are restricted to Fabry-Perot lasers. The distortion is then usually calculated from the rate equations (as presented in chapter 2), by the introduction of a similar (but second or third order) expansion as (2.3.16):

$$J = J_0 + \mathrm{Re}\{J_1 e^{j\Omega t}\}$$

$$I_m = I_{m,0} + \mathrm{Re}\{I_{m,1} e^{j\Omega t} + I_{m,2} e^{2j\Omega t} + I_{m,3} e^{3j\Omega t}\}$$

$$N_0 = N_{00} + \mathrm{Re}\{N_{01} e^{j\Omega t} + N_{02} e^{2j\Omega t} + N_{03} e^{3j\Omega t}\}$$

$$\omega_m = \omega_{m,0} + \mathrm{Re}\{\omega_{m,1} e^{j\Omega t} + \omega_{m,2} e^{2j\Omega t} + \omega_{m,3} e^{3j\Omega t}\} \qquad (6.1.2)$$

Only the influence of a small number of non-linearities on the distortion has been studied so far and only amplitude modulation has been considerd. Amplitude modulation is currently strongly favoured for the design of analog communication systems, partly because the present television distribution is based on AM-formatting.

First of all it must be mentioned here that distortion can occur even if the power current relation of a laser is perfectly linear. This is due to the clipping at threshold [6.10]. This clipping effect is a consequence of the fact that, at certain moments in time, the total current can decrease below the threshold current if the number of channels N and/or the modulation index m_i of these channels are too large. The optical power remains zero if the total current decreases below the threshold current and, obviously, the linear relation between small signal power and current is lost therby. The effect can be avoided by restricting the modulation index m of each

channel so that $m \leq 1/N$. Such a restriction is often regarded as far too severe and in many cases it is believed that accepting a little distortion and choosing m larger than 1/N may be more advantageous. The distortion, described above, is often referred to as the Saleh limit.

It must also be mentioned that the distortion is not only originating from the laser diode, but also from e.g. the photodetector [6.11]. The distortion in an APD diode mainly occurs at high optical powers or in an state with large amplification and it results from the sharp increase in amplification with increasing bias voltage. The distortion in a PIN diode mainly occurs at low bias voltages where fotovoltaïc effects can be observed.

In [6.12] and [6.13], the effect of spontaneous emission and of relaxation oscillations on the distortion in Fabry-Perot lasers is described. These effects are only important at low power levels, resp. at high modulation frequencies. The damping of the relaxation oscillations due to e.g. spectral hole burning has not been considered in both papers. Diffusion of carriers has been taken into account in [6.14], but again no spectral hole burning was taken into account and the analysis is restricted to Fabry-Perot lasers.

More recent studies also treat DFB-lasers and/or take into account spectral hole burning. The damping of the relaxation oscillations due to spectral hole burning is described in [6.15] for both Fabry-Perot and DFB lasers. The influence of spatial hole burning on the low frequency (LF) distortion in DFB lasers on the other hand has been studied in [6.16]. The distortion is calculated from the variation of the efficiency with the output power in this case and it is found that the distortion is minimal for a normalized coupling constant of about one. [6.17] reports on a dip in the power dependence of the distortion in DFB lasers, which has been explained as being a result of the leakage currents.

Our study goes beyond that in the sense that relaxation oscillations, spontaneous emission and spectral and spatial hole burning can be taken into account at the same time and in a more detailed way. It must indeed be remarked that the different non-linearities can influence each other mutually. The spatial hole burning furthermore depends on the modulation frequency; the effect becomes weaker at higher modulation frequencies (e.g. above 500 MHz).

This approach has led to some interesting results about the distortion in the AM-response. E.g. it appears that the distortion caused by the spatial hole burning originates from a non-linear relation between output power and average intracavity power. As the facet loss is proportional with the output power, it can be concluded that the distortion decreases if the ratio of absorption loss to facet loss decreases. Our analysis also confirms that the distortion is minimal for κL-values between 1 and 1.5.

It was also found that the presence of a dip in the power dependence of the distortion can also be attributed to an interaction between spatial and spectral hole burning. Moreover, a dip in the frequency dependence is sometimes resulting from an interaction between the spatial hole burning and the relaxation oscillations.

VI.2 Small signal modulation: overview

From now on, we will only consider lasers with good single mode behaviour and we leave the mode index m behind. In the following we will also use the definition 'low frequent' for modulation frequencies between 1 MHz and a few hundred MHz.

VI.2.1 The AM-response

The AM-response can, even for DFB lasers, be approximated very well by the analytical formula (2.3.18). Longitudinal spatial hole burning merely has an influence on the low frequency AM-response and it can only cause a small increase or decrease of the amplitude of the response. As the cut-off frequency of spatial hole burning is normally smaller than the resonance frequency, there is no influence on the damping of the relaxation oscillations either. This damping is practically identical to the value which can be derived from the formula (2.3.18a). Gain suppression and spontaneous emission also cause, in addition to the damping, a small variation in the amplitude of the AM-response.

The actual AM-response however must be calculated from the relation between the number of photons I and the output power P_{out}. In general, this relation is non-linear in Fabry-Perot lasers with small facet reflectivities and in DFB lasers and one can write:

$$P_{out,1} \sim (1 - 2\,\xi_{spat,2}\,I_0)\,I_1 \qquad (6.2.1)$$

It can be remarked though that the factor between brackets will practically equal one in normal situations and that the frequency dependence of $\xi_{spat,2}$ will not be reflected in the frequency dependence of the AM response.

The AM response remains flat as function of the modulation frequency until the relaxation oscillations occur. Its amplitude at low frequencies is furthermore proportional with the ratio of the facet loss to the total loss. Fig. 6.2.1 shows as an illustration the AM response of a 300 μm long $\lambda/4$-shifted DFB-laser with $\kappa L=1$, and this for different values of the injected current. The laser has a threshold current of 22.5 mA and a ΔgL value of 0.7. Spontaneous emission has been neglected in the calculations, while the response was calculated both with and without taking into account the gain suppression (with an ε-value of 11 W^{-1}). One can see that the effect of gain suppression is very small.

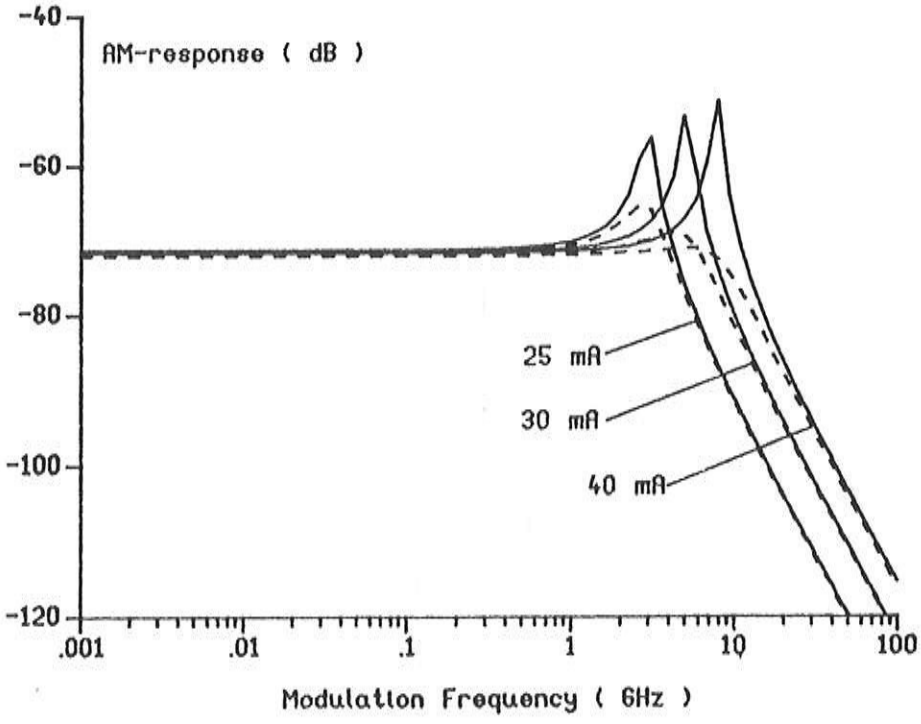

Fig. 6.2.1: AM response of a 300 μm long $\lambda/4$-shifted laser with $\kappa L=1$, (--) with and without (—) gain suppression.

VI.2.2 The FM response

The behaviour of the FM-response is far more complicated, especially for DFB lasers. The anomalous behaviour is due to the relatively large influence of spatial hole burning in this case.

Spatial hole burning has no influence on the FM response of F-P lasers. The low frequency FM in this case is determined by spontaneous emission (at low power levels) and by gain suppression and the analytical expression (2.3.18b) is an excellent approximation in this case. The resonance frequency and the damping of the relaxation oscillations are identical as in the case of the AM response and they can easily be derived analytically. As a first example of the FM response of DFB lasers, we have given the FM response of the 300 μm long $\lambda/4$-shifted laser with $\kappa L=1$ in fig. 6.2.2. Fig. 6.2.2a shows the influence of spatial hole burning and fig. 6.2.2b the influence of gain suppression. The last phenomenon is dominating, but this may not be generalized. Spatial hole burning as well as gain suppression give rise to contributions with phase zero. The contribution of gain suppression always has a phase zero, but we will see furtheron that this is not the case for the contribution of spatial hole burning. The contribution of the gain suppression can again be approximated very well from a rate equation analysis.

The contribution of spatial hole burning can be estimated from the earlier calculations of the gain and loss suppression caused by the spatial hole burning. If we denote by $\xi_{spat,1}$, resp. $\xi_{spat,2}$ the gain, resp. the loss suppression (see II.3.3.1) and if we neglect the phase ϕ_R, we find:

$$G = [A N_0 - B]\{1 - \xi_{spat,1} I\}$$
$$\gamma = \gamma_{fac,0}\{1 - \xi_{spat,2} I\} + \gamma_{int} \qquad (6.2.2)$$

and for the contribution to the FM response:

$$\omega_1 = \frac{\alpha}{2} A N_{01} = \frac{\alpha}{2} \frac{A\{\xi_{spat,1}\gamma - \xi_{spat,2}\gamma_{fac}\}\frac{\eta J_1}{qd}}{A\gamma V_a^{-1} + \tau_{rd}^{-1}\{\xi_{spat,1}\gamma - \xi_{spat,2}\gamma_{fac}\}} \qquad (6.2.3)$$

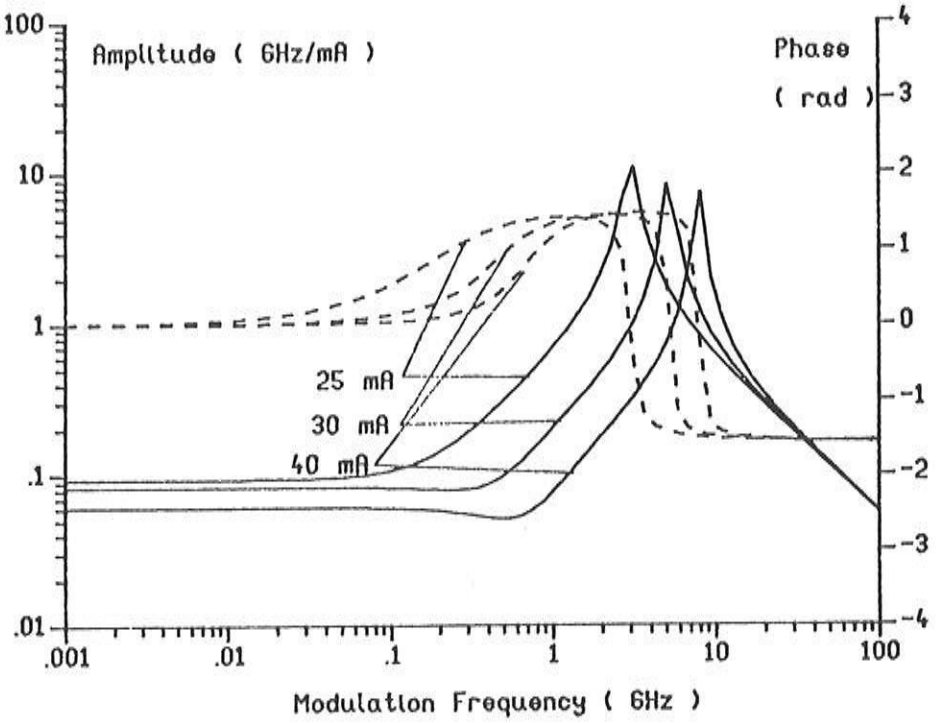

Fig. 6.2.2a: FM response of a 300 μm long λ/4-shifted laser with κL=1, no gain suppression taken into account.

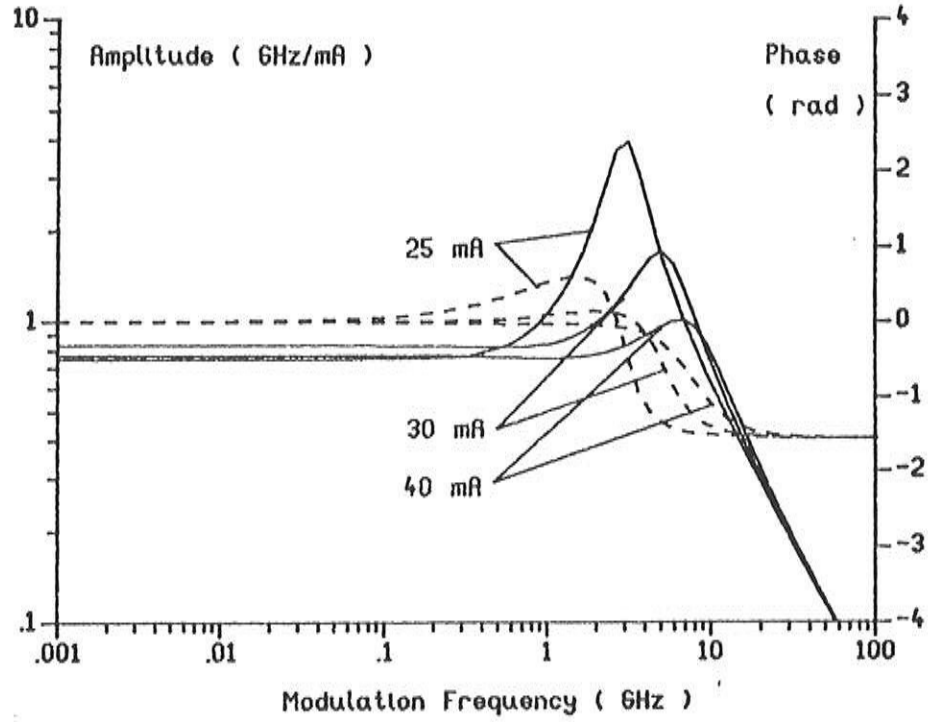

Fig. 6.2.2b: FM response of a 300 μm long λ/4-shifted laser with κL=1, gain suppression is taken into account.

For the laser under consideration one has: $\gamma_{fac} = 7.62\ 10^{11}\ s^{-1}$ and $\gamma_{int} = 3.75\ 10^{11}\ s^{-1}$, $\xi_{spat,1} = 0.266\ 10^{-6}$ and $\xi_{spat,2} = 0.618\ 10^{-6}$. Substitution of these values in the formula (6.2.3) shows that an FM response with a phase π can be expected. The fact that fig. 6.2.a shows that this phase equals zero indicates that the influence of the term ϕ_R can be decisive, even for lasers such as $\lambda/4$-shifted lasers. This thesis is supported also by numerical calculations with CLADISS. For the laser under consideration, it is found that the average electron density N_0 decreases with a rate of 2700 $\mu m^{-3}/mA$ at a current of 25 mA.

It can therefore be concluded that spatial hole burning not only comes to expression in a power dependence of gain and loss but also through the reflection phase ϕ_R, and that one of these aspects cannot be neglected a priori. It can be noticed that this also holds for the influence of spatial hole burning on the linewidth, although it was not explicitly mentioned in chapter 5.

In fig. 6.2.2a, a dip occurs in the FM response at 40 mA and at a modulation frequency of ± 1 GHz. The cause of this dip can be found in the weakening of the spatial hole burning beyond the cut-off frequency. The phase of the spatial hole burning contribution to the FM thereby gradually decreases to the value $-\pi/2$. The contribution of the relaxation oscillation on the other hand has a phase $\pi/2$, and, under appropriate conditions, this can lead to a destructive interference between the two contributions, which in turn causes a decrease of the FM-amplitude and a dip. Whether such a minimum will occur depends on the cut-off frequency of the spatial hole burning (which is mainly determined by τ_{rd} at low power levels) and on the resonance frequency f_r. E.g., the resonance frequency at 25 and 30 mA is far too small and the amplitude of the contribution of the relaxation oscillation is already too large near the cut-off frequency of the spatial hole burning; the minimum is not present or at least not visible.

As a second example we have shown the FM response of a 300μm long DFB-laser with $\kappa L=2$ and with facet reflectivities $\rho_f = 0.566\ e^{j\pi/4}$ and $\rho_b = 0$ in fig. 6.2.3. The threshold current of this laser is 16.5 mA and one finds the value 0.32 for ΔgL. Fig. 6..2.3a, resp.b shows the FM response of this laser if gain suppression (with $\varepsilon = 11\ W^{-1}$) is not taken into account, resp. is taken into

account. From fig. 6.2.3a, it follows that spatial hole burning now gives a contribution with a phase π at low frequencies. A minimum in the frequency dependence of the FM response is now longer present. The contributions from spatial hole burning and from the relaxation oscillations now both have a phase $\pi/2$ beyond the cut-off frequency of the spatial hole burning and they interfere constructively in stead of destructively.

The influence of the spatial hole burning is again expressed through the reflection phase ϕ_R. Numerical calculations indeed show that the average carrier density increases as a function of the injected current, with a rate of 815 μm^{-3}/mA at 20 mA. This increase of the carrier density induces a decrease of the average effective refractive n and, as a result of the resonance condition ωn = cte, an increase of the frequency. The phase π of the FM response in fig. 6.2.3a thus indicates a dominant influence of ϕ_R.

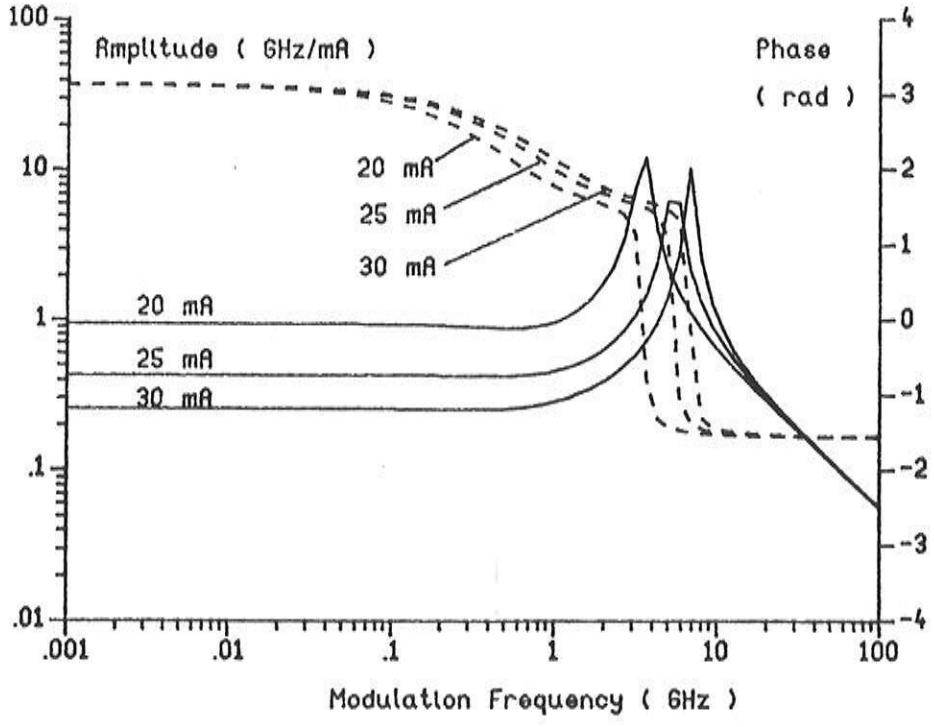

Fig. 6.2.3a: FM response of a 300 μm long DFB laser (see text) with κL=2, no gain suppression taken into account.

As the gain suppression always gives a contribution to the FM response with a phase zero, destructive interference between the contributions of spatial and spectral hole burning can occur for the

laser under consideration. However, the contribution of the gain suppression depends little on the power level, while the contribution of the spatial hole burning generally becomes weaker with increasing bias level (see fig. 6.2.3a). A minimum in the bias dependence of the low frequency FM response will therefore often occur. The typical course can be seen on fig. 6.2.3b. The contribution of spatial hole burning is usually dominant at low power levels and the FM response then has a phase π. With increasing bias level, the contribution of spatial hole burning decreases and more and more destructive interference occurs, until, at a certain power level, the contributions of spatial and spectral hole burning have identical amplitudes. Both effects then cancel each other and a minimal value for the low frequency FM is found. The FM response is then solely caused by the relaxation oscillations and has a phase equal to $\pi/2$. At even higher power levels, one finds that the contribution of the spatial hole burning still decreases and that the gain suppression becomes more and more dominant. The low frequency FM response then has a phase zero.

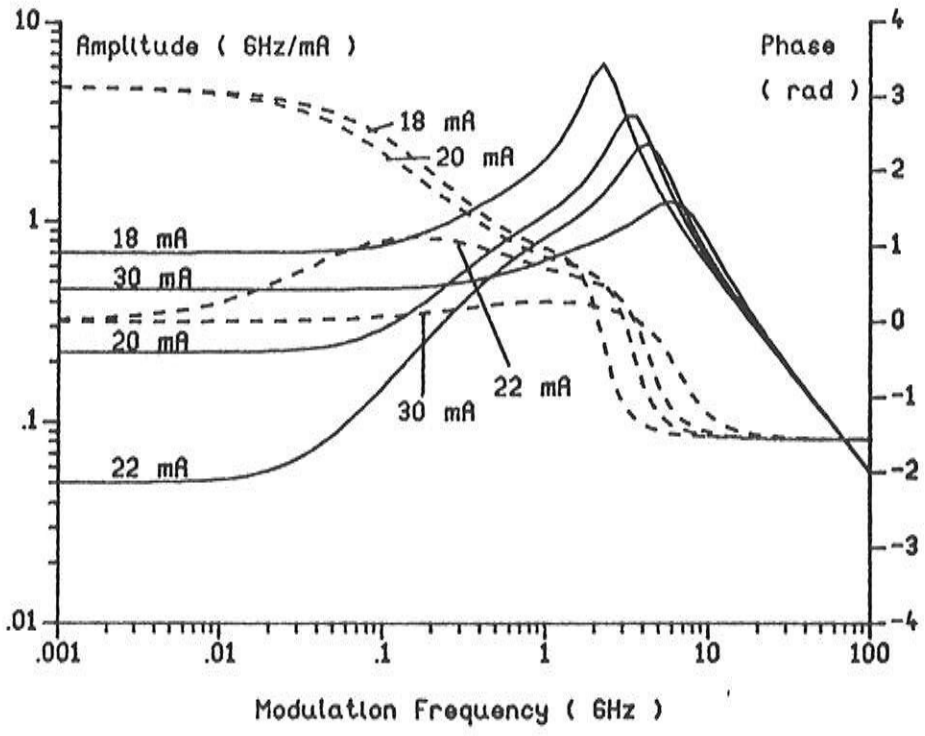

Fig. 6.2.3b: FM response of a 300 µm long DFB laser (see text) with $\kappa L=2$, gain suppression is taken into account.

VI.3 Harmonic distortion in Fabry-Perot lasers

In order to be able to eliminate spatial hole burning and dispersion completely, we first investigate the distortion in Fabry-Perot lasers. We will apply a single mode analysis, although such lasers are seldom single mode. This allows us to assess the influence of spontaneous emission, gain suppression and of the relaxation oscillations. Since it can be assumed that these effects will have similar influence on the distortion in DFB lasers, a study of F-P lasers might be interesting in the investigation of DFB lasers and might contribute to a better understanding of the non-linear behaviour of DFB lasers.

We will also show how the spatial hole burning in long F-P lasers with small facet reflectivities gives rise to a non-linear power current relation and which quantities are of special importance for this phenomenon. Mainly the distortion in the AM response will be covered here. In the case of F-P lasers, a good approximation can always be obtained from the rate equations and therefore the distortion will in general be described with the help of analytical formulas here.

We first investigate the influence of the different non-linearities separately here. Although the superposition principle can not be applied for non-linear systems, we will see that in many cases one of the non-linearities has a dominant influence. This also makes the analysis a lot easier. Indeed, taking into account different non-linearities leads immediately to very complex, unpractical formulas. Sometimes however, we will consider the combined effect of 2 non-linearities if it is of special importance.

Before considering the distortion in the AM response, we will briefly discuss the distortion in the FM response. With the help of an analytical small signal approximation, we will show that this distortion in the FM response can be relatively large, so that our small signal analysis is not really justified anymore. The dominant contribution to this large distortion has its origin in the relaxation oscillations, even at relatively small modulation frequencies.

On the other hand, from the relatively good linearity of the static power current relation, it can be concluded that the distor-

tion in the AM response will be rather small and that a small signal approximation is justified in this case.

VI.3.1 Distortion in the FM response

It can be shown that the low frequency, n-th order distortion in the FM response due to the relaxation oscillations is given by:

$$\frac{\omega_n}{\omega_1} = \left(-\frac{1}{2}\frac{I_1}{I_0} \right)^{n-1} \qquad (6.3.1)$$

This formula is easily derived from the static rate equation for the number of photons. If we assume that no other non-linearities exist, it follows that the power current relation will be perfectly linear so that under modulation $I_n=0$ for $n>1$. Furthermore, the loss is constant in this case and the gain depends only and linearly on the carrier density. The rate equation for the number of photons reduces to:

$$\{(AN_0-B)I - \gamma I\} = 0 \qquad (6.3.2)$$

And after substitution of the expansions (6.1.2), one can easily derive the following recursive relation:

$$\frac{N_{0n}}{N_{0n-1}} = -\frac{I_1}{I_0} \qquad (6.3.3)$$

The expression (6.3.1) immediately follows from this relation after introduction of a factor 1/2, which takes into account the fact that: $\cos^n(x) = 2^{-n} \cos(nx) + \ldots$

From (6.3.1) it follows that especially the 2nd order distortion can become relatively large if a large OMD is persuited. For an OMD of 20 % e.g., one finds a 2nd order distortion of 10 %, which appears to be too large to justify the use of a small signal analysis.

It can be remarked here that this contribution of the relaxation oscillations disappears if I is left behind as a common factor in (6.3.2). If, on the other hand, one takes into account the derivati-

ve with respect to the time, one again finds the contribution (6.3.1). The inclusion of I also makes the equation (6.3.2) more physical since the different term then describe the creation and the annihilation of photons (or power). Leaving I behind only leaves a mathematically deduced condition for oscillation. The author therefore believes that the relaxation oscillations constitute a real source of low frequency distortion.

VI.3.2 Distortion in the AM response

VI.3.2.1 Influence of the spontaneous emission and of the relaxation oscillations

The variations in the optical power are mainly caused by variations in the gain (which is not yet clamped) and in the carrier density for those bias points where the spontaneous emission has a substantial influence (i.e. in the vicinity of the threshold current). The stimulated emission can then still be neglected in the rate equation for the carriers, while the number of photons is determined by:

$$I = \frac{S}{\gamma - G} = \frac{S}{\gamma - (AN_0 - B)} \qquad (6.3.4)$$

The distortion in the AM response can be derived from this equation after introduction of the series expansion:

$$I = \frac{S}{\gamma - G_0}\left\{1 + \frac{A\,(N_0 - N_{00})}{\gamma - G_0} + \left(\frac{A\,(N_0 - N_{00})}{\gamma - G_0}\right)^2 + \ldots\right\} \qquad (6.3.5)$$

with G_0 being the gain under static injection. One finds:

$$I_0 = \frac{S}{\gamma - G_0} \quad \text{en} \quad I_n = I_0\left(\frac{A\,N_{01}}{\gamma - G_0}\right)^n, \; n > 0 \qquad (6.3.6)$$

It has been assumed that the laser is biased above threshold so that the difference between gain and loss is relatively small. The influence of the higher order carrier density can be neglected in

this case and only the dominating term must be retained in (6.3.6). One finds for the distortion:

$$\frac{I_n}{I_1} = \left(\frac{1}{2}\frac{I_1}{I_0}\right)^{n-1} \qquad (6.3.7)$$

An expression which, however, is only valid if the laser is biased sufficiently close to the threshold.

A more accurate expression for the 2nd order distortion, which also takes into account the dynamics, is given by:

$$\frac{I_2}{I_1} = \frac{1}{2}\frac{\left(j\Omega + \frac{S}{I_0}\right)\left(2j\Omega + \frac{1}{\tau_{rd}}\right) - \frac{1}{2A\,V_a}\frac{\partial}{\partial N_0}\left(\frac{1}{\tau_{rd}}\right)\left(j\Omega + \frac{S}{I_0}\right)^2}{\left(2j\Omega + \frac{S}{I_0}\right)\left(2j\Omega + \frac{1}{\tau_{rd}} + \frac{AI_0}{V_a}\right) + G_0\frac{AI_0}{V_a}}\frac{I_1}{I_0} \qquad (6.3.8)$$

in which the derivative of the dynamic carrier lifetime τ_{rd} is determined by the bimolecular and the Auger recombination. One can see from (6.3.8) that the static distortion caused by the spontaneous emission strongly depends on the spontaneous carrier recombination (via τ_{rd}). For small values of I_0 and in the static case, (6.3.8) reduces to (6.3.7).

This is illustrated in fig. 6.3.11 for a 300 μm long, symmetric Fabry-Perot laser with an 80 % facet reflectivity (laser FP1). The threshold current of this laser is 10.8 mA. Fig. 6.3.1 shows the 2nd order distortion caused by the spontaneous emission and the relaxation oscillations for a bias current of 15 mA and a modulation current of 1 mA. One can see that the effect of the spontaneous emission is already very small at the power level considered in fig. 6.3.11.

The relaxation oscillations dominate already for modulation frequencies above a few MHz. Resonance peaks (n peaks in the n-th order distortion) can be observed at even higher modulation frequencies (± 1GHz) and the distortion rapidly decreases beyond these resonances. It must be remarked that this decrease of the distortion is due to the decrease of the OMD.

The distortion caused by the spontaneous emission has a phase zero. The contribution of the relaxation oscillations has a phase

which equals $\pi/2$ at low frequencies, but which gradually increases to the value π in the vicinity of the resonance frequency.

Fig. 6.3.2 shows the 3rd order distortion caused by the spontaneous emission and the relaxation oscillations for the same laser and under identical circumstances. The contribution of the spontaneous emission at static frequencies, which, sufficiently far above threshold can be approximated by:

$$\frac{I_3}{I_1} = -\frac{1}{4}\,\frac{\frac{1}{\tau_{rd}}\frac{S}{I_0}}{G_0\frac{AI_0}{V_a}}\left(\frac{I_1}{I_0}\right)^2 \qquad (6.3.9)$$

is also very small and now has a phase π. The contribution of the relaxation oscillations has a phase $-\pi/2$ at low frequencies and a phase 0 near the resonance frequency.

Formuli (6.3.8) and (6.3.9) illustrate that the n-th order distortion is generally proportional with the (n-1)-th power of the OMD. This property is found both theoretically and experimentally.

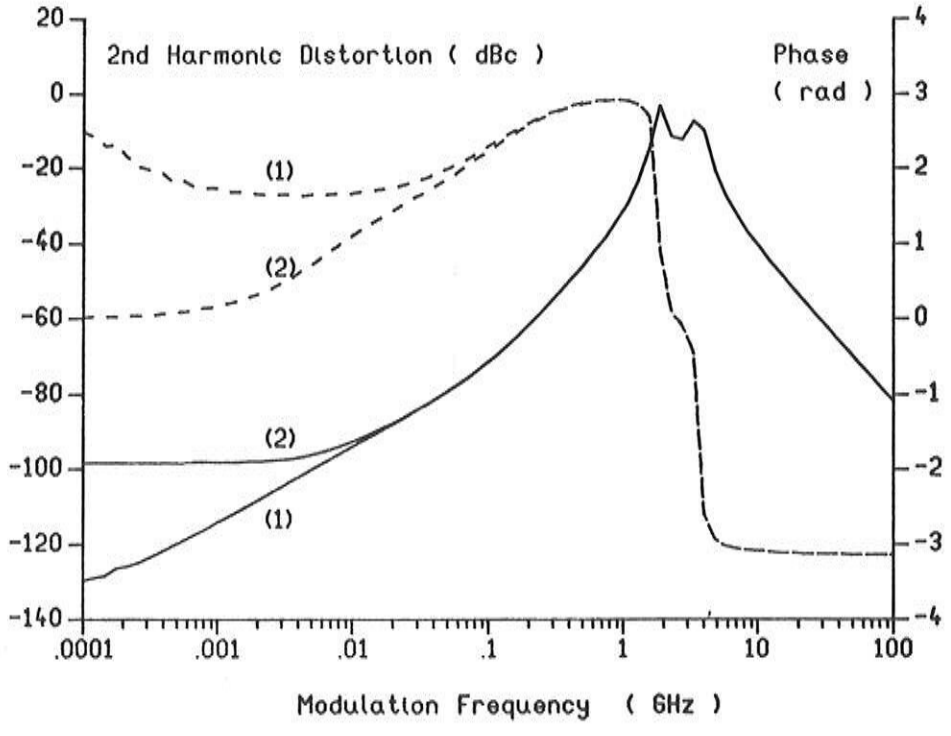

Fig. 6.3.1: 2nd order distortion in the AM response due to spontaneous emission and relaxation oscillations for laser FP1; OMD=0.24.

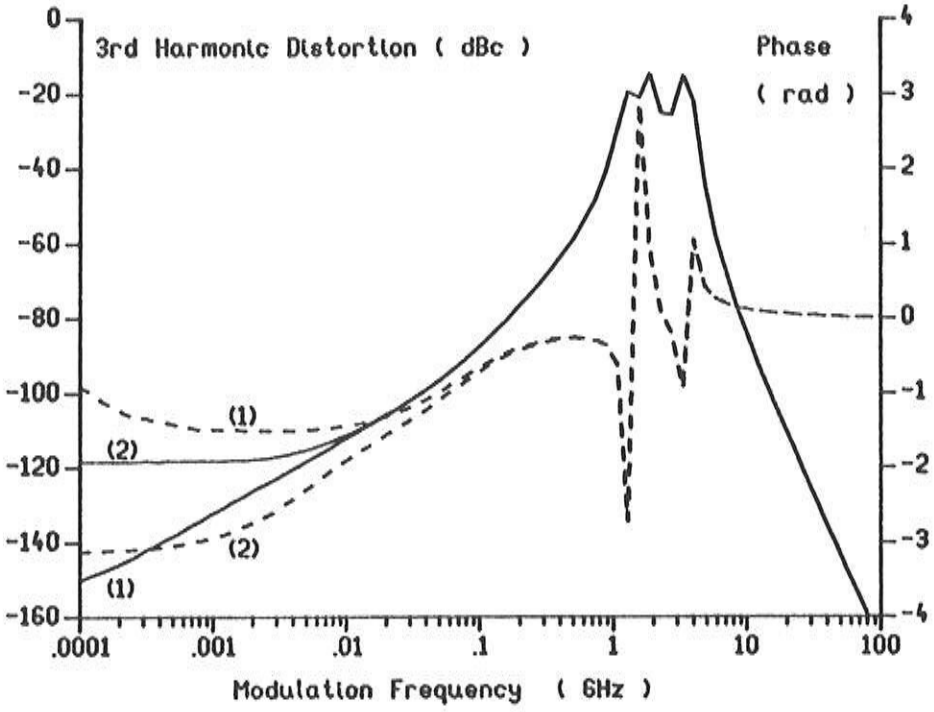

Fig. 6.3.2: 3rd order distortion in the AM response due to spontaneous emission and relaxation oscillations for laser FP1; OMD=0.24.

VI.3.2.2 Influence of the gain suppression

The gain suppression has no influence on the actual value of the gain, but it results in an increase of the carrier density, which is required to obtain this value of the gain, with increasing power. The distortion in the AM response caused by this gain suppression therefore has its origin in the increase of the spontaneous carrier recombination, which makes that an increase in injected current is not completely transferred into an increase of the stimulated emission. A similar effect can be expected to result from the presence of leakage currents (an effect which we do not consider here). Both effects will result in a sublinear P/I-curve and the 2nd order distortion will have a phase π at low modulation frequencies.

After manipulation of the rate equations, one finds the following expressions for the 2nd and 3rd order distortion at low modulation frequencies:

$$\frac{I_2}{I_1} = -\frac{1}{2}\,\frac{\xi^2 G_0\left(\frac{1}{\tau_{rd}} + \frac{G_0}{2A}\frac{\partial}{\partial N_0}\left(\frac{1}{\tau_{rd}}\right)\right)}{\left(\xi G_0 \frac{1}{\tau_{rd}} + \frac{G_0 A}{V_a}\right)} I_1 \qquad (6.3.10a)$$

$$\frac{I_3}{I_1} = -\frac{1}{4}\,\frac{\xi^3 G_0\left(\frac{1}{\tau_{rd}} + \frac{G_0}{A}\frac{\partial}{\partial N_0}\left(\frac{1}{\tau_{rd}}\right) + \frac{G_0^2}{6A^2}\frac{\partial^2}{\partial N_0^2}\left(\frac{1}{\tau_{rd}}\right)\right)}{\left(\xi G_0 \frac{1}{\tau_{rd}} + \frac{G_0 A}{V_a}\right)} I_1^2 + 2\left(\frac{I_2}{I_1}\right)^2 \qquad (6.3.10b)$$

The 2nd order distortion is proportional with the square of ξ and always has a phase π. The distortion increases with increasing power level if a constant OMD is used. The 3rd order distortion consists of a term with phase π, which is proportional with the 3rd power of ξ and which is normally dominant and a term with phase 0 and proportional with 4th power of ξ. The 3rd order distortion also increases with increasing bias level if the OMD is kept constant. It can easily be shown that these properties remain valid if another form for the gain suppression (see (5.2.10)) is assumed.

Fig. 6.3.3 and 6.3.4 illustrate the influence of gain suppression on the distortion of the laser FP1. The modulation current is again 1 mA and different values (15, 20, 25 en 30 mA) for the static current have been considered. It is clear that the low frequency distortion is practically independent of the static power and that the phase of 2nd and 3rd order distortion equals π. The relaxation resonances are again strongly damped as a result of this gain suppression.

The presence of a dip in the frequency range from 100 MHz to 1 GHz can be observed in fig. 6.3.4. This dip can be attributed to the interference between the contribution of the gain suppression (with phase π) and the contribution of the relaxation oscillations (the phase of which approaches the value 0 in the frequency region under consideration). The contribution of the relaxation oscillations increases with increasing modulation frequency, while the contribution of the gain suppression is rather constant. At a certain, well-determined modulation frequency, both contributions cancel each other and only a component with a phase $-\pi/2$, stemming from the relaxation oscillations, remains. The contribution of

the relaxation oscillations still increases beyond this frequency and it dominates the contribution of the gain suppression.

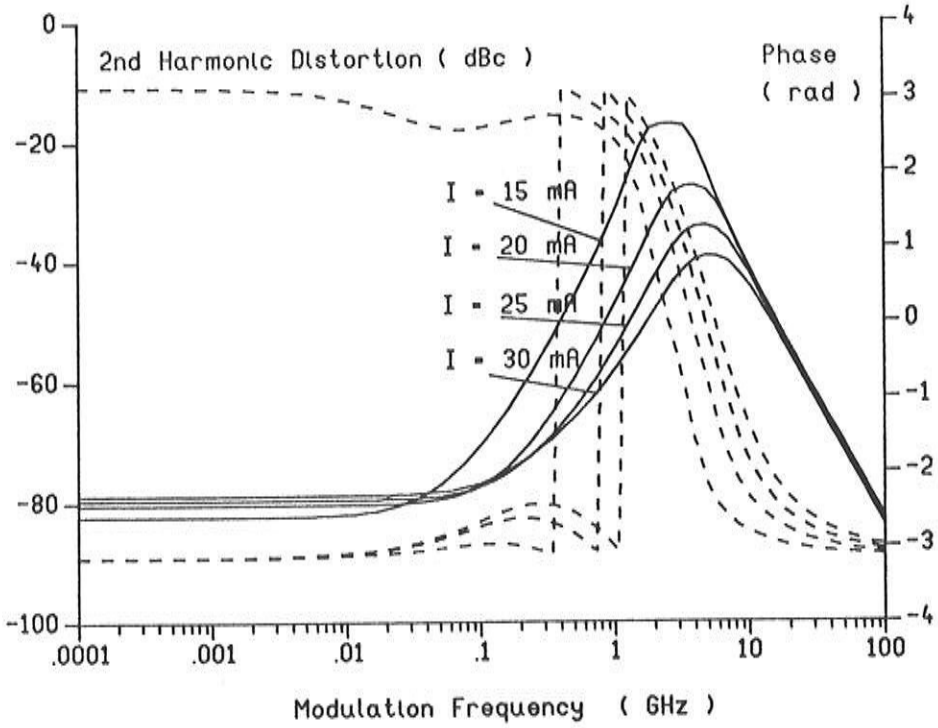

Fig. 6.3.3: 2nd order distortion in the AM due to gain suppression for laser FP1 at 15 (1), 20 (2), 25 (3) and 30 mA (4).

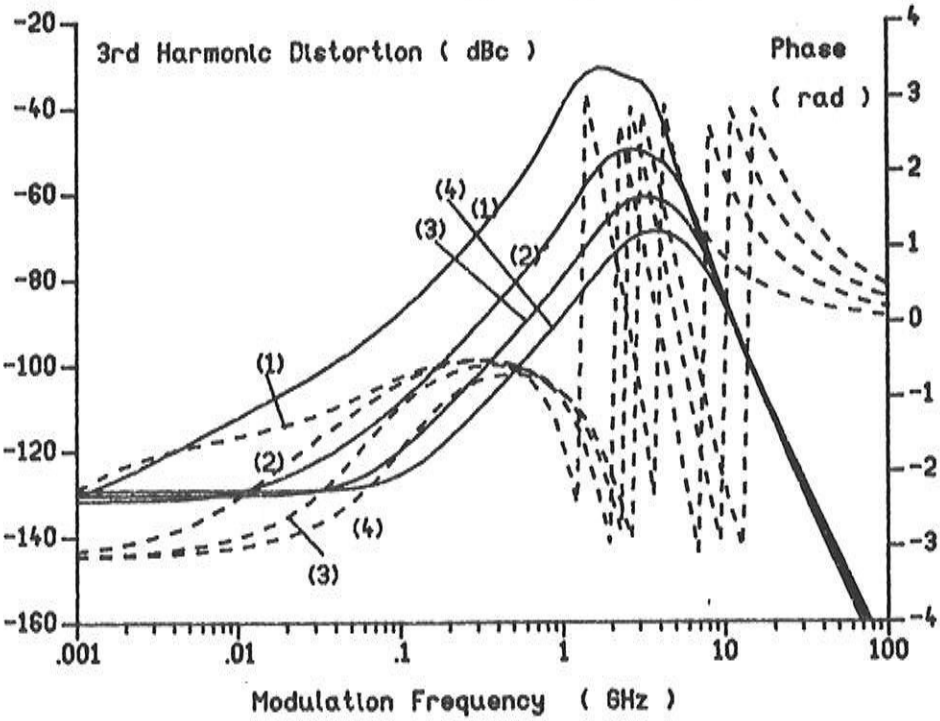

Fig. 6.3.4: 3rd order distortion in the AM due to gain suppression for laser FP1 at 15 (1), 20 (2), 25 (3) and 30 mA (4).

VI.3.2.3 Influence of spatial hole burning

It was shown in chapter II (II.3.31) how, even in Fabry-Perot lasers, the longitudinal variation of the optical power results in a non-linear relation between output power and the number of photons. The gain and the loss are both suppressed as a result of this effect, but the carrier density still remains clamped and is independent of the power level. If all other non-linearities are disregarded, there will be no influence on the FM response. There exists however an influence of the spatial hole burning on the distortion in the AM response. From the rate equation for the carrier density it follows that the quantity $I(1-\xi_{spat}I)$ will vary proportionally with the injected current, since no variations in the carrier density occur. The distortion in the output power can then be derived from the relation (2.3.34):

$$P \sim \{(AN_0 - B)(1 - \xi_{spat}I) - \alpha_{int}v_g\} I \qquad (6.3.11)$$

For a laser of length L with facetreflectivities R_1 and R_2, one finds:

$$\frac{P_n}{P_1} = \frac{2\alpha_{int}L}{\ln(R_1R_2)} \frac{I_n}{I_1} \qquad (6.3.12)$$

and hence:

$$\frac{P_2}{P_1} = \frac{\alpha_{int}L\,\xi_{spat}I_0}{\ln(R_1R_2)} \frac{P_1}{P_0} \qquad (6.3.13a)$$

$$\frac{P_3}{P_1} = \frac{\alpha_{int}L\,\xi_{spat}^2 I_0^2}{\ln(R_1R_2)} \left(\frac{P_1}{P_0}\right)^2 \qquad (6.3.13b)$$

The value of ξ_{spat} has been depicted in fig. 2.3.1 for 300 μm long lasers. For the laser FP1, ξ_{spat} is too small to have any visible effect. ξ_{spat} is also relatively small for e.g. as-cleaved lasers. The distortion in F-P lasers will therefore usually be dominated by the spectral hole burning.

From the expressions (6.3.13), it can be concluded that the distortion, resulting from spatial hole burning, varies strongly as a

function of the internal absorption. This is illustrated in fig. 6.3.5 and 6.3.6, which give the 2nd and 3rd order distortion in the AM response of a 300μm long F-P laser with cleaved facets for different values of the internal absorption. The distortion has been calculated at an output power of 1 mW and for an OMD of 20 % in both cases and the spontaneous emission and the spectral hole burning have been neglected.

The 2nd order distortion has a phase π at low modulation frequencies, in agreement with the expression (6.3.13). The phase of the 3rd order distortion equals 0, which is different than what can be expected from (6.3.13). A possible explanation for this deviation could perhaps be found in the power dependence of ξ_{spat} (see formula (2.3.31)), which was not taken into account in the derivation of (6.3.13). The spatial hole burning is taken into account in a more detailed way in the numerical model. ξ_{spat} furthermore decreases with increasing modulation frequency and its value is already sufficiently low at the relaxation resonance, so that any influence on the damping of this resonance is not very likely.

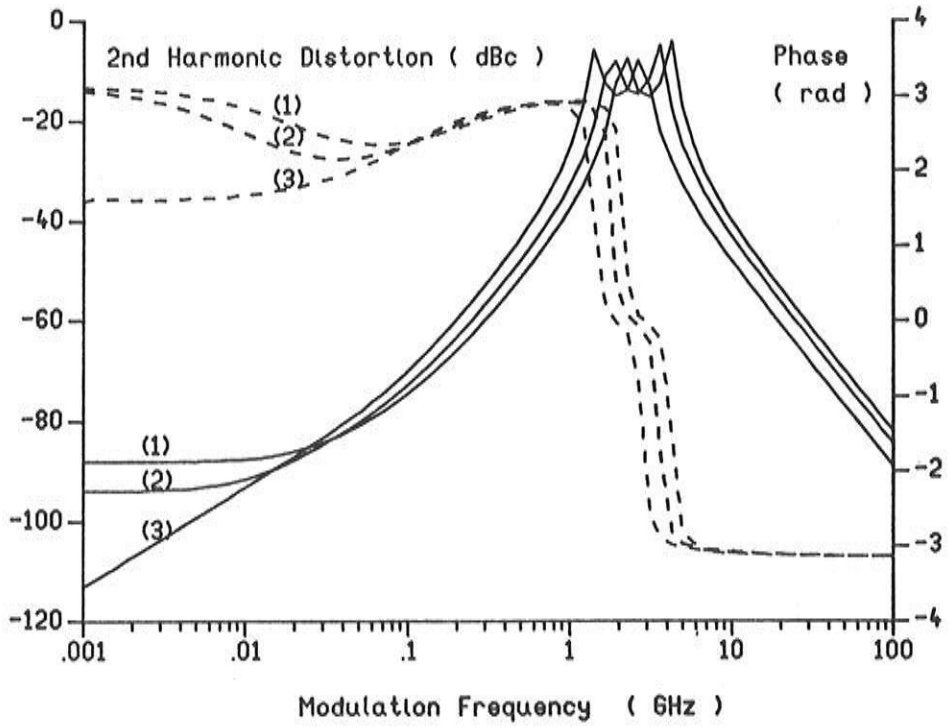

Fig. 6.3.5: 2nd order distortion due to spatial hole burning for laser FP2 α_{int}=50 cm^{-1} (1), α_{int}=25 cm^{-1} (2) en α_{int}=0 cm^{-1} (3).

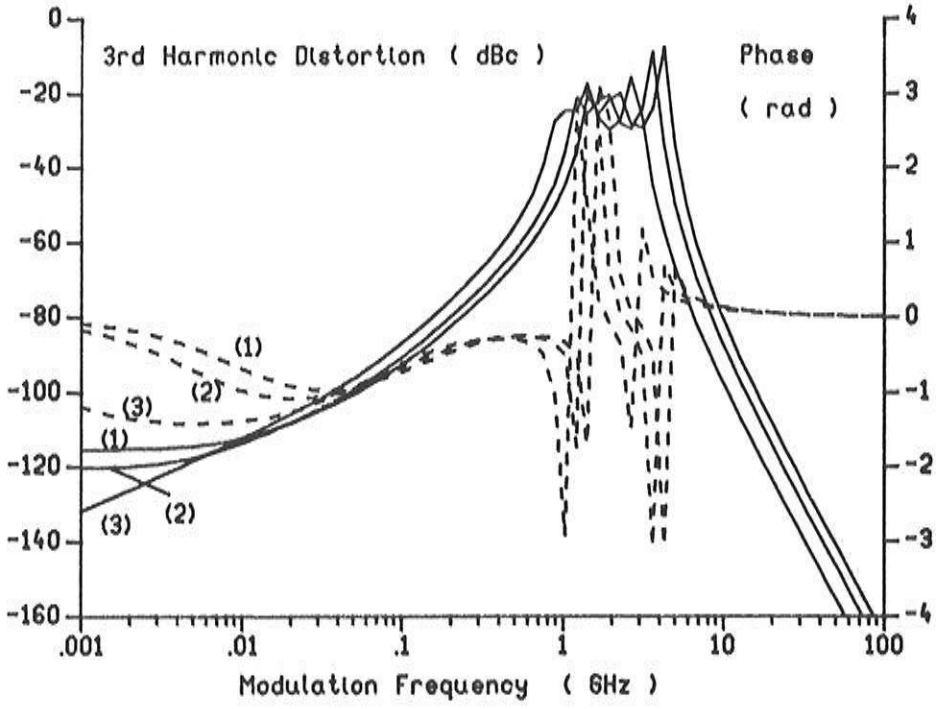

Fig. 6.3.6: 3rd order distortion due to spatial hole burning for laser FP2 α_{int}=50 cm^{-1} (1), α_{int} =25 cm^{-1} (2) en α_{int} = 0 cm^{-1} (3).

VI.4 Distortion in DFB lasers

DFB lasers distinct themselves from F-P lasers by the more pronounced spatial hole burning and by their sometimes strong dispersion. Here, we first discuss $\lambda/4$-shifted or similar lasers for which the dispersion can be disregarded. Since the cut-off frequency of the spatial hole burning is normally far below the resonance frequency f_r of the relaxation oscillations, we can afford to refer to the previous paragraph (VI.3) for what concerns the distortion at such high modulation frequencies.

Spectral hole burning can be taken into account simultaneously with the spatial hole burning in the derivation of the analytical formuli. Both effects lead to gain suppressions, which can be superposed. One must nonetheless keep in mind that the spectral hole burning is independent of the power and the' frequency, while the spatial hole burning certainly depends on power and frequency. Here, we will mainly focuss on the interferences between contributions from spatial hole burning, spectral hole burning and relaxation oscillations.

VI.4.1 Influence of the spatial hole burning.

The effect of spatial hole burning on the distortion is again a consequence of the non-linear relation between the output power and the average power inside the cavity. This non-linearity is, in lasers which emit at the Bragg wavelength (such as λ/4-shifted lasers) and at low power levels, mainly caused by the longitudinal variation of the gain and one can show analytically that in this case, the modal gain and the loss can be expressed as:

$$G = (AN_0 - B)(1 - \xi_{spat,1} I) = G_0(1 - \xi_{spat,1} I)$$
$$\gamma = \gamma_{fac} + \gamma_{int} = \gamma_{fac,0}(1 - \xi_{spat,2} I) + \gamma_{int} \qquad (6.4.1)$$

Both $\xi_{spat,1}$ and $\xi_{spat,2}$ decrease with increasing power level, but, in contrast with the case of F-P lasers, $\xi_{spat,2}$ can now be positive as well as negative. The values of $\xi_{spat,i}$ are also substantially larger now. The inclusion of spectral hole burning does not require a modification of the expression (6.4.1) and one can write:

$$G = G_0(1 - \xi_1 I) \; ; \; \xi_1 = \xi_{spat,1} + \xi_{spectr}$$
$$\gamma = \gamma_{fac,0}(1 - \xi_2 I) \; ; \; \xi_2 = \xi_{spat,2} \qquad (6.4.2)$$

Typical values for the coefficients $\xi_{spat,i}$ at the threshold of 300 μm long λ/4-shifted lasers have already been given in chapter 2 (fig. 2.3.2). Both coefficients are minimal for $\kappa L = 1.25$, a value which is known to result in minimal spatial hole burning for λ/4-shifted lasers.
The output power can again be expressed as:

$$P \sim I(1 - \xi_2 I) \qquad (6.4.3)$$

With the help of the expressions (6.4.2) and (6.4.3), one finds for the low frequency 2nd and 3rd order distortion:

$$\frac{P_2}{P_1} = -\xi_2 P_1 \frac{\gamma_{int}}{2\gamma} - (\xi_2\gamma_{int} + \Delta\xi G_0)\frac{V_a P_1}{\gamma 2A}\left\{\frac{\Delta\xi}{\tau_{rd}} + \frac{(\xi_2\gamma_{int} + \Delta\xi G_0)}{2A}\frac{\partial}{\partial N_0}\left(\frac{1}{\tau_{rd}}\right)\right\}$$

$$\frac{P_3}{P_1} = 2\left(\frac{P_2}{P_1}\right)^2 - (\xi_2\gamma_{int} + \Delta\xi G_0)\frac{V_a P_1^2}{4\gamma A}\frac{\Delta\xi^2}{\tau_{rd}} -$$

$$(\xi_2\gamma_{int}+\Delta\xi G_0)^2\frac{V_a P_1^2}{4\gamma A^2}\left\{\Delta\xi\frac{\partial}{\partial N_0}\left(\frac{1}{\tau_{rd}}\right) + \frac{(\xi_2\gamma_{int}+\Delta\xi G_0)}{6A}\frac{\partial^2}{\partial N_0^2}\left(\frac{1}{\tau_{rd}}\right)\right\} \quad (6.4.4)$$

with $\Delta\xi = \xi_1 - \xi_2$.

We first consider the effect of spatial hole burning on the 2nd order distortion. By substitution of typical numerical values in the expression (6.4.4) it can easily be checked that the first term will dominate at low power levels, except for those κL-values in the vicinity of 1.25 for which ξ_2 is very small. Since ξ_2 can assume positive as well as negative values, it follows that the 2nd order distortion can have a phase π as well as a phase 0.

The 2nd order distortion induced by spatial hole burning is illustrated in fig. 6.4.1, resp. 6.4.2 for 300 μm long $\lambda/4$-shifted lasers with $\kappa L = 1$ (laser L1, with a threshold current of 22.5 mA), resp. $\kappa L = 2$ (laser L2, with a threshold current of 15 mA) for a static OMD of 20 %.

It can be seen that the low frequency distortion has a phase π for the case $\kappa L=1$ and a phase 0 for the case $\kappa L=2$. This agrees with the expression (6.4.4), since, in the limit of low power levels, one finds for $\kappa L = 1$ the values $\xi_1 = 8.35\ W^{-1}$ and $\xi_2 = 19.4\ W^{-1}$ and for $\kappa L = 2$ the values $\xi_1 = 47.4\ W^{-1}$ and $\xi_2 = -18.9\ W^{-1}$. According to the expression (6.4.4), it can also be expected that the distortion increases with increasing static output power if the OMD is kept constant. In fig. 6.4.1 and 6.4.2, such a behaviour can only be observed at low power levels, while the distortion at high power levels decreases monotonically with increasing power level. This deviation could again be explained by taking into account the power dependence of ξ_1 and ξ_2.

As for Fabry-Perot lasers and for the same reasons, the distortion induced by the spatial hole burning strongly depends on the ratio of absorption loss to facet loss. The distortion diminishes as the absorption decreases or as the reflection loss increases (e.g. if lower κL-values are being used).

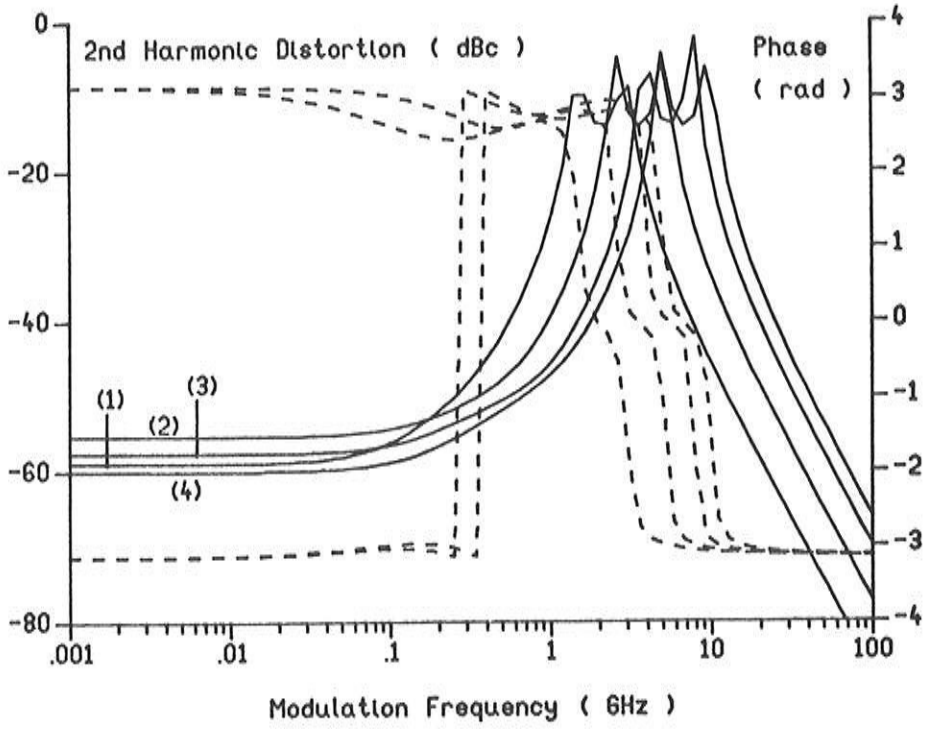

Fig. 6.4.1: 2nd order distortion due to spatial hole burning for laser L1 at 25 mA (1), 30 mA (2), 40 mA (3) and 50 mA (4).

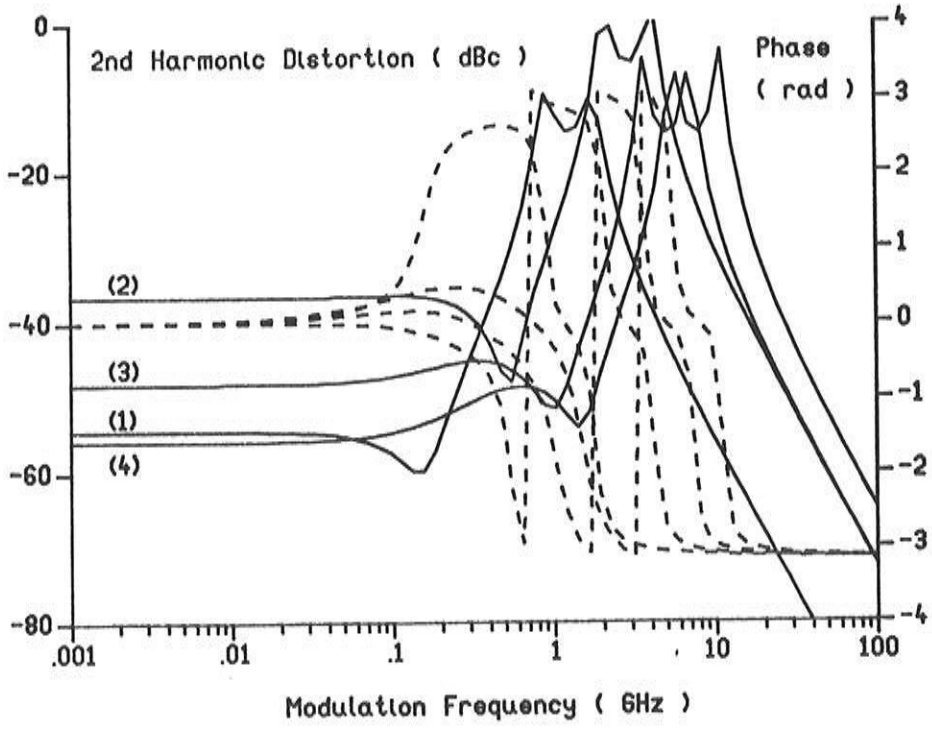

Fig. 6.4.2: 2nd order distortion due to spatial hole burning for laser L2 at 16 mA (1), 20 mA (2), 30 mA (3) and 50 mA (4).

For modulation frequencies above ± 100 MHz, the relaxation oscillations (giving a contribution with a phase $\pi/2$ and a contribution with a phase π) become important as well. The contribution of the relaxation oscillations then interferes with the contribution of the spatial hole burning, which already starts decreasing at these high frequencies. Destructive interference can occur if the distortion caused by the spatial hole burning has a phase 0. The interference results in a dip in this case, as can be seen in fig. 6.4.2. This dip shifts towards higher frequencies with increasing static output power, since both the relaxation oscillations as well as the cut-off frequency of the spatial hole burning are located at higher frequencies. Such a dip may be interesting and it can lead to a distortion that is small even for frequencies of e.g. 1 GHz. It can be noticed that the distortion at 1 GHz has increased by 10 dB with respect to the low frequency value in fig. 6.4.1, while both values are almost identical in fig. 6.4.2.

The third order distortion consists of two contributions with opposite sign (see (6.4.4)). The first term is equal to twice the square of the second order distortion, its phase is zero and its magnitude can be derived immediately from the second order distortion. The second contribution, which is related to the variation of the spontaneous carrier recombination due to spatial and spectral hole burning, may have a phase zero as well as a phase π. Which one of the two contributions dominates is hard to predict and depends on the modulation depth, on the bias point and on the laser structure. We will discuss this distortion here with the help of a few numerical examples. It will become clear that the third order distortion is usually a lot smaller than the second order distortion.

The third order distortion as a function of the modulation frequency is depicted in fig. 6.4.3 for the laser L1 and in fig. 6.4.4 for the laser L2. The OMD and the bias points have been chosen as in fig. 6.4.1, resp. 6.4.2, so that the magnitude of the first contribution can be estimated from these figures. Since the second order distortion of the laser L1 (for $\xi_{spec}=0$) varies between -60 and -55 dBc, it follows that the first term in formule (6.4.4b) will vary between -124 and -104 dBc. The second order distortion of the laser L1 varies between ±-56 and ±-37 dBc and the first term in (6.4.4b) will assume a value between -106 and -68 dBc.

The second contribution always seems to dominate for the case $\kappa L=1$ and the third order distortion always has a phase zero. It can be noticed that $\Delta\xi$ is negative in this case (at least at low power levels where $\Delta\xi = -11\ W^{-1}$) and that $G_0 \gg \gamma_{int}$ so that the phase of the second contribution is zero indeed. However, both contributions are very small (approximately -110 dBc) for very low power levels (the curve (1) in fig. 6.4.3); mainly as a result of the small value of P_1. The influence of the relaxation oscillations already becomes visible at very low modulation frequencies (e.g. 10 MHz). The phase of the distortion then approaches the value $-\pi/2$.

The phase of the third order distortion is for $\kappa L=2$ always equal to π, from which it can be concluded that the second contribution again dominates. The value of $\Delta\xi$ is positive now and larger, $\Delta\xi = 66.3\ W^{-1}$, while the value of γ also has become smaller. The second contribution therefore can have an amplitude that is a lot larger than the -80 dBc which was found for $\kappa L=1$ and it can dominate the relatively large contribution of the first term. Again, the value of P_1 is so small at low power levels that the relaxation oscillations can be visible already at low modulation frequencies. This can be seen from the phase corresponding with the curve (1) in fig. 6.4.4.

It must finally be remarked that destructive interference occurs between contributions from the relaxation oscillations (with phase 0) and from the spatial hole burning, if the latter contribution has a phase π. This leads to a dip in the frequency region between 100 MHz and 1 GHz, as can be observed in fig. 6.4.4. We also notice that the presence of a dip in the frequency dependence of the 2nd order distortion implies here a dip in the frequency dependence of the 3rd order distortion and vice versa. We suspect that this phenomenon is related with the sign of ξ_2, which determines the phase of the first term in (6.4.4a) (and thus of the 2nd order distortion), but also the sign of $\Delta\xi$ and of the second contribution in (6.4.4b) and of the 3rd order distortion.

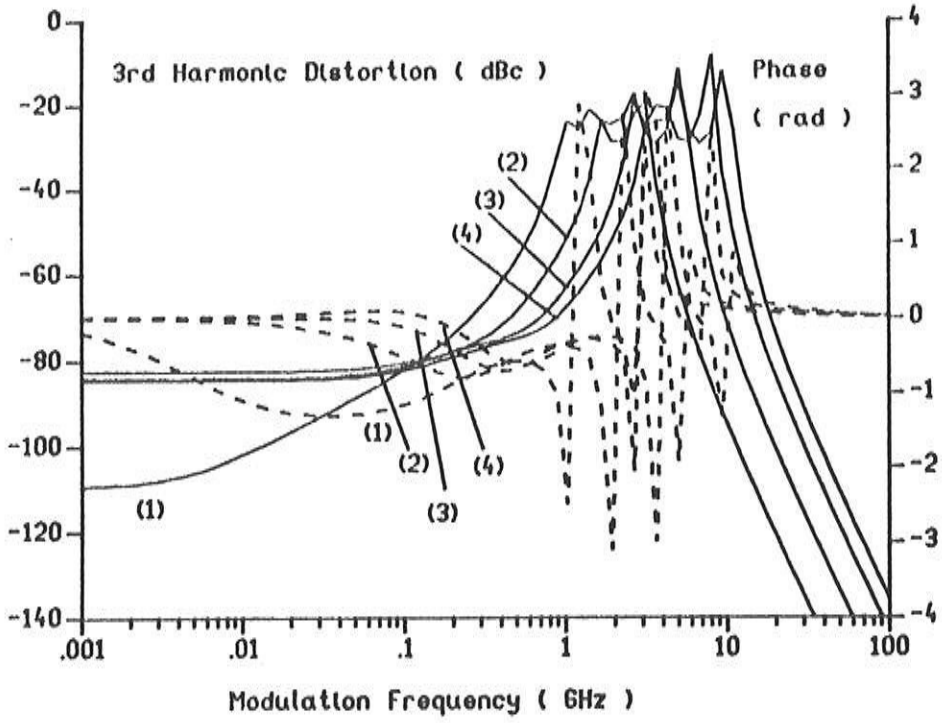

Fig. 6.4.3: 3rd order distorton due to spatial hole burning for laser L1 at 25 mA (1), 30 mA (2), 40 mA (3) and 50 mA (4).

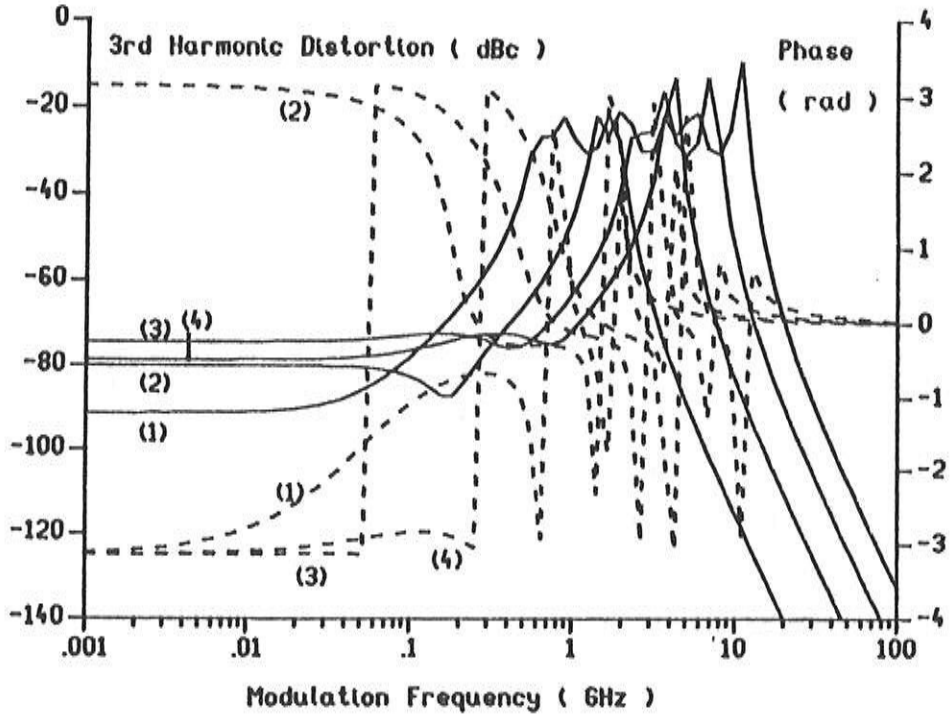

Fig. 6.4.4: 3rd order distortion due to spatial hole burning for laser L2 at 16 mA (1), 20 mA (2), 30 mA (3) and 50 mA (4).

6.4.2 Dips in the bias dependence of the distortion

Taking into account spectral hole burning does not require a modification of the analytical approximations (6.4.4), though the value of ξ_{spectr} must be added to ξ_1. At very high power levels, spatial hole burning can be neglected and one again finds the approximations (6.3.10). At high power levels, one therefore always finds a 2nd and 3rd order distortion with a phase π.

On the other hand, it may be possible that spatial hole burning dominates at low power levels and that the phase of the 2nd and 3rd order distortion is zero in this case. The transition from a phase 0 at low power levels to a phase π at high power levels then assures the existence of a bias point for which the distortion is minimum and for which the phase equals $\pi/2$. The contributions of spectral and spatial hole burning interfere destructively at this point and only the contribution of the relaxation oscillations (with phase $\pi/2$ at low modulation frequencies) remains.

An example of this phenomenon is shown in fig. 6.4.5. Fig. 6.4.5 shows the 2nd order distortion of the laser L2 for the case $\xi_{spectr} = 11\ W^{-1}$. It can be seen how the spatial hole burning dominates at low power levels and how the spectral hole burning dominates at high power levels. Both effects almost cancel each other for the 3rd bias point (the curve labeled (3)), the low frequency distortion is very small and the relaxation oscillations start dominating already at 10 MHz. Such a minimum can not be observed for the laser L1, where both the contributions from spatial and spectral hole burning have a phase π.

Such a minimum in the bias dependence of the 3rd order distortion can be observed for laser L1, although this is not shown here. The minimum in the 3rd order distortion can now not be observed for the laser L2, for which the contributions of spatial and spectral hole burning both have a phase π.

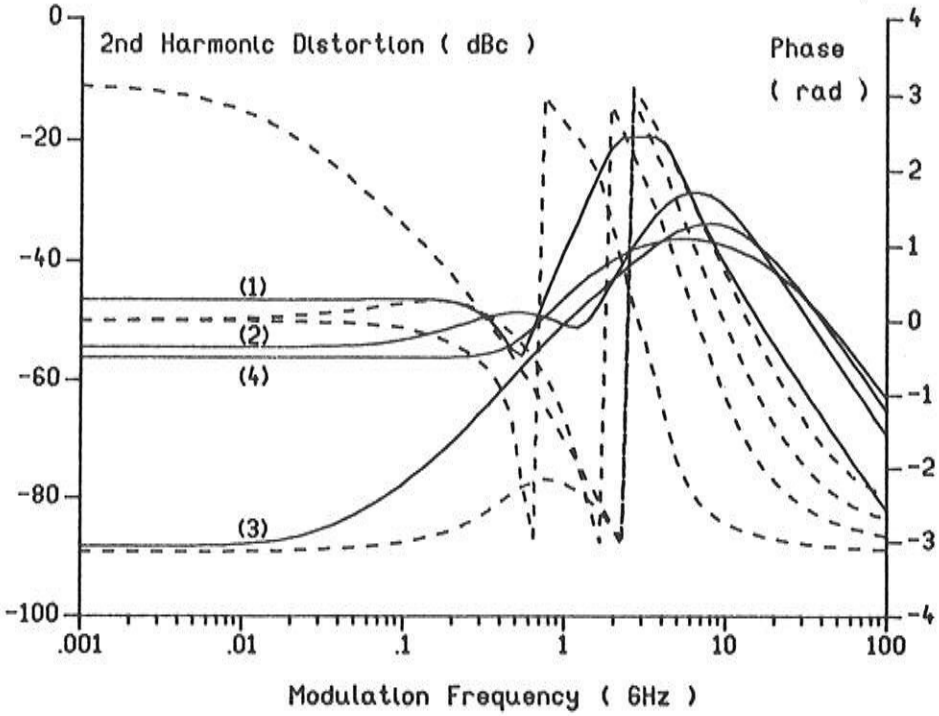

Fig. 6.4.5: 2nd order distortion due to spatial and spectral hole burning for laser L2 at 20 (1), 40 (2), 60 (3) and 80 mA (4).

VI.5 The system dependent quantities CSO and CTB

A system design usually imposes no restriction on the harmonic distortion, but rather on the, on the system depending, quantities such as the CSO ('Composite Second Order') and the CTB ('Composite Triple Beat'). For mutual harmonic carriers, the CSO, resp. the CTB can be defined as the ratio of the peak power in the carrier to the peak power in the second order, resp. the third order intermodulation tone. The relation between the system dependent quantities CSO and CTB and the laser dependent quantities, 2nd and 3rd order harmonic distortion, will only be addressed briefly here. We refer to the literature (e.g. [6.18] and [6.19]) for a more detailed account.

We first show how the intermodulation distortion is related to the harmonic distortion. We assume for the sake of simplicity

that only 3 carriers (with frequencies f_1, f_2 and f_3 and with an identical OMD) are used and that the current injection is therefore given by:

$$J = J_0 \left\{ 1 + \frac{m}{3} [\cos(\Omega_1 t) + \cos(\Omega_2 t) + \cos(\Omega_3 t)] \right\} \qquad (6.5.1)$$

m is the total modulation depth. We also assume that the harmonic distortion is nearly flat in the frequency region that contains f_1, f_2 and f_3. The optical output power can then be approximated as:

$$P = a + b\,J + c\,J^2 + d\,J^3 \qquad (6.5.2)$$

After substitution of (6.5.1) into (6.5.2) one finds that the light intensity not only consists of components with frequency f_i (linear response), $2f_i$ (2^e order harmonic distortion) and $3f_i$ (3^e order harmonic distortion), but also components at the frequencies $f_i \pm f_j$ and at the frequenties $f_i \pm f_j \pm f_k$. Moreover, it can easily be checked that the amplitude of the components at the frequencies $f_i \pm f_j$ ($i \neq j$) is a factor 2 (6 dB) larger than the amplitude of the components at the frequencies $2f_i$. The amplitude of the components at the frequencies $f_i \pm f_j \pm f_k$ ($i \neq j \neq k$) is a factor 6 (15.5 dB) larger than the amplitude of the components at frequencies $3f_i$ and a factor 2 (6 dB) larger than the amplitude of the componens at frequencies $2f_i \pm f_j$ ($i \neq j$). The intermodulation distortion can simply be derived from the harmonic distortion with the help of these relations.

The CSO and the CTB for a given carrier can then be obtained as the sum of all possible intermodulation products with a frequency in this channel. We now assume that all carrier frequencies are given by $f_i = i\,f$, $i = N_{min} \ldots N_{max}$. The number of second order intermodulation products is maximum for the channel with the lowest frequency in this case and this maximum is equal to $N_{max} - 2\,N_{min}$. The number of third order intermodulation products is maximum in the centre of the band and this maximum equals $3/8\ N^2$, with N being the number of channels.

References

[6.1] M. Ito, T. Kimura, 'Stationary and Transient Thermal Properties of Semiconductor Laser Diodes', IEEE Journ. Quant. El., Vol. 17, pp. 787-795, May, 1981.

[6.2] S. Kobayashi, Y. Yamamoto, M. Ito, T. Kimura, 'Direct Frequency Modulation in AlGaAs Semiconductor Lasers', IEEE Journ. Quant. El., Vol. 18, pp. 582-595, April, 1982.

[6.3] R. Tucker, D. Pope, 'Circuit modeling of the effects of diffusion damping in a narrow-stripe semiconductor laser', IEEE Journ. Quant. El., Vol. 19, pp. 1179-1183, July, 1983.

[6.4] P. Vankwikelberge, Ph. D. thesis (in Dutch), LEA, University of Gent.

[6.5] R. Olshansky, P. Hill, V. Lanzisera, W. Powazinik, 'Frequency Response of 1.3 μm InGaAsP High Speed Semiconductor Lasers', IEEE Journ. Quant. El., Vol. 23, pp. 1410-1418, September, 1987.

[6.6] R. Tucker, 'High-Speed Modulation of Semiconductor Lasers', IEEE Journ. Lightw. Techn., Vol. 3, pp. 1180-1192, December, 1985.

[6.7] J. Kinoshita, K. Matsumoto, 'Transient Chirping in Distributed Feedback Lasers: Effect of Spatial Hole-Burning Along the Laser Axis', IEEE Journ. Quant. El., Vol. 24, pp. 2160-2169, Nov., 1988.

[6.8] K. Kikuchi, 'Static Frequency Chirping in λ/4-Phase-Shifted Distributed-Feedback Semiconductor Lasers: Influence of Carrier-Density Nonuniformity Due to Spatial Hole Burning', IEEE Journ. Quant. El., Vol. 26, pp. 45-49, Jan., 1990.

[6.9] Y. Yoshikuni, G. Motosugi, 'Multielectrode Distributed Feedback Laser for Pure Frequency Modulation and Chirping Suppressed Amplitude Modulation', IEEE Journ. Lightw. Techn., Vol. 5, pp. 517-522, April, 1987.

[6.10] A. Saleh, 'Fundamental limit on number of channels in subcarrier-multiplexed lightwave CATV system', El. Lett., Vol. 25, pp. 776-777, June, 1989.

[6.11] T. Okezi, E. Hara, 'Measurement of nonlinear distortion in photodiodes', El. Lett., Vol. 12, pp. 80-81, Febr., 1976.

[6.12] K. Stubkjaer, M. Danielsen, 'Nonlinearities of GaAlAs Lasers - Harmonic Distortion', IEEE Journ. Quant. El., Vol. 16, pp. 531-537, May, 1980.

[6.13] K. Lau, A. Yariv, 'Intermodulation distortion in a directly modulated semiconductor injection laser', Appl. Phys. Lett., Vol. 45, pp. 1034-1036, Nov., 1984.

[6.14] M. Maeda, K. Nagano, K. Saito, 'Harmonic distortion in semiconductor injection lasers', Proceedings of ECOC '79, paper 18.5, Amsterdam, 1979.

[6.15] T. Darcie, R. Tucker, 'Intermodulation and harmonic distortion in InGaAsP lasers', El. Lett., Vol. 21, pp. 665-666, August, 1985.

[6.16] A. Takemoto, H. Watanabe, Y. Nakajima, Y. Sakakibara, S. Kakimoto, H. Namizaki, 'Low harmonic distortion distributed feedback laser diode and module for CATV systems', Proceedings of the Opt. Fiber Communications Conf. (OFC '90), p. 214, San Francisco, 1990.

[6.17] M. Lin, S. Wang, N. Dutta, 'Frequency dependence of the harmonic distortion in InGaAsP distributed feedback lasers', Proceedings of the Opt. Fiber Communications Conf. (OFC '90), p. 213, San Francisco, 1990.

[6.18] J. Daly, 'Fiber optic intermodulation distortion', IEEE Trans. Commun., Vol. 30, pp. 1954-1958, 1982.

[6.19] R. Olshansky, 'SCM Techniques for Video Distribution, Basic Principles and Options for Upgrades', Proceedings of ECOC'90, pp. 855 - 885, Amsterdam, 1990.

[6.20] K. A. Simons, 'The Decibel Relationships Between Amplifier Distortion Products', Proc. of the IEEE, Vol. 58, pp. 1071 - 1086, July, 1970.

Chapter VII

CONCLUSION

In this doctorate, we have attempted to give a contribution to the theoretical description of DFB laser diodes and to improve the understanding of the operation of such lasers. To this end, we have paid relatively much attention on a rigourous derivation of the coupled wave equations and on the inclusion of spontaneous emission. For the same reason, we have derived several analytical approximations and illustrated how the coupled wave equations can be manipulated in several ways e.g. to derive rate equations or to derive structures with axially uniform power.

One nevertheless needs a numerical solution of the longitudinal equations to obtain accurate results. An existing computer-model has been extended in several ways. The original version of this model, named CLADISS (Compound LAser DIode Simulation Software), was restricted to a single mode static analysis and a single mode, small signal AC-analysis. It is now a multi mode model that also allows to analyze the harmonic distortion and the influence of the noise.

In the doctorate, by far most of the attention is paid to a physical description of the behaviour of diode lasers. In chapter 4, where the static behaviour is treated, we first show how longitudinal spatial hole burning at higher power levels can give rise to the onset of side modes and how this phenomenon depends on parameters such as the laserlength, the coupling constant, the internal absorption, the carrier lifetime and the linewidth enhancement factor. Subsequently, we show how in general terms how an axially uniform power can be obtained by varying the coupling constant, the net gain or the Bragg deviation in the axial direction. Several structures that can be realized in practice are then derived and discussed.

The study of the noise in DFB lasers is mainly concentrated on the linewidth and its rebroadening at high power levels, a phenomenon that was not yet fully understood. We have shown that

this rebroadening can be the result of a side mode onset and that the side mode can thereby influence the noise in the main mode via spectral or spatial hole burning. Possible explanations have also been found for single mode lasers. The rebroadening of the linewidth in this case can be attributed to a power dependence of the linewidth enhancement factor or, in a limited number of cases, to the power and frequency dependence of the reflection loss.

The last chapter treats the distortion in the AM-response of DFB lasers, a quantity that is of interest for analog communication. We particularly illustrate the influence of spatial and spectral hole burning and of the relaxation oscillations, and how the interference of the different non-linearities can lead to the presence of dips in the frequency and/or the power dependence of the distortion. The knowledge of these influences allows to minimize the distortion, somehow by choosing the appropriate laser structure as function of the frequency allocation and of the desired bias level.

To conclude, we remark however that this study is far from complete. In particular the influence of the temperature, of leakage currents and of the carrier dependence of the absorption on the static, dynamic and noise behaviour must still be investigated. Furthermore, the study can be extended to the behaviour of quantum well lasers, where the gain is a non-linear function of the carrier density, which results in other interesting effects.

In addition, a model for laser amplifiers can be developed starting from CLADISS and can then be followed by a detailed study of the behaviour of such amplifiers.